Tectonics of Gedemsa Magmatic Segment: Insight from Paleomagnetic Investigation, Central Main Ethiopian Rift

MSc. Thesis

By

YOSEPH MUHABAW

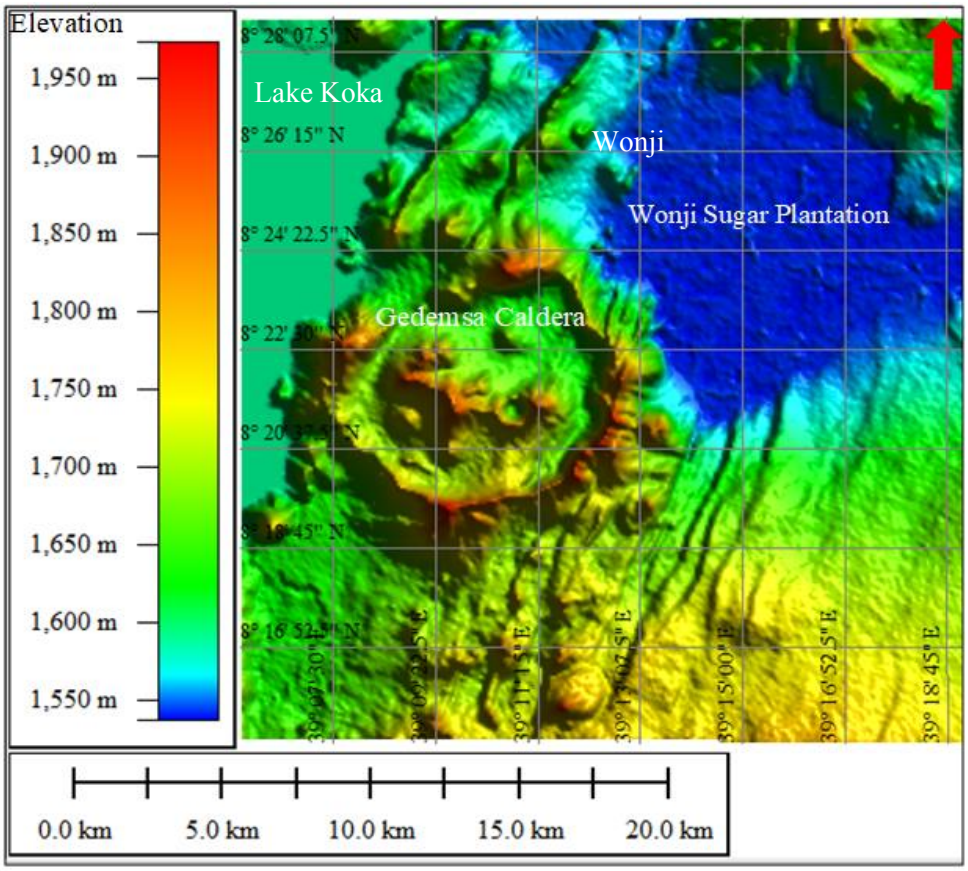

A THESIS SUBMITTED TO SCHOOL OF GRADUATE STUDIES OF ADDIS ABABA UNIVERSITY, IN PARTIAL FULFILLMENT OF THE REQUIREMENTS FOR THE DEGREE OF MASTER OF SCIENCE IN EARTH SCIENCES (STRUCTURAL GEOLOGY)

ADDIS ABABA UNIVERSITY

ADDIS ABABA, ETHIOPIA

SEPTEMBER 2020

ADDIS ABABA UNIVERSITY

SCHOOL OF GRADUATE STUDIES

SCHOOL OF EARTH SCIENCES

Tectonics of Gedemsa Magmatic Segment: Insight from Paleomagnetic Investigation, Central Main Ethiopian Rift

By

Yoseph Muhabaw

Advisors: Prof. Tesfaye Kidane

Dr. Ameha Atnafu Muluneh

A Thesis Submitted to School of Graduate Studies of Addis Ababa University, in Partial Fulfillment of the Requirements for the Degree of Master of Science in Earth Sciences (Structural Geology)

Addis Ababa, Ethiopia

September 2020

ADDIS ABABA UNIVERSITY
SCHOOL OF GRADUATE STUDIES
SCHOOL OF EARTH SCIENCES

This is to certify that the thesis prepared by Yoseph Muhabaw entitled *"TECTONICS OF GEDEMSA MAGMATIC SEGMENT: INSIGHT FROM PALEOMAGNETIC INVESTIGATION, CENTRAL MAIN ETHIOPIAN RIFT,"* submitted in partial fulfillment of the requirement for the degree of Master of Science in Structural Geology complies with the regulations of the university, and meets the accepted standards concerning originality and quality.

Approved by examining committee:

	Signature	Date
Dr. Balemwal Atnafu	_____	_____
(Head of School of Earth Sciences)		
Prof. Tesfaye Kidane	_____	_____
(Advisor)		
Dr. Ameha Atnafu	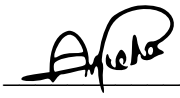	28 Sept 2020
(Advisor)		
Prof. Bekele Abebe	_____	_____
(Examiner)		
Prof. Gezahegn Yirgu	_____	_____
(Examiner)		

Declaration

I, the undersigned, hereby declared that the thesis entitled **"TECTONICS OF GEDEMSA MAGMATIC SEGMENT: INSIGHT FROM PALEOMAGNETIC INVESTIGATION, CENTRAL MAIN ETHIOPIAN RIFT"** is my original work. I carried it out under the supervision of Prof. Tesfaye Kidane and Dr. Ameha Atnafu and has not presented to any university or institution for the award of any degree or diploma program. All sources of materials used for the thesis are duly acknowledged.

Name of the candidate	Signature	Date
Yoseph Muhabaw	_____	_____

We, the undersigned, now certify that the above declaration made by the candidate is correct to the best of our knowledge and it has been submitted for examination with our approval as university advisors.

	Signature	Date
Prof. Tesfaye Kidane	_____	_____
Dr. Ameha Atnafu	_____	_____

ABSTRACT

The paleomagnetic and tectonic investigation was conducted on Gedemsa Magmatic Segment, Central Main Ethiopian Rift. The main objective of this study was to investigate crustal block rotation of the Gedemsa magmatic segment and to identify the magnetization carrier minerals in the sampled rock units. To address the set scientific objectives, a total of 170 core samples (from 23 sites) were sampled and analysed from the outcrop of basalts, ignimbrites, volcanic tuffs and rhyolite units. From these samples a total of 243 specimens were prepared. The specimens were then subjected to progressive demagnetization to isolate the ChRM from the secondary overprint magnetization, and impulse magnetization (23 specimens) to identify magnetization carrier minerals. Rock magnetic experiments show that the dominant magnetic minerals are titanomagnetite, magnetite, titano-hematite and small amount of hematite. The demagnetization analyses reveal two components (low stability and high stability components) of Natural Remanent Magnetization (NRM). Demagnetization process removes the low stability components by applying up to 30mT or by heating up to 520^{o}C. The high stability ChRM components were isolated above those steps and the ChRM vector direction characterized to be directed towards the origin with a straight line segment. All the selected sites show normal polarity. An overall mean direction calculated from individual accepted site mean directions were D=359.1^{0}, I=9.6^{0}, N=20, K =20, α95=7.5^{0}. When these observed mean directions are compared with the mean expected reference geomagnetic field direction for stable Africa (D=1^{0}, I=13.5^{0}, N=32, K=105.6, and α95 =2.5), from the apparent polar wander path reference curve for Africa, found to be statistically different in small amount. This suggests that a small amount of counter-clockwise crustal block rotation (~3^{0}) about the vertical axis has occurred at the Gedemsa Magmatic Segment relative to stable Africa. The result is in agreement with most of other paleomagnetic investigations which advocates an increasing magnitude of counter-clockwise vertical axis rotation towards the north which characterised the heterogeneous deformation of the Main Ethiopian Rift. The study area is characterised by normal faults with NNE-SSW, NE-SW and some N-S orientation which are part of the WFB.

***Key words**: Characteristic remanent magnetization, Crustal block rotation, Magmatic segment, Paleomagnetism, Tectonics*

ACKNOWLEDGMENT

I gratefully acknowledge Addis Ababa University and Bahir Dar University for providing me with an opportunity to study my master‘s degree and funding the budget for the research work.

I wish to express my heartfelt gratitude to my advisors; Prof. Tesfaye Kidane and Dr. Ameha Atnafu, for their genuine supervision, and continuous follow up throughout the accomplishment of this thesis work. I would like to acknowledge Prof. Gezahegn Yirgu for his constructive comments and suggestions on my work. Special thank goes to Mr. Ermias Filflu, who was with me during all the field works. Mr Kahsay Nugsse also highly acknowledged for his continuous suggestions and valuable comments on the thesis work.

I would like to thank very much Addis Ababa University School of Earth Sciences staff members, especially Dr. Balemwal Atnafu, head of the department, Dr. Bayisa Regassa, head of the school of graduate committee, Prof. Bekele Abebe and Dr Abera Alemu for their encouragement and moral support during the laboratory work. All my friends are highly acknowledged for their respective contribution to the accomplishment of this thesis work successfully.

At last but not the least, my lovely families deserved a special appreciation for their encouragement and support throughout my life.

TABLE OF CONTENTS

LIST OF FIGURES

LIST OF TABLES

LIST OF ABBREVIATIONS

AFD: Alternative Field Demagnetization

AMS: Anisotropy of Magnetic Susceptibility

APWP: Apparent Polar Wander Path

BRZ: Broadly Rifted Zone

CCWR: Counter Clockwise block Rotation

ChRM: Characteristic Remanent Magnetisation

CMER: Central Main Ethiopian Rift

D/I: Declination / Inclination

DRM: Detrital Remanent Magnetization

EAP: East African plateau

EARS: East African Rift System

Elv: Elevation

GAD: Geocentric Axial Dipole

GMS: Gedemsa Magmatic Segment

HTC: High Temperature Component

IM: Impulse Magnetizer

IRM: Induced Remanent Magnetization

K: Precision Parameter

LTC: Low Temperature Component

MAD: Medium Angular Deviation

MER: Main Ethiopian Rift

Mmax: Maximum intensity of magnetization

Mmax /M: Maximum value of magnetization normalized by M

MMTD: Magnetic Measurements Thermal Demagnetizer

mT: milliTesla

M x, M y, M z: Magnetic moment along x, y, z axis, respectively

NMER: Northern Main Ethiopian Rift

NRM: Natural Remanent Magnetization

PCA: Principal Component Analysis

SDZFZ: Silti-Debre Zeit Fault Zones

SMER: Southern Main Ethiopian Rift

SRTM: Shuttle Radar Topography Mission

TB: Blocking Temperature

THD: Thermal Demagnetization

TRM: Thermal Remanent Magnetization

V: Voltage

VRM: Viscous Remanent Magnetization

WFB: Wonji Fault Belts

YTVL: Yerer-Tullu-Wellel Volcanotectonic Lineament

α95: Confidence Limit

k: precision parameter

CHAPTER ONE

INTRODUCTION

1.1 General Background

The East Africa Rift System (EARS) is a place where the earth's tectonic forces are currently trying to create new plates (https://geology.com/articles/east-africa-rift.shtml). The EARS encompasses a series of rifts that prolongs ~5,000 km long fault-bounded depressions characterized by active extensional tectonics accommodating ~6–7 mm/yr relative movement between the Somalian and African plates (Fernandes et al., 2004).

The Main Ethiopian Rift (MER) is the northern portion of the EARS trending NE across the Ethiopian plateaus, characterized by magmatically segmented, seismically vigorous (Kurtz et al., 2007) region. Besides, it has uplifted flanks and steep border faults which invite geoscientists with its excellent location to study how continental rifts progress into oceanic ridges (Mehatsente et al., 1999, Keranen et al., 2004). The MER accounts for all the different phases of rift evolution from rift initiation to break up and incipient oceanic spreading (Ebinger, 2005). Thus, it is an ideal and promising region to understand and examine the evolution of continental rift. So that, the Main Ethiopian Rift has attracted the attention of many geoscientists and research teams (Corti, 2009).

The Main Ethiopian Rift is also the best example of oblique continental rifting where the ongoing continental breakup is associated with an extension direction oblique to the trend of the rift (Corti et al., 2013). This oblique rifting is due to the oblique motion and deformation of the Somalian plate relative to the Nubian plate along with the MER. The MER progressively opened and developing through a system of interacting half-grabens marking the boundary between the Nubian and Somalian plates during the Pliocene and the Quaternary (Hayward and Ebinger 1996). This forms a narrow active zone of overlapping magmatic segments that are arranged in a right stepping en-echelon manner. Thus, the MER displays variations in rift architecture, geometry, orientation and style of deformation along the strike of the rift (Tesfaye Kidane et al., 2009; Corti et al., 2013). This variation is

supposed to be controlled by inherited structures that underlie the Somalian and Ethiopian plateau (Corti et al., 2018).

The extension direction of the MER has been contrarily understood based on local geologic studies. Gidey Woldegabriel et al., (1990) suggested an east-west extension direction during the entire rift evolution; on the other hand, NW-SE extension direction has been offered by Chorowicz et al., (1994). Several authors (e.g. Bonini et al., 1997; Agostini et al., 2009; Corti, 2008) determined the extension direction along both sets of faults to be pure dip-slip, irrespective of their difference in the strike. This geometry required local deflection in the orientation of the extension direction at the border faults that force the block to rotate counterclockwise to accommodate these variations (Corti et al., 2013). In order to characterize the deformation style and quantify the vertical axis crustal block rotation related to the rift axis overlap, different studies have been carried out in the Main Ethiopian Rift (e.g Tesfaye Kidane et al., 2009, Kahsay Nugsse et al., 2018); all these studies suggested the presence of counter-clockwise rotation along the strike of the rift. The result of this study is also consistent with those studies with minor counter-clockwise crustal block rotation even though the small amount of rotation is observed.

In this thesis results, paleomagnetic investigation in the central MER from the Gedemsa Magmatic Segment is presented. The Gedemsa magmatic segment provides an excellent setting to investigate along strike variation in rotation of crustal blocks about a vertical axis for two reasons. First, because young faults persistently shatter this magmatic segment providing outcrops and secondly, the rocks are sound recorders of the paleomagnetic direction. The collection of data in this region is particularly important in defining the extent of the block rotations; typically, it provides a high-quality recording of the ancient magnetic field during the time of rock formation. To this end, oriented core samples from basalt, ignimbrite and rhyolite rock units were collected. After a routine laboratory analysis, a mean declination and inclination values were estimated, which is later compared with APWP curve (Besse and Courtillot, 2003). The difference in inclination and declination between the observed and expected direction is interpreted as inclination shallowing and vertical axis block rotation, respectively.

1.2 Description of the Study Area

1.2.1 Location and Accessibility

The study area is situated in the central sector of the Main Ethiopian Rift, 25km southwest of Adama town notably close to the eastern rift margin. Geographically, it lies within 39^0 05' E and 39°20'E longitude and 8º 14'N and 8º28'N latitude. It covers approximately 730 square kilometers. The study area is bounded to the North by the Awash River, to the West by the Koka Lake and to the East by Wonji sugar plantation.

The study area is accessed by vehicles through two roads. One of the roads starts from Addis Ababa to Adama then to Wonji sugar factory and then goes to the northeast and western rim of the Gedemsa caldera, the other one runs from Adama town directly to Dera town then goes to the west of Dera town.

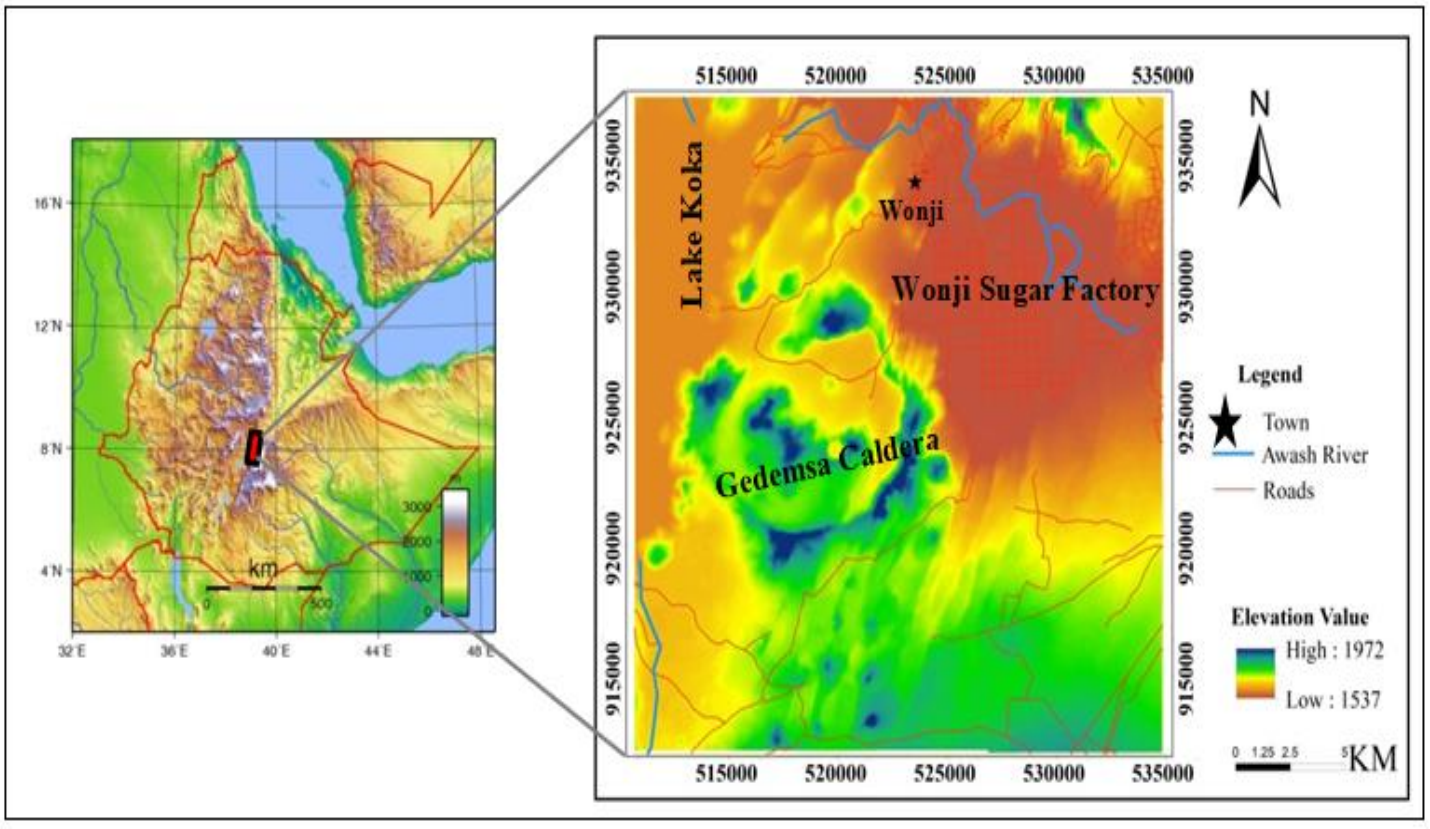

Fig 1.1) Location and accessibility map of the study area prepared from the Digital elevation model of Ethiopia using Arc GIS 10.1 version. The green to blue colors shows the highest elevation and the yellow to orange color shows the lowest elevation value.

1.2.2 Physiography of the Study Area

The study area, as a volcanic complex, is characterized by the existence of rugged topography (Fig 1.2), elongated and relatively narrow (1-5m) extension fractures (Tesfaye Korme et al., 1997). Brecciated lava flows, lava domes, cinder cones, crater and calderas are the main notable features within the study area. The central part of the caldera is occupied by an irregular chain of hills which results from the coalescence of several volcanic edifices. One of these volcanoes, sited at the edge of the chain, contains an explosion crater (Kore Crater).

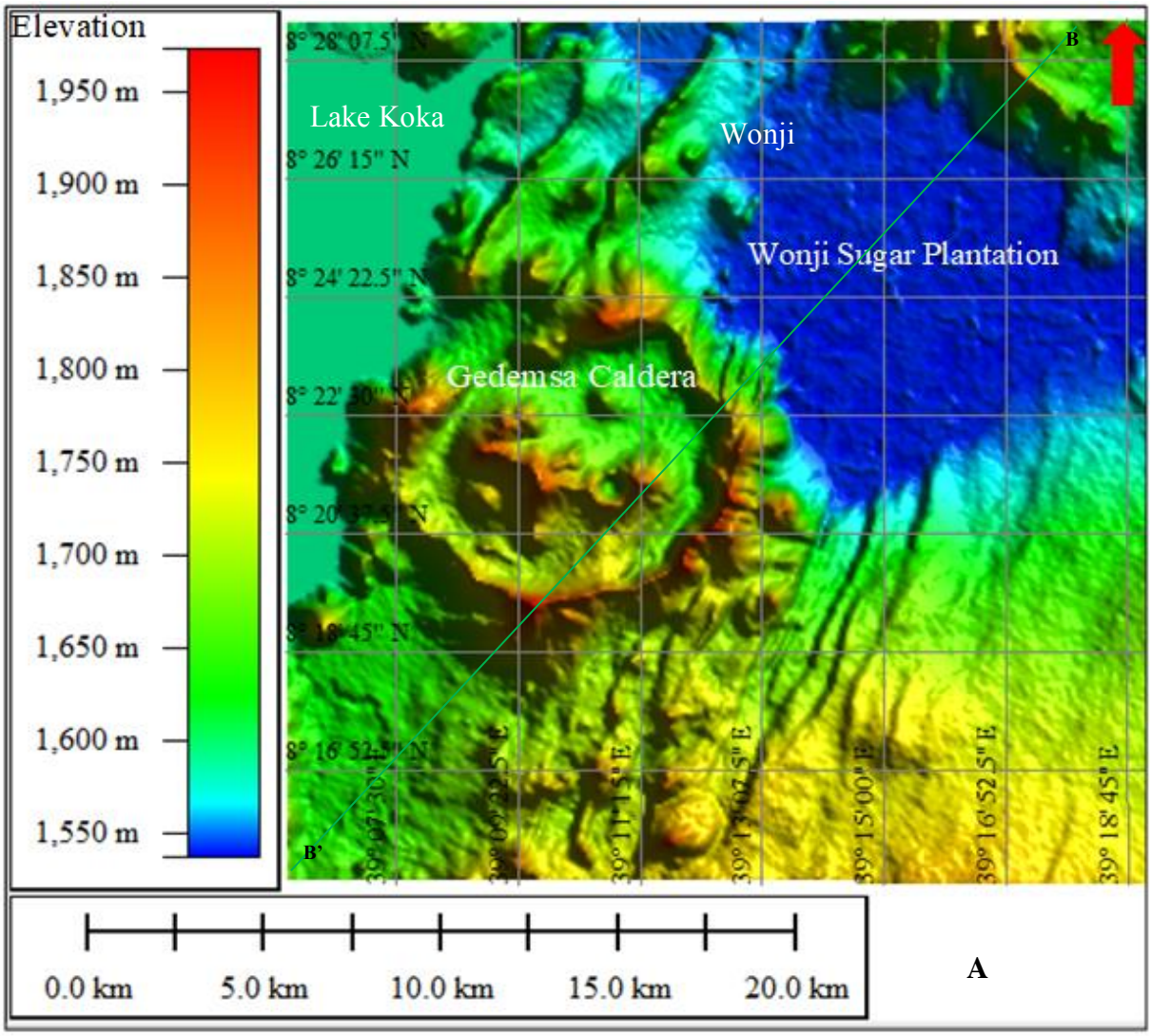

Fig 1.2) Physiographic map of the study area (A), elevation profile of the study area (B). From elevation profile we can observe that the Gedemsa volcano shows a complex morphology, the

depressed area is the Wonji sugar factory, it is covered by a lacustrine and alluvial deposit, made by Global Mapper.

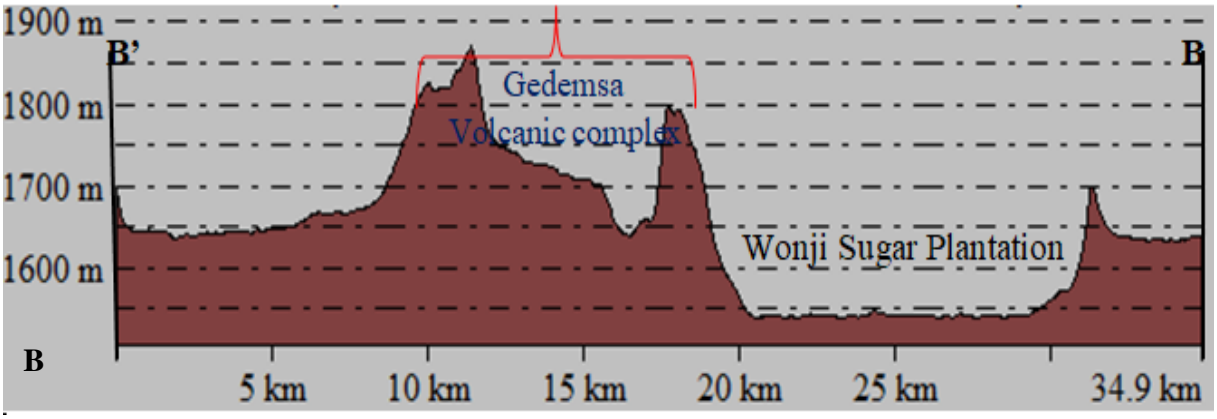

1.2.3 Population and Settlement of the Study Area

Generally, the study area is dominantly inhabited by Oromo nationalities with some other small nationalities like Amhara, Guraghe, and Silte. The dominant religions are Islam and Protestant Christians with few orthodox Christians. Amharic and Afan Oromo are the dominant languages spoken in the study area. The distribution of population varies in rural areas and towns. In rural areas, the population is sparse and unevenly distributed. The population distribution varies due to the socio-economic factors and lack of infrastructure. They engage in agricultural practice cultivating different kinds of crops such as wheat, barley, teff, etc. In addition to farming activity, most of the rural dwellers engage also in breeding domestic animals like Cattle, Horses, mules, and donkeys.

1.3 Statement of the Problem

The MER shows variations in the rift architecture, geometry, orientation and style of deformation along the strike of the rift (Tesfaye Kidane et al., 2009; Corti et al., 2013). To characterize the deformation style and quantify crustal block rotation, different paleomagnetic studies have been conducted in the MER (e.g Tesfaye Kidane et al. 2006; 2009, Kahsay Nugsse et al. 2018). Results from geophysical and structural investigations (Ebinger and Casey 2001, Casey et al., 2006, Siegburg et al. 2020) support a notion that the MER may have experienced differential kinematics with subsequent temporal and spatial variations in deformational style. Paleomagnetic investigations along the magmatic segments

of the Main Ethiopian rift offered valuable evidence about the crustal block motion along the strike of the rift.

Paleomagnetic investigation presented by Tesfaye Kidane et al., (2006) shows negligible crustal block rotations about the vertical axes around Assela area which is situated south of the present study area. However, another work of Tesfaye Kidane et al., (2009) indicates $\sim 7^0$ counterclockwise block rotations about the vertical axis consistent with the transtentional deformations that characterize the Fentale magmatic segment, north of the present study area. Further north, in the Dofan magmatic segment, Kahsay Nigusse et al., (2018) identified a $\sim 7^0$ counterclockwise crustal block rotation about vertical axis consistent with paleomagnetic reports and analogue modeling in Fentale magmatic segment (Corti et al. 2013).

Constraining crustal block rotation along the Gedemsa magmatic segment provides a better understanding on the along strike variation in deformation style of the MER, as previous studies show no rotation and $\sim 7^0$ counter-clockwise rotation to the south and the north of the study area respectively.

1.4 Objectives

1.4.1 General Objective

The main objective of this study is to conduct tectonic and paleomagnetic investigation on the Gedemsa magmatic segment, central Main Ethiopian Rift.

1.4.2 Specific Objectives

- To quantify the mean paleomagnetic direction and determine the sense of block rotation of the Gedemsa magmatic segment.
- To identify magnetization carrier minerals.
- To describe tectonic history and deformation style of the study area, and to characterize the variation of deformation along the strike of the MER.

1.5 Significance of the Study

Detailed understanding of the tectonics of the Gedemsa magmatic segment has paramount importance as the area hosts one of the potential geothermal fields in the MER. This study provides a systematic understanding of the kinematics of the crustal block in Gedemsa

magmatic segment relative to the stable Africa. It helps to understand the heterogeneous deformation style of the Main Ethiopian rift by considering the results of previously published works. Besides, intended peoples and research institutions will be benefited from this research paper either directly or indirectly.

1. 6 Pervious Paleomagnetic Studies in the Ethiopian Rifts

The volcanic rocks of Afar depression and Main Ethiopian Rift have given emphasis to conduct paleomagnetic investigation for the last few years Acton et al., (2000). Those studies presented different scale of crustal block rotation along the axis and margin of the rift. The present study has contributed new interest in the crustal block rotation of the Main Ethiopian Rift, especially on determining crustal block rotation of Gedemsa magmatic segment.

The paleomagnetic study conducted by Tesfaye Kidane et al., (2009) presented that 7º counter-clockwise crustal block rotation (CCWR) about vertical axis that characterizes the Fentale magmatic segment and its surrounding. Further North, recent observation by Kahsay Nigusse et al., (2018) also shows similar counter-clockwise block rotation at the Dofan magmatic segment. So that, these two magmatic segments both found in the northern Main Ethiopian rift, Fantale and Dofan are characterized by similar sense of crustal block rotation. On the other hand, south of the present study area, Tesfaye Kidane et al., (2006) detected no significant crustal block rotation of the vertical axis for Assela and surrounding area.

Acton et al., (2000) investigated the volcanic rocks of central Afar to characterize its tectonics and to compare with the eastern Afar. The outcome suggested that central Afar experienced insignificant crustal block rotation whereas the eastern Afar has experienced significant clockwise crustal block rotation of 9^0. According to the results, there are two main factors for the more minor crustal block rotations in the central Afar. The first one is the localization and propagation within the central Afar are still in progress while the process nearly completed in the eastern Afar; the other factor, the rate of the localization and the propagation happening in the central Afar is more faster.

The volcanic rocks of the Danakil blocks have been investigated Paleomagnetically, suggesting that the Danakil horst has experienced counter-clockwise crustal block rotation relative to Africa. However, the magnitude of the crustal block rotation was not clear. Brock

et al., (1970) estimated at least 25^0 counter-clockwise crustal block rotation since the Miocene; on the other hand, Schult (1974) estimated a 10^0 counter-clockwise rotation since the early Pliocene.

Ameha Atnafu Muluneh et al., (2013) conducted paleomagnetic investigation on the major overlap between Red Sea and Gulf of Aden rift, eastern Dabbahu magmatic segment to investigate the influence of the series right stepping southward propagation of Red Sea Rift on the movement of the block that are connected to them. The result suggested that counter-clockwise rotation about the vertical axis that resulted due to south-ward propagation and overlap of the Earta'Ale–Alayta-Dabbahu magmatic segments and Manda Hararo rifts.

CHAPTER TWO

REGIONAL GEOLOGY AND TECTONIC SETTING

2.1 Regional Geology of the Main Ethiopian Rift

The MER has experienced a very complex geological evolution and tectonic history (Gidey Woldegabriel et al., 1990). It divides the wide uplifted Ethiopian volcanic province asymmetrically in to the Southeastern and Northwestern plateaus. Volcanic rocks of Pliocene and Pleistocene age such as pantelleritic rhyolite, trachytes, ignimbrites and basalts are abundant within the rift floor and on the adjoining plateaus (Kazmin, 1972, Gidey Woldegabriel et al., 1990).

The oldest volcanic rocks are exposed in the western escarpment and comprise of basaltic lava with interbedded ignimbrites beds, superimposed by massive rhyolites and intervening tuffs and basalt (Gidey Woldegabriel et al., 1990). Radiometric ages range from 40-25 Ma in the basalt and from 37- 27Ma in the Rhyolites. The early Tertiary volcanic units are unconformably overlain by Middle Miocene to Pliocene (15-3Ma) basalt flows; rhyolites and tuffs (Merla et al., 1979; Gidey WoldeGabriel et al., 1990).

Pliocene to early Pleistocene (4.6-1.6Ma) aged shield volcano (Chilalo, 4005m; Kekha 4245m; Badda, 4170m) covers the eastern margin. This consists of trachytes with subordinate basalt (Gidey WoldeGabriel et al., 1990; Bigazzi et al., 1993). Early-middle Pliocene (4.2-3Ma) age silicic pyroclastic materials mainly peralkaline rhyolitic ignimbrites interlayered with basalts and tuffs cover the floor of MER (Mohr, 1962; Di Paola, 1972; Gidey WoldeGabriel et al., 1990). Alkaline and peralkaline rhyolitic lava flows and domes associated with ash and pumice characterize the late silicic volcanic events (Di Paola, 1972).

A more recent volcanic rocks outcrop along the WFB (Di Paola, 1972; Kazmin et al., 1980) and the Silti-Debre Zeit Fault Zones (SDZFZ); it encompassed of basaltic lava flows with the associated scoria cones. It is very recent, as testified by radiometric ages of 0.13Ma (Gidey WoldeGabriel et al., 1990). The final products of volcanic activities are represented by Obsidian flows (Di Paola, 1972), started to be active from the middle Pleistocene (about 0.25Ma, Di Paola, 1972; Mohr et al., 1980; Gidey WoldeGabriel et al 1990).

The basement rocks in the Ethiopian Rift System, except in the Northern Afar and at the extreme South of the Ethiopian Rift, are mostly covered by more recent Tertiary volcanic rocks and Mesozoic sediments (Mohr, 1962). However, there are windows of metamorphic basement rocks of Precambrian age and Mesozoic sedimentary rocks in a few localities. These pre-Tertiary rocks are exposed along the eastern, western and southern Afar margins. Restricted outcrops of basement rocks overlain by Early Mesozoic fluvial sandstones, marine shales and limestones, occur along the west margin of the central sector of the MER at Kella Horst, and Amaro Horst in the southern sector of the MER (Levitte et al., 1974).

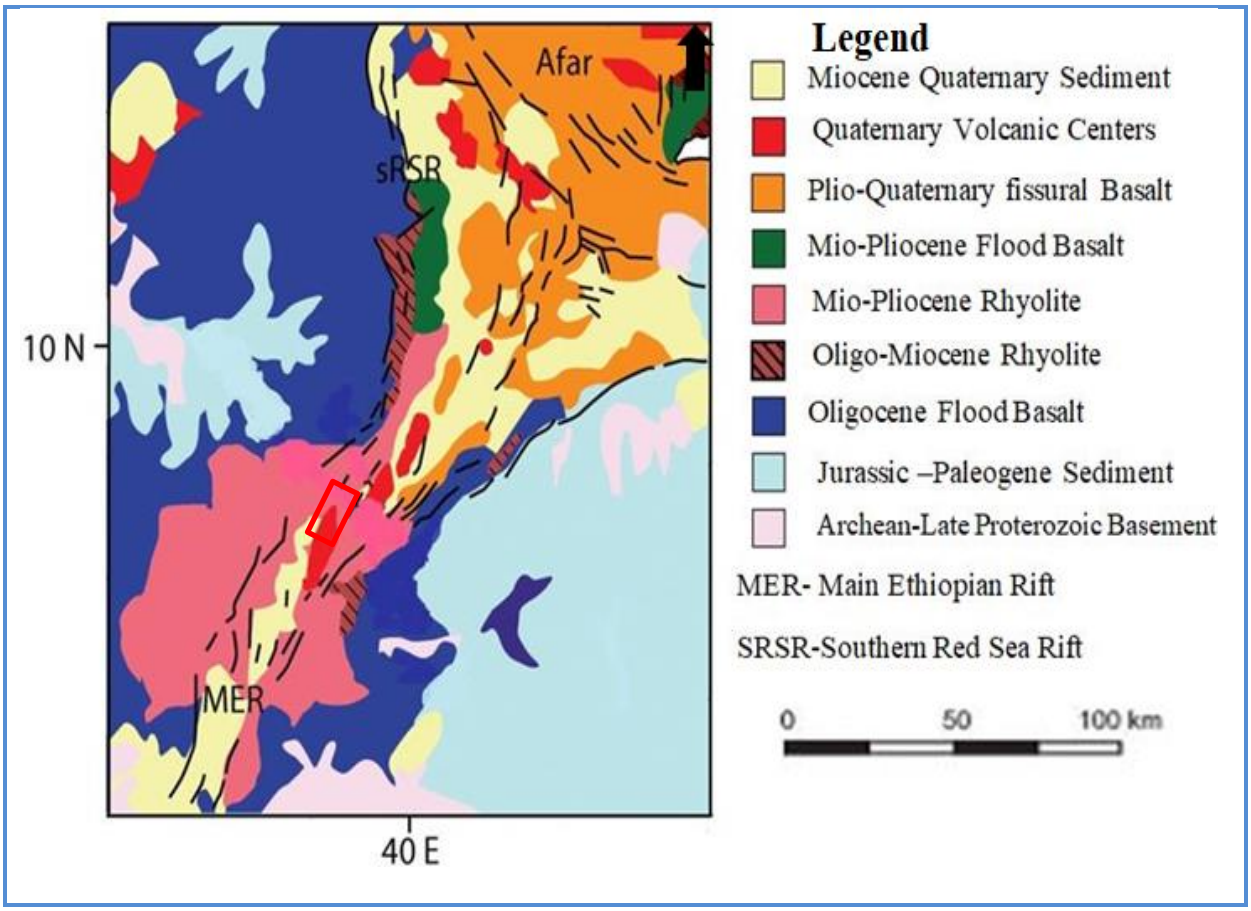

Fig 2.1) Simplified geological map of the Ethiopian rift (Both the Afar rift and the Main Ethiopian Rift) (adopted from Wolfenden 2003). Red open box shows the approximate location of the study area

2.2 Tectonic Setting

Recent volcano-tectonic activity along the Main Ethiopian Rift is mostly situated on the Wonji Fault Belt (WFB) (Bilham et al., 1999; Ebinger and Casey, 2001). Based on geology

and surface geomorphology the Main Ethiopian Rift divided in to three sectors (Keranen and Klemper, 2008); southern (SMER), central (CMER), and the northern (NMER). Those sectors described by different phases of the continental extension process. They are characterized by different fault architecture, the timing of volcanism and deformation, crustal and lithospheric structure (Hayward and Ebinger, 1996).

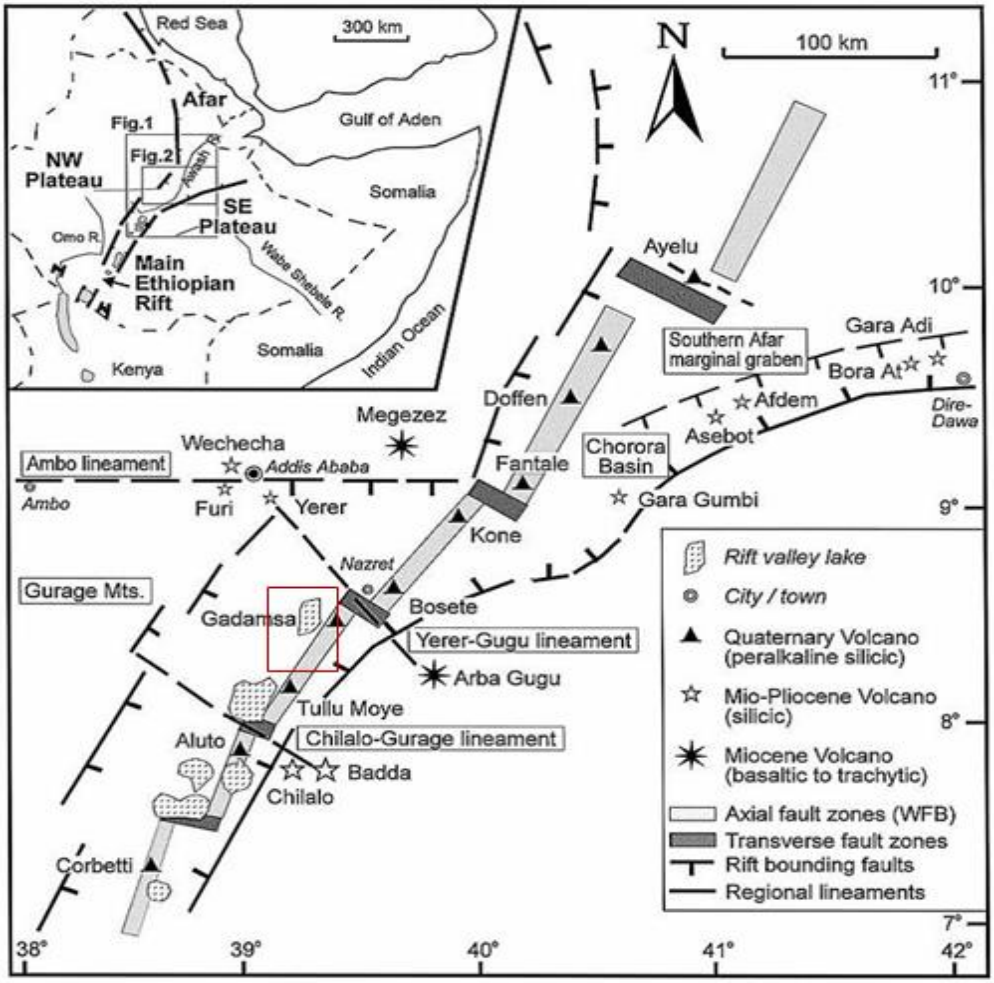

Fig 2.2) Regional setting, the inset map illustrates the tectonic setting of Main Ethiopian Rift and Southern Afar transition region. Here the axial fault zone, WFB, shows En echelon pattern which accommodates the recent deformation of the Main Ethiopian Rift and Afar rift. The approximate location of the study area is demonstrated by red Square (after Tadiwos Chernet et al., 1998).

The NMER extends for ~200 km from the Afar to near Lake Koka with steep boundary faults that trend on average at N50°E (Keranen and Klemper, 2008). The northern Main Ethiopian Rift is recognized as the merger of MER border faults and the southern Afar marginal faults,

have formed since 10–11Ma (Wolfenden et al., 2004). This sector has the lowest elevation and consequently thin crust (shallow Moho depth) compared to the CMER. The abrupt and apparent change in physiography and crustal properties is observed at the junction between the CMER and NMER (Keranen and Klemper, 2008). Significant crustal extension accompanied by rift deepening and widening are apparent for the CMER during the late Miocene–early Pliocene, with intensive volcano-tectonic activity after 5 Ma (Tsegaye Abebe et al., 2010). Based on seismic and gravity data, the crustal thickness of the CMER increases rapidly from the boundary with the NMER (33–35 km) to the middle of the CMER (38–40 km) (Keranen and Klemper, 2008).

The SMER, in which rifting initiates, extends south from Lake Awasa into the broadly rifted zone of southern Ethiopia (Ebinger et al., 2000) with faults trending N-S to N20°E. Faulting in the SMER was well-established by ~18 Ma. The three sectors of the Main Ethiopian Rift can be understood as representing different phases of rift extension processes, from the early rift initiation in the southern MER to the more evolved stages in the central and northern MER preceding the incipient seafloor spreading in the Afar rift.

The different MER sectors can be characterized by two distinct systems of normal faults that differ in terms of orientation, structural characteristics (e.g. vertical throw, length), the timing of activation and relation with magmatism. Those are the border faults and a set of faults affecting the rift floor usually referred to as the Wonji Fault Belt (Boccaletti et al., 1998; Mohr, 1962).

The border faults are generally widely spaced, long and characterized by large vertical offset and variable orientation in the different MER sectors. The activation period of these faults shows variation along the strike of the rift axis; in the NMER it is commonly understood to have occurred in the Late Miocene (~11Ma; Wolfenden et al., 2004), to the Late Miocene–Early Pliocene in the CMER (~6–8 Ma Gidey WoldeGabriel et al., 1990), and to the Plio-Pleistocene in the SMER.

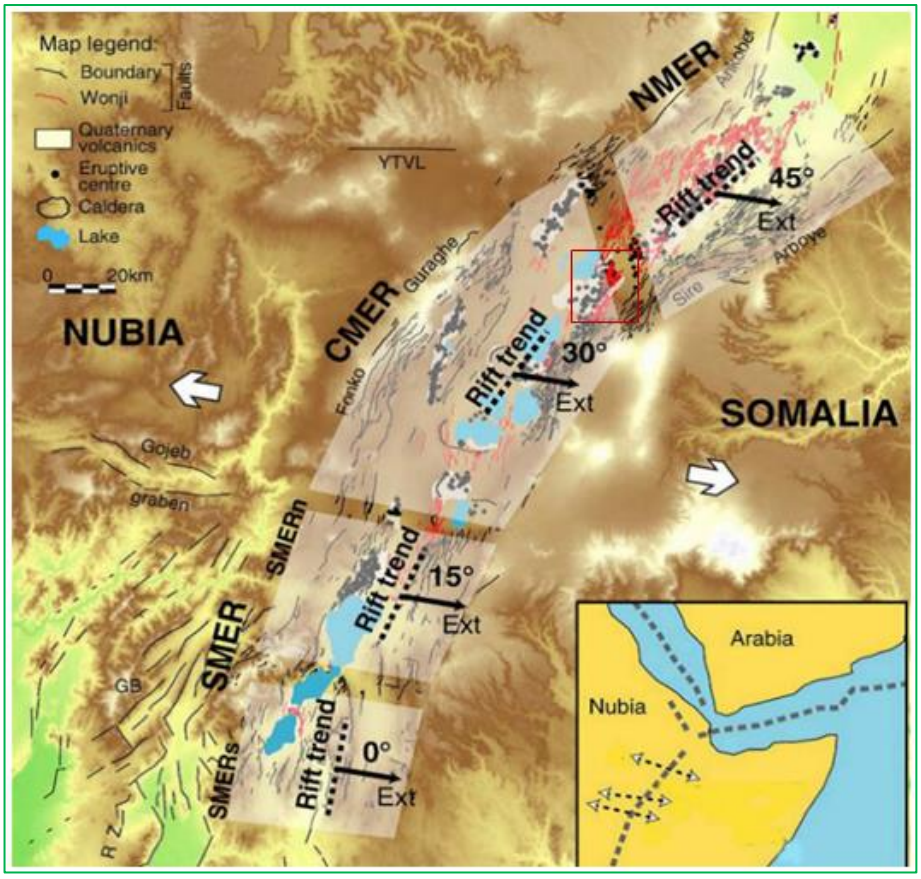

Fig 2.3) Structural setting of the MER superimposed onto a digital elevation model showing the trend of each rift sector and the Nubia–Somalia extension direction. (Adopted from Agostini et al., 2011a) the solid square shows the approximate location of the study area which is situated in the central MER and it is near the boundary of NMER and CMER.

Geological data and analysis of the instrumental and historical seismicity suggest that the boundary faults are mostly inactive and eroded in the Northern MER (Keir et al., 2006; Wolfenden et al., 2004). Morphostructural and geological data together with the analysis of local seismicity, on the other hand, suggests that the boundary faults are still accommodating some extensional deformation in the CMER and SMER (Keir et al., 2006).

The youngest Wonji Fault Belts (WFB) are characterized by closely spaced, short, active faults that exhibit minor vertical throw. They are believed to be developed in the last 2 My (Ebinger and Casey, 2001) and was intimately associated with the intense Quaternary magmatism of the rift floor. These faults (WFBs) are well established in the NMER, forming right-stepping en-echelon segment obliquely cutting the rift floor. The existence of this fault system decreases southwards. Magma intrusion occurs throughout the lithosphere beneath

the WFB (Kendall et al., 2005). Segmented high velocity anomalies, interpreted to be of regions of mafic intrusion in the mid-upper crust below the MER axis are spatially coincident with the segmentation of the rift axis identified from the surface expression of Quaternary volcanism and faulting (e.g Bekele Abebe et al., 2007; Hayward and Ebinger, 1996; Mohr, 1962). These interpretations permit to consider the WFB as distinct tectono magmatic segments within the rift depression (Ebinger and Casey, 2001; Keranen et al., 2004).

the Main Ethiopian Rift (MER) is the best example of oblique continental rifting where ongoing continental break-up is associated with an extension direction oblique to the trend of the rift (Corti et al., 2013). This oblique rifting is due to the oblique motion and deformation of Somalia plate with respect to the Nubian plate along with the MER. During Pliocene and Quaternary, the MER has been progressively deepened and opened, growing through a system of interacting half-graben segments (Hayward and Ebinger, 1996). The along-strike variation in rift architecture, asymmetry is controlled by inherited structures that underlie the contrasting Somalian and Ethiopian plateau, (Corti et al., 2018).

2.3 Geology of Central MER

The Central sector of the Main Ethiopian Rift and its shoulders are made of pyroclastic rocks and other volcanic rocks. Volcano-lacustrine and fluvio-lacustrine deposits cover large areas of the rift floor (Gidey WoldeGabriel et al., 1990). Limited outcrops of Precambrian biotite gneiss, covered by Early Mesozoic fluvial sandstone, marine shales and limestone, occur in a complex horst structure on the western margin (Gidey Woldegabriel et al., 1990; Di Paola et al., 1993).

The geology of central Ethiopia is classified in to different lithologic-units (Tsegaye Abebe et al., 2010). These lithologies are described below;

2.3.1 Pre-Cambrian Crystalline Basement and Pre-Tertiary Sediments

The pre-rift geology is hardly exposed along with the rift system (Gidey Woldegabriel et al., 2002). The crystalline basement rocks are exposed by the boundary faults beneath tertiary volcanic rocks in the southern sector of the MER. Pre-Tertiary crystalline basement and Mesozoic sedimentary rocks are exposed in the western margin of the central sector at the Guraghe escarpment (Gidey Woldegabriel et al., 1990).

2.3.2 Oligocene and Lower Miocene Plateau Volcanics

The Oligocene rocks are dominated by basalt with limited rhyolite and sedimentary rocks (Gidey Woldegabriel, 1990). The main parts of the Ethiopian volcanics consist of the Trap Series (e.g Hofmann, 1997) and are in age of 32-29 Ma. They cover an area of more than 600,000km^2 and locally reach thickness exceeding 3000m (Gidey Woldegabriel, 1990). After a long period of ~11-8 Ma age less voluminous and more local volcanic activity happened. This resulted in the development of shield volcanoes (Corti, 2009), basaltic-trachytic lava flows and associated pyroclastic. They constitute the most substantial part of the Guraghe escarpment and extend for several tens of kilometers west of the escarpment (Tsegaye Abebe et al., 2010).

2.3.3 Miocene–Pliocene Trachytic–Rhyolitic Volcanics and Pyroclastic Layers

Different pyroclastic rock layers associated with rhyolitic and trachytic lava domes and flows together with some central volcanoes were formed in this period. The products of this episode consist of unwelded pumice fall and flow deposits, rhyolitic–trachytic lava flows forming central volcanic edifices, fissural basaltic lava flows with associated scoria and phreatomagmatic cones, and interbedded lacustrine deposits. This highly differentiated fissural effusive and central eruption products indicate that volcanism during this period was very intensive and vigorous (Tsegaye Abebe et al, 2010).

2.3.4 Plio-Pleistocene Rift Volcanics

Volcanic rocks of Pliocene and Pleistocene age such as trachytes, pantelleritic rhyolite, basalts and ignimbrites are abundant within the Main Ethiopian rift floor and on the adjoining plateaus (Kazmin, 1972). Pliocene to early Pleistocene (4.6-1.6Ma) shield volcanoes (Chilalo, 4005m; Badda, 4170m; Kekha 4245m) covers the eastern margin. These comprise of trachytes with subordinate basalt (Di Paola., 1972; Merla et al., 1979; Gidey WoldeGabriel et al., 1990; Bigazzi et al., 1993). Most of the MER floor is covered by silicic pyroclastic materials, they are Early to Middle Pliocene (4.2-3Ma, Gidey WoldeGabriel et al., 1990), predominantly peralkaline rhyolitic ignimbrites interlayered with basalts and tuffs.

2.3.5 Quaternary Central Volcanics

Quaternary volcanism was associated with the oblique faults of the Wonji fault belt cutting the rift floor. These episodes are characterized by basaltic lava flows, associated scoria cones and Phreato-magmatic deposits. Silicic rocks form large central volcanoes like Gedemsa, some characterized by well-developed calderas, which give rise to lava flows, ignimbrites, domes and Phreato-magmatic deposits, with compositions varying from trachyte to peralkaline rhyolites; basalts form small lava flows, scoria cones and Phreato-magmatic deposits. Radiometric ages of this activity are generally <1.8 Ma (e.g. Gidey WoldeGabriel et al., 1990).

2.3.6 Quaternary Lacustrine Sediments and Pyroclastic Deposits

During the Quaternary (<1.6–1.8 Ma), bimodal volcanic rocks were closely associated with Wonji Fault Belt affecting the rift floor (e.g., Gidey WoldeGabriel et al., 1990). Pleistocene-Holocene lacustrine sediments covered a significant tract of the ground and were deposited in a huge lake (Kazmin et al., 1980). Interlayering of primary fall pyroclastic deposits and lacustrine deposits are common in the rift floor. The subaqueous pyroclastic deposits can be identified by reverse graded bedding of pumice layers. Rounded rock fragments indicate abrasion during transportation by waves of lakes and rivers. Presence of evaporites and poor consolidation distinguish subaqueous pyroclastic materials from reworked sedimentary deposits

CHAPTER THREE

MATERIALS, METHODOLOGY AND PRINCIPLES OF THE STUDY

3.1 Instruments used in Field and Laboratory Works

3.1.1 Field Instruments

Sampling of oriented core samples for paleomagnetic investigation encompasses both removals of samples from their natural environments and marking them with their known original orientation using the field instrument (Butler 1992). The sampling instruments used to perform paleomagnetic core sampling includes; portable gasoline-powered driller with diamond drilling bit, water pump, orientation fixture, magnetic compass, tank for fuel and nonmagnetic slotted tube with an adjustable platform around the sample (sun compass). Besides, geologic hammer, topographic map, GPS, digital camera, marker pen, note book, hand lenses and so on were used.

Fig 3.1) Instruments used during field work A) Orientation stage with sun and magnetic compass, B) Portable gasoline-powered driller with diamond drilling bit, C) Water pump, D) geologic hammer, E) Paleomagnetic bag, F) Note book, G) fuel container, H) Water container.

3.1.2 Laboratory Instruments

Laboratory instruments used for paleomagnetic measurements include; JR-6A spinner magnetometer attached to Dell machine, ASC Impulse Magnetizer, MMTD Thermal Demagnetizer, LDA-3A Alternating field Demagnetizer and Dual blade core slicing saw. All of these instruments are found in the school of Earth sciences, Addis Ababa University Paleomagnetic laboratory.

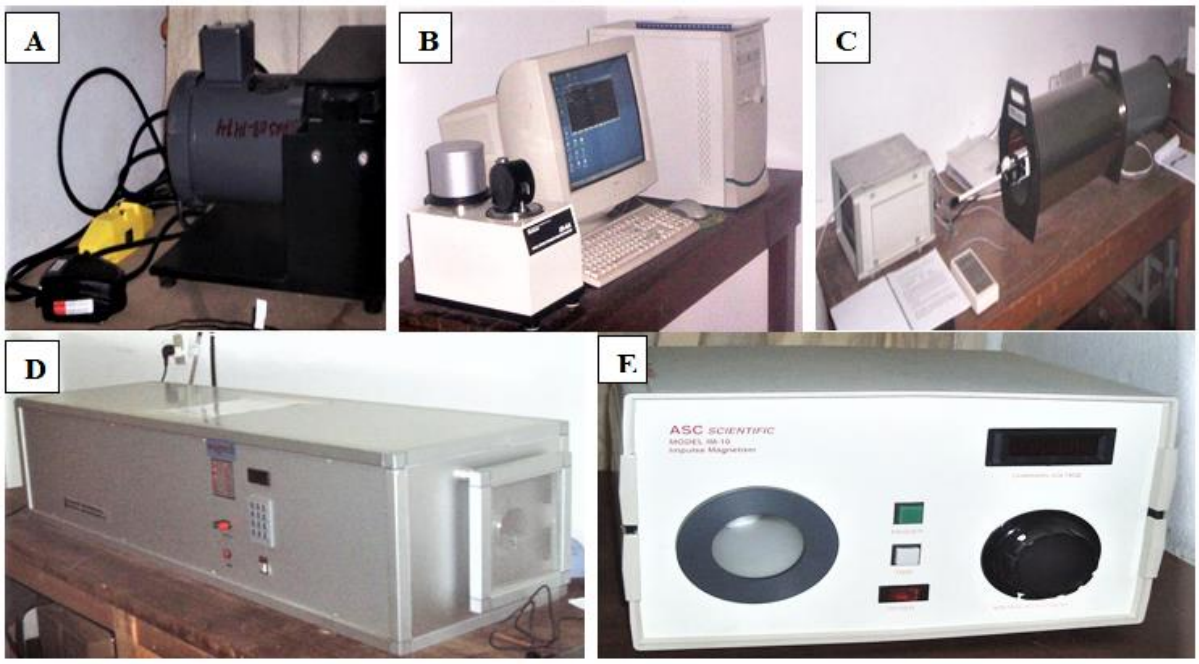

Fig 3.2) Instruments used in Laboratory work (A) dual blade core slicer saw. It slices each sample from all sites into specimens. (B) JR6-A spinner magnetometer lined with a desktop computer to measure the intensity of magnetization (C) LDA-3, alternating field demagnetizer, (D) MMTD 80 furnace thermal demagnetizer. (E) ASC-IM impulse magnetizer for the acquisition of isothermal remnant magnetization.

3.2 Principles of Paleomagnetism for Tectonic Rotation

Paleomagnetic study is primarily based on the measurement of the NRM of geologic material, which is the relict magnetism naturally present in a rock (Butler 1992). The primary magnetization is the component of the Natural Remanent Magnetization (NRM) that was attained when the rock was formed and may represent all or part of the NRM. The original magnetic intensity may decay with time either partially or completely and additional soft overprints, referred to as secondary magnetization, may be added by various processes.

The main duty in the paleomagnetic analysis is to recognize and isolate the magnetic components in the NRM, through a range of demagnetization and analysis procedures (Butler 1992). Progressive demagnetization of specimens and subsequent measurement of the remaining magnetization after each demagnetization step are the main laboratory analysis to identify and isolate the different paleomagnetic components recorded during the rock-geological history. Two separate techniques, thermal (TH) and alternating field (AF); have been utilized to conduct progressive demagnetization of specimens. During these demagnetization experiments, specimens were subjected to stepwise increasing values of temperature or alternating field in the absence of magnetic field. The residual magnetisation is measured after each demagnetization step and the resulting changes in direction and intensity are displayed and analysed to reconstruct the complete component structure of the NRM. The three components (Mx, My and Mz) of magnetic moment of the specimen then measured through multiple measurements steps of each component, permitting assessment of homogeneity of NRM in the specimen (Butler, 1992). The values then fed into a computer containing orientation data for the sample and calculation of the best-fit direction of NRM in the sample geographic coordinates is carried out.

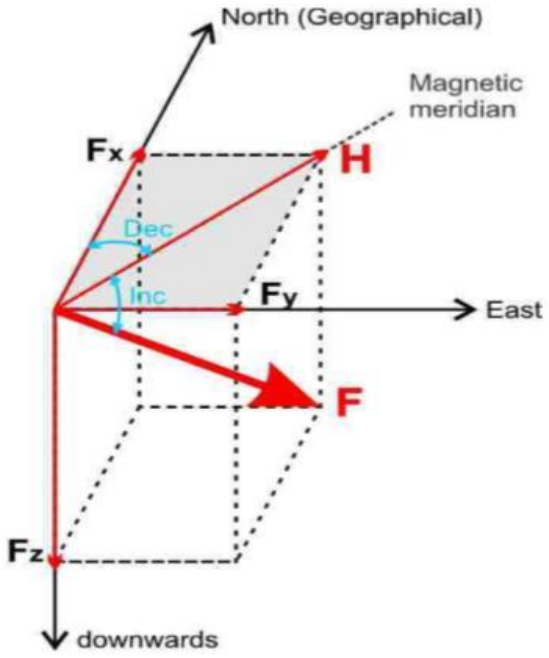

Fig 3.3) Description of the direction of the magnetic field (F), Inclination (Inc) is the vertical angle (dip) between the horizontal and F; declination (Dec), is the azimuthal angle between the horizontal component of F (H) and the geographic north.

Vector directions are described in terms of declination (D) and inclination (I) (fig 3.3). After the complete demagnetization of the samples, these directions are displayed with a projection that depicts three-dimensional information on a two-dimension environment. The most common presentation of results of progressive demagnetization is in orthogonal projection diagrams, also known as Zijderveld diagrams (Zijderveld, 1967). The quality of this diagram is the ability to display intensity and directional information on a single graph by projecting the vector onto two orthogonal planes. Magnetic components are then displayed from the Zijderveld diagrams using least-square analysis (Kirschvink 1980). The most consistent and stable component that can be isolated is referred to as the characteristic remanent magnetisation (ChRM).

The ChRM is then further examined to confirm if it represents a record of the original geomagnetic field attained during the time of rock formation, or an overprint magnetisation acquired later in geologic history.

At any point of the earth surface, the magnetic field (F) can be defined by two angles (Fig 3.3). Declination (Dec) is the angle between geographic north and the horizontal component of F, with values ranging from 0 to 360º; inclination (Inc) is the vertical angle or the angle between F and the horizontal, with values ranging from -90^0 to 90º.

3.3 Methodology

The methodologies to address the stated problems and objectives of the study were mainly paleomagnetic investigation associated with field observation and structural analysis. This section discuss about the activities and methods performed from the field work to the final laboratory work. The study conducted on three separate phases of activities. Pre-field, field and post-field work (Laboratory analysis) were the approaches/activities this thesis was accomplished.

3.3.1 Pre-Field Work

The pre-field work primarily includes literature reviews, collection of existing data, analysis of DEM, satellite imageries and aerial photos of the study area. Delineating the study area from the topographic map of Koka sub-sheet, lithologic and structural contacts were

extracted from Google earth and previous map (Alula Damte et al 1992). Preliminary paleomagnetic sites were also selected through Google earth and satellite images.

3.3. 2 Field Work

3.3.2.1 Paleomagnetic Sampling

There are three techniques of paleomagnetic sample collection (Butler 1992). Those are block sampling, oriented core sampling, and Lake-bottom or sea-bottom core sampling. For the present research work oriented core sampling technique with a portable drill is utilized to take oriented core samples from the outcrops.

Paleomagnetic Sampling in the Study Area

For this study twenty-three sites were sampled during the field work. Sampling sites were systematically selected to be on fault scarps, quarry sites, road cut and river cuts to collect fresh and unweathered samples. Oriented core samples were then drilled from the selected sites by using a gasoline-powered portable drilling apparatus with a water-cooled diamond bit (Fig 3.5A). The diameter of the cores is ~2.5 cm. After coring of the core samples to a 6 to 12 cm, an orientation stage is slipped over the sample before removing the core samples from the outcrop (Fig B, C). Orientation stage has two components magnetic or sun compass (or both) for determining the azimuth of the core axis and the inclinometer for determining inclination (dip) of the core axis. After taking the orientation, the core is extracted from the outcrop, marked for orientation identification (Fig 3.5E), and returned to the laboratory.

A minimum of six and a maximum of fourteen oriented core samples per site were cored/drilled with an average of ~ nine cores per each site. Totally 220 cores were collected and 170 of them were used for this thesis work. Sampling was conducted on different lithologies (basalt, ignimbrite and volcanic tuff and rhyolite) well exposed in the study area.

Most of the paleomagnetic samples are collected from sites on basalt (mafic lava flow) and welded ignimbrite (felsic pyroclastic flows), while a few sites are from volcanic tuff and rhyolite rocks. The rhyolites and vesiculated basalts were relatively challenging to drill and shorter and fewer number of samples were collected.

3.3.2.2 Drilling and Sample Orientation

The samples were oriented before they are extracted from the outcrop by using the orientation stage. Care has been taken in moving of magnetic materials faraway enough so that there was no effect on the accuracy of Brunton compass. The sun angle and local time were recorded because of possible magnetic disturbances that might affect the magnetic compass reading. For each core samples alpha mag, beta and alpha-sol with their time of measurement are documented during field work. The most important consideration is that the sample which is returned to the laboratory will be fully oriented with respect to a geographic coordinate system as well as necessary pieces of information have been recorded accordingly.

The appropriate procedures (Butler, 1992) taken for this study to drill and sample orientations during field works are as follows:

- The appropriate exposures of rocks have been selected;
- Cores were drilled by using a portable gasoline-powered drill with a diamond drilling bit;
- After drilling, the orientation stage has been inserted over the sample before extracting the core;
- Rotate the slot to the top of the sample and note the azimuth and hade of the drill direction (into the outcrop) with sun and or Burton compass;
- Before the orientation stage has removed, a mark was scratched on the sample using copper wire not to miss the exact orientation;
- The sun angle and local time were recorded to determine magnetic disturbances that might cause the magnetic compass record;
- Carefully extract sample; mark a fixed arrow on the side of the sample in the direction of the drilling and label the sample with an informative sample name;
- Make a note of the orientation data in the field note book, and about the information needed to the laboratory work
- After the sample was extracted, label the samples with the appropriate sample name

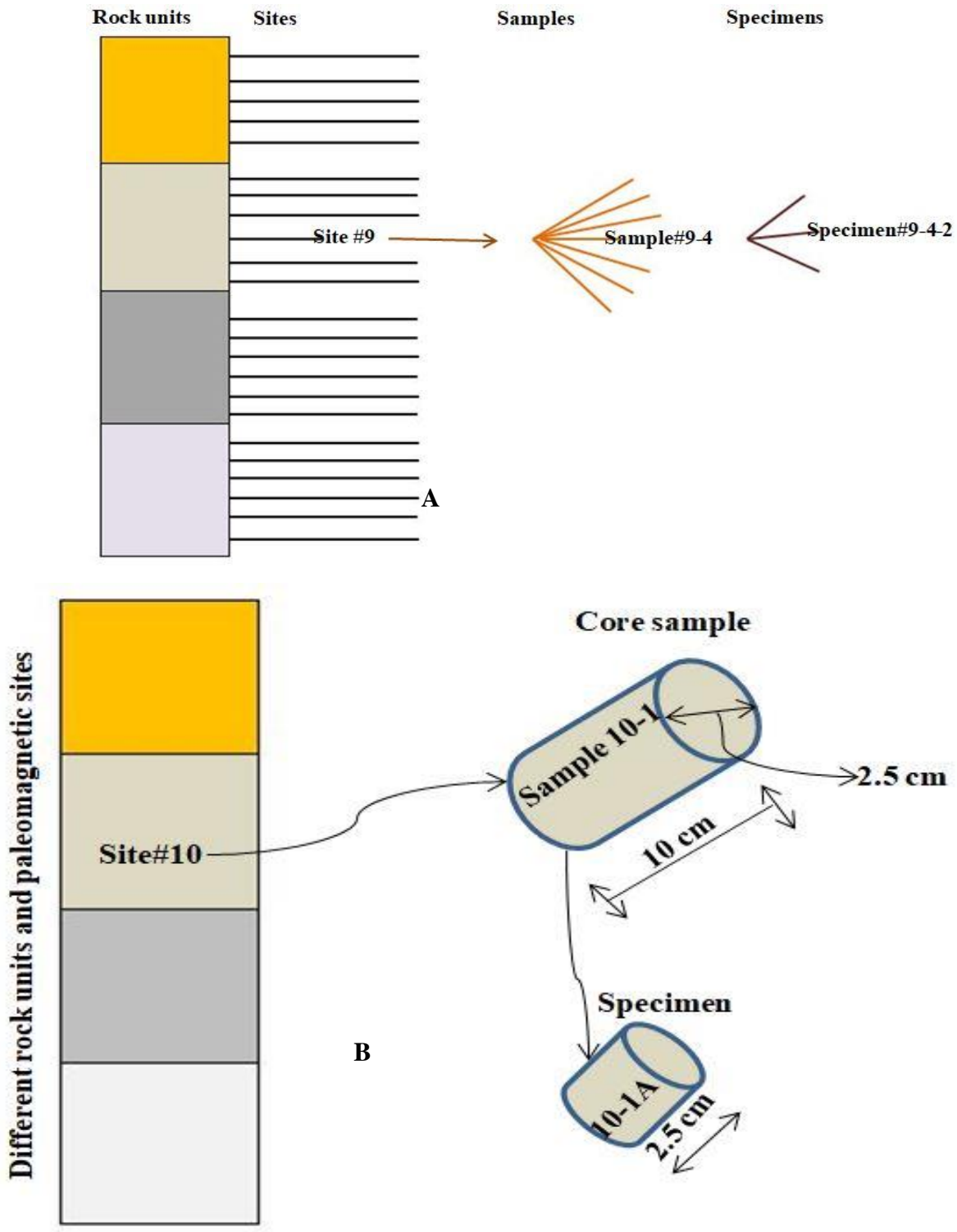

Fig 3.4) Generalized paleomagnetic sampling scheme, (A) several sites were collected from the rock unit; multiple samples were collected from each site; (Modified from Butler, 1992). (B) Several samples were collected from each site, several specimens for laboratory measurement from each sample.

Fig 3.5) Field photographs showing the procedures followed in drilling and sample orientation under the study area in Gedemsa magmatic segment: A) Drilling the sample using gasoline-powered drill with diamond drilling bit, B) Insert the orientation stage and measuring the orientation of the samples, C&D) Measuring orientation of core sample: Note the azimuth and dip of the drill direction with sun and magnetic compass and inclinometer, E) Make a permanent arrow on the upper side of the sample in the direction of drilling and label the sample with the sample name; F) Paleomagnetic holes after the core sample s are extracted.

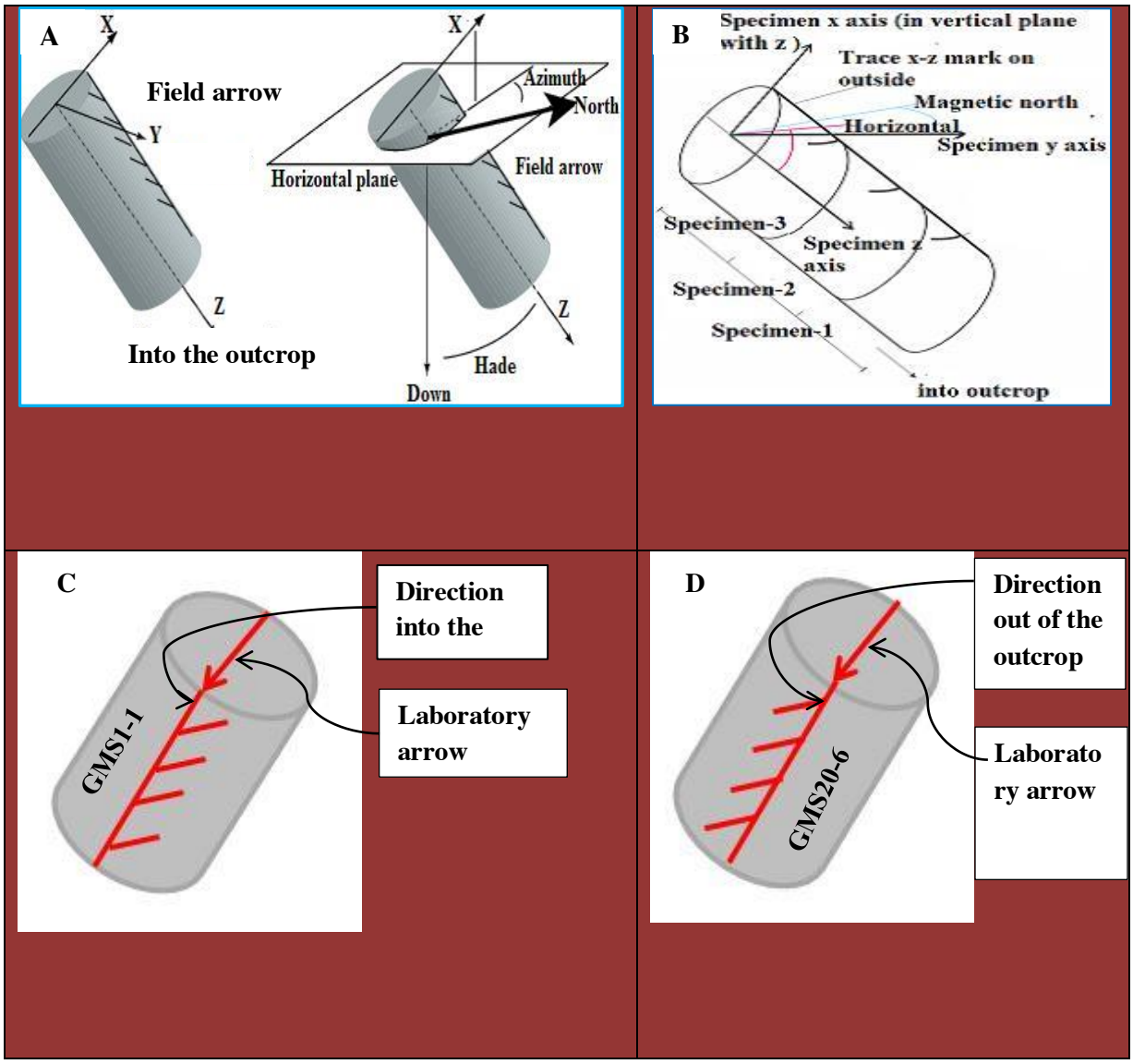

Fig 3.6) Orientation systems of samples drilled by portable core drill; (A) diagram on the left is a schematic representation of the core sample in situ. The z-axis points into the outcrop; the x-axis is in the vertical plane; the y-axis is horizontal. The diagram on the right shows orientation angles for core samples. The angles measured are the hade of the z-axis (angle of z from vertical) and the geographic azimuth of the horizontal projection of the +x axis measured clockwise from geographic north (After Collinson, 1983 as cited in Butler, 1992). (B) Shows different specimens that can be extracted from a single core sample. (C and D) show the two types of possible specimen shape and orientation convention, (C) Into and (D) Out to outcrop during laboratory measurement, GMS1-1=Gedemsa Magmatic Segment site one core sample one, GMS20-6= Gedemsa Magmatic Segment site twenty core sample six.

Table 3.1 General information about the paleomagnetic sites in the study area

Paleomagnetic site name	Location		Number of Cores per site	Lithologic unit
	Latitude	Longitude		
GMS1	522920	936682	9	Ignimbrite
GMS2	522932	936717	11	Ignimbrite
GMS3	518693	913105	10	Basalt
GMS4	517978	914366	9	Basalt
GMS5	517978	914366	9	Basalt
GMS6	520581	912560	10	Basalt
GMS7	519179	913329	6	Ignimbrite
GMS8	522081	913763	6	Basalt
GMS9	522684	912915	6	Basalt
GMS10	523556	914437	7	Basalt
GMS11	524118	916290	7	Ignimbrite
GMS12	524371	916560	6	Ignimbrite
GMS13	524718	916579	7	Basalt
GMS14	525522	916501	7	Basalt
GMS15	527808	916837	7	Volcanic tuff
GMS16	533254	919355	6	Ignimbrite
GMS17	517452	921844	7	Ignimbrite
GMS18	524822	935333	7	Basalt
GMS19	520530	922336	7	Volcanic tuff
GMS20	522744	924711	6	Rhyolite
GMS21	521969	927210	7	Ignimbrite
GMS22	522490	927946	7	Ignimbrite
GMS23	522148	932645	6	Volcanic tuff

Table 3.2 age determination of rock units available from the study area

Rock unit	Locality	Age	Reference
Fluvio-lacustrine	outside the caldera	0.1 My	Laury and Albritton(1975)

deposits	all around		
post-caldera deposits	In and outside the caldera	between 0.2 and 0.1 My	Bigazzi et al (1981).
Pantelleritic Pre-caldera lava flow	NE rim of Gedemsa caldera	0.212±0.032 My	Bigazzi et al (1981).
Pantelleritic Pre-caldera lava flow	SE rim of Gedemsa caldera	0.267±0.040 My	Bigazzi et al (1981).
Recent Basalt lava flow	-	0.13My	WoldeGabriel et al., 1990

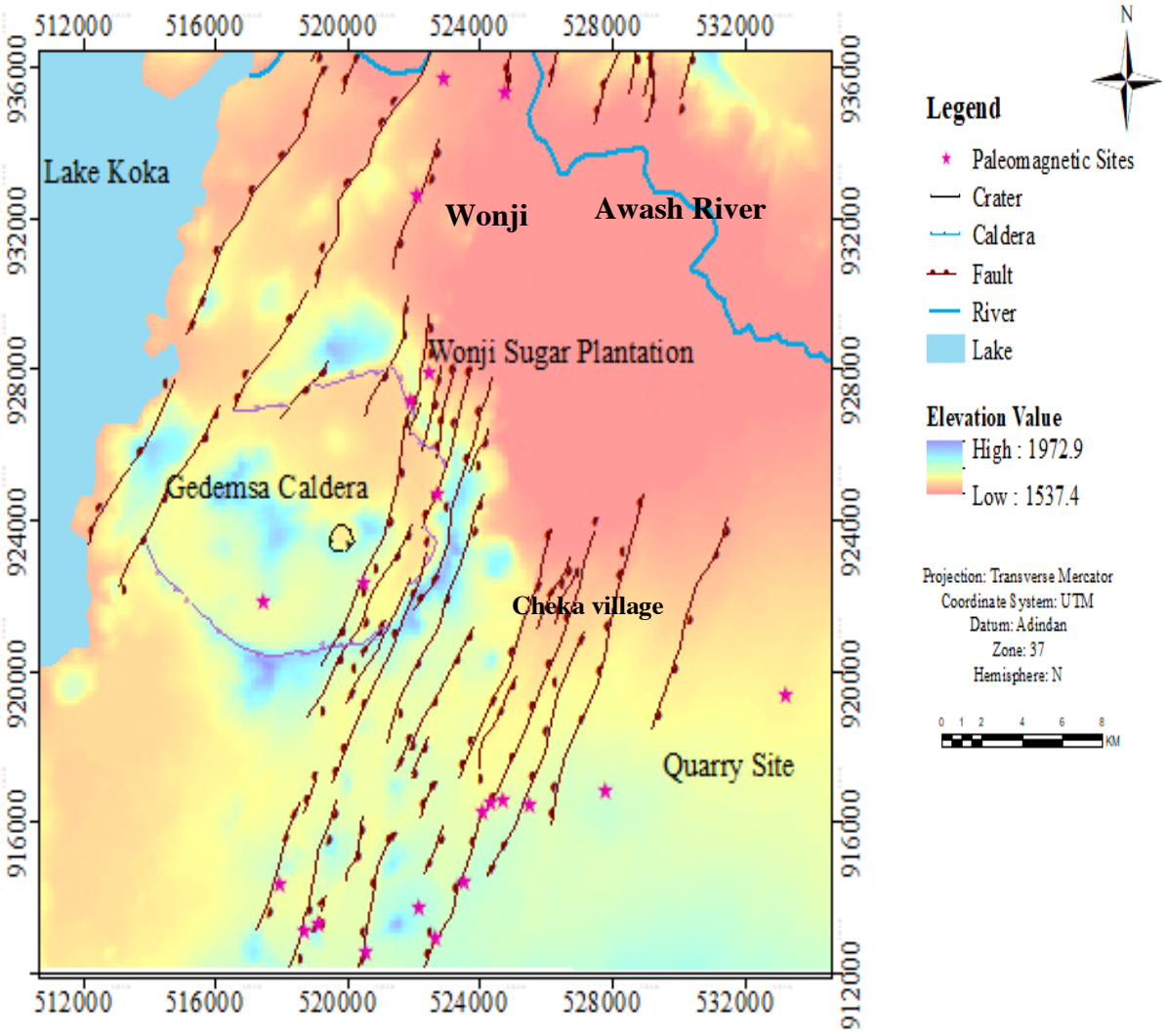

Fig 3.7) The distribution of paleomagnetic site locations on the DEM of the study area

3.3.3 Laboratory Work

All the laboratory works were conducted in Addis Ababa University School of Earth Science, Paleomagnetic laboratory. After the oriented paleomagnetic core samples were collected, different paleomagnetic laboratory works have been performed accordingly. The laboratory work started from the selection and preparation of enough specimens from the collected paleomagnetic core sample during field work. The core samples then cut into standard cylindrical specimens by using Diamond Blade Cutting Machine. Specimens have been prepared for other partial demagnetization and magnetization laboratory techniques.

In the laboratory, the collected ~10 cm long core samples cut in to specimens of 2.2 cm length. One specimen subjected to step wise Alternating field demagnetization (NRM, 5mT, 10mT, 15mT, 20mT, 25mT, 30mT, 40mT, 60mT, 80mT, 100mT), the second one subjected to Thermal demagnetization with step wise heating (150^0c, 200^0c, 250^0c, 300^0c, 330^0c, 360^0c, 390^0c, 420^0c, 450^0c, 490^0c, 520^0c, 540^0c, 560^0c, 580^0c, 600^0c, 640^0c, 680^0c). The third specimen is used for a rock-magnetic analysis and as such subjected to step wise magnetic intensity acquisition using the impulse magnetizer and stepwise thermal demagnetizations to get information on the Curie temperature there by determining the magnetic mineralogy.

3.3.3.1 Specimen Preparation

One hundred seventy core samples were sliced into the standard size of 242 specimens with approximately 2.5cm length (Fig. 3.4) of each specimen. Some core samples gave three specimens, most of the samples gave twin specimens and few of the samples gave only one specimen. Specimens were then marked and labelled for the next steps. Those dimensions are optimal for measurement using the JR6 spinner magnetometer to fit the automatic sample holder (Butler, 1992). After specimen preparation, classifications of specimens were performed. From a total of 242 specimens: 147 specimens for AFD, 72 specimens for THD and 23 for IRM acquisition.

3.3.3.2 Measurement of NRM and Progressive Demagnetization

After the preparation of appropriate specimens, NRM measurements have been done before any laboratory treatment (demagnetization and magnetization) for all specimens. Identification and removal of secondary overprint components of NRM is the principal aim of different paleomagnetic laboratory work (Butler 1992). To come up with the objectives of

this thesis different paleomagnetic laboratory works like partial demagnetizations (Alternating-Field Demagnetization, Thermal Demagnetization), and impulse magnetization techniques were accompanied, and a spinner magnetometer is used to measure magnetic remanence after each experiment.

As mentioned earlier, the natural remanent magnetization (NRM) of a rock characterizes the sum of all magnetic components throughout a rock's history. However, the main intention of palaeomagnetic investigation is to come up with the earliest component, defined as the characteristic remanent magnetization (ChRM) direction, for tectonic interpretation. That direction denotes the geomagnetic field at the time of acquisition of the magnetization. Consequently, low stability secondary magnetizations (commonly carried by the lowest coercivity or blocking temperature grains) required to be removed.

To isolate the ChRM, there are two different techniques. The first is alternating field (AF) demagnetization and the second one is thermal demagnetization technique. In this thesis Alternating field and Thermal demagnetizations were employed to eliminate the secondary magnetizations. The IRM acquisition experiment also conducted for the identification of magnetic carrier minerals.

3.3.3.3 Alternative Field Demagnetization

In AF demagnetization experiment, a specimen was stumbled in an alternating field in the absence of direct magnetic field environment made by magnetic shielding. Grains having smaller coercivity values than the applied field track the alternating field direction as the specimen are tumbled, and as the field is gradually reduced to zero the magnetization of these grains becomes randomized and cancel each other out. This successfully eliminates secondary magnetization components carried by grains with coercivity less than the peak applied field.

LDA-3 AF demagnetizer (Fig. 3.2C) with maximum peak field of 100 mT was used for this study. Each specimen was put separately inside the specimen holder. Alternating fields were applied in 5 mT steps from 5 mT to 30mT and in 20 mT steps from 40mT to 100mT. These demagnetization steps were used based on the previous work of Tesfaye Kidane et al. (1999; 2003). After each step, remanent magnetizations were measured using an AGICO JR6 spinner magnetometer.

3.3.3.4 Thermal Demagnetization

Thermal demagnetization was carried out by MMTD-80 thermal demagnetizer (Fig 3.2D). The procedure of thermal demagnetization encompasses heating of a specimen to an increasing temperature (T_{demag}) below the Curie temperature of the magnetic minerals, then cooling to room temperature in the absence of magnetic field. Heating and cooling of the specimens made stepwise. As the specimen is heated, the relaxation time of all contained magnetic particles is reduced exponentially. It means that the grain with low relaxation time will, when heated, easily erase the remanence.

The magnetization of all grains having blocking temperature (TB) ≤ Tdemag was randomized. MMTD-80 thermal demagnetizer has a dual chamber for simultaneous heating and cooling of the samples from room temperature up to 680^{o}C in the variable steps. Initially, representative specimens were selected and demagnetized in 18 steps (NRM, 150°C, 200°C, 250°C, 300°C, 330°C, 360°C, 390°C, 420°C, 450°C, 490°C, 520°C, 540°C, 560°C, 580°C, 600°C, 640°C and 680°C) for thermal demagnetization experiment. Demagnetization steps were used based on the previous work of Tesfaye Kidane et al. (1999; 2003). After each step, the remanent magnetizations were measured using the AGICO-JR6 spinner Magnetometer.

Table 3.3 Summary of demagnetization and magnetization procedures used in the laboratory work

Methods	No of steps	No of specimens	# steps in mT/^{0}c
AFD	11	147	NRM, 5, 10, 15, 20, 25, 30, 40, 60, 80, 100
THD	18	72	NMR, 150, 200 , 250 , 300 , 330 , 360 , 390, 420, 450, 490, 520, 540 , 560 , 580 , 600 , 640 , 680
IRM	16	23	NRM, 10, 20, 30, 40, 60, 80 , 100, 150, 300, 400, 500, 750, 900, 1000

3.3.3.5 Rock Magnetic Experiment

The rock magnetic experiment has been performed primarily to identify the magnetic/ferromagnetic minerals carrying the magnetic remanence of rock sampled and assess the ability of these rocks to record an ancient magnetic field. In this study an induced isothermal remanent magnetization (IRM) acquisition study was conducted using an ASC-IM

impulse magnetizer. A total of 23 specimens were utilized for this IRM acquisition experiment one specimen per site (except for site 16, in which the specimen was broken during the experiment).

3.3.4 Data Analysis and Interpretation

Characteristic remanent magnetization ChRM directions of the specimens were determined using a combination of Zijderveld diagram analysis (Zijderveld, 1967), principal component analysis (Kirschvink, 1980) and Stereoplot /remagnetization circle analysis (Halls, 1976). *PaleoMac6.5*, *remasoft3.0 and Rema6* softwares were utilized for paleomagnetic data processing and analysis. Zijderveld diagrams and stereographic projection were used to display the results of progressive demagnetization. Principal component analysis was conducted to define the ChRM direction by determining the best-fit line of Kirschvink (1980). The ChRM directions for each specimen, determined using partial step demagnetization, were averaged to obtain the site mean direction, and then averaged in turn to get the overall mean ChRM direction for the target geologic unit using Fisher (1953) and Paleomagnetic software (Cogne, 2003).

3.3.5 Data Reliability Criteria

Remanence components for this study are principally evaluated on the basis of the following standards:

- Sampling should be adequate to average secular variation, thus sample number should not be less than six per site (Tarling, 1983).
- Sites were rejected from the group mean calculations if components calculated by Principal Component Analysis (PCA) gives, $\alpha 95 > 25^{o}$ (Irving, 1964), $k < 10^{o}$ (Tarling, 1983), MAD $>10^{o}$ (Turner et al., 2012).
- Components calculated for different specimens of the same core should display directional agreement ($<10^{0}$) (Turner et al., 2012).
- There should be adequate evidence that primary ferromagnetic minerals carry the ChRM. Rock magnetic experiments were conducted to investigate the magnetic mineralogy of sampled rocks.

CHAPTER FOUR

GEOLOGY AND STRUCTURES OF THE STUDY AREA

4.1 Introduction

Gedemsa Magmatic Segment is one of the tectono-magmatic segments situated on the central Main Ethiopian Rift. It is close to the large eastern rift marginal faults that cut through the volcanics of the Nazret group and in the rift floor which is affected by Wonji Fault System (Mohr 1971, Peccerillo et al, 2003).

The Gedemsa volcano is situated in an extensional tectonic setting in rift where voluminous volcanism occurs (Di Poala, 1970). The lowest exposed products are represented by acidic lavas, which are covered by thick pumice fall deposits followed by an ignimbrite deposits and intra-caldera lava flows, and interbedded pyroclastic products. The formation of the caldera is a composite structure resulting from the occurrence of several collapses. A separate stage of volcanic activity (basaltic volcanism) formed surge deposits and numerous basaltic cinder cones and lavas, both within and outside the caldera depression.

Gedemsa caldera is dissected by Wonji Fault Belt, both at its internal floor and outer flanks (Peccerillo et al, 2003). The inner floor of Gedemsa is covered by lacustrine, subordinated alluvial deposits, and intercalated tuffs. This fact can be well seen on the eastern side, where normal faults with several meters of the vertical throw are present.

Fluvio-lacustrine deposits are also found outside the caldera all around it. They are considered to be 0.1 My old as this is the age suggested by Laury and Albritton (1975). The final eruptive phase of Gedemsa is characterized by basaltic effusions (Di Poala, 1970).

Two scoria cones are found inside Gedemsa, a bigger one on its NE part and a very small one on its SW part. These basalts are related to the intense tensional tectonics which affected the caldera structure. The NE cone, which is located close to the rim of the caldera, has been successively cut by the same fault from which magma rose. It lies over and is associated with a series of thin cross-laminated wet surges deposits. It has been generated by the explosive activity terminated probably when the vent become insulated from the water by the

accumulation of surge deposits; at that moment a purely magmatic activity (strombolian) began forming the scoria cone.

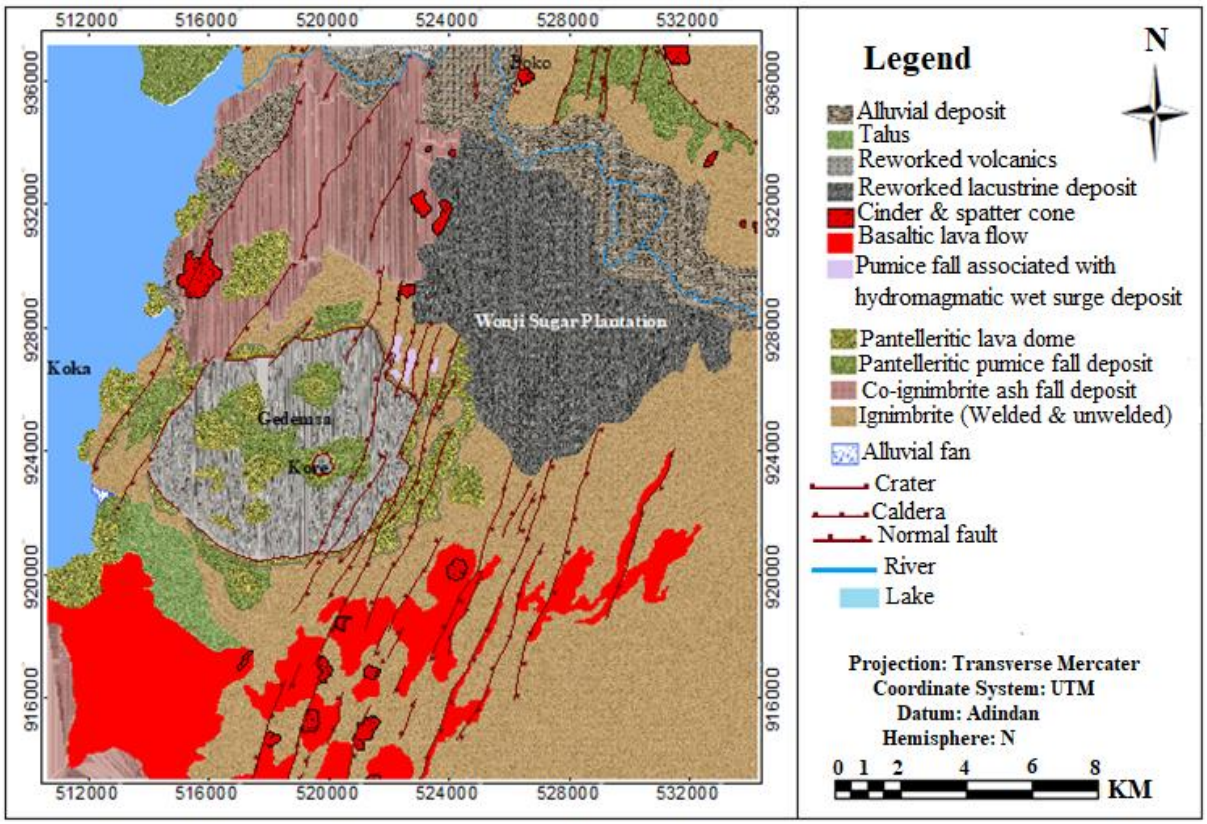

Fig 4.1) Geological map of the study area (Modified from Alula Damte et al, 1992)

4.2 Lithologic Units

4.2.1 Alluvial and Lacustrine Deposit

Along the Northern and Northeastern part of the Gedemsa caldera following the Awash River there are well exposed alluvial sediments constituting relatively large area. This unit covers mainly the Wonji plain currently used for agricultural purpose and Wonji sugar plantation. Its colour varies from dark grey to black. Particularly the recent alluvial deposit cover the area following the Awash River, where as those the lacustrine deposits cover the Wonji sugar plantation.

4.2.2 Basaltic Flows and Associated Scoria Deposits

Basalt is one of the dominant rock types in the study area. They are exposed on a different part of the study area as lava flow forming flat morphology, like small ridges and forming

scoria cones. Mostly they are exposed in Eastern, Southern part of the Gedemsa caldera and near the rim of the Gedemsa caldera. There are vesiculated basalts on the eastern and north-eastern part of the area, and they are highly weathered. The basalts vary from aphyric to porphyritic, especially those near the caldera on the east and southern portion-having phenocrysts of plagioclase-the dominant one and minor phenocrysts of olivine and pyroxene.

In general, these basalts are moderately fractured and weathered, vertically to sub-vertically jointed, porphyritic, aphanitic and often vesicular in texture, dark-grey to black in color when the out crop is fresh and bluish grey when weathered and forms cliffs in some part, scoria cones while in some part flat-lying. These rocks cut by NNE-SSW and N-S trending faults. Notably, different scoria cones inside the caldera are dissected by those Wonji faults.

Fig 4.2) Field photographs of Basalts; A) Porphyritic and vesicular basalts (E= 517978, N= 914366, Elv= 1697±3m), B) Scoria cone dissected by the Wonji faults C) Porphyritic basalt with phenocrysts of plagioclase (dominant) and olivine (minor), fault scarp exposure. (E=518693, N=913105, Elv=1727±3m), D) Aphanitic basalt (E= 520809, N= 913763, Elv= 1732±3m) GMS8,

4.2.3 Rhyolitic Lava Flows and Domes

It is one of the lithologic units in the study area, exposed on the wall of the caldera rim, in the northern tip and in the southeastern of the caldera as well as outside of the caldera. It is revealed by lava dome/hill side, road cut and fault scarp exposure. It has both weathered and fresh colour with grey colour for fresh and brownish grey for weathered rock. It is affected by systematic to non-systematic joints and fractures. It is intensely jointed /fractured like the ignimbrites and basalts rock units but the joints are dominantly NW trending. Very thick rhyolites are found on fault scarps forming rhyolitic lava domes. Rhyolite domes are emplaced in the SE parts of the study area that is on the Southern part of the caldera. Most of these domes are not cut by the NNE-SSW trending fault systems which may indicate that the domes postdate the faulting activities.

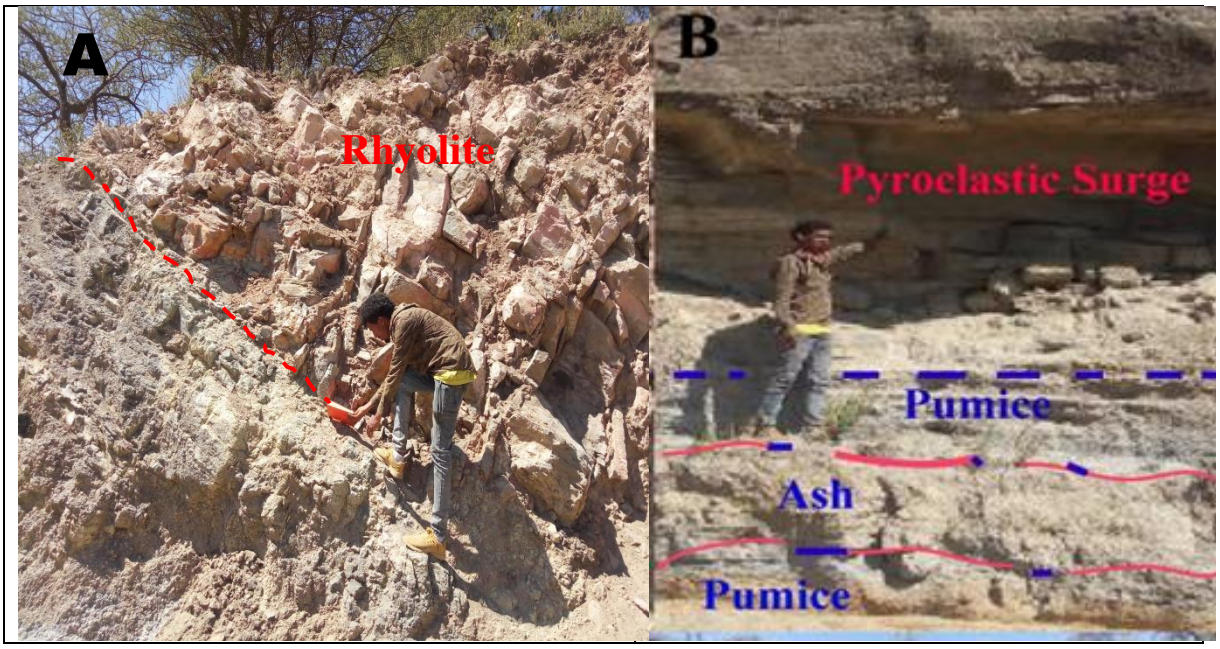

Fig 4.3) Field photograph of; (A) Contact between ignimbrite and rhyolite units exposed along the road, (E=521969, N=927210, Elv=1666±3m); (B) Pumice, volcanic ash and pyroclastic surge deposit exposed along with road cut (E=521969, N=927210, Elv=1666±3m)

4.2.4 Pumice Fall Deposit

The pumice fall deposit is dominantly exposed within Gedemsa caldera, and along the Adama-Wonji road near the bridge on the Awash River. This pumice fall deposit is found associated with ignimbrites and rhyolite forming a horizontal layering as well as it is also

associated with volcanic ash. It is yellowish to grey in colour and light pyroclastic materials. It is also found associated with silicic lava domes and ash flows. It is light grey, less dense and shows vesiculated in texture.

4.2.5 Ignimbrite Units

It is one of the dominant lithologic units in the study area. Ignimbrite deposits are found at a different part of the study area, particularly in the northeast, southeast and east of the Gedemsa caldera. These rocks are exposed along fault scarps, quarry site and road cuts. It is affected by systematic joints (which are orthogonal to each other, one parallel to magmatic layering and the other is vertical joint). The ignimbrites are mostly fine to medium-grained, brownish/light to light-dark grey. Ignimbrite is one of the rock units used to determine paleomagnetic experiments to assess the vertical axis block rotation and magnetic mineralogy of the sampled rocks. Especially the Main Ethiopian Rift ignimbrites are potential lithologic unit for paleomagnetic investigation because they are pantelleritic in composition which helps the ignimbrites to have ferromagnetic minerals.

There are varieties of ignimbrite, for instance there is crystal rich ignimbrite in the North-east of the area at the beginning of Wonji town, in most cases, ignimbrite with a fiamme feature especially those in the North, South and South-east portion of the study area, welded and hard ignimbrite near the Dera town which is quarry site exposure, and some part of the ignimbrite are very weak and friable especially in the flat part of the area and it is associated with reworked volcanic-clastic sediment and reworked lacustrine sediment. Most ignimbrite exposure in the paleomagnetic site were selected as fault scarp exposure, quarry site exposure and road cut exposure.

This lithologic unit represents a large part of the study area and in general it is exposed mostly outside of the caldera. There are also obsidian glasses which align horizontally to the layer of the different ignimbrite layers and they are stretched horizontally and show evident elongation. When observed, the exposure mostly the upper surface (up to some depth) of the ignimbrite is affected by weathering and alteration due to the percolation of water and further profound it becomes fresh. The fresh colour of the rock unit is mostly grey and the weathered colour is just brownish to yellowish.

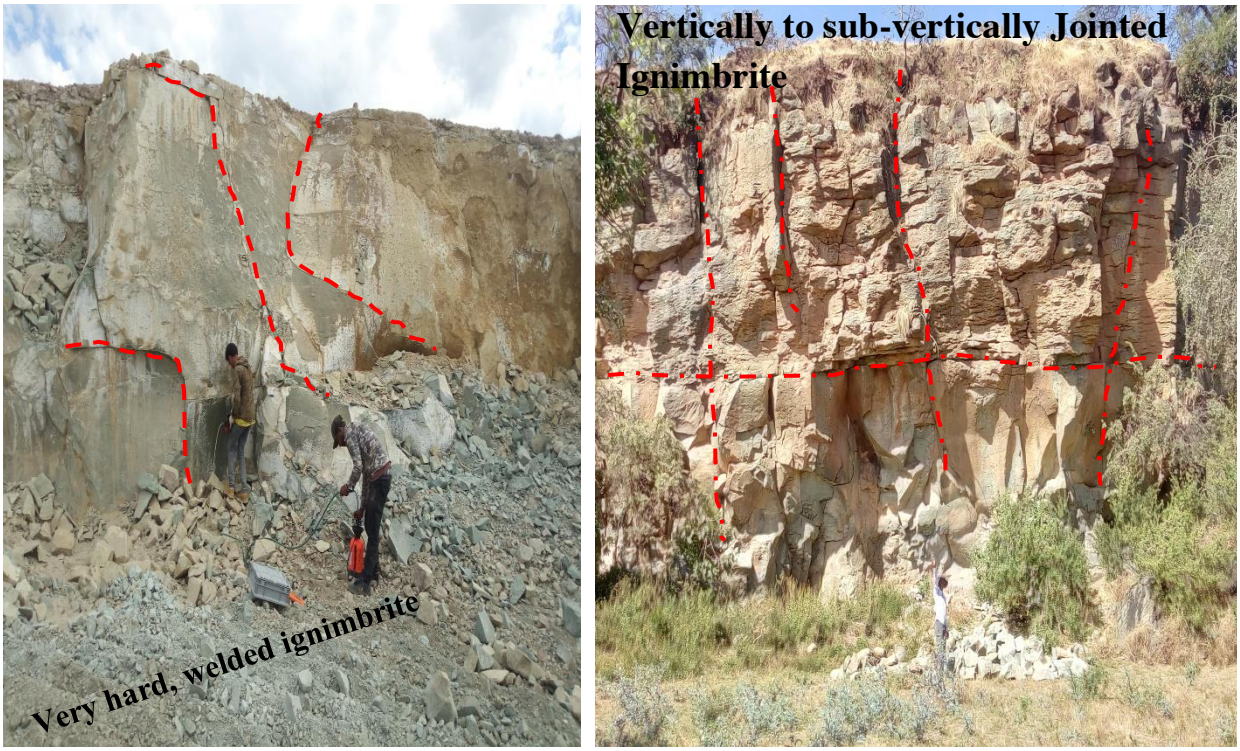

Fig 4.4) Field photograph of; (A) Ignimbrite exposed in the quarry site characterized by curving joint (E=521969, N=927210, Elv=1666±3m); B) Ignimbrite affected by orthogonal joints along with fault scarp exposure (E=519179, N=913229, Elv=1708±3m) GMS 7.

Especially on the north-eastern, eastern, southern, and south-eastern part of Gedemsa volcano along the escarpments a series of ignimbrite rock units are exposed which are intensely dissected by parallel to sub-parallel aligned NNE-SSW and NE-SW trending Wonji faults. The ignimbrite is also exposed on small ridges and flat laying terrains. It is strongly layered and distinguished one from the other either by variation in colour and mostly they form stair-step features. Stratification is mostly horizontal to sub-horizontal forming scarps due to faulting. These rocks show fracturing and jointing. Fractures are oriented horizontal, perpendicular and oblique to the bedding planes. Ignimbrites, especially those in the Main Ethiopian Rift, are one of the best rock units used to determine magnetic experiments to assess the block rotation and magnetic mineralogy of the sampled rocks.

4.2 Geologic Structures of the Study Area

The study area is characterized by intense NE-SW, NNE-SSW and some N-S oriented tensional tectonics which produced a highly developed system of Wonji faults.

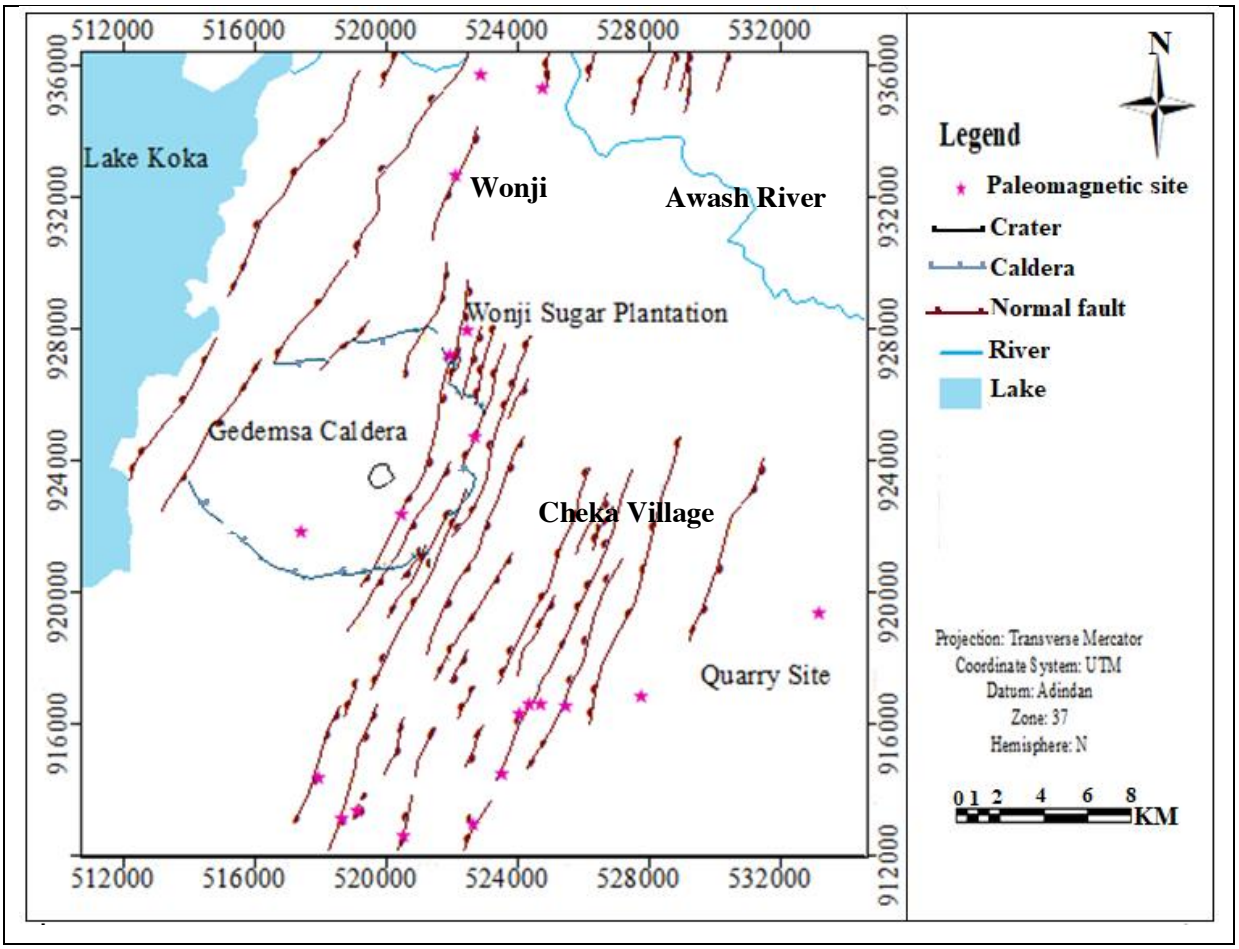

Fig 4.5) Structural map of the study area

The rift floor is affected by several tectonic and volcanotectonic features such as "en echelon" array of faults and partly preserved calderas, elongated domes and aligned spatter cones. From the volcano-tectonic point of view the area is characterized by preserved caldera (Gedemsa) and Kore crater inside the Gedemsa caldera.

The major geological structures in the study area show a series of NNE-SSW and N-S oriented normal faults (fig 4.7) with variable length and differently oriented joints. The tectonic structures are associated with the regional extensional tectonics. In general the volcanic rocks of Gedemsa magmatic segment have been subjected to brittle deformations mainly faulting and jointing which have variable magnitude and orientation as discussed below.

4.2.1 Normal Faults

The most dominant structural features of the study area are normal fault characterized by NNE-SSW and N-S trending faults with vertical displacements and dipping towards the west

as well as to the east direction. Since most of the faults are regional fault they are characterized by very large in length and high vertical throw. In some case these faults are terminated near rhyolitic and lava dome this indicates that the faults are younger than the domes and these domes postdated the development of fault.

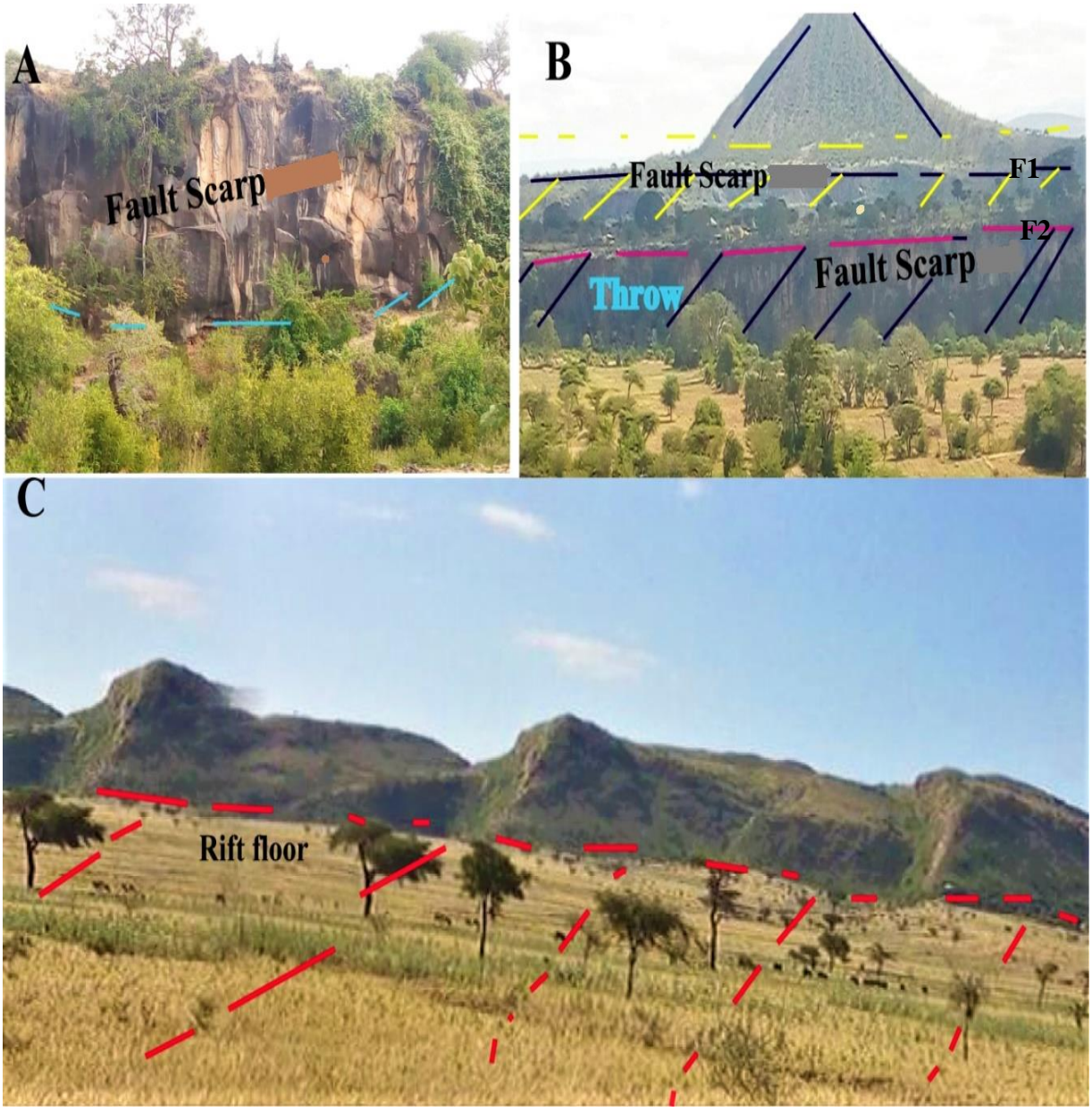

Fig 4.6) Field photographs of, A-normal fault affecting the ignimbrite with significant vertical displacement and with vertical dip, B-faults (F1-Fault1, F2=Fault2) with vertical to sub-vertical dip showing half-graben fault system from a series of normal faults, C-series of faults affecting the eastern rim of the Gedemsa caldera, D-scoria cones inside the rift floor along with the trend of the Ethiopian rift, some of them affected by regional normal faults (the Wonji fault belts).

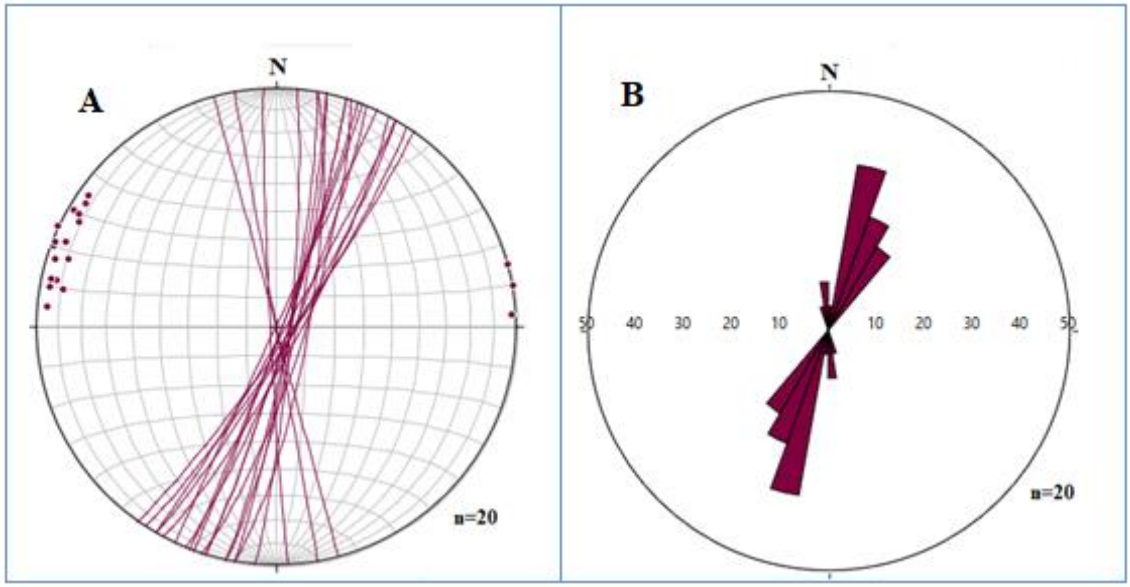

Fig 4.7) (A) Stereo plot using equal-area projection for the fault data measured from the study area on different rock units shows the fault planes and poles to the planes, (B) rose diagram shows NNE, NE and some of NNW trending fault

The Main Ethiopian Rift floor is characterized by a persistent belt of intense fresh faulting which has been named as the Wonji Fault Belt (Mohr, 1960). The faults are short in length, arranged in "en echelon" fashion, normal fault type and oriented dominantly in north-northeast direction (Gibson and Tazief, 1970). The faulting is in general younger along the medial line of the rift valley, becoming progressively older as one approaches the rift margins (Gibson and Tazief, 1970). The more recent faults are associated with the recent basaltic fissure eruptions. These Wonji Faults also cut the Gedemsa caldera and the scoria cones inside and outside the caldera. These faults are normal faults with dominantly NNE and with small N trending characterized by vertical to sub-vertical dip (Fig 4.5). The faults have variable throws ranging from 20m to 35m, the average being about 25m. Bigazzi et al (1981) presumed that the age of these faults is younger than 0.1Ma. In the Easter margin of Gedemsa caldera, in the vicinity of Cheka village is dominantly affected by these faults.

Generally, the faults observed in the study area are part of the Wonji fault belt. The dominant orientation of the fault in the study area is NNE with some of the faults with N and NE orientation (Fig 4.5)

4.2.2 Joint

Joints are fractures which have no or insignificant relative displacement between the blocks found on the two side of the fracture. This structure is predominantly observed in the study area and it affects most of the rock units. They are diverse in morphology; mostly, they are orthogonal (Fig 4.8B) forming two sets of joint. Some are radiating joint (Fig 4.8D) in which originated in common point and growth in to branches, and few of them are curving and dying joints (Fig 4.8A). In general there are two dominant trends of the joints NW-SE and NE-SW which characterize most of the joint populations.

Most of the joints are systematic to non-systematic and shows the variable orientation and dip amount except those joints which affect the rhyolites and volcanic tuff. They are trending NE-SW whereas joints affecting the rhyolite are trending NW-SW. This implies that in some case the nature/composition of the host rock can change the orientation of the joints.

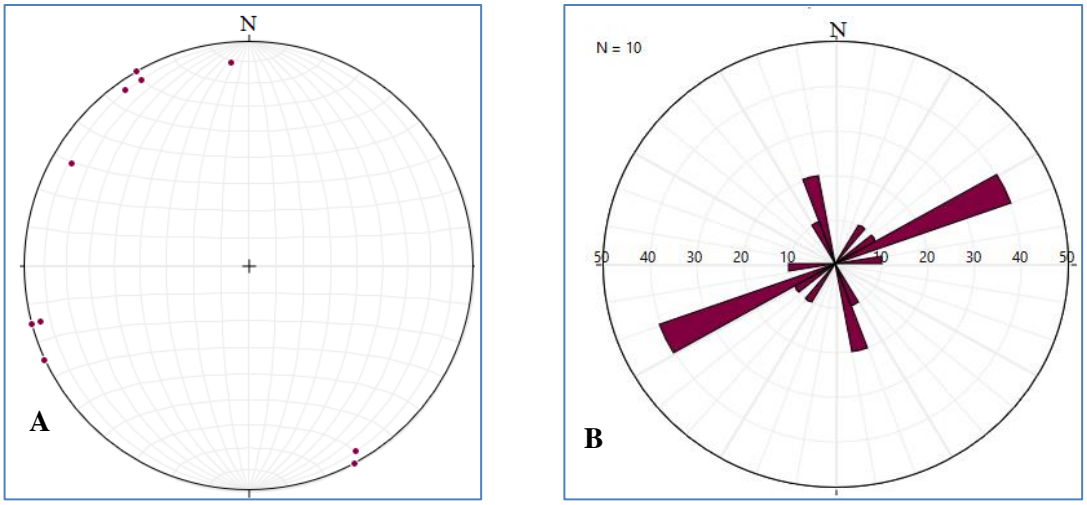

Fig 4.8) Stereo plot using equal-area projection for the joint data measured from the study area on basaltic rock units A) Stereoplot (poles) to the joints and B) rose diagram of the joint showing dominantly of NE and NNW orientation

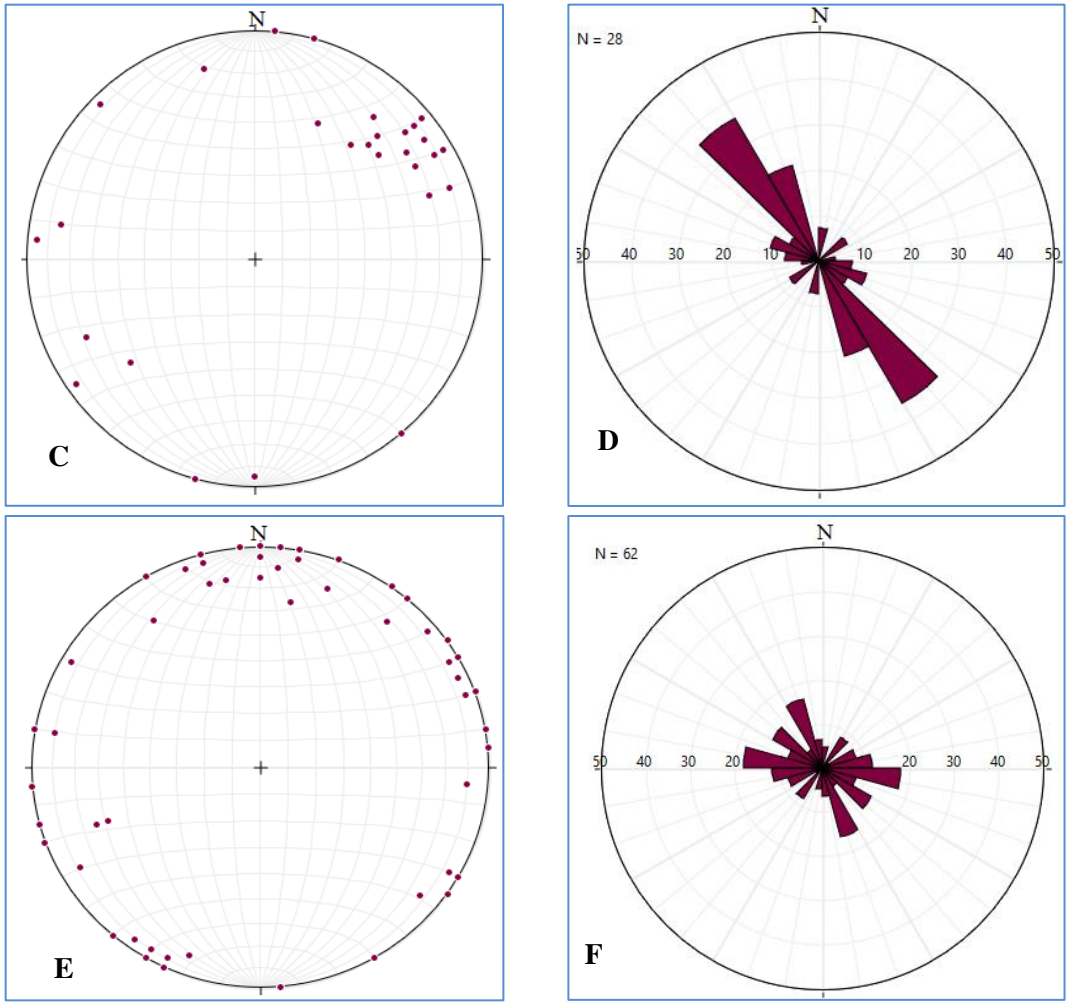

Fig 4.9) Stereo plot using equal-area projection for the joint data measured from the study area on different rock units; C & D Stereoplot (poles) to the joints and rose diagram of the joint on the rhyolites and volcanic tuff showing dominantly of NW orientation; E & F Stereoplot (poles) to the joints and rose diagram of the joint on ignimbrite rock units variable orientation

As can be observed on the rose diagrams, the joint that is observed on the basaltic lava flows has a general orientation of NE-SW strike with some of the joints trending to NNW to NW direction characterized by vertical to sub vertical dip amount, the dip direction fall on the SE direction (and some NE). On the volcanic tuff and on the rhyolites, the general orientation of the strike is NW-SE (some NE-SW) with relatively sub vertical dip amount. The orientation measurements of all joints are presented on Appendix-E. Generally the dominant orientation of joint observed during field work is NE-SW and NW-SE (see the stereonet analysis in Fig.4.9).

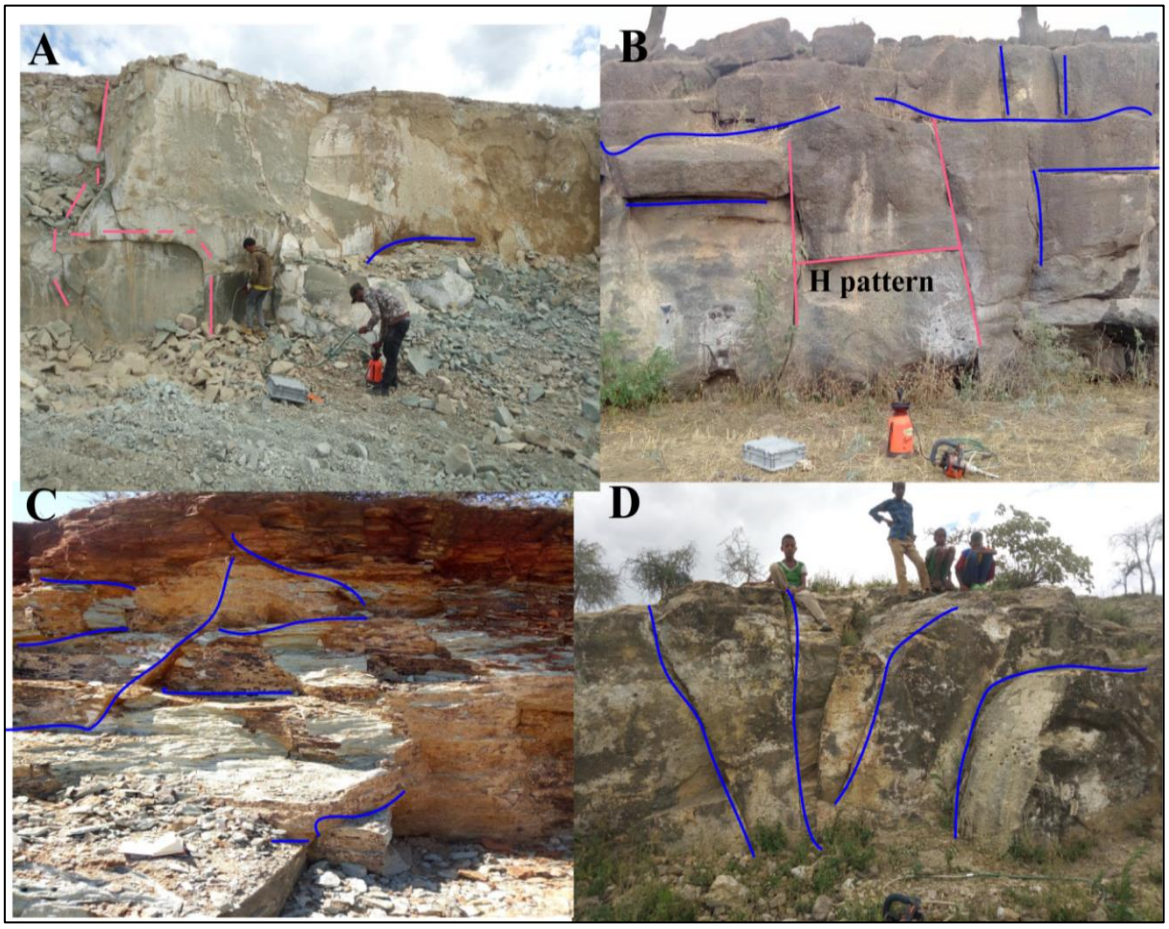

Fig 4.10) Field photographs of Joints; A-curving and dying joint affecting the welded ignimbrite, B-orthogonal joint affecting basalt which shows H-pattern, C-joints affecting the ignimbrite, D-radiating joint affecting the volcanic tuff

CHAPTER FIVE

PALEOMAGNETIC RESULTS

5.1 Introduction

Oriented paleomagnetic core samples from twenty-three sites were collected from Gedemsa magmatic segment. Samples were taken from different lithologic units such as basalts, ignimbrites, rhyolites and volcanic tuffs along the fault scarps, road cut and quarry sites. A total of about 170 core samples were used, and in the laboratory nearly 243 specimens were prepared for paleomagnetic analysis. The samples were collected from horizontal to sub-horizontal rock units. For each core samples, alpha mag, sun angle (alpha sol), and beta measurement were documented during the fieldwork. Most of the core samples were assigned for twin specimens, and some of them yield three specimens, as well as few samples yield only one specimen. One of the specimens was assigned for alternative field demagnetization, the second one for thermal demagnetization and the third specimen was for rock magnetic experiment. Thus, NRM, AFD, THD, and IRM results were determined for each selected specimen. After the laboratory analysis, the results were then further utilized to determine ChRM, rock magnetic minerals, paleomagnetic direction, and tectonic rotation of study area.

5.2 NRM Measurement Results

Measurements of the Natural Remnant Magnetization (NRM) of specimens were done using Spinner Magnetometer (existed in Addis Ababa University paleomagnetic laboratory). The Natural Remanent Magnetization (NRM) measurements were conducted before any laboratory treatment. The results exhibited significant variations among different rock types due to the difference in the nature and composition of the magnetic minerals present in rocks (Butler, 1992). The initial NRM measurements were done for all 243 specimens. Those specimens latter classified 147 for Alternative field demagnetization, 72 for Thermal demagnetization, and the remaining 24 are left for IRM-THD analysis to describe the magnetic mineralogy. The NRM value measured before any laboratory treatment ranges from 0.0009236 A/M to 243.3 A/M. The smallest magnetization intensity value (0.0009236 A/M) was recorded from GMS20-2A of rhyolitic rock unit whereas the highest value observed to

be 243.3 A/M recorded from basalt but this highest intensity value is expected to be due to the effect of a lightning strike. Most of the measured samples within the site show minor variations in the NRM intensity value.

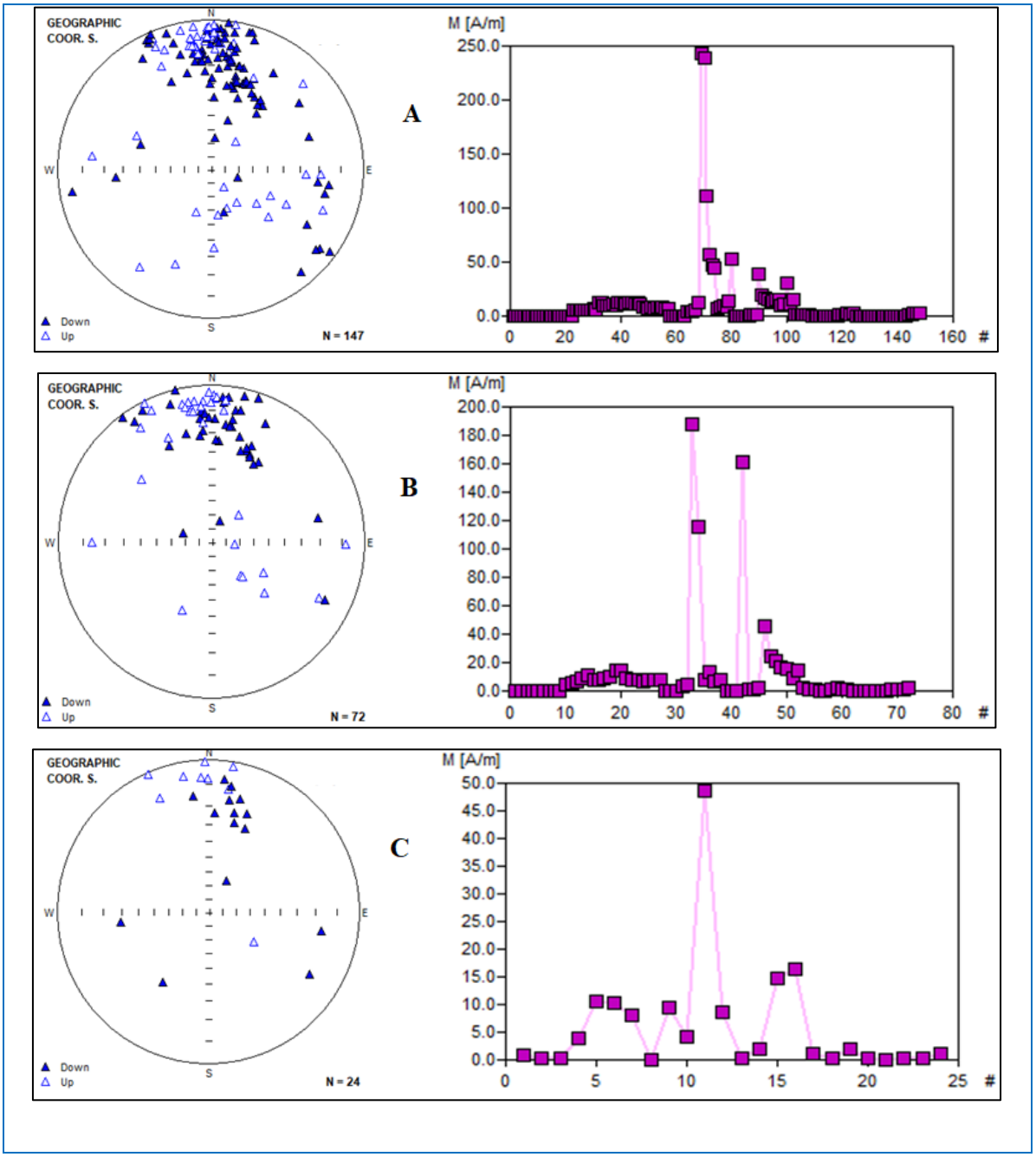

Fig 5.1) Distribution of NRM value before any laboratory treatment within the Stereographic projection and bar graph A) NRM values of specimens selected for AFD B) NRM values of specimens selected for THD C) NRM values of specimens selected for IRM acquisition

5.3 Progressive Demagnetization Results

Progressive demagnetization experiments were executed following the measurements of NRM of all specimens in a collection. The demagnetization experiments yield distinct components of remanence magnetization which can be taken as the ChRM. Secondary magnetizations, which latter need to be removed, were evidenced from the deflection of magnetization directions to anomalous declination and curvilinear trajectories in the Zijderveld diagrams and Stereoplots. Those secondary magnetizations were characterized by low blocking temperature and coercivity ranges in demagnetization experiments. The secondary magnetization of the rocks attained during their subsequent history like the alteration affecting the ferromagnetic minerals, lightning strike or long term exposure to the geomagnetic field (Butler, 1992).

AF and TH demagnetization techniques were accompanied to clean the secondary magnetizations to come up with the ChRM. As mentioned earlier, this ChRM is characterized by a straight line segment directed towards the origin. AF demagnetization experiment was not able to demagnetize the specimens to its origin in most specimens. In contrast, TH demagnetization was able to erase all the secondary components of magnetization in all most all specimens. During thermal demagnetization the low components of magnetizations (secondary magnetization) were randomized at a temperature up to 520^0C on the other hand during AF demagnetization it needs up to 30mT on average. Demagnetization results of the specimens were then presented on Zijderveld diagram, stereographic projections, and normalized intensity decay curves to allow detailed analysis of this study.

5.3.1 AFD Measurement Results

Alternative field demagnetization (AFD) technique was effective on demagnetizing specimens with low coercivity. One hundred forty-seven specimens from 23 sites were progressively demagnetized in an alternating field (AF) with (5) mT increments up to (30) mT and with 10 mT increment up to 100 mT. Remanence NRM of these pilot specimens was measured by a spinner magnetometer existed in (Addis Ababa University) (See appendix-A). 50% of the magnetization intensity of the specimens was removed using the applied fields between 30 and 40mT and almost 85% to 90% of the magnetization was removed on the

applied peak alternative magnetizing field (100mT). The stereographic projections show a useful clustering of the magnetic declination values towards the North, Northeast and northwest and also it indicates almost shallow inclination values. Some of the selected AFD results are presented here to analyze the behaviour of the rocks with the applied field.

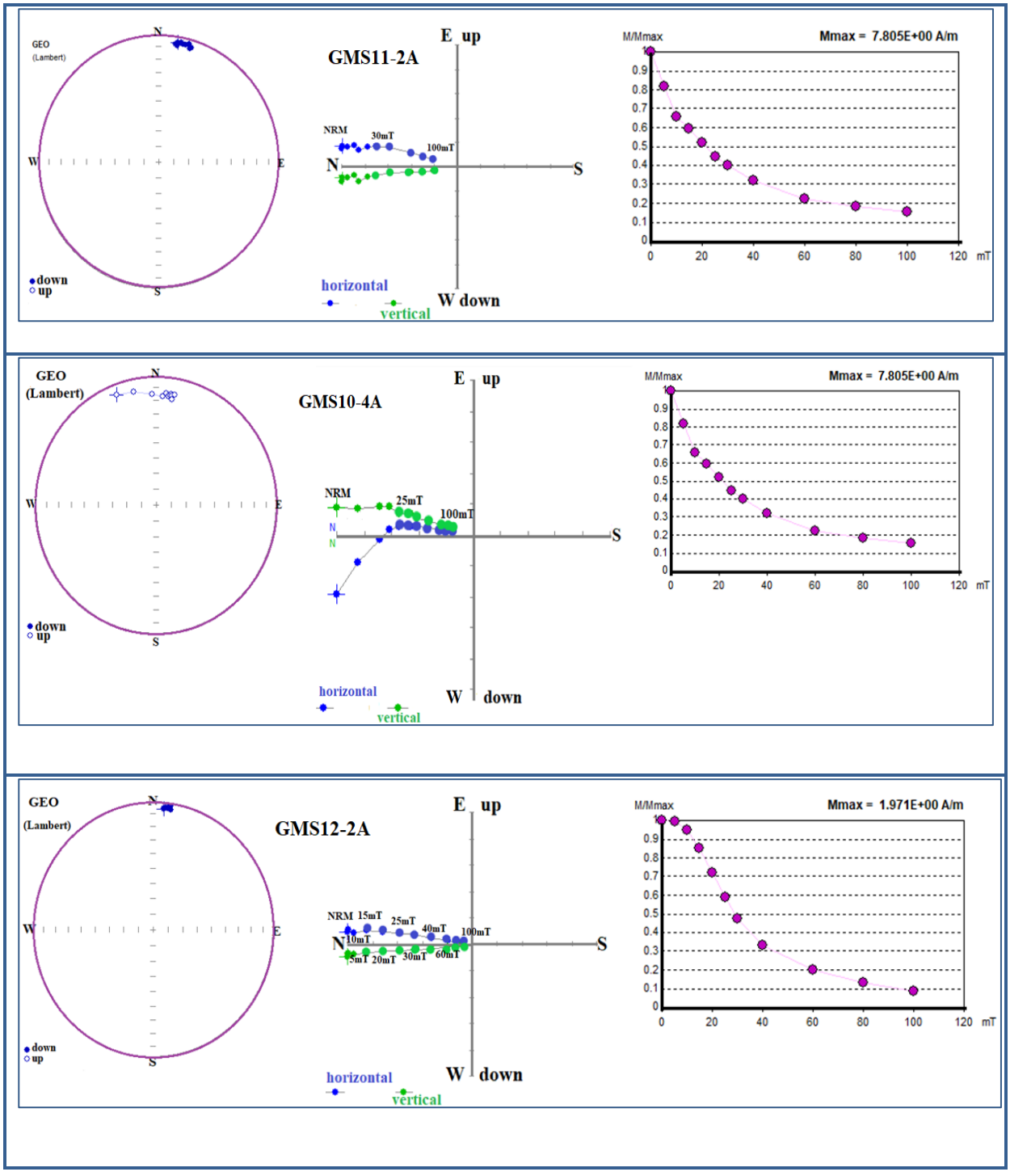

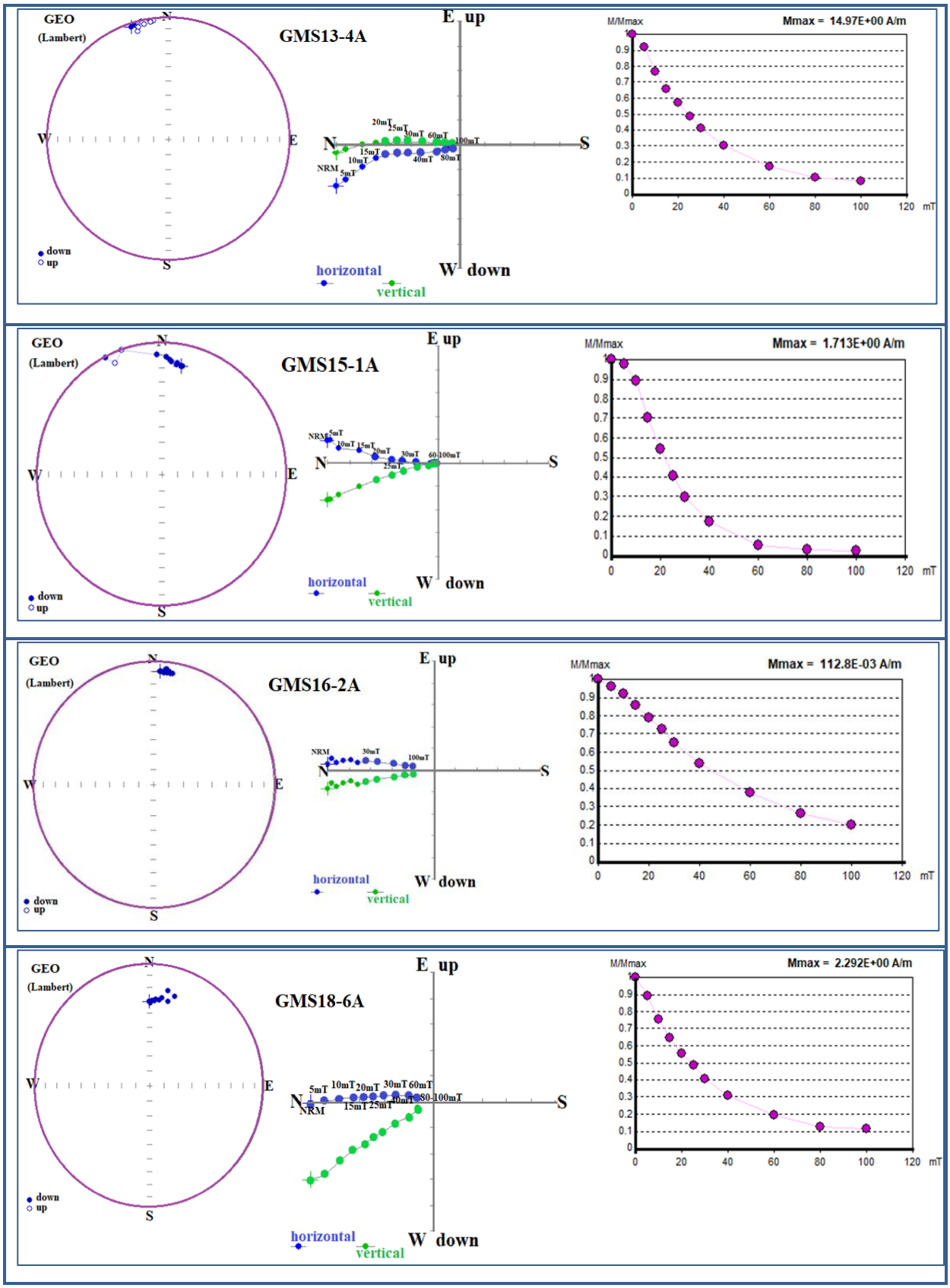
GEO
(Lambert)
N
W
E
S
down
up
GMS13-4A
E up
N
S
W down
horizontal
vertical
NRM
5mT
10mT
15mT
20mT
25mT
30mT
40mT
60mT
80mT
100mT
M/Mmax
Mmax = 14.97E+00 A/m
0 20 40 60 80 100 120 mT
GMS15-1A
Mmax = 1.713E+00 A/m
GMS16-2A
Mmax = 112.8E-03 A/m
GMS18-6A
Mmax = 2.292E+00 A/m

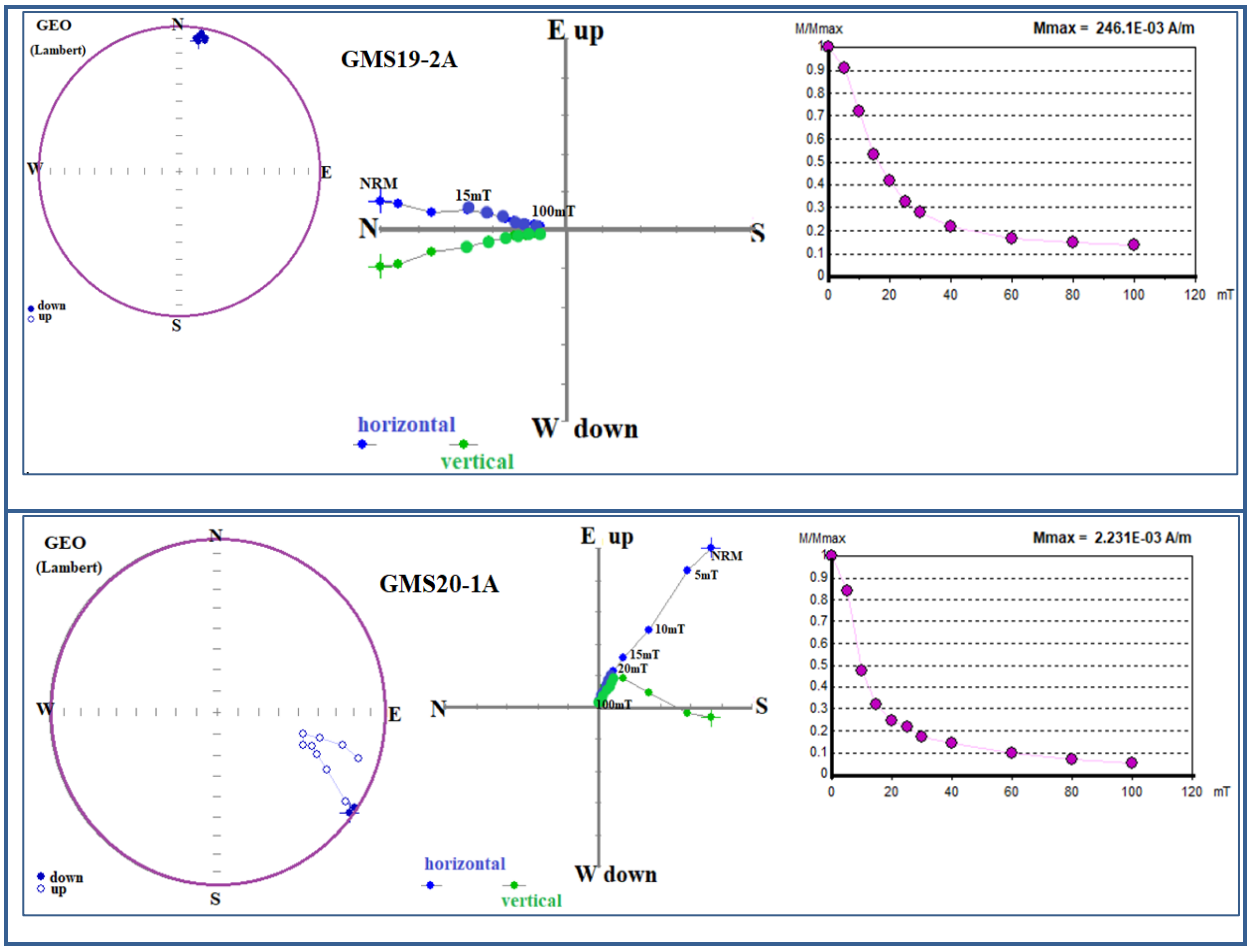

Fig 5.2) Progressive Alternative field demagnetization diagrams (Lambert-equal area stereographic projection, Zijderveld diagrams and normalized intensity decay curves) of nine specimens (GMS11-2A, GMS10-4A, GMS12-2A, GMS13-4A, GMS15-1A, GMS16-2A, GMS16-2A, GMS18-6A, GMS19-2A and GMS20-1A)

In all specimens, the normalized intensity versus the applied field shows a gradual drop in magnetization intensity values with increasing applied field. Normalized intensity curves for specimens (GMS11-2A, GMS10-4A, GMS12-2A, and GMS18-6a) reveal that their magnetic intensities individually lost by 80-85% from their original intensities after subjected to the applied field of 60mT indicating that the rocks have low to moderate coercivity field with normal polarity.

In specimen GMS11-2A, the secondary magnetization (low coercivity) was cleaned at 30mT and only 85% of magnetization was cleaned at peak demagnetizing field (100mT). In GMS10-4B the overprint has been removed at the demagnetization level of 20-25mT and the ChRM is observed in a straight line segment directed towards the origin. 50% of its original

magnetization is removed at 20mT and 85% is removed after a peak demagnetizing field. The orthogonal vector shows a trajectory towards the origin with no significant change in the direction of NRM for specimen GMS12-2A and almost 90% of its original magnetization lost by the maximum magnetizing field. The ChRM well oriented and clustered towards NNE direction with a shallow inclination and it shows normal polarity. For GMS13-4A the secondary overprint was cleaned at a demagnetization field of 15mT and its ChRM directed towards NNW direction. As well the peak demagnetization level erased 90% of its original magnetization. For GMS15-1A 98 to 100% of the magnetization lost at a maximum applied demagnetizing field of 100mT on the other hand half of its magnetization lost only at 20mT. Specimen GMS16-2A gained its ChRM direction after a demagnetization level of 30mT directed and well clustered towards NNW with shallow inclination. Half of its original magnetization lost at 40mT.

For specimen 18-6A, the orthogonal vector diagram shows a trajectory towards the origin with no significant change in direction with NRM value and its ChRM directed towards North with significant inclination. Its median destructive field is observed to be 20mT and it lost its 97-99% of original magnetization at peak demagnetization field. GMS19-2A, half of its magnetization lost at only 15mT and 85% of its magnetization lost at the peak demagnetization applied field of 100mT. The ChRM was well-oriented and clustered towards the NNE direction. For GMS20-1A anomalous ChRM direction and polarity have been observed. The overprint has been removed at 20mT and the ChRM oriented towards SE direction. Half of its original magnetization lost only at 10mT and 95% of its magnetization value lost at the peak demagnetization level.

In general, stable NNE-directed ChRMs (GMS11-2A, GMS10-4A, GMS12-2A, GMS15-1A, GMS16-2A, GMS16-2A, GMS18-6A, and GMS19-2A) with shallow inclinations (in geographic coordinate system) and NNW-directed ChRMs (GMS13-4A) with normal polarity were identified in the above specimens. On the other hand specimen GMS20-1A shows reversed polarity.

In most of the specimens, their secondary overprint was removed at the applied demagnetization field ranged between 10-30mT allowing a stable ChRM to be easily isolated. In GMS22-4A orthogonal vector diagram shows a trajectory towards the origin with

no significant change in direction with NRM value and its ChRM directed towards North with shallow inclination. Half of its original magnetization removed at 30mT and 80% of the magnetization was lost at the maximum applied demagnetizing filed. The same thing occurred for GMS22-6A that no directional change during the course of demagnetization. However, the stable ChRM directed towards NNE direction and its median destructive field is observed to be 40mT with almost 88% percent of its original magnetization lost at a peak demagnetization level. GMS2-6A gained its stable ChRM direction at only 5mT and it oriented towards NNE with shallow inclination. The median destructive filed to be 30mT and almost 88% of its magnetization was cleaned at 100mT which is the peak demagnetization level.

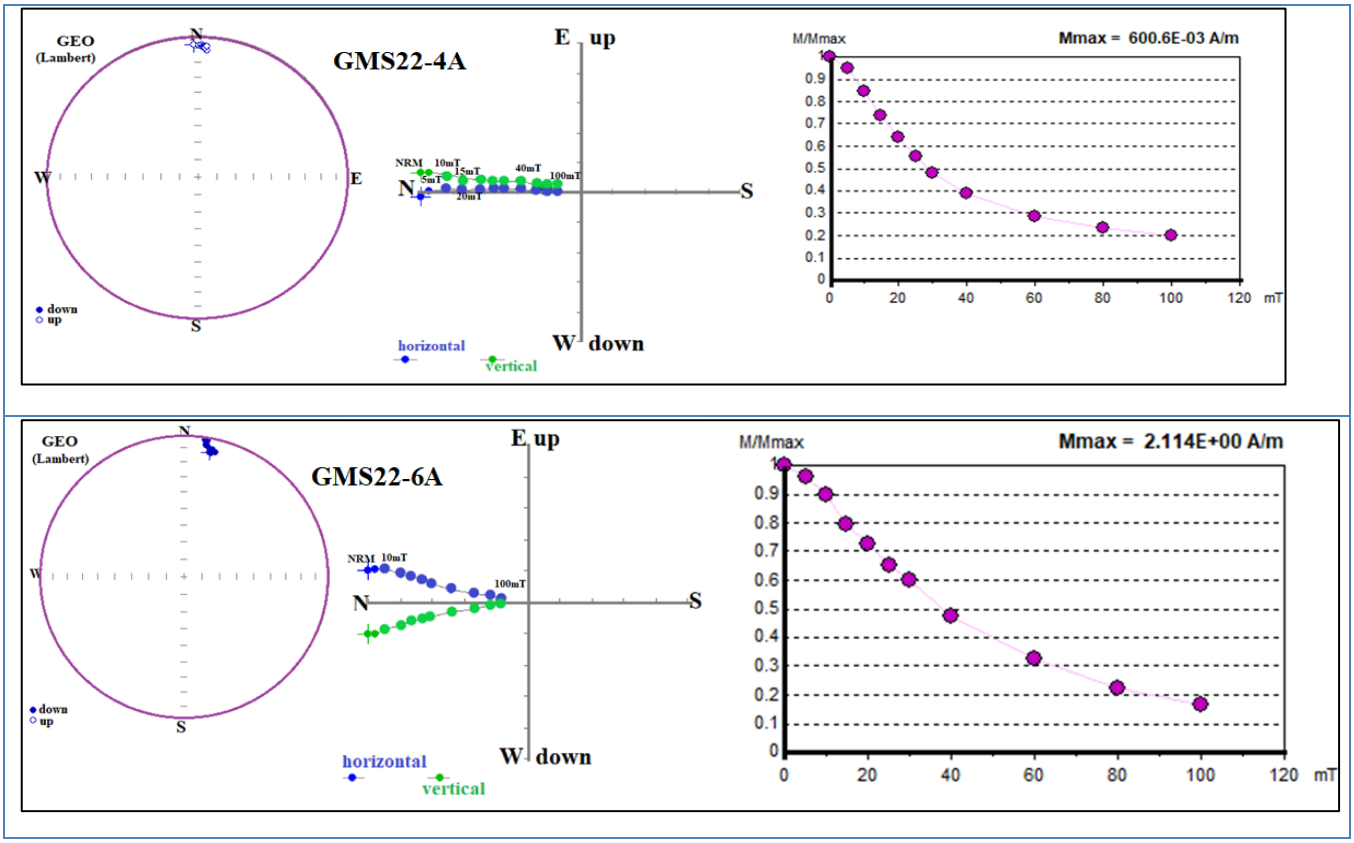

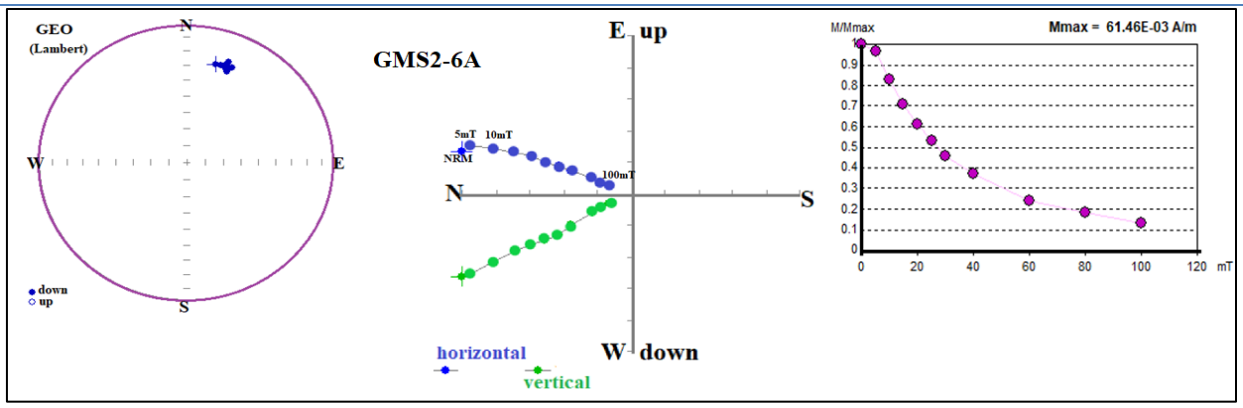
GEO
(Lambert)
N
W
E
S
down
up
GMS2-6A
E up
5mT
10mT
NRM
100mT
N
S
W down
horizontal
vertical
M/Mmax
Mmax = 61.46E-03 A/m
0
0.1
0.2
0.3
0.4
0.5
0.6
0.7
0.8
0.9
0
20
40
60
80
100
120
mT

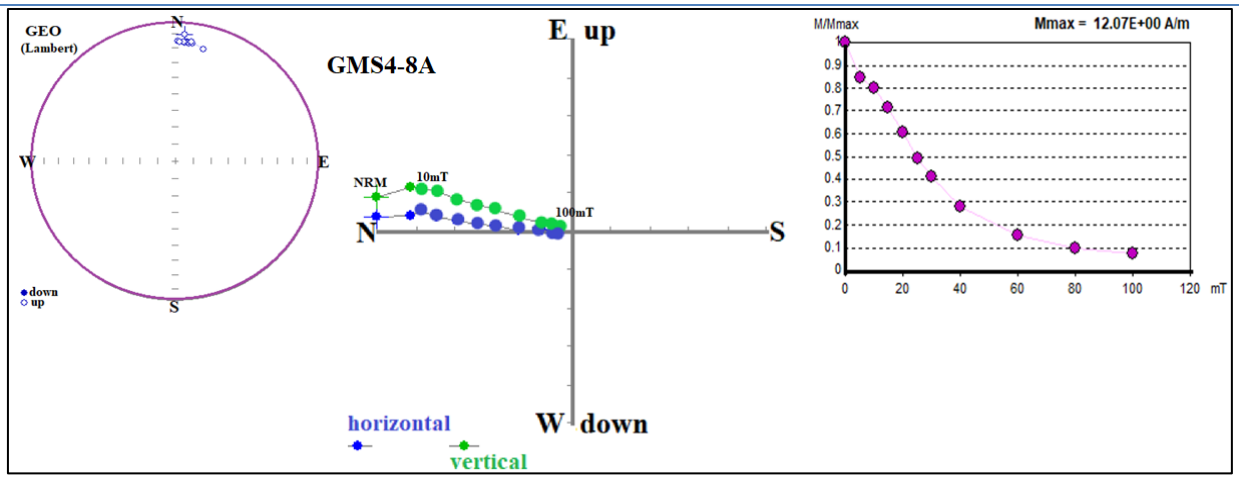
GEO
(Lambert)
N
W
E
S
down
up
GMS4-8A
E up
NRM
10mT
100mT
N
S
W down
horizontal
vertical
M/Mmax
Mmax = 12.07E+00 A/m
0
0.1
0.2
0.3
0.4
0.5
0.6
0.7
0.8
0.9
0
20
40
60
80
100
120
mT

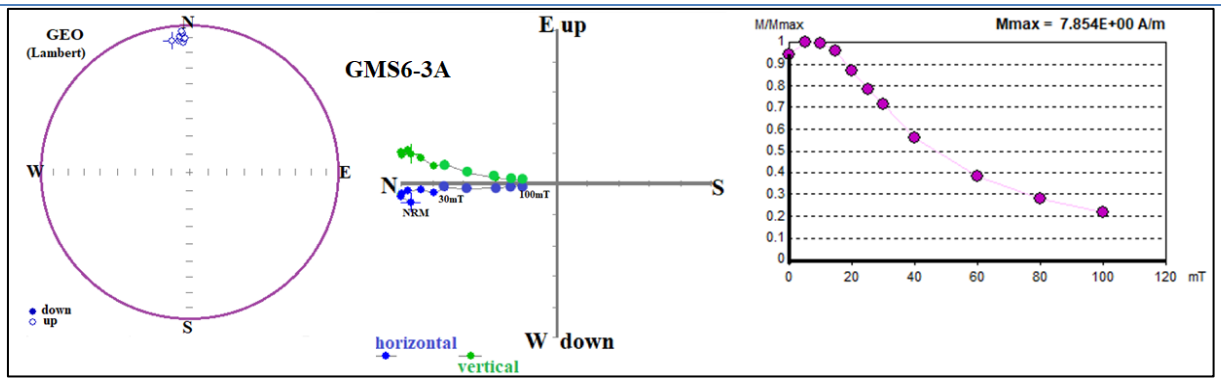
GEO
(Lambert)
N
W
E
S
down
up
GMS6-3A
E up
N
S
30mT
100mT
NRM
W down
horizontal
vertical
M/Mmax
Mmax = 7.854E+00 A/m
0
0.1
0.2
0.3
0.4
0.5
0.6
0.7
0.8
0.9
1
0
20
40
60
80
100
120
mT

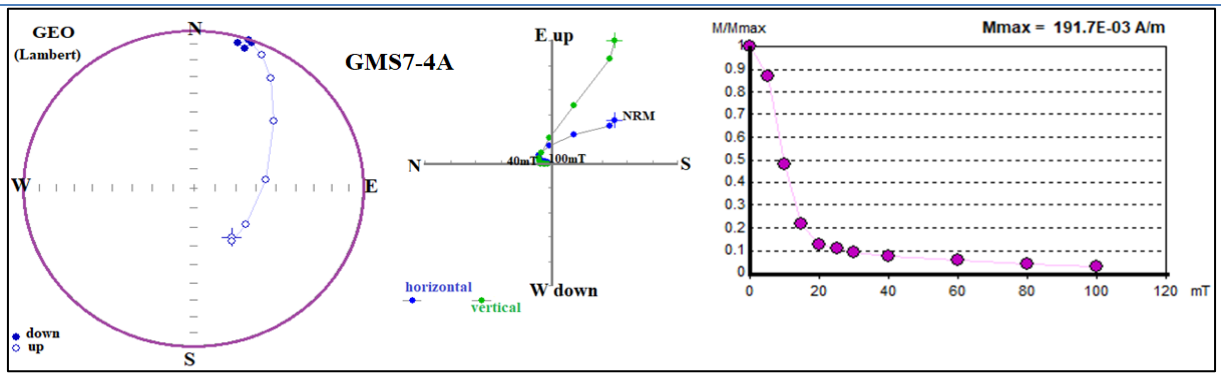
GEO
(Lambert)
N
W
E
S
down
up
GMS7-4A
E up
NRM
N
40mT
100mT
S
W down
horizontal
vertical
M/Mmax
Mmax = 191.7E-03 A/m
0
0.1
0.2
0.3
0.4
0.5
0.6
0.7
0.8
0.9
1
0
20
40
60
80
100
120
mT

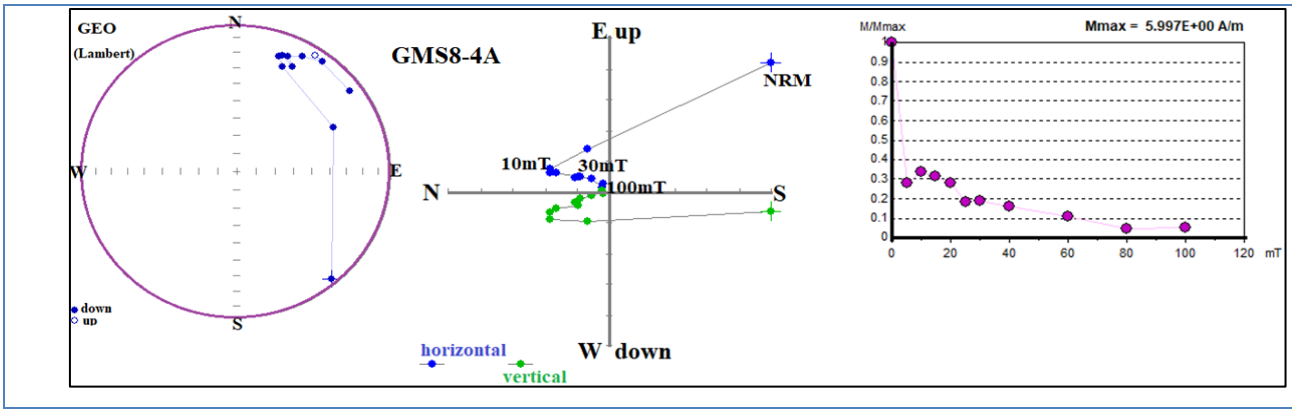

Fig 5.3) Progressive Alternative field demagnetization diagrams (Lambert-equal area stereographic projection, Zijderveld diagrams, and normalized intensity decay curves) of seven specimens (GMS22-4A, GMS22-6A, GMS2-6A, GMS4-8A, GMS6-3A, GMS7-4A, and GMS8-4A)

Only 10mT needed to remove the secondary overprint for GMS4-8A and the stable ChRM is directed towards the North. 90% of its initial magnetization lost at the peak demagnetization level of 100mT. GMS7-4A and GMS8-4A, on the contrary, showed the reverse secondary overprint which later cleaned at a low applied demagnetizing field of 40mT and 10mT respectively. For GMS7-4A even though the overprint shows reverse polarity, the stable ChRM directed towards NNE direction with normal polarity. 90% of its initial magnetization has been lost by only 20mT and all its magnetization lost at the peak demagnetization level with 100mT. The same thing for GMS8-4A in which the reversed polarity secondary overprint erased at 10mT but the decay curve didn't show a horizontal pattern. Unlike others, the ChRM is not well clustered but directed towards NE with normal polarity. Generally, the Alternative Field Demagnetization was effective in removing secondary overprint magnetization with a different degree on different specimens.

5.3.2 THD Measurement Results

Progressive thermal demagnetization of specimens was carried out with the aim to study their magnetic behaviour and also to isolate the ChRM from the secondary overprint magnetization. Thermal demagnetization analysis was conducted for (72) specimens using the thermal demagnetizer model (MMTD80) available in Paleomagnetic laboratory, Addis Ababa University. The selected specimens were heated and then cooled in a laboratory-built, shielded furnace. The demagnetization was carried out by heating to 150°C and then in (18)

steps up to (680) °C (except GMS15-1B that was broken during the heating at 600°C). The thermal demagnetization results are presented in appendix-B.

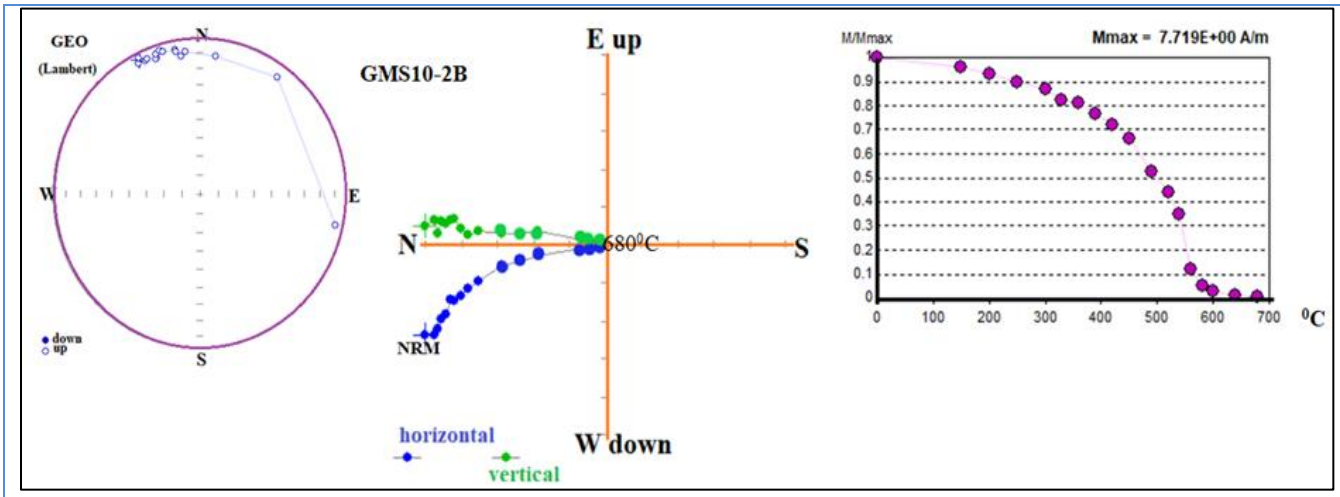

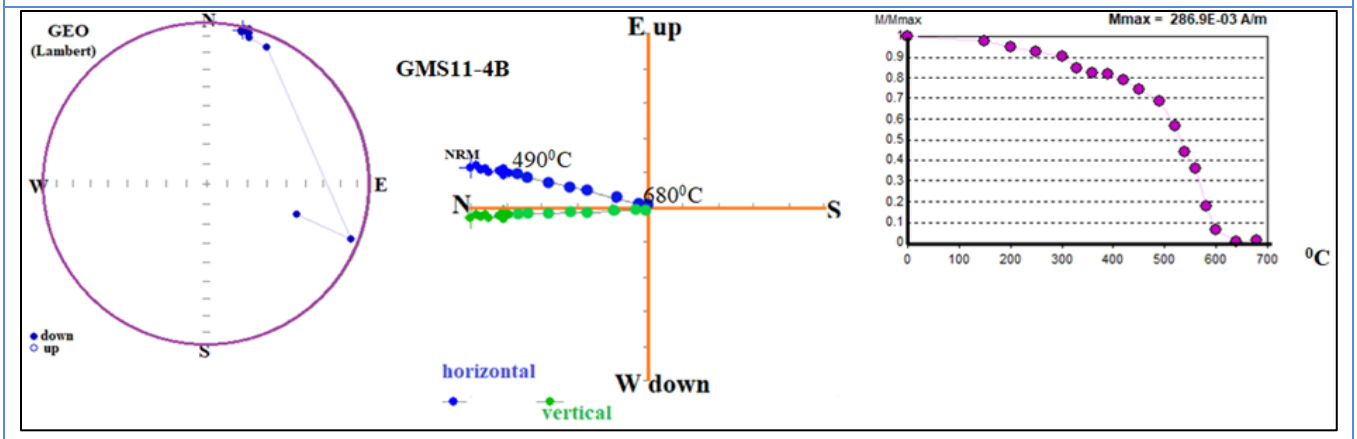

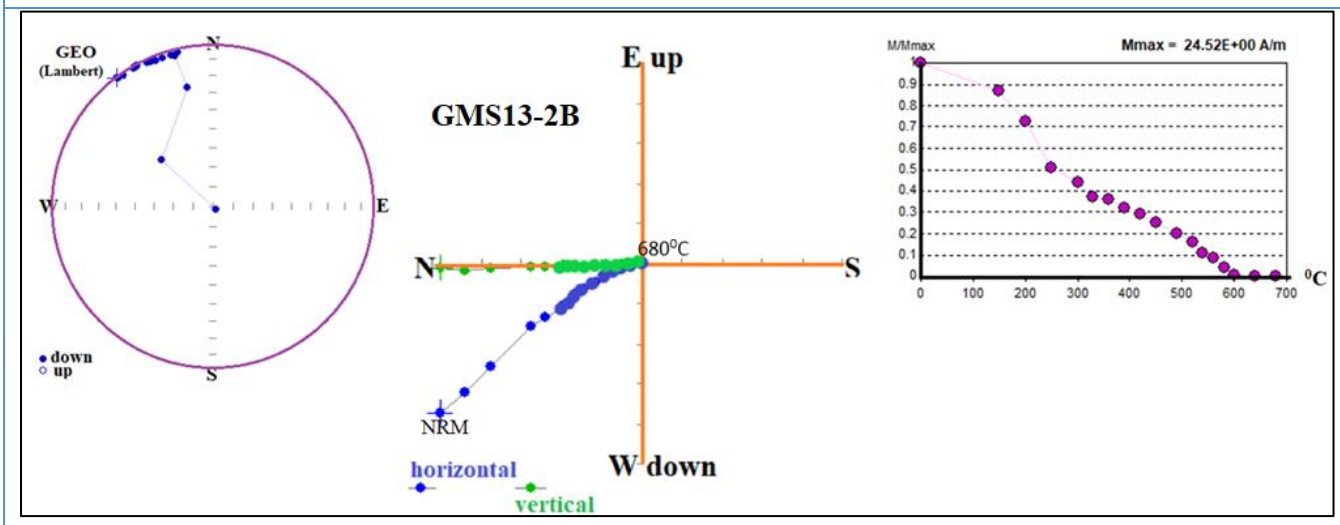

Fig 5.4 Progressive thermal demagnetization diagrams (Lambert equal-area stereographic projection and Zijderveld diagrams and their corresponding normalized intensity decay curves from left to right) for three specimens (GMS10-2B, GMS11-4B, and GMS13-2B)

As in the case of AF demagnetizations, TH demagnetizations also revealed the stable ChRM components after a certain demagnetization levels. The weak secondary overprint was removed by the application of temperature up to 520^0C. From the intensity decay curves, it could be noticed that the magnetization intensity was dropped significantly between 450^0C and 590^0C demagnetization levels. These may suggest that the dominance magnetization carrier minerals are magnetite and titanomagnetite. Some specimens lost their magnetization up to a demagnetization levels up to 640^0C. These also may indicate the presence of titanohematite and minor hematite as a magnetic mineralogy in some rock samples.

For GMS10-2B the normalized intensity versus temperature curve shows a gradual drop in intensity value (Fig 5.4) with shallow inclination. The declination of this specimen shows a good cluster around the NNW direction in which the secondary overprint has been cleaned at 520^0C. Specimen GMS11-4B, the secondary overprint has been removed after the demagnetization temperature of 360^0C and the stable ChRM directed towards the NNE direction with shallow inclination. For specimen GMS13-2B, the orthogonal vector shows a trajectory towards the origin with no significant change in direction with NRM value and its ChRM with less clustering directed towards Northwest with shallow inclination.

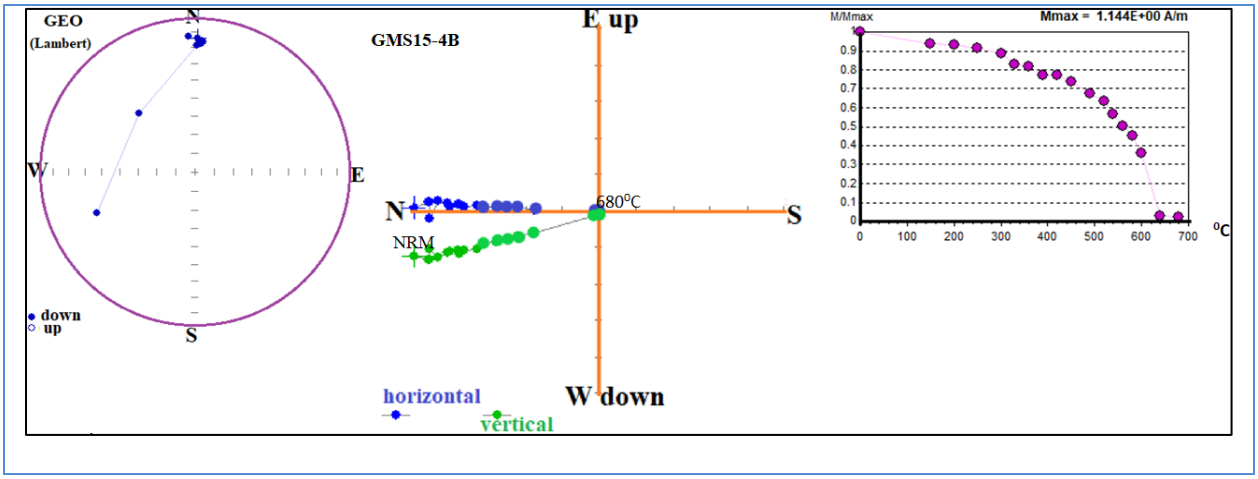

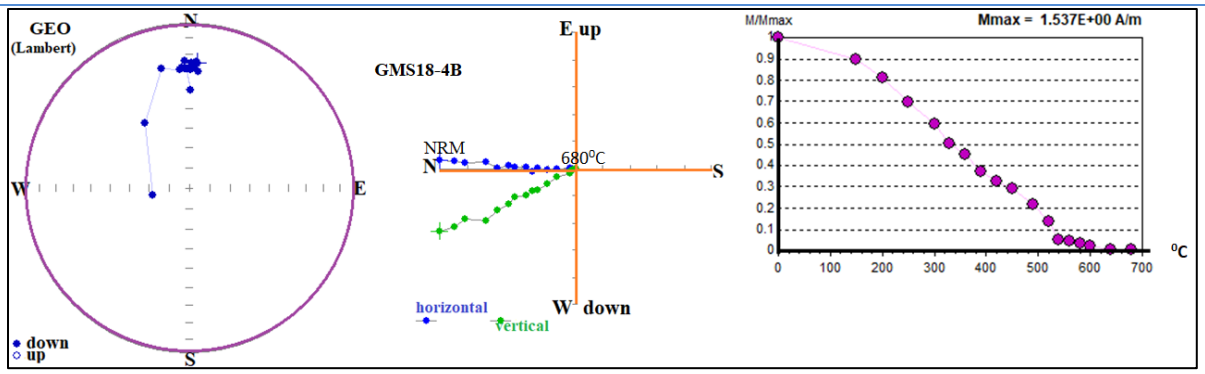
GEO
(Lambert)
N
W
E
S
down
up
GMS18-4B
E up
NRM
N
680°C
S
W down
horizontal
vertical
M/Mmax
Mmax = 1.537E+00 A/m
0.9
0.8
0.7
0.6
0.5
0.4
0.3
0.2
0.1
0
0 100 200 300 400 500 600 700
°C

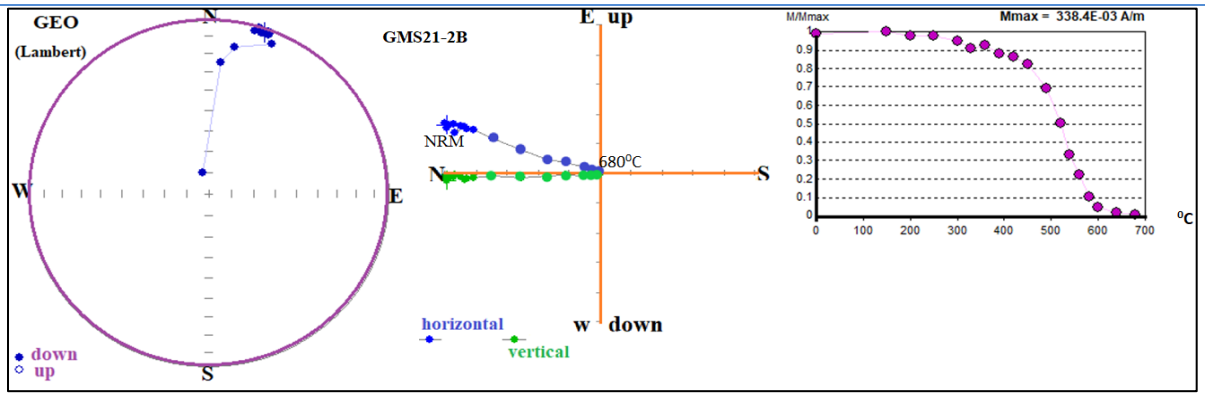
GEO
(Lambert)
N
W
E
S
down
up
GMS21-2B
E up
NRM
N
680°C
S
w down
horizontal
vertical
M/Mmax
Mmax = 338.4E-03 A/m
0.9
0.8
0.7
0.6
0.5
0.4
0.3
0.2
0.1
0
0 100 200 300 400 500 600 700
°C

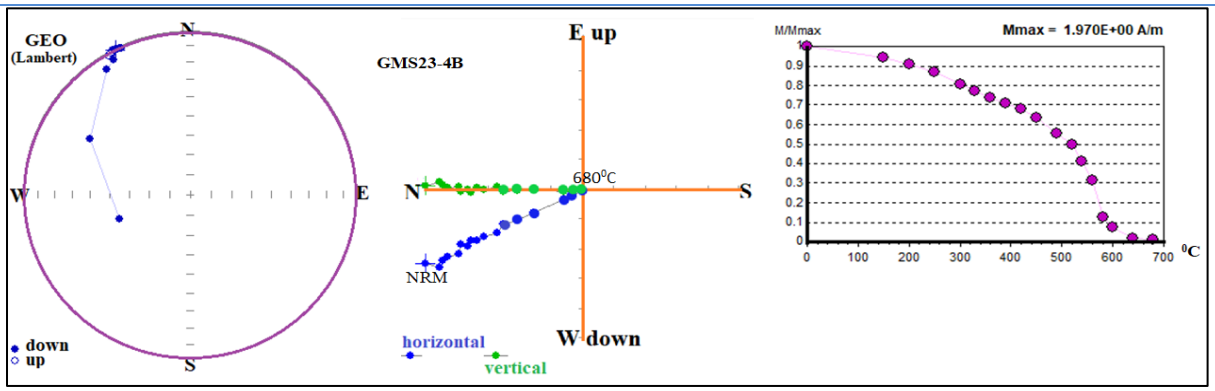
GEO
(Lambert)
N
W
E
S
down
up
GMS23-4B
E up
N
680°C
S
NRM
W down
horizontal
vertical
M/Mmax
Mmax = 1.970E+00 A/m
0.9
0.8
0.7
0.6
0.5
0.4
0.3
0.2
0.1
0
0 100 200 300 400 500 600 700
°C

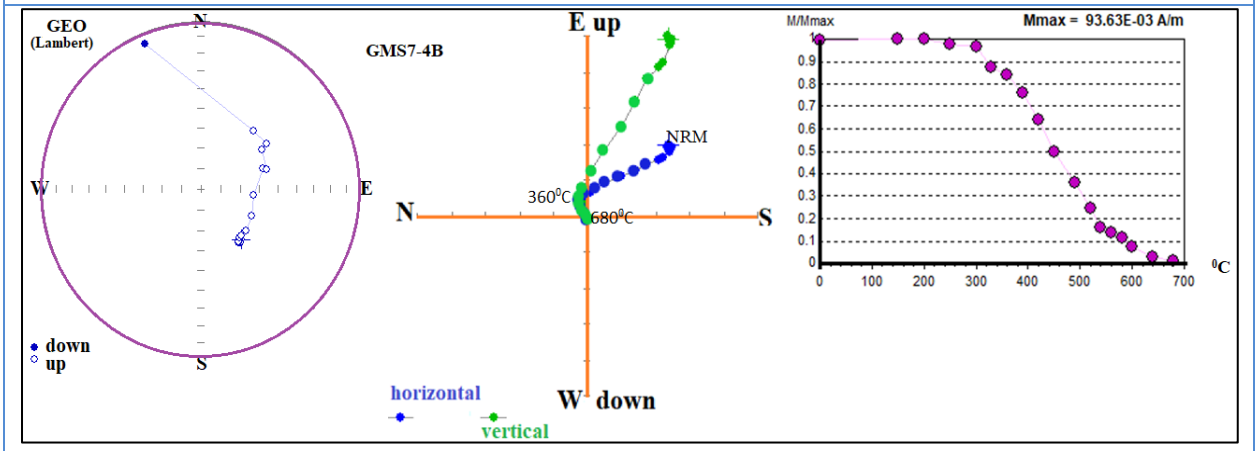
GEO
(Lambert)
N
W
E
S
down
up
GMS7-4B
E up
NRM
360°C
N
680°C
S
W down
horizontal
vertical
M/Mmax
Mmax = 93.63E-03 A/m
0.9
0.8
0.7
0.6
0.5
0.4
0.3
0.2
0.1
0
0 100 200 300 400 500 600 700
°C

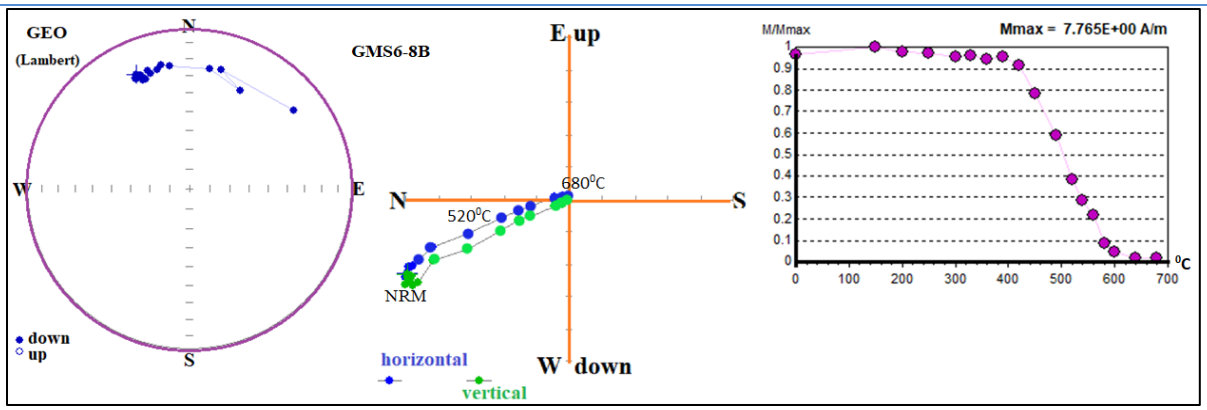
GEO
(Lambert)
N
W
E
S
down
up
GMS6-8B
E up
N
S
W down
680°C
520°C
NRM
horizontal
vertical
M/Mmax
Mmax = 7.765E+00 A/m
0 100 200 300 400 500 600 700
°C

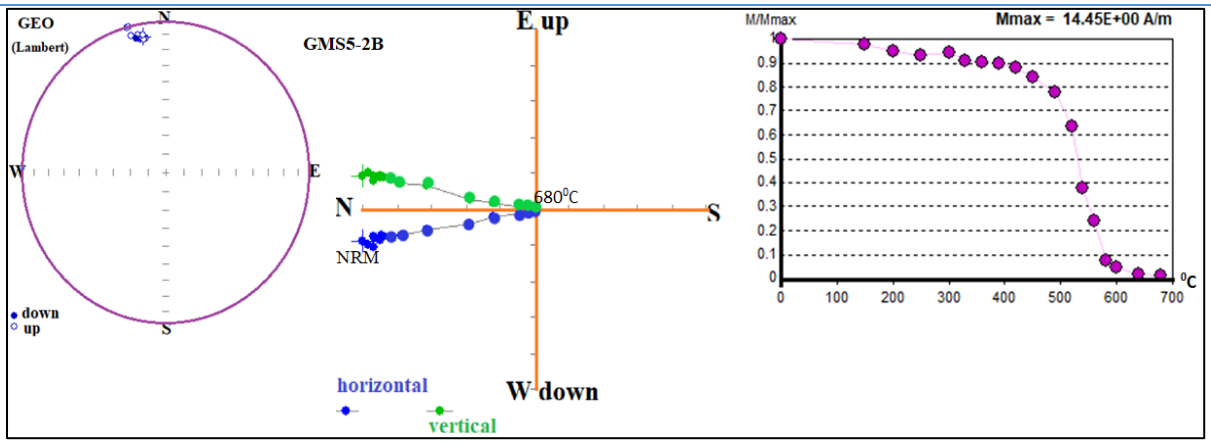
GEO
(Lambert)
N
W
E
S
down
up
GMS5-2B
E up
N
S
W down
680°C
NRM
horizontal
vertical
M/Mmax
Mmax = 14.45E+00 A/m
0 100 200 300 400 500 600 700
°C

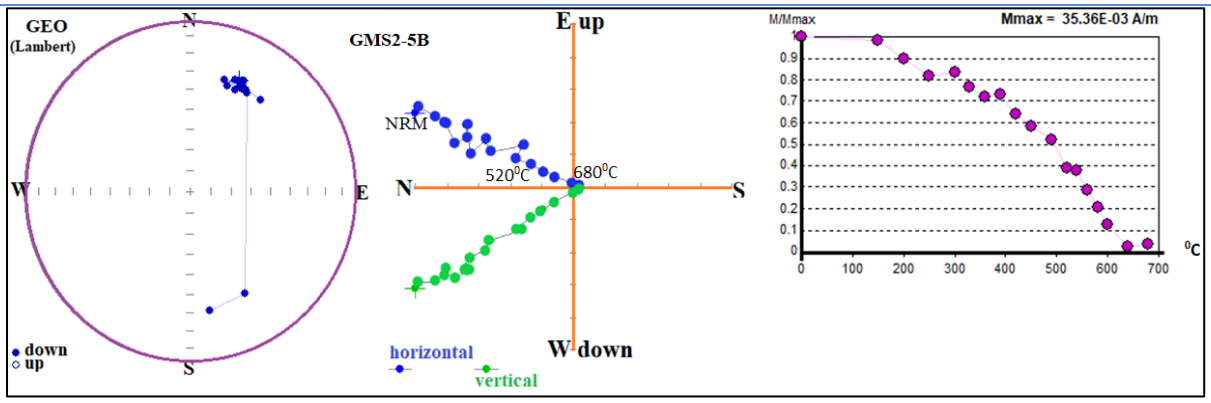
GEO
(Lambert)
N
W
E
S
down
up
GMS2-5B
E up
N
S
W down
NRM
520°C
680°C
horizontal
vertical
M/Mmax
Mmax = 35.36E-03 A/m
0 100 200 300 400 500 600 700
°C

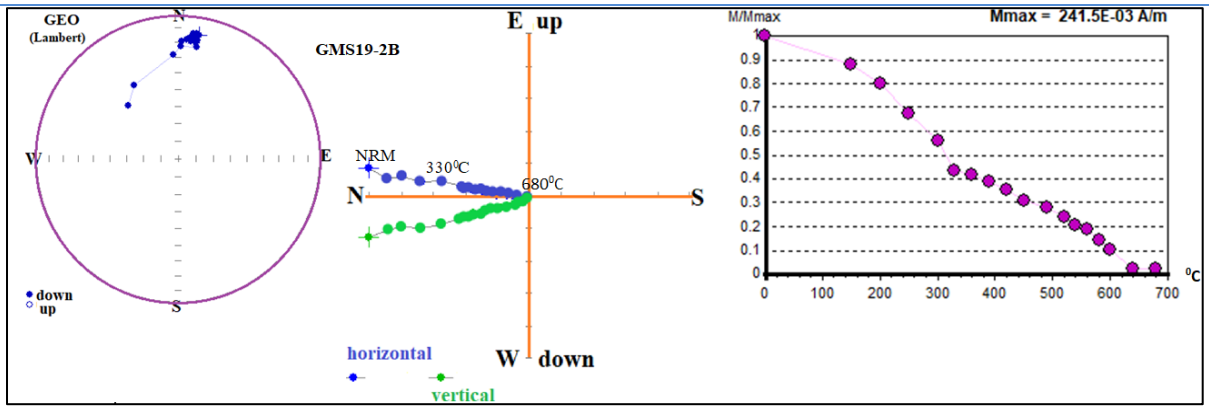
GEO
(Lambert)
N
W
E
S
down
up
GMS19-2B
E up
N
S
W down
NRM
330°C
680°C
horizontal
vertical
M/Mmax
Mmax = 241.5E-03 A/m
0 100 200 300 400 500 600 700
°C

Fig 5.5) Progressive thermal demagnetization diagrams (Lambert equal-area stereographic projection and Zijderveld diagrams and their corresponding normalized intensity decay curves from left to right) for nine specimens (GMS15-4B, GMS18-4B, GMS21-2B, GMS23-4B, GMS7-4B, GMS6-8B, GMS5-2B, GMS2-5B and GMS19-2B)

In most cases, the magnetic direction of thermally demagnetized specimens (Fig.5.5) showed shallow to intermediate inclinations with the stable ChRM directed towards the Northeast and the Northwest direction suggesting variable degrees of overprinting in a normal polarity field. In most of the samples, the secondary overprints were removed at a temperature of 420-520^{0}C. Some representative samples also show reverse polarity (e.g GMS7-4B) in the secondary overprint magnetization. All of the pilot specimens showed almost regular normalized intensity decay curves which intern showed a regular drop in the intensity value. Moreover, between 490 and 680ºC, a systematic movement was noticed in the Zijderveld diagram which characterized the stable ChRM value. This suggests that some overprinting components hide the primary magnetization. With increasing temperature, the intensity gradually decreased with the removal of secondary soft components and left the stable ones in less than 520ºC. Then the sample began to lose the remaining magnetization up to 680ºC slowly and the direction headed toward the plot origin yielding a relatively well-defined high-temperature component between 520ºC and 680ºC.

Here, all the specimens exhibit a gradual drop in their normalized intensity to less than 20% of their initial NRMs between 300-400°C. This is the indication of maghemitization process that might occur in these temperatures (Løvlie and Sandnes, 1987). A considerable rise in magnetic intensities was perceived at 250-300°C in Specimens (GMS2-5B and GMS5-2B). The concave shape that existed in the normalized intensity curves of these specimens may represent the conversion of one or more of the magnetic minerals as a result of the heating. The declination values of almost all specimens showed good grouping around or near the earth's magnetic pole (especially GMS18-4B, GMS15-4B, GMS5-2B and GMS19-2B), which could suggest normal polarity components.

Specimen GMS15-4B radically lost its total magnetization after a temperature of 600^{0}C and the secondary overprint was erased after 420^{0}C. The stable ChRM is well clustered and oriented towards the North. Specimen GMS18-4B, its secondary overprint magnetization has

been lost at a temperature of 330^0C with a moderate inclination and good clustering of the declination value which was well clustered and well-oriented towards the North. This specimen (GMS18-4B) lost its magnetization at 580^0C, so that the magnetic mineralogy is most probably magnetite. For specimen GMS21-2B, the orthogonal vector diagram shows a trajectory towards the origin with no significant change in direction with NRM value and its ChRM with less clustering directed towards Northeast with shallow inclination. Specimen GMS7-4B shows a reversed secondary overprint magnetization which then demagnetized and removed at a temperature up to 360^0C and the stable ChRM obtained after this demagnetization level and directed to the origin.

In all case (Fig 5.6), the two demagnetization techniques show identical Zijderveld diagram pattern in the same direction. The main difference is then in the case of alternative filed demagnetization, the straight line segment which is the ChRM didn't reach to the origin, and 10-20% magnetization stay unremoved. This means the alternative field demagnetization was able to erase 80-90% of magnetization (see the normalized intensity decay curve). On the contrary, thermal demagnetization techniques cleaned all the magnetization and the straight line segment reaches to the origin means it was very effective to remove 100% of the magnetization (see the normalized intensity decay curve).

For most of the samples analysed, the ChRM recognized by AF and TH techniques are matching for the twin specimens obtained from the same core samples (e.g. Fig 5.6). Even though both AF and TH treatments were done on the expectations that for some cases one or the other technique would better identify the vector components present. In this study, however, both AF and TH generally resulted in identical Zijderveld diagrams (Figs 5.6). These happen because; for the most part the vector components of various specimens are characterized by non-overlapping unblocking temperatures and non-overlapping coercivity spectra (Tesfaye Kidane et al, 2006).

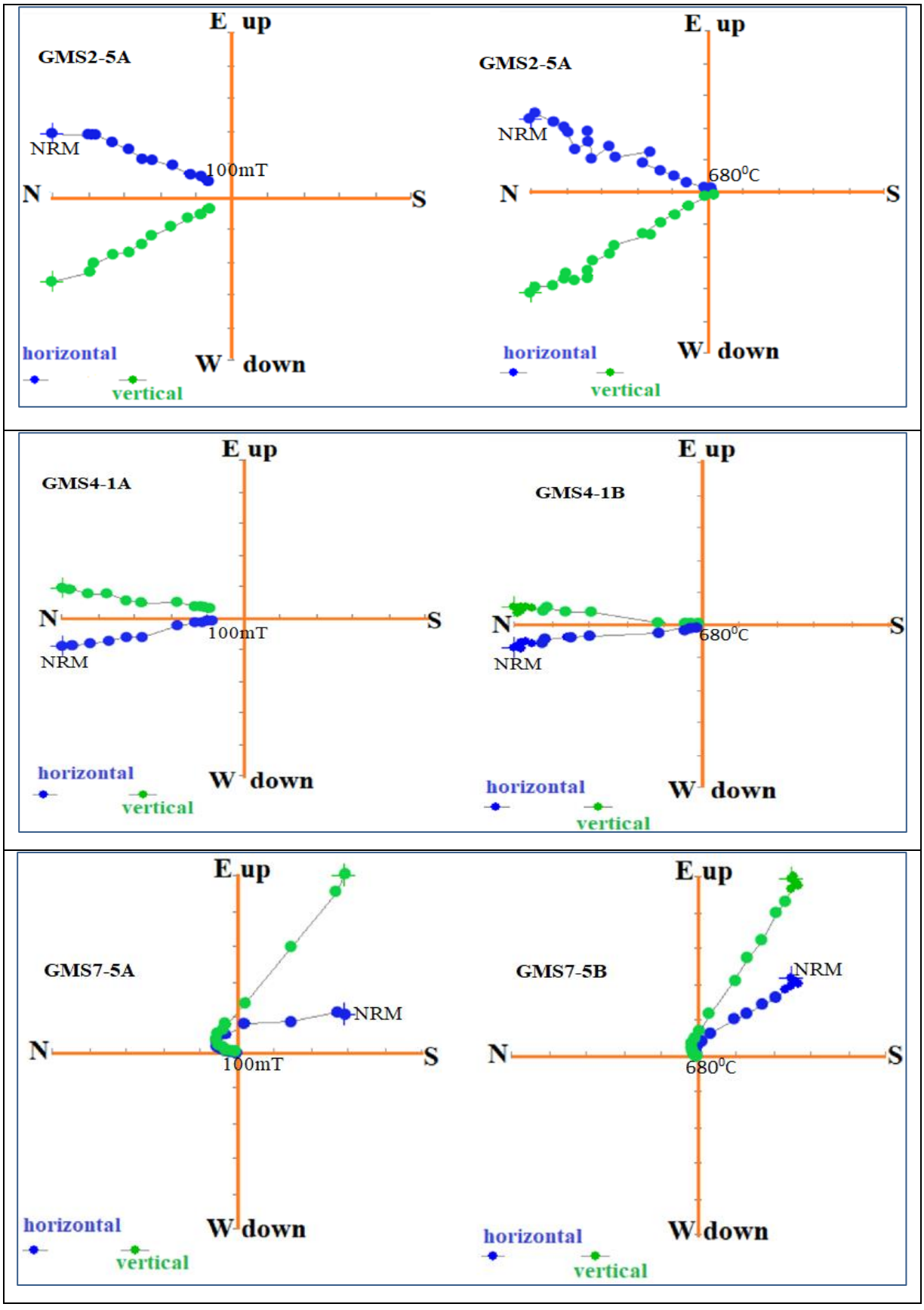
GMS2-5A
E up
NRM
100mT
N
S
W down
horizontal
vertical
GMS2-5A
E up
NRM
680°C
N
S
W down
horizontal
vertical
GMS4-1A
E up
N
S
100mT
NRM
W down
horizontal
vertical
GMS4-1B
E up
N
S
680°C
NRM
W down
horizontal
vertical
GMS7-5A
E up
NRM
N
S
100mT
W down
horizontal
vertical
GMS7-5B
E up
NRM
N
S
680°C
W down
horizontal
vertical

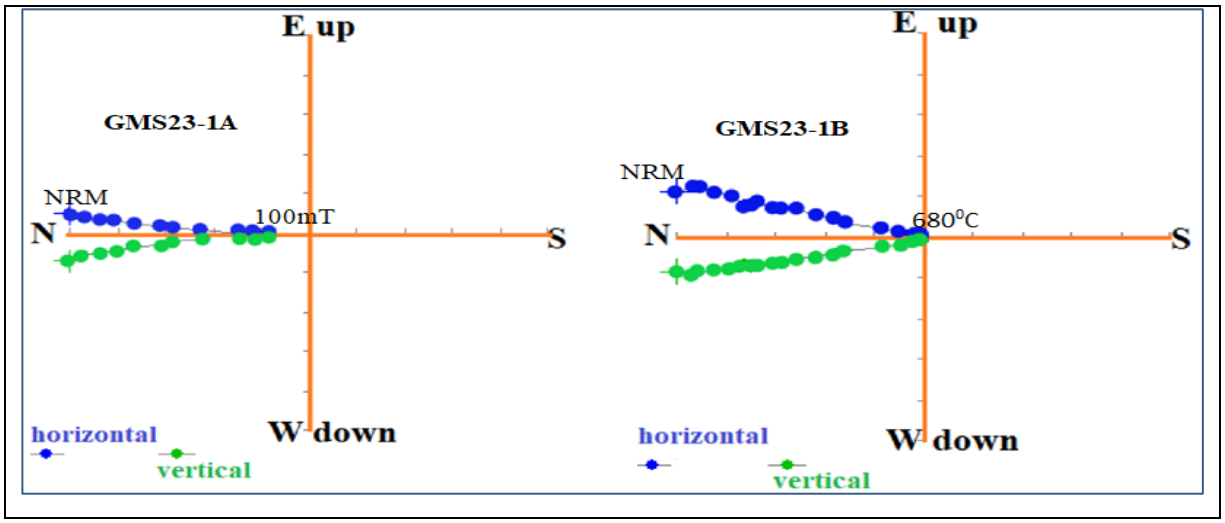

Fig 5.6) Examples of Zijderveld diagrams for representative twin specimens (GMS2-5A&B, GMS4-1A&B, GMS7-5A&B, GMS23-1A&B) treated by AF and TH, to show the reliability of the two types of demagnetization techniques with the same core sample

Analyses of the paleomagnetic results accomplished by a graphic assessment of Zijderveld diagrams and determination of component direction by PCA, paleomagnetic specimens generally consists of two components of magnetization; the first one is attributed to a low-temperature-component-LTC that is usually of small magnitude which was removed by a temperature less than 300-520ºC, that is regarded as overprint secondary unstable magnetic component with magnetic direction around the present earth magnetic field. The second high-temperature-HTC with elevated temperature > 520ºC is considered to be the characteristic remanent magnetization. It forms rather a straight line directed towards the origin in the Zijderveld diagram. HTC shows stable direction up to (300-680°C).

In general from the demagnetization experiment, after the removal of the secondary overprint magnetization, mostly NNE and NNW directed stable, well oriented and clustered ChRM with shallow inclination (with geographic coordinate) were identified.

5.4 Rock Magnetic Experiment

Rock magnetic experiments have been conducted for a specimen per site to associate particular components of NRM with a particular ferromagnetic mineral. Hopefully to determine the magnetization carrier minerals too, rock magnetic experiment has been done. There are three techniques of rock magnetic experiment for identification of ferromagnetic

minerals (Butler, 1992). Those are (1) Optical microscopy techniques; (2) determination of Curie temperature; and (3) coercivity spectrum analysis. In this study coercivity spectrum analysis followed by Curie temperature estimations were accompanied to identify ferromagnetic minerals.

5.4.1 IRM Acquisition Study

From twenty-three sites, one specimen per site has been selected for this IRM acquisition study except for site GMS16; the specimen was broken during the experiment. This magnetization acquisition study aims to identify ferromagnetic minerals of the sampled rocks in the study area, by their coercivity and Curie temperature determination.

In this study, coercivity spectrum analyses followed by Curie temperature were conducted to identify ferromagnetic minerals. The procedure attended in coercivity spectrum analysis is to induce IRM by exposing the specimen to a magnetizing field (H), using impulse magnetizer; measurement of the resulting IRM using spinner magnetometer, then repeat the procedure using the stronger magnetizing field with the following magnetizing levels (table 5.1). Progressive direct magnetic fields up to 1T (1000mT) were applied to the representative specimens to determine the IRM acquisition patterns for a short time up to (a minute).

Table 5.1 Applied field (mT) and voltage (v) used for IRM curve determination of the selected specimens

S. No	Applied Field (mT)	Voltage (v)
1	0	0
2	10	3
3	20	6
4	30	9
5	40	12
6	60	18
7	80	24
8	100	30
9	150	45
10	300	90
11	400	120
12	500	150
13	750	225
14	900	270
15	1000	300

The magnetic field applied to the specimens from each site to do magnetization acquisition experiments is as a function of applied voltage which is converted into a magnetic field in mT. The IRM intensity values were normalized to the saturation value according to the behaviour of the specimens. An essential part of every paleomagnetic study is the identification of magnetic minerals which carries the magnetic remanence and how the sampled rocks got magnetized.

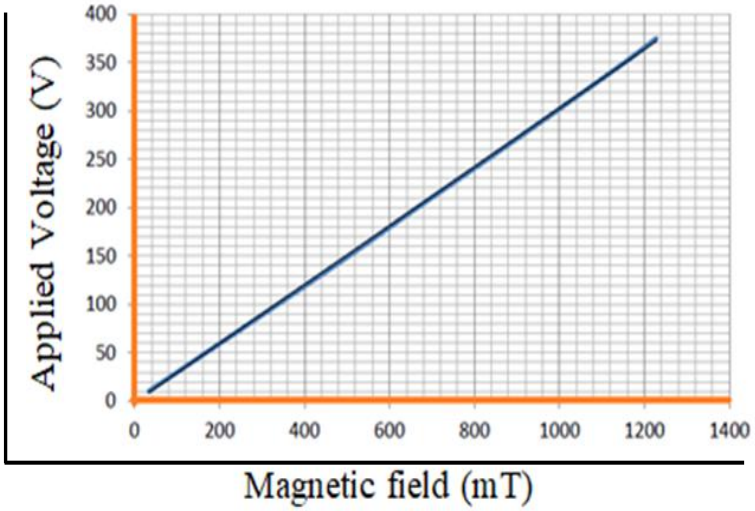

Fig 5.7) a graph shows the direct proportionality of the applied voltage and the magnetic field used in the IRM acquisition experiment

By plotting a curve for IRM against the applied field, the nature of the magnetic mineral can be identified. There are standard curves for magnetite and hematite (Fig 5.8). Each mineral has its own behaviour under the applied field. The magnetite can be saturated at about 220 to 300mT, while the hematite shows a gradual increase and no saturation beyond the maximum applied field for the case of standard curves below. In general a sample containing only titanomagnetite (magnetite) acquires IRM in H≤300mT, but no additional IRM is acquired in

higher H. Maghemite shows the behaviour in between magnetite and hematite minerals. Thus, the IRM method can identify the magnetic minerals.

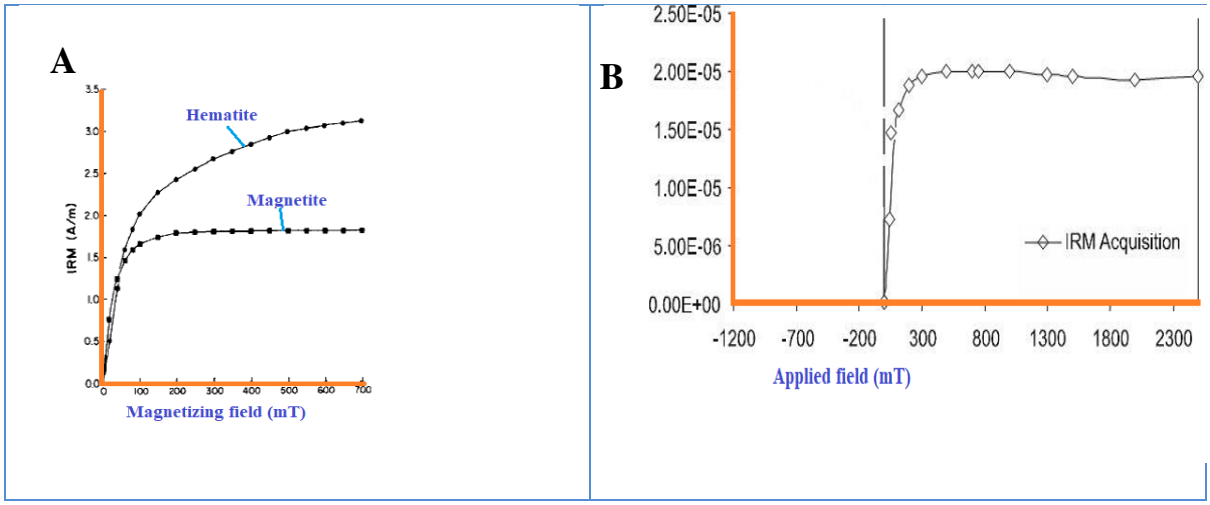

Figure 5.8 Representative isothermal remanent magnetization acquisition curves for (A) magnetite and hematite, (B) hematite.

Coercivity in hematite is commonly higher than that observed in magnetite. Hence, during IRM acquisition, it is more challenging to saturate hematite than magnetite. Magnetite is typically saturated by about 300-400mT. The magnetite-rich sample shows a steep rise in IRM acquisition up to 0.3T (300mT) at which point single domain magnetite grains are aligned in the field direction.

The IRM acquisition curves for most of the specimens investigated under this study (Fig 5.8) are characterized by low, medium and high coercivity components. The specimens with low coercivity component <400mT includes (GMS18-7B, 14-4B, 12-6B, 13-7B, 21-6B, 1-8B, 3-2B, 9-4B and 8-3B). Some specimens show a medium coercivity component with a saturation field of approximately 500mT (GMS15-5B, 19-6B, 1-9B, 2-2B, 5-9B, 6-10B, 7-6B and 10-4B) as well there are also specimens with high coercivity component that could not reach saturation at 1000mT (GMS23-6B, 22-6B and GMS17-4B). In the next pages the IRM acquisition curves are clearly described for the specimens that have been examined with their corresponding illustrations.

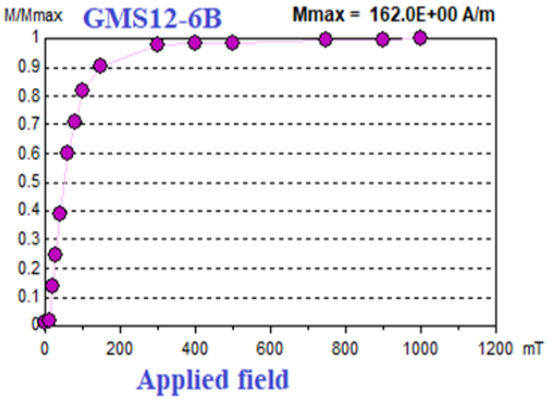
M/Mmax
GMS12-6B
Mmax = 162.0E+00 A/m
Applied field
mT

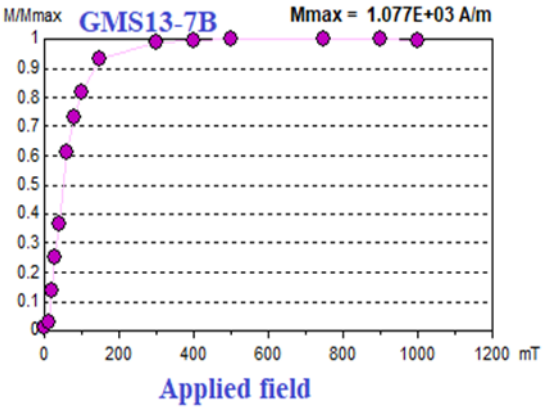
M/Mmax
GMS13-7B
Mmax = 1.077E+03 A/m
Applied field
mT

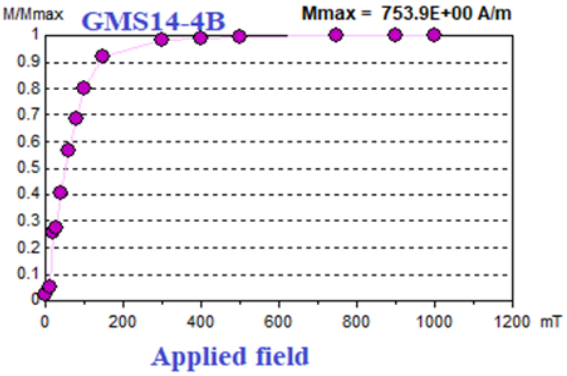
M/Mmax
GMS14-4B
Mmax = 753.9E+00 A/m
Applied field
mT

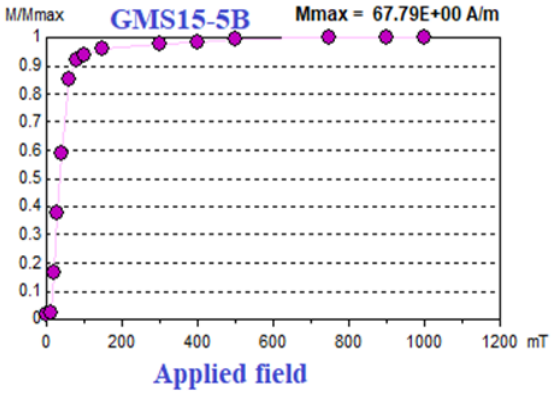
M/Mmax
GMS15-5B
Mmax = 67.79E+00 A/m
Applied field
mT

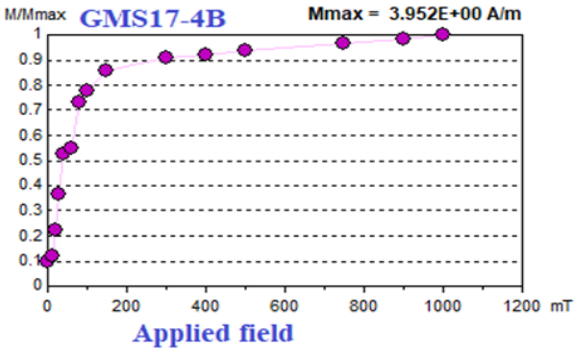
M/Mmax
GMS17-4B
Mmax = 3.952E+00 A/m
Applied field
mT

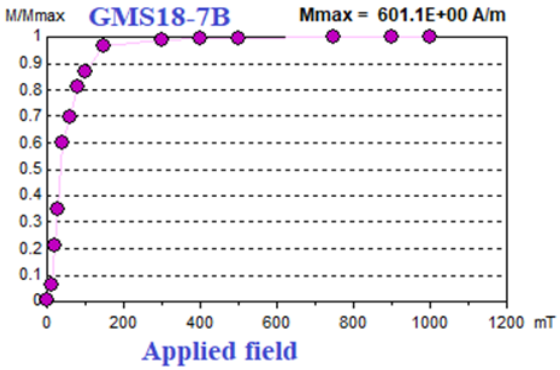
M/Mmax
GMS18-7B
Mmax = 601.1E+00 A/m
Applied field
mT

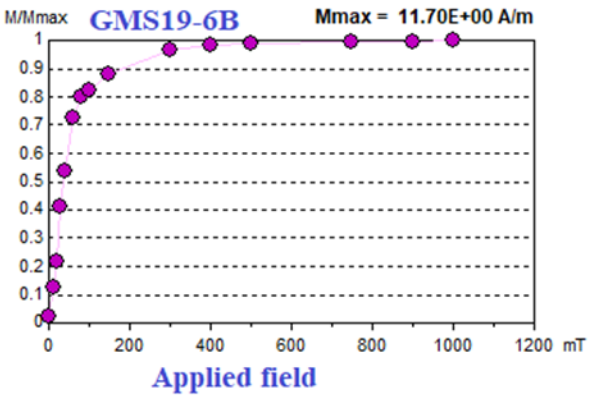
M/Mmax
GMS19-6B
Mmax = 11.70E+00 A/m
Applied field
mT

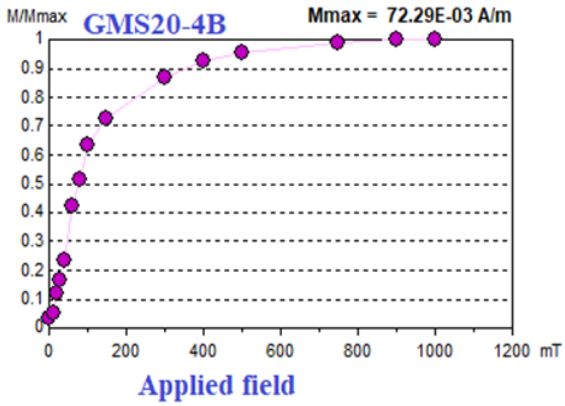
M/Mmax
GMS20-4B
Mmax = 72.29E-03 A/m
Applied field
mT

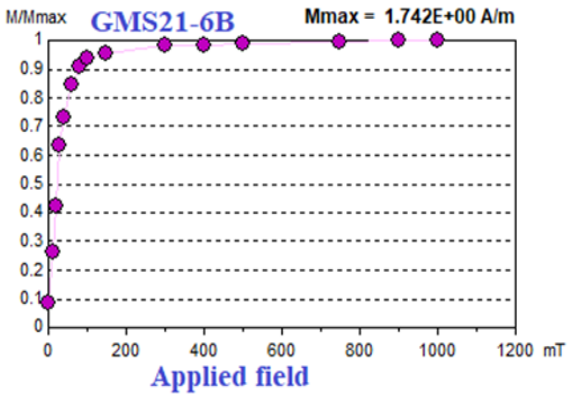
M/Mmax
GMS21-6B
Mmax = 1.742E+00 A/m
Applied field

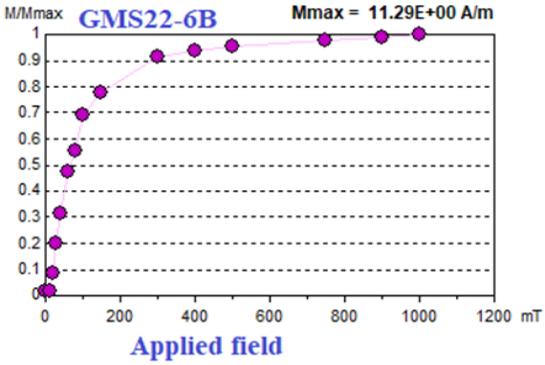
M/Mmax
GMS22-6B
Mmax = 11.29E+00 A/m
Applied field

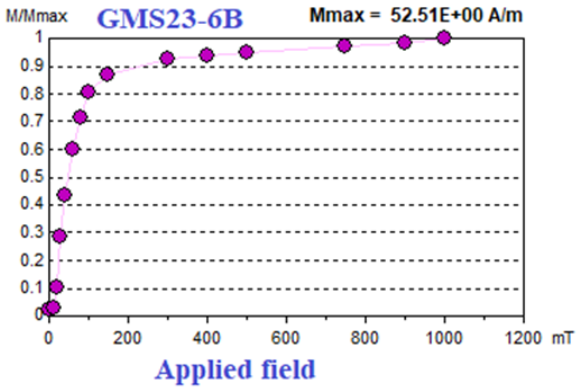
M/Mmax
GMS23-6B
Mmax = 52.51E+00 A/m
Applied field

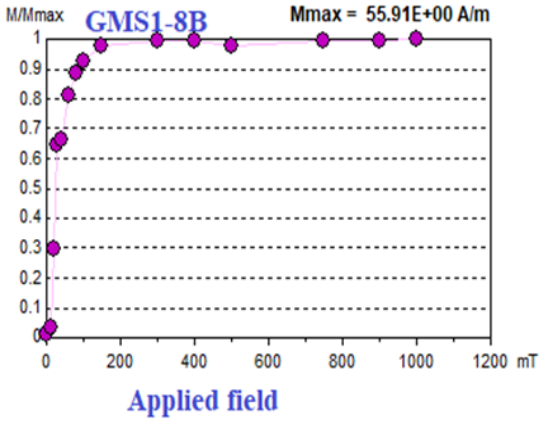
M/Mmax
GMS1-8B
Mmax = 55.91E+00 A/m
Applied field

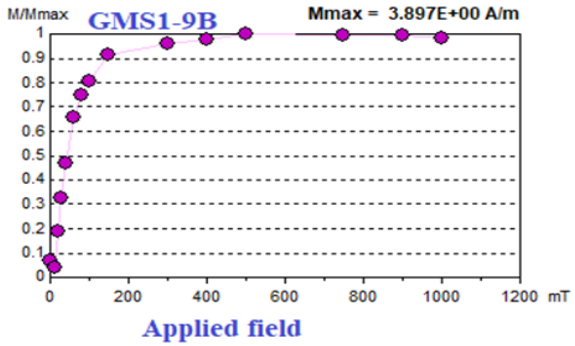
M/Mmax
GMS1-9B
Mmax = 3.897E+00 A/m
Applied field

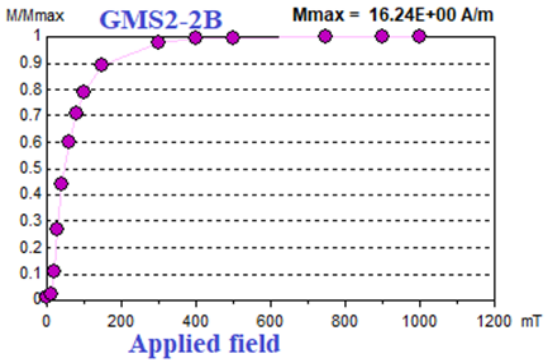
M/Mmax
GMS2-2B
Mmax = 16.24E+00 A/m
Applied field

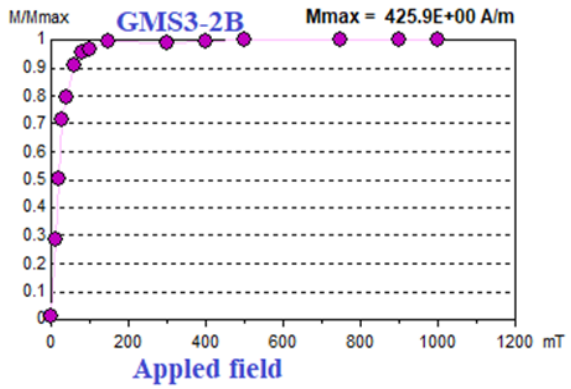
M/Mmax
GMS3-2B
Mmax = 425.9E+00 A/m
Appled field

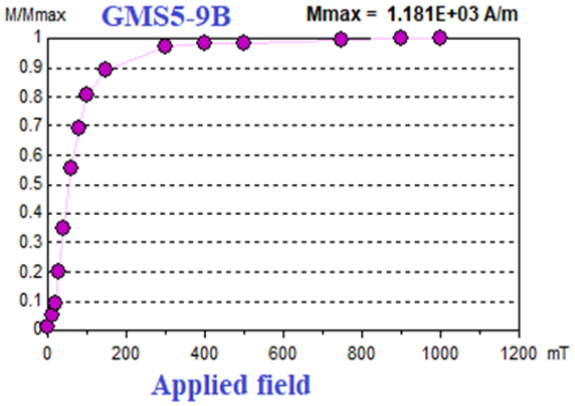
M/Mmax
GMS5-9B
Mmax = 1.181E+03 A/m
Applied field

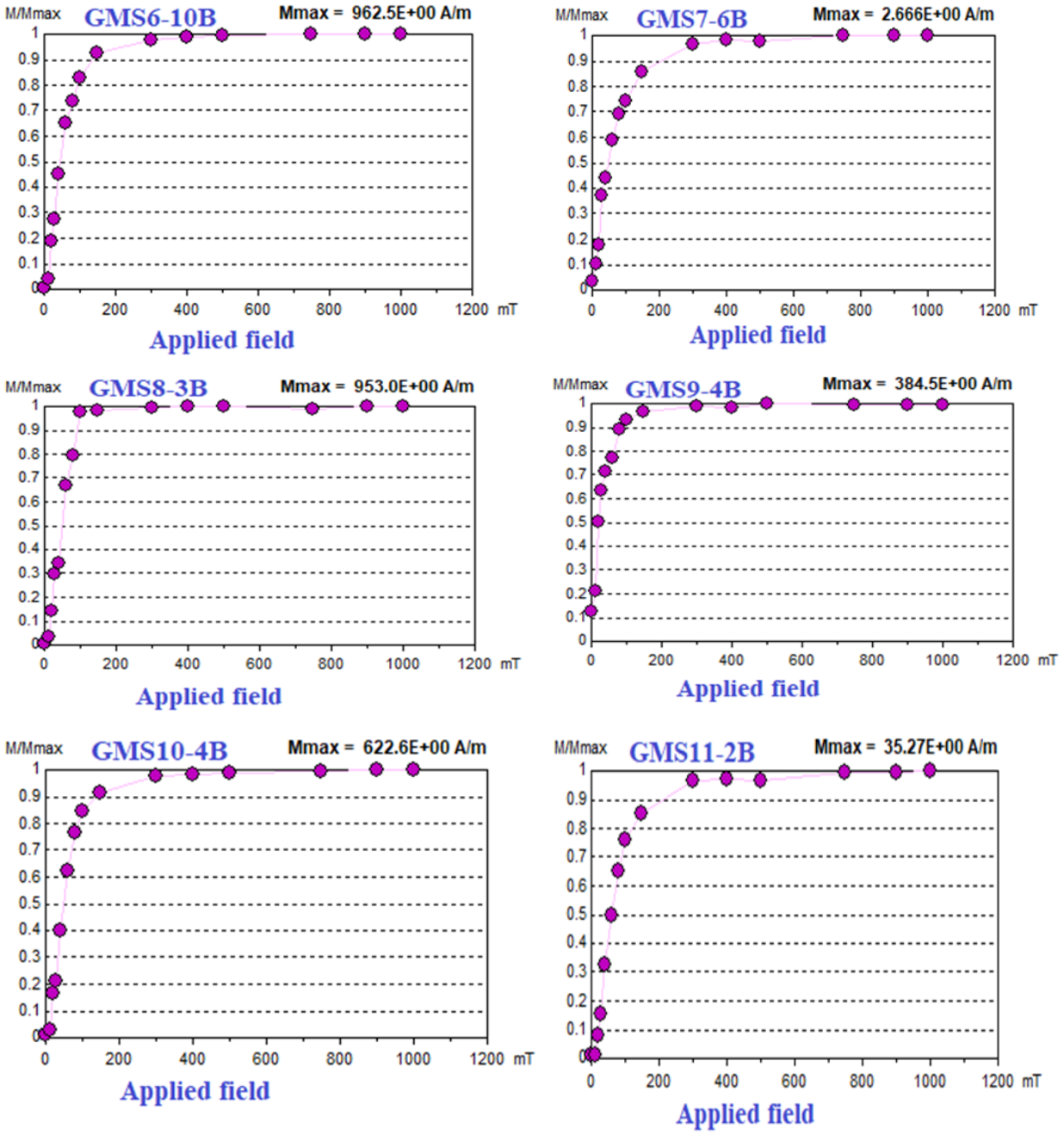

Fig 5.9) Isothermal Remanent Magnetization (IRM) acquisition for 22 representative specimens from each site (GMS12-6B, 13-7B, 14-4B, 15-5B, 17-4B, 18-7B, 19-6B, 20-4B, 21-6B, 22-6B, 23-6B, 1-8B, 1-9B, 2-2B, 3-2B, 5-9B, 6-10B, 7-6B, 8-3B, 9-4B, 10-4B and GMS11-2B) from the Gedemsa Magmatic Segment.

For basalt specimens (GMS13-7B, 14-4B, 18-78, 3-2B, *5-9B*, 6-10B, 8-3B, 9-4B, 10-4B), the IRM acquisition curve showed an initial rapid acquisition of ~98% of the maximum IRM typically reaches saturation by an applied magnetic field of <300mT, followed by smooth

coercivity field spectrum up to the maximum applied field of 1T(mT). The normalized NRM acquisitions of magnetization intensity curves show a steep increase in intensity up to 300 mT to saturation. But after about 300mT, a further increase in the applied magnetic field did not result in a corresponding rise in an acquisition. This indicates that magnetite whose coercivity spectrum of 300mT, is probably the main ferromagnetic mineral present in all the basalt specimens with some titanomagnetite.

Unlike basaltic specimens, which have dominantly of magnetite as ferromagnetic minerals, for ignimbrite specimens, more than one ferromagnetic mineral are perceived from the IRM acquisition curves. Specimens GMS21-6B and GMS1-9B reach a saturation magnetization at about 500mT. The normalized NRM acquisition of the magnetization intensity curve of these specimens show up to 500mT steeply increased intensity of magnetization due to the applied magnetic field. But after about 500mT, further increase in the applied magnetic field did not result in increased in the acquisition. This indicates that magnetite is probably the dominant ferromagnetic mineral present in these two ignimbrite specimens while minor amounts of titano-hematite could also be present. The same thing also happened for ignimbrite specimen GMS2-2B which reaches its saturation at 400mTand the probable ferromagnetic mineral for this specimen is magnetite with minor titano-hematite.

As observed from the IRM acquisition curves, specimen GMS1-8B is characterized by two ferromagnetic minerals which are saturated by different magnetizing field. One of the magnetic mineral in this site is most probably magnetite, which is saturated at 300mT; on the other hand the other magnetic mineral may be maghematite which has magnetic character between magnetite and hematite. Specimens GMS7-6B and GMS11-2B can be characterized by two magnetic minerals. The one which reaches 99% magnetization at 400mT applied magnetic field and the other which reaches saturation at 700-800mT. In this case the magnetic minerals most probably magnetite as the dominant and titanohematite proportion. The other ignimbrite specimens are GMS22-6B and GMS23-6B. In both cases, both of the specimens got 90% magnetization at 500mT but they did not saturation magnetization at the peak applied magnetic field of 1000mT (1T). These specimens indicate that the presence of both high and low coercivity of magnetic minerals (Fig.5.8) which reflecting the presence of

both magnetite (the low coercivity) and hematite (the high coercivity) as the magnetic carrier minerals in these two specimens.

The rhyolitic specimen, GMS20-4B, also got 90% magnetization at 400mT applied field and again got saturation magnetization at 900mT applied magnetic field. This indicates that this specimen is characterized by two magnetic carrier minerals, magnetite and titanohematite. The other specimen, GMS15-5B, reaches saturation magnetization at 400mT applied magnetic field. The normalized NRM acquisition of the magnetization intensity curve of this specimen shows up to 400mT steeply increased intensity of magnetization due to the applied magnetic field. But after about 400mT, further increase in the applied magnetic field did not result in an increased in the acquisition. This indicates that magnetite is the main ferromagnetic mineral in this specimen.

In general, results from IRM experiment on basalt, ignimbrite, and rhyolite specimens show different applied magnetic field was required for saturation magnetization to be reached. The IRM acquisition curves suggest that titanomagnetite, magnetite and titanohematite are the dominant magnetization carrier minerals for most of the sites. But, very few sites also showed the presence of a minor amount of hematite. The igneous rock yield two magnetic vectors, the primary magnetite vector acquired during the beginning stages of cooling processes which can be termed as ChRM and the secondary magnetic vector which came from the substantial alteration of magnetite due to the geological processes, lightning strike and due to other processes.

The IRM experiment was successful to recognize the magnetization carrier minerals, but sometimes it is rather useful to do other mineral identification techniques. So that, Curie temperature analysis has been conducted for those specimens investigated under the IRM acquisition study.

5.4.2 Curie Temperature Analysis

A Curie temperature analysis was conducted for 23 specimens, one specimen per site except for site 16 in which the specimen was broken during the laboratory work. This Curie temperature analysis provides a simple diagnosis of the magnetic minerals present within the rocks.

The selected specimens were subjected to heat in increasing steps with the presence of a steady magnetic field and then measuring the resulting remanent magnetization as a function of temperature as THD. Each of the procedures was the same as performed for the thermal demagnetization experiment. The main difference is that for Curie temperature analysis specimens first should be magnetized to their saturation level using an impulse magnetizer as described under the IRM acquisition study.

Thermal demagnetization was conducted following the IRM acquisition experiment for each specimen. The IRM decreases during thermal demagnetization as blocking temperatures are reached. The inflexion point determines the Curie temperature on the heating curve. From the investigated specimens, almost all components were unblocked between 560°C and 640°C. Graphic analyses of the thermal demagnetization curve of the acquired IRMs in Fig.5.9 indicate that the magnetite is dominant magnetic mineral and also hematite is present in less considerable quantity. These results indicate the dominance of magnetite minerals as clearly stated in the IRM acquisition experiment.

Table 5.2 Standard Curie temperatures for most common ferromagnetic minerals (Dunlop and Özdemir 1997)

Mineral	Curie/Neel temperature °C
Magnetite	580
Hematite	680
Maghemite	590-675
Goethite	120
Pyrrhotite	320

Maghemite exhibits magnetic character in between magnetite and hematite.

As can be inferred from Fig 5.9, specimens (GMS3-2B, 6-10B, 10-4B, 11-2B, 14-4B, and 21-6B) show a maximum unblocking temperature at 580^0C. This indicates that the main magnetic mineral in these specimens is magnetite. On the other hand, specimen GMS22-6A shows a maximum unblocking temperature at 640^0C. This temperature is characteristic for magnetite with some hematite which can be named Maghemite (table 5.2) mineral.

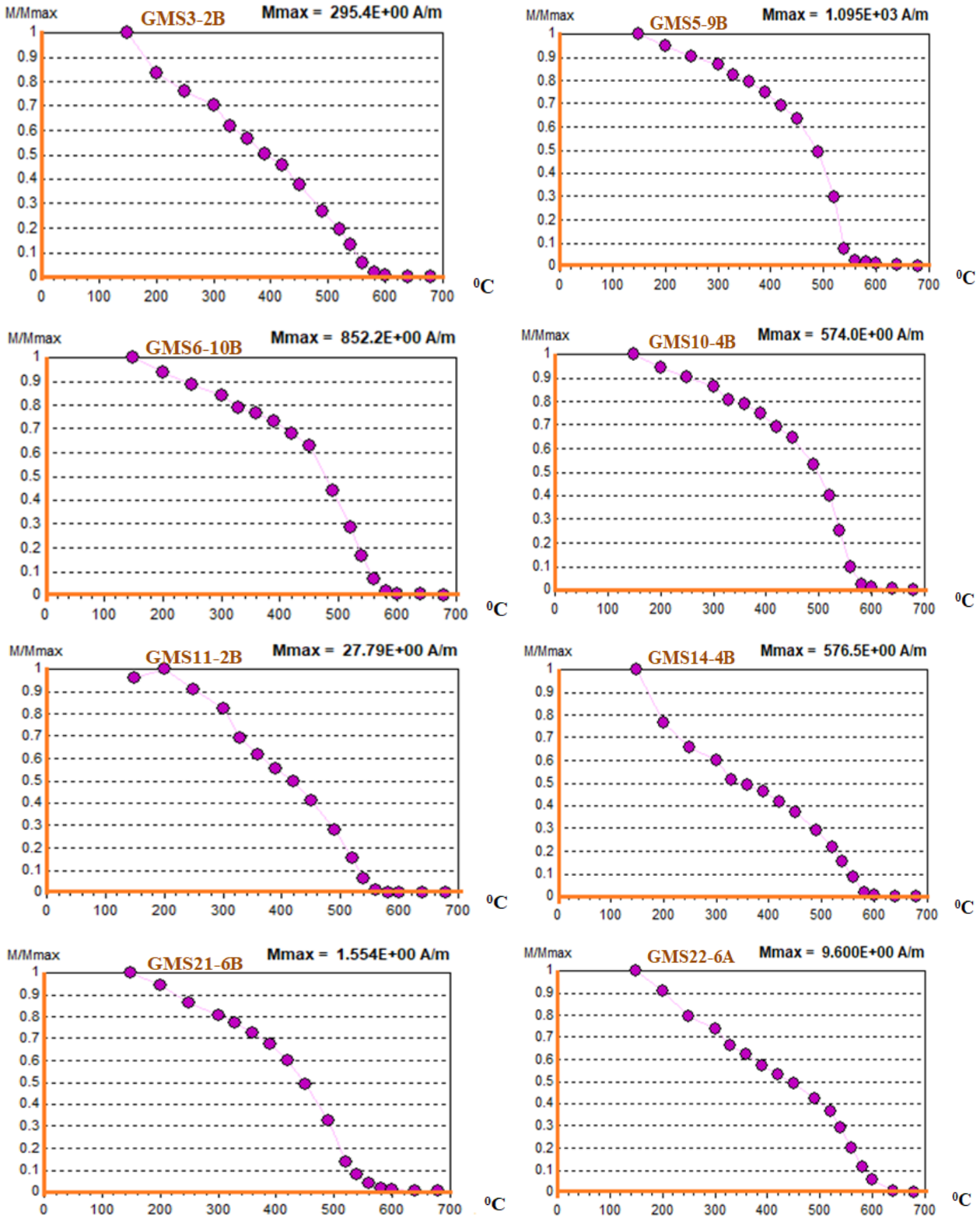

Fig 5.10) Selected specimens of thermal demagnetization which were analyzed for IRM acquisition study and now for Curie temperature analysis to confirm the magnetic mineralogy for representative specimens

Generally from the IRM acquisition experiment and the Curie temperature analyses it can be concluded that the magnetite is the primary dominant magnetic carrier remanent magnetization for most of the sites. But there is also a small amount of hematite mineral which came from the substantial alteration of magnetite due to the geological processes occurring in the area.

5.5 Paleomagnetic Direction

Both AF and TH partial demagnetization revealed two components of NRM (low stability and high stability components). The low stability component mostly has been cleaned by imposing an applied field of 10-30mT and/or a heating temperature of 330^0C-520^0C. The high stability component represents the Characteristic Remanent Magnetization (ChRM) which is characterized by a straight line segment directed to the origin in the Zijderveld diagram. It is this ChRM direction in which the calculation of the paleomagnetic direction relays on.

The directions of the ChRM component were determined by the principal component analysis using the best-fitting line of least square technique passing through the origin (Kirschvink, 1980). The maximum angular deviation (MAD) for most of the ChRM is less than five and no specimen had MAD >10. The ChRM components determined at specimen level then used to calculate the site mean direction using Fisher (1953) statistics for combined analysis of remagnetization circles and stable linear segments. Finally, the site's mean direction was utilized to calculate the overall mean direction of the study area using the Paleomac6.5 software (Cogne, 2003).

In calculating the overall mean direction for several levels of paleomagnetic data the following points are considered (Butler, 1992);

- When more than one specimen is prepared from a single core sample, the ChRM directions for multiple specimens must be averaged.
- A site-mean ChRM direction is then calculated from the specimens ChRM directions.
- The Paleomagnetic investigation involves numerous sites within the particular rock unit, which are then combined to give the overall ChRM mean direction of the formation.

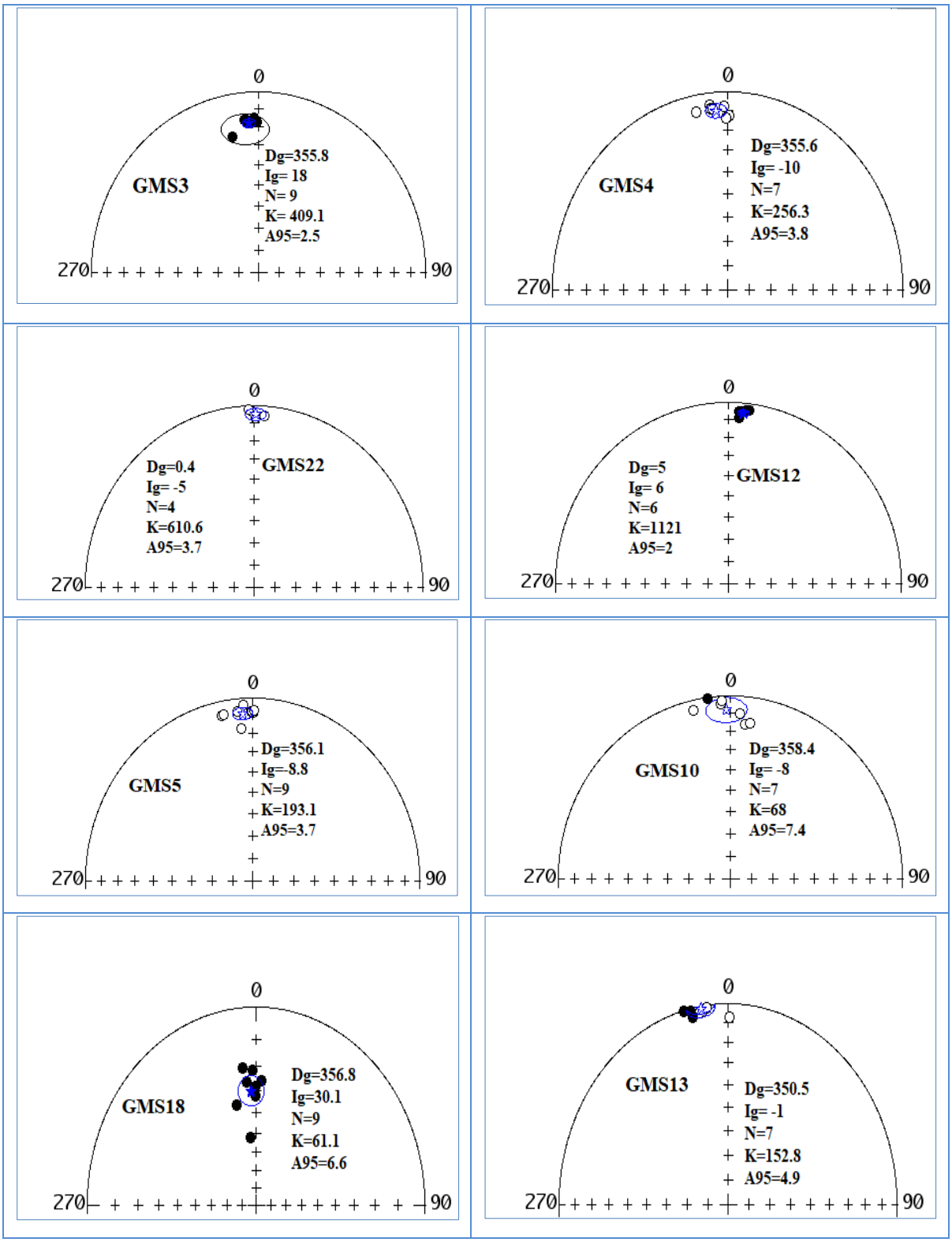

Fig 5.11) some of the selected sites mean direction showing the Characteristic remanent direction after the removal of the secondary soft overprint through Thermal and Alternating field demagnetization

Table 5.3 Paleomagnetic site mean directions for all the analyzed rocks are reported. The overall mean directions calculated for the 20 sites considered are also given. Colored numbers indicate the rejected sites in the mean paleomagnetic direction calculation.

Site Id	Coordinates		N	Dg(^{0})	Ig(^{0})	K	α95	P
	Lat.	Long.						
GMS1	522920	936682	4	18.7	25.7	153.9	7.4	N
GMS2	522932	936717	7	17.7	28.6	193.6	4.3	N
GMS3	518693	913105	9	355.8	18	409.1	2.5	N
GMS4	517978	914366	7	355.6	10	256.3	3.9	N
GMS5	517978	914366	9	356.1	-8.8	193.1	3.7	N
GMS6	520581	912560	14	352.5	-2.6	37.5	6.6	N
GMS7	519179	913329	3	332.4	39.6	25	15	N
GMS8	520890	913763	4	355.4	24.8	39.5	14.8	N
GMS9	522684	912915	5	59.6	-13.7	3.4	49.9	N
GMS10	523556	914437	7	358.4	-8	68	7.4	N
GMS11	524118	916290	5	12.4	4.4	231.9	5	N
GMS12	524371	916560	6	5	6	1121	2	N
GMS13	524718	916579	7	350.1	-1	152.8	4.9	N
GMS14	525522	916501	4	8.8	12.6	64.3	11.5	N
GMS15	527808	916837	6	358.1	11.2	36.8	11.2	N
GMS16	533254	919355	4	4.4	8.2	137.1	7.9	N
GMS17	517452	921844	5	356.8	0.8	25.1	15.6	N
GMS18	524822	935333	9	356.8	30.1	61.1	6.6	N
GMS19	520530	922336	5	8.7	15.7	157.7	6.1	N
GMS20	522724	924711	5	110.5	-11	3.5	48.1	N
GMS21	521969	927210	6	344.3	-19.1	1.1	0	N
GMS22	522490	927946	4	0.4	-5	610.6	3.7	N
GMS23	522148	932645	3	335.5	0.4	1146	7.4	N
Over all mean direction			20	359.1	9.6	20	7.5	N
Expected mean direction			32	1.9	13.5	105.6	2.5	

Remark: Site ID, site name; location coordinates (latitude and longitude); N, number of samples; Dg and Ig, declination and inclination in geographic coordinates: K, Fischer precision

parameter; A95, 95% confidence interval. GMS9, 20 and 21 highlighted in blue are sites rejected from overall mean direction based on statistical criteria

As shown from the table (5.3), in different paleomagnetic sites, the results have different quality parameters, for instance, K and α95 are excellent for sites GMS23, 12, 22, and 3 whereas relatively poor for sites GMS7 and 17 since statistical parameters, K needs to be large, and at least a minimum of 25 and α95 need to be very small. According to these parameters paleomagnetic results from sites GMS9, 20, and 21were rejected from overall mean direction based on statistical criteria.

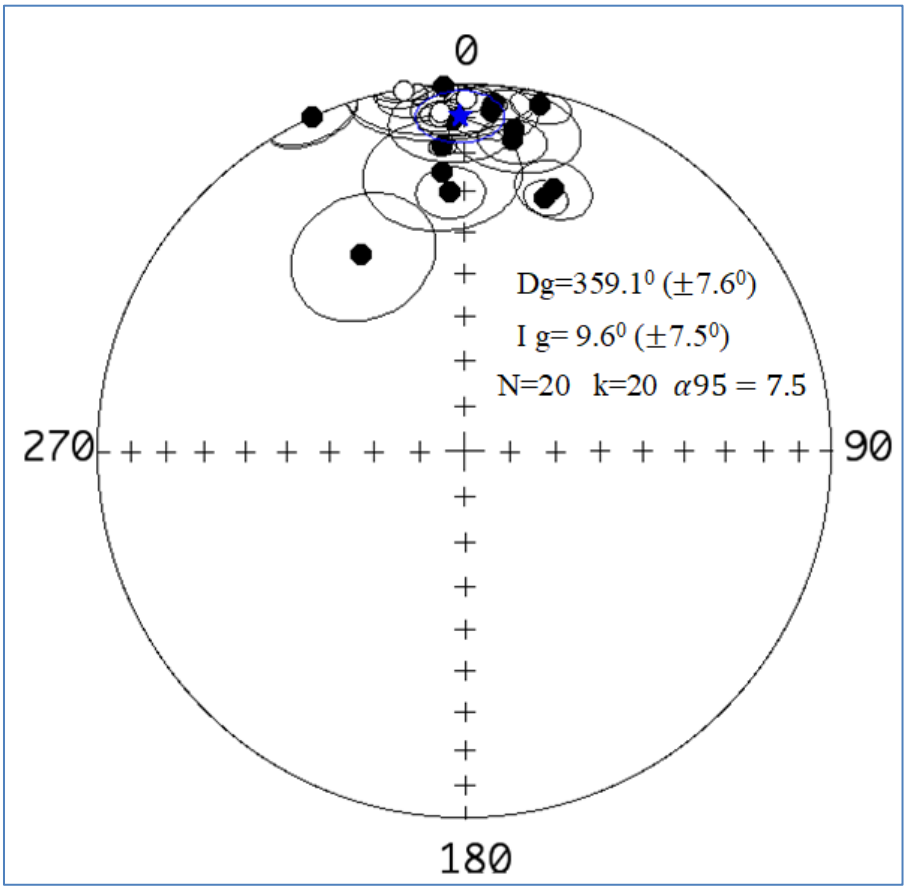

Fig 5.12) Stereographic projections of site mean ChRM directions (after the removal of secondary overprints), 20 sites of normal polarity out of 23 sites, three of them rejected according to the statistical criteria followed, the solid blue star shows the ChRM mean direction, the surrounding black circle shows 95% confidence limit

CHAPTER SIX

DISCUSSION

6.1 INTRODUCTION

This paleomagnetic investigation from the Gedemsa and surrounding area of the central MER provides important constraints on the deformation style of the region. Previous studies from the Assela area (south of the present study area) shows negligible vertical axis rotation. Whereas, in the northern MER (near Fantale and Dofan), crustal blocks have been rotated by about $\sim 7^0$ counter-clockwise senses (Tesfaye Kidane et al., 2009; Kahsay Nugsse et al., 2018). These studies are in perfect agreement with recent structural analysis on faults, which indicate that transtensional deformation increase as we go towards the northern MER (Siegburg et al., 2020). Hence, the result of this study which is situated in the Gedemsa magmatic segment of the central MER shows $\sim 3^0$ counter-clockwise crustal block rotation. It can be suggested that the transtensional deformation increase towards the northern MER.

6.2 Statistical Criterias and Magnetization Components

To select the reliable paleomagnetic directions, the cone of confidence at 95 levels is used as the primary statistical criteria. In the present study, the values of α95 for the group mean values are less than or equal to 15^0 with only one site having α95=15.6. The precision parameter, K, is also considered as one of the statistical criteria. In this study all the selected site means have a precision parameter greater than ten.

The intensity and directional results of demagnetization of the specimens after the isolation of ChRM have been averaged per each site to determine the groups mean paleomagnetic directions. Based on the above criterias, groups/sites were selected to calculate the overall mean paleomagnetic direction. The observed paleomagnetic direction later compared with the expected paleomagnetic direction to investigate the crustal block rotation with the vertical axis in the study area.

From the progressive demagnetization analyses, two magnetic remanence components have been identified. The first one is the secondary overprint carried by magnetic minerals of low blocking temperature (mostly $<300^0$C) and low coercivity (<20-30mT). This component

leads to uncertainty and confusion on the interpretation of the ChRM direction. Since these components did not represent the original magnetization of rocks acquired during the formation of the rock.

The secondary overprint magnetizations were developed due to the different tectonic and geological processes. As well as the lightning strike also played its own role in developing these magnetizations. These components cause some scattered directions around the present earth's magnetic field. These components were effectively removed by the progressive demagnetization processes. Since the rocks sampled were igneous rocks, and in addition based on the results obtained, the ChRM seems to be of primary origin and could be understood as the primary thermal remnant magnetization (TRM). This indicates that the paleomagnetic fields were developed at the time of cooling of these rocks.

The second and an essential magnetic remanent component is the ChRM directions which is characterized by a straight line segment directed to the origin in the Zijderveld diagram. This component identified after the demagnetization of the specimen for approximately 520^0C and 30mT in thermal and alternative field demagnetization, respectively. This component is used for the interpretation of paleomagnetic results.

6.3 Magnetization Carrier Minerals

Routine rock magnetic experiments have been accompanied for the identification of magnetization Carrier Minerals. First, IRM acquisition experiment for selected specimens of each paleomagnetic sites was performed. Those specimens were utilized for the identification of magnetic mineralogy by analyzing the saturation magnetization obtained from the experiment. After analyzing the saturation magnetization, specimens again subjected to thermal demagnetization to confirm the identification of the magnetic mineralogy through the analysis of the Curie temperature.

From the IRM acquisition experiments, it can be observed that all the studied basaltic specimens were begun to saturate in the applied field of 200 to 300mT and/or completely saturated at 400mT indicating that the dominant magnetic mineral in the samples are magnetite and titanomagnetite. This can also be confirmed from the heating curves of thermal

demagnetization, and it can be observed that the curve drops to zero at 580^0C-585^0C (Curie point of magnetite) indicating the magnetite as the primary magnetic mineral in the samples.

In the case of the ignimbrites, rhyolites and volcanic tuff samples, the rock magnetic experiment shows a little bit variation in saturation magnetization and also different Curie points. This suggests that these rocks may contain multiple magnetization carrier minerals. For instance, ignimbrite specimens GMS7-6B and GMS11-2B can be characterized by two magnetic minerals. These are, the one which reaches 99% magnetization at 400mT magnetic field, and the other at 700-800mT. This indicates that magnetite is the dominant magnetization carrier minerals with small titanohematite for both specimens. The other ignimbrite specimens are GMS22-6B and GMS23-6B. In both cases, both of the specimens attain 90% magnetization at 500mT but they did not attain saturation magnetization at the peak applied magnetic field of 1000mT (1T). These specimens indicate that the presence of hematite and magnetite as the magnetization carrier minerals (Fig.5.8).

Similarly, the rhyolitic specimen, GMS20-4B, attain 90% magnetization at 400mT applied field and again got saturation magnetization at 900mT applied magnetic field. This also suggests that the rock contains magnetite and titanohematite as magnetization carrier minerals. The other specimen, which is volcanic tuff, GMS15-5B, reaches saturation magnetization at 400mT applied magnetic field. The normalized NRM acquisition of magnetization intensity curve of these specimens shows up to 400mT steeply increased intensity of magnetization due to the applied magnetic field. But, after about 400mT, further increase in the applied magnetic field did not result in an increased saturation. This suggests that magnetite is the main magnetization carrier mineral in this specimen.

Similar to the basalt specimens, some ignimbrite specimens are characterized by magnetite as the dominance of magnetic minerals without the evidence of significant hematite. As mentioned earlier, this indicates that these parts of ignimbrites are not subjected to chemical alteration by the ongoing geological processes. For example (Fig 5.8), specimens GMS21-6B and GMS1-9B reach saturation magnetization at only 500mT. The normalized NRM acquisition of magnetization intensity curve of these specimens shows up to 500mT steeply increased intensity of magnetization due to the applied magnetic field. But after about 500mT further increase in the applied magnetic field did not result in increased in an acquisition.

This indicates that magnetite and titanomagnetite are probably the dominant ferromagnetic mineral present in these two ignimbrite specimens.

The Curie temperature analysis results also consistent with the Isothermal remanent magnetization experiments. Progressive heating and temperature measurements indicated Curie temperature ranging between 560°C-580°C for most basalt and some ignimbrite specimens and between 600°C - 640°C for ignimbrites and other rock units, suggesting the magnetic mineralogy to be titanomagnetite and magnetite for the former and magnetite and titanohematite for the latter (Fig 5.9) Curie points. It is observed that specimens GMS3-2B, GMS5-9B, GMS6-10B, GMS10-4B, GMS11-2B, GMS14-4B and GMS21-6B reach their Curie temperature at or below 580^0C, suggesting that titanomagnetite and magnetite are the dominant magnetic minerals in the sampled rocks. The Curie temperature for specimen (GMS22-6A) is 640°C, an indication of titanohematite as magnetization carrier minerals.

In conclusion, the IRM experiment shows titanomagnetite and magnetite are the main magnetic mineralogies for most of the sites (especially for basaltic specimens) with small amount of titanohematite and hematite magnetic minerals mostly on the ignimbrites, rhyolites and volcanic tuff specimens. The igneous rocks, in this case, can yield two magnetic vectors, primary magnetite vector acquiring during the beginning stages of cooling processes and secondary magnetic vectors which came from the strong alteration of primary minerals like magnetite due to the geological processes and due to other processes. Generally, it can be concluded that the IRM experiments and the Curie temperature analysis were effective for recognizing the magnetization carrier minerals.

6.4 Tectonic Rotation

Rotation of crustal block about the vertical axis is determined by comparing the observed declination and inclination values with the Apparent Polar Wander Path curve (Besse and Courtillot, 2003). The overall mean paleomagnetic directions of the ChRM result from 20 selected sites mean directions out of 23 sites in the Gedemsa Magmatic Segment (Dec=359.1^0, Inc=9.6^0, $\alpha 95$=7.5, N=20 and K=20) were compared with the corresponding expected mean paleomagnetic reference field direction of the stable African Apparent Polar Wander Path (AAPWP) curve of Besse and Courtillot (2003) for an average age of 1.5Ma

($D_{exp}=1.9^0$, $I_{exp}=13.5^0$, α=2.5, N=32, K=32). Vertical axis block rotation is computed by calculating the difference between the observed and expected declination values (eqn.1). The vertical-axis rotation, R is (Butler, 1992);

$$R = Do - Dx \quad \text{.....eqn1}$$

$$R = 359.1 - 361.9$$

$$\boldsymbol{R = -2.8}$$

The negative value indicates that the rotation is in counterclockwise sense

Where, Do is the observed declination

Dx is the expected declination .

The flattening of inclination is labeled F and is defined as;

$$F = Fx - Fo \quad \text{.....eqn2}$$

$F = 13.5 - 9.6$ Where, Fx observed inclination

$\boldsymbol{F = 3.9}$ Fo observed inclination

The positive flattening value suggests the observed inclination is flatter or shallower than the expected inclination.

From the above calculation, the result suggests that statistically small amount of counterclockwise vertical axis rotation has occurred at the Gedemsa Magmatic Segment on the Central Main Ethiopian Rift.

A model on the northern-central MER transition area (Corti et al. 2013) and paleomagnetic laboratory experiments performed in NMER suggested that both the border and rift axis faults exhibit almost pure dip-slip motion, and indicate significant local deflection in orientation of the extension direction at rift margins. That can be able to cause a local rotation/change in the orientation of the extension direction at rift margins. Minor counter-clockwise block rotations are required to accommodate the difference in slip direction along with the different fault systems. Most of the paleomagnetic, structural and geophysical data

from the northern MER and in the northern-central MER transition area suggested a consistent pattern of counterclockwise block rotation which is in agreement to the findings of the present study even though the rotation in this study is small in amount.

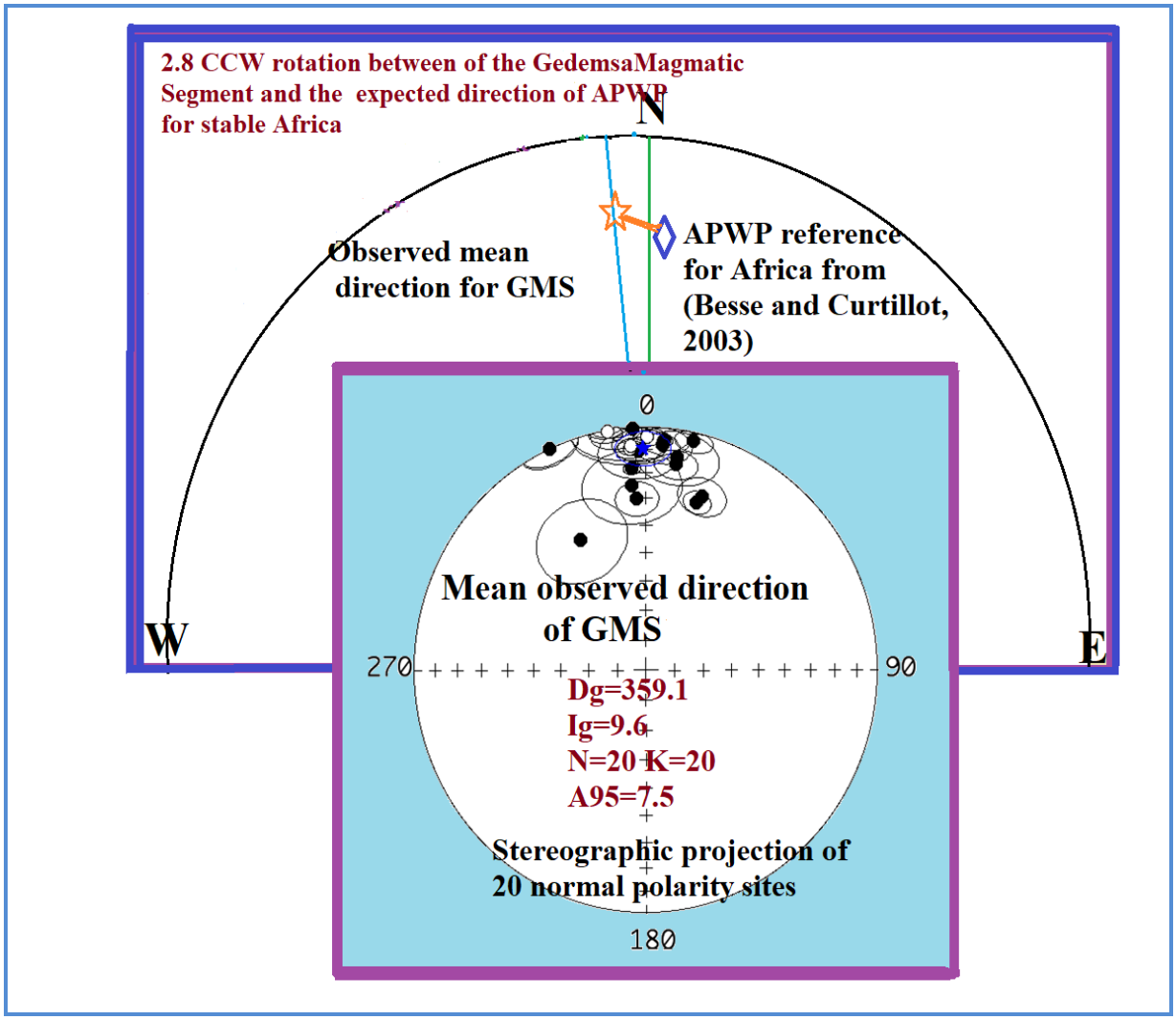

Fig 6.1) Schematic diagram, comparison of the site mean directions and the expected field directions for stable Africa, mean paleomagnetic directions computed from cooling unit in GMS (orange star) and expected paleomagnetic direction for ~1.5Ma stable African of APWP (blue diamond).

The observed rotation in the Gedemsa magmatic segment agrees well with previous paleomagnetic (Tesfaye Kidane et al. 2009, Kahsay Nugsse et al. 2018) and structural analysis (Siegburg et al., 2020). Paleomagnetic investigation (Tesfaye Kidane et al., 2009) suggests counter-clockwise rotation about the vertical axis with transtensional deformation has occurred in the Fantale magmatic segment. This result is in perfect agreement with the

analogue models of transtensional rifting fault geometry of the Main Ethiopian Rift (Casey et al., 2006). Kahsay Nugsse et al. (2018) in their paleomagnetic investigation on the Dofan magmatic segment also have identified a counterclockwise rotation (6.9^0) consistent with the prior results of Tesfaye Kidane et al., (2009) and the analogue modelling of Corti, et al. (2013). The result of this study also suggests the presence of counter-clockwise rotational deformation in the Gedemsa magmatic segment.

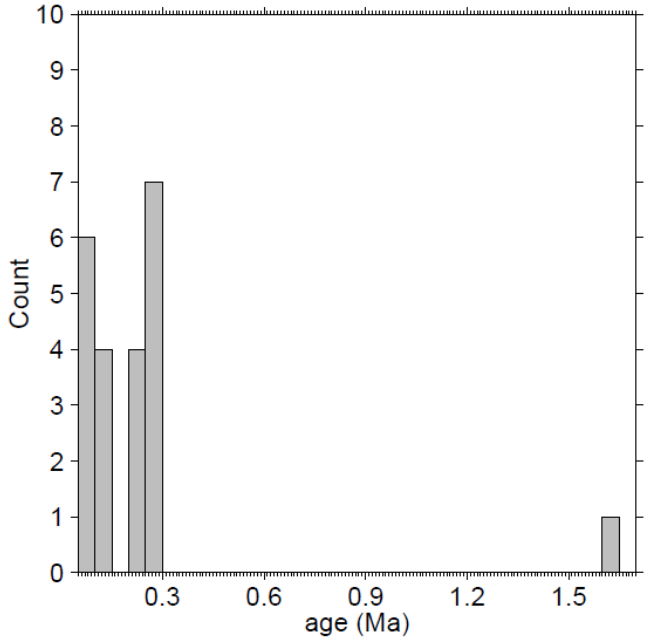

Fig 6.2) Histogram of the age data, Most of the rock units age younger than 0.3Ma and only one unit with an age of 1.6Ma

The small rotation in the Gedemsa area could be due to the young age of rocks sampled nevertheless it agrees with the recent fault slip analysis suggesting that transtensional deformation increases as we go to the northern MER (Siegburg et al., 2020).

Generally, the magmatic segments of the MER show trends of increasing counter-clockwise crustal block rotation towards the north. Similarly, the width of the rift and the number of identified faults increase in different magmatic segments towards the northern MER (Bastow et al., 2005; Maguire et al., 2006).

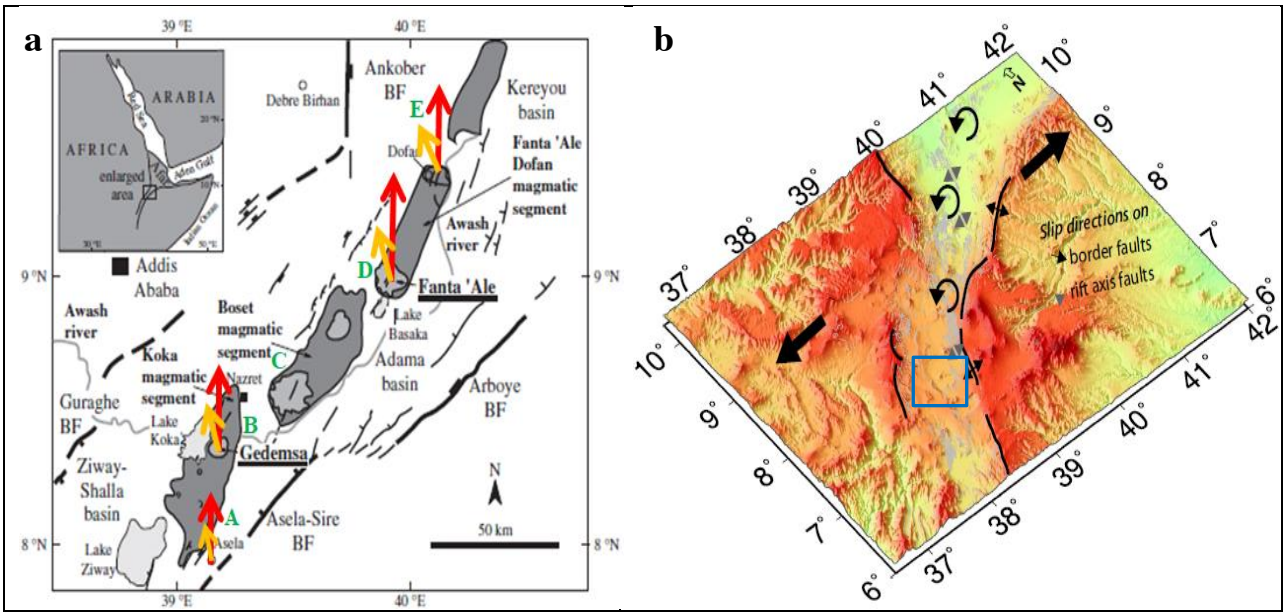

Fig 6.3 a) Structural map of the northern and central portions of the Main Ethiopian Rift including the magmatic segments (modified after Wolfenden et al., 2004): red arrows show the earth geographic north and the yellow arrows show the amount of counter-clockwise block rotation obtained on the different magmatic segments of the MER by different paleomagnetic investigations ; b) DEM map shows the pattern of the rift margin and rift axis faults with the slip direction on these faults and the general opening direction of the rift shown with arrows of different types (Adopted from Kahsay Nugsse et al., 2018), the blue open box shows the approximate location of the study area.

As observed in the Fig 6.3a, the MER experienced an increasing magnitude of counter-clockwise block rotation towards the north. From the Figure 6.3a; **A**- the result of Tesfaye Kidane et al., 2006 suggested that the Late Pliocene-Pleistocene rocks of the MER in the Asela area do not experienced significant vertical axis rotation (only 0.4^0). **B**-the result of the present study, suggests that small counter-clockwise crustal block rotation (2.8^0) characterize the Gedemsa magmatic segment. **C**-structural analysis presented by Siegburg et al., 2020 on the Boset magmatic segment; suggested that Large-scale obliquity in the northern MER increases towards Afar with transtensional kinematics for individual magmatic segments (from Gedemsa to Fantale). **D**-the result of Tesfaye Kidane et al., 2009 presented ~6.7^0 counterclockwise crustal block rotations about vertical axis consistent with the transtentional deformations that characterize the Fentale magmatic segment. **E**-the results of Kahsay Nugsse et al., 2018 suggested counterclockwise rotation about the vertical axis (6.9^0) with the transtentional deformations that characterize the Dofan magmatic segment.

Thus, from the above paleomagnetic investigations and structural analysis, it can be proposed that an increasing magnitude of counter clockwise vertical-axis rotation along the different magmatic segments in the MER characterised the heterogeneous deformation style along the strike of the Rift (e.g Tesfaye Kidane et al., 2006; 2009, Kahsay Nugsse et al., 2018, Siegburg et al., 2020).

CHAPTER SEVEN

CONCLUSION AND RECOMMENDATION

7.1 Conclusion

The paleomagnetic investigation was carried out in the Gedemsa magmatic segments, central MER. The rock magnetic experiment showed that titano-magnetite, magnetite, titano-hematite and a minor amount of hematite are the magnetization carrier minerals with a sound paleomagnetic direction. Thus, it can be concluded that the igneous rocks in the study area are an excellent recorder of paleomagnetic direction.

In all most all cases, for basalt samples the magnetization carrier minerals are titanomagnetite and magnetite with a minor amount of titano-hematite this indicates that basalts are not that much subjected to alteration effect since no significant hematite is observed which is considered to be the result of the alteration of magnetite. The primary magnetizations were acquired during the cooling of lava from TRM. On the other hand, the other lithologies sampled like ignimbrites and rhyolites, the remanent carriers are magnetite, titanohematite and some hematite. The presence of hematite is suggested to be the alteration product of magnetite due to the ongoing geological and tectonic processes.

Both the TH and AF techniques revealed identical orthogonal vector component diagrams for most samples. The thermal demagnetization and the alternative filed demagnetization techniques of the NRM of the pilot specimens showed two main magnetic components. The first one, the low-temperature (LTC)/ low coercivity component. These components regarded as the secondary overprint magnetization which may be due to a lightning strike, chemical alteration or other geological processes. These components were effectively erased during the demagnetization processes. The second magnetic components were a medium to high-temperature components/ medium to high-coercivity components which are carried by stable magnetic minerals. These components showed normal magnetic polarity, and it is these components interpreted as Characteristic Remanent Magnetization in which this paleomagnetic investigation relays on.

The characteristic remanent magnetization components were isolated successfully by the progressive demagnetization processes. From these ChRM the overall mean paleomagnetic direction were obtained in this study as D= 359.1, I= 9.6, N=20, K=20 and α95=7.4º.

The sites mean ChRM directions demonstrate excellent directional data sets recorded from the well exposed fresh basalt, ignimbrite and some other volcanic rocks. It is observed that a 2.8° counter-clockwise rotation of crustal blocks about a vertical axis in the Gedemsa magmatic segment has occurred. The observed rotation agrees very well with previous paleomagnetic and structural studies suggesting an increasing extension as we go from the central MER to the northern MER.

The northward increasing of the extension direction along the Main Ethiopian Rift is best characterised by the magmatic segments as indicated by the deformed volcanic edifices and an intense normal faults from Boset-Kone to Fantale-Dofan magmatic segments (Bastow et al., 2005; Maguire et al., 2006). Geochemical investigation along the MER (Furman et al. 2006) also suggested a south to the north increase in the amount of crustal and mantle lithospheric thinning. Paleomagnetic investigation on different magmatic segments (e.g. Tesfaye Kidane et al 2009, Kahsay Nugsse et al 2018) also suggests a north-ward increase in the crustal block rotation. Since this paleomagnetic investigation was conducted on the southernmost magmatic segment, Gedemsa Magmatic segment, relative to other magmatic segment, its result is consistent with increasing magnitude of counterclockwise rotation towards the northern MER. Hence the magnitude of the crustal block rotation in the Gedemsa magmatic segment is small relative to the result of other magmatic segments situated in the northern MER.

The study area is characterized by NNE–SSW, N-S and NE-SW few trending youngest rift axis normal faults which are part of the Wonji fault belts.

In this study ignimbrite and basalt rocks are considered as very good rocks for paleomagnetic investigations, because they recorded stable paleomagnetic directions and kept them through the geologic times. Thus, it can be concluded that these rocks can be considered an excellent recorder of paleomagnetic direction and used to conduct further tectonic studies in the Main Ethiopian Rift.

7.2 Recommendation

- Detailed paleomagnetic study along the MER should be conducted with having good radiometric age data to explain regional tectonics and geologic both along the rift axis and marginal faults.
- Polished section and petrographic analysis should be conducted to further characterize the magnetic mineralogy.
- Further studies should be conducted by comparing GPS and paleomagnetic studies to fully understand how the transtensional deformation is partitioned between strike-slip, dip-slip and block rotation.

References

Acton, G.D, Abera Tessema, Jackson, M. and Bilham, R. (2000). The tectonic and geomagnetic significance of paleomagnetic observations from volcanic rocks from central Afar. *Africa Earth and Planetary Science Letters*. **180(3)**:225-241.

Acocella, V. and Tesfaye Korme. (2002). Holocene extension direction along the main Ethiopian rift. East Africa. *Terra Nova,* **14(3)**:191-197. DOI:10.1046/j.1365-3121.2002.00403.x.

Agostini, A., G. Corti, A. Zeoli, and Genene Mulugeta. (2009). Evolution, pattern, and partitioning of deformation during oblique continental rifting: Inferences from lithospheric-scale centrifuge models, *Geochem*. *Geophys*. *Geosyst*, **10:**11-15, DOI:10.1029/2009GC002676.

Agostini, A., Bonini, M., Corti, G., Sani, F., Mazzarini, F. (2011a). Fault architecture in the Main Ethiopian Rift and comparison with experimental models: Implications for rift evolution and Nubia-Somalia kinematics. *Earth and Planetary Science Letters*, **301(3-4)**:479–492. https://DOI.org/10.1016/j.epsl.2010.11.024.

Alula Damte, Boccaleti Mario, Getaneh Assefa, Mazzouli Roberto, and Tortorici Luigi. (1992). Geological Map of the Nazret-Dera region (Main Ethiopian Rift). Consiglio Nazionale Delle Ricerche, Italy.

Ameha Atnafu, Tesfaye Kidane, Rowland, J. and Bachtadse, V. (2013). Counter clockwise block rotation linked to southward propagation and overlap of sub-aerial Red Sea Rift segments, Afar Depression: Insight from paleomagnetism. *Tectonophysics,* **593:** 111-120.

Argus, D. F., and R. G. Gordon. (1991). No-net-rotation model of current plate velocities incorporating plate motion model NUVEL-1, *Geophys*. *Res*. *Lett*., **18**: 2039–2042.

Atalay Ayele. (2000). Normal left-oblique fault mechanisms as an indication of sinistral deformation between the Nubian and Somalian plates in the Main Ethiopian Rift, J. *Afr*. *Earth Sci*., **31**: 359–367.

Bastow, I. D., Stuart, G. W., Kendall, J.M. and Ebinger, C. J. (2005). Upper-mantle seismic structure in a region of incipient continental breakup: northern Ethiopian rift. *Geophysical Journal International*, ***162*(2)**: 479-493.

Bekele Abebe, Tilahun Mammo, Asfaw Teklu and Yiheyis Kebede. (2007). Compilation of the geoscientific study of the Dofan-Fantale geothermal prospect, Ethiopia. Geological Survey of Ethiopia, Addis Ababa.

Besse, J. and Courtillot, V. (1991). Revised and synthetic apparent polar wander paths of the African, Eurasian, North American and Indian plates and true polar wander since 200 Ma. *Journal of Geophysical Research: Solid Earth (1978–2012)*, ***96*****(B3)**: 4029-4050.

Besse, J. and Courtillot, V. (2003). Apparent and True Polar wander and the geometry of the geomagnetic field in the last 200 million years. *J*. *Geophys*. *Res*. **108(B10):**2469, *DOI:10.1029/2003JB002684*.

Bigazzi, G., Bonadonna, F., Di Paola, G. and Giuliani, A. (1981). New K-Ar and Fission-track ages of the last volcanotectonic phase in the Ethiopian Rift Valley. (Tullu-Moye area). Proceedings of the First International Symposium on Crustal Movements in Africa. 141-159.

Bigazzi, B., Bonadonna, F., Di Paola, G. and Giuliani, A. (1993). K-Ar and fission track ages of the last volcano tectonic phase in the Ethiopian Rift Valley (Tullu Moye area). Geology and mineral resources of Somalia and surrounding regions. Istituto Agronomico Oltremare, Firenze, *Relazioni Monografie*, **113:** 311-322.

Bilham, R., Bendick, R., Larson, K., Mohr, P., Braun, J., Samson Tesfaye and Laikemariam Asfaw. (1999). Secular and tidal strain across the Main Ethiopian Rift. *Geophysical Research Letters*, **26(18)**: 2789-2792.

Boccaletti, M., Getaneh Asefa and Tortorici, L. (1992). The Main Ethiopian Rift: an example of oblique rifting. *Ann*. *Tecton*. **6**: 20–25.

Boccaletti, M. et al. (1995). Chemical variations in a bimodal magma system: the Plio-quaternary volcanism in the Dera Nazret area (MER, Ethiopia). *Africa Geosciences Review*, **1**: 37-60.

Boccaletti, M., Bonini, M., Mazzuoli, R., Bekele Abebe, Piccardi, L. and Tortorici, L. (1998). Quaternary oblique extensional tectonics in the Ethiopian Rift (Horn of Africa). *Tectonophysics*, **287(1):** 97-116.

Bonini, M., Souriot, T., Boccaletti, M. and Brun, J. P. (1997). Successive orthogonal and oblique extension episodes in a rift zone: laboratory experiments with application to the Ethiopian Rift. *Tectonics,* **16(2)**: 347-362.

Bonini, M., Corti, G., Innocenti, F., Manetti, P., Mazzarini, F., Tsegaye Abebe and Pecskay, Z. (2005). Evolution of the Main Ethiopian Rift in the frame of Afar and Kenya rifts propagation. *Tectonics, **24*** **(1)**.

Brock, A., Gibson, I. and Gacii, P. (1970). The Palaeomagnetism of the Ethiopian flood basalt succession near Addis Ababa. *Geophysical Journal International,* **19(5)**: 485-497.

Butler, R. F. (1992). Paleomagnetism: magnetic domains to geologic terranes. Oxford, *Black well Scientific Publications Boston*.

Casey, M., Ebinger, C., Keir, D., Gloaguen, R. and Mohamed, F. (2006). Strain accommodation in transitional rifts: extension by magma intrusion and faulting in Ethiopian rift magmatic segments. *Special publication-geological Society of London,* **259**: 143.

Chorowicz, J., Collet, B., Bonavia, F. F. and Tesfay Korme. (1994). Northwest to north-northwest extension direction in the Ethiopian rift deduced from the orientation of extension structures and fault-slip analysis. *Geological Society of America Bulletin, **106*****(12):*** 1560-1570.

Chorowicz, J. (2005). The East African Rift System. Journal of African Earth Sciences, **43**: 379– 410.

Cogne, J. (2003). PaleoMac: a Macintosh™ application for treating paleomagnetic data and making plate reconstructions. *Geochemistry, Geophysics, Geosystems,* **4(1).**

Collinson, D. (1983). Methods in palaeomagnetism and rock magnetism. Chapman and Hall, London.

Corti, G. (2008). Control of rift obliquity on the evolution and segmentation of the main Ethiopian rift. *Nature Geoscience,* **1(4)**: 258-262.

Corti, G. (2009). Continental rift evolution: From rift initiation to incipient break-up in the Main Ethiopian Rift, East Africa. *Earth-Sci. Review,* **96**: 1–53.

Corti, G., Philippon, M., Sani, F., Keir, D. and Tesfaye Kidane. (2013). Re-orientation of the extension direction and pure extensional faulting at oblique rift margins: comparison between the Main Ethiopian Rift and laboratory experiments. *Terra Nova*, **25(5):** 396-404.

Corti, G., Paola Molin, Andrea Sembroni, Ian D. Bastow, Derek Keir. (2018). Control of pre-rift lithospheric structure on the architecture and evolution of continental rifts: insights from the Main Ethiopian Rift, East Africa. DOI: **10**: 1002/2017TC004799.

Courtillot, V., Achache, J., Landre, F., Bonhommet, N., Montigny, R. and Féraud, G. (1984). Episodic spreading and rift propagation: new paleomagnetic and geochronologic data from the Afar nascent passive margin. *Journal of Geophysical Research: Solid Earth*, **89(B5):** 3315-3333.

Dankers, P. (1981). Relationship between median destructive field and remanent coercive forces for dispersed natural magnetite, titanomagnetite and hematite, *Geophys*. *J*. *Roy*. *Astr*. *Soc*. **64**:461-477.

Davidson, A. and Rex, D. (1980). Age of volcanism and rifting in southwestern Ethiopia.

Di Paola, G. M. (1970). Geological-Geothermal report on the central part of the Ethiopian rift valley. Report Ethiopian Institute Geological Survey, 46.

Di Paola, G.M. (1972). The Ethiopian Rift Valley (between 7° and 8°40_ lat North). *Bull*. *Volcano*. **35**:497–506.

Dunlop, D.J. (1972). Magnetic mineralogy of unheated and heated red sediments by coercivity spectrum analysis, *Geophys*. *J*. *Roy*. *Astr*. *Soc*., **27**: 37-55.

Dunlop, D.J. and Özdemir, O., (1997). Rock Magnetism: Fundamentals and Frontiers. Cambridge Uni. Press, 117-118.

Ebinger, C. et al. (2000). Rift deflection, migration, and propagation: Linkage of the Ethiopian and Eastern rifts, *Africa*. *Geological Society of America Bulletin*, **112(2)**: 163-176.

Ebinger, C. and Casey, M. (2001). Continental breakup in magmatic provinces: An Ethiopian example. *Geology*, **29(6)**: 527-530.

Ebinger, C. (2005). Continental break-up: The East African perspective. *Astron*. *Geophys*. **46**: 216–221.

Fernandes, R., et al. (2004). Angular velocities of Nubia and Somalia from continuous GPS data: Implications on present-day relative kinematics, *Earth planet*.*sci*. *Lett*. **222**: 197-208.

Fisher, R. (1953). *Dispersion on a sphere*, **217**: 295-305.

Furman, T., Bryce, J., Rooney, T., Hanan, B., Gezahegn Yirgu and Dereje Ayalew. (2006). Heads and tails: 30 million years of the Afar plume. Geological Society, *London, Special Publications*, **259(1)**: 95-119.

Gibson, I., Tazieff, H. and Hepworth, J. (1970). The structure of Afar and the northern part of the Ethiopian rift. Philosophical Transactions of the Royal Society of London A. *Mathematical, Physical and Engineering Sciences*, **267(1181):** 331-338.

Gidey Woldegabriel, Aronson, J. L. and Walter, R. C. (1990). Geology, geochronology, and rift basin development in the central sector of the main Ethiopia rift. *Geological Society of America Bulletin*, **102(4)**: 439-458.

Gidey Woldegabriel, et al. (1992). Kesem-Kebena: a newly discovered paleoanthropological research area in Ethiopia. *Journal of Field Archaeology*, 471-493.

Halls, H.C. (1976). A least-squares method to find a remanence direction from converging remagnetization circles. *Geophysical Journal International*, **45(2):** 297-304.

Hayward, N.J., Ebinger, C.J,. (1996). Variations in the along-axis segmentation of the Afar rift system. *Tectonics* **15**: 244–257.

Hofmann, C., et al. (1997). Timing of the Ethiopian flood basalt event and implications for plume and global change. *Nature*, **389:**838–841.

(https://geology.com/articles/east-africa-rift.shtml).

Irving, E. (1979). Paleopoles and paleolatitudes of North America and speculations about displaced terrains. *Canadian Journal of Earth Sciences*, **16(3):** 669-694.

Jestin, F., P. Huchon, and M. Gaulier. (1994). The Somalia plate and the East African Rift system: Present-day kinematics, Geophys. J. Int., **116**:637–654.

Kahsay Nigusse, Ameha Atnafu & Tesfaye Kidane. (2018). Paleomagnetic evidence for counterclockwise rotation of the Dofan magmatic segment, Main Ethiopian Rift, *Tectonophysics*. **732***:85-94*

Kazmin, V. (1972). Geological map of Ethiopia, scale 1:2,000,000. Ethiopian Institute of Geological Survey, Addis Ababa, Ethiopia.

Kazmin, V., Seifemichael Berhe, Nicoletti, M. and Petrucciani, C. (1980). Evolution of the northern part of the Ethiopian rift. *Atti Convegni Lincei*, **47:** 275-292.

Keir, D., Ebinger, C. J., Stuart, G. W., Daly, E. &, Atalay Ayele. (2006). Strain accommodation by magmatism and faulting as rifting proceeds to breakup: Seismicity of the northern Ethiopian rift, *Geophys*. *Res*. **111**: 1-17.

Kendall, J.M., Stuart, G.W., Ebinger, C.J., Bastow, I.D. and Keir, D. (2005). Magma assisted rifting in Ethiopia, *Nature*, **433**: 146–148.

Keranen, K., Klemperer, S., Gloaguen, R., Eagle Working group. (2004). Imaging a porridge axis in the Main Ethiopian Rift. *Geology* **39:**949–952.

Keranen, K., and S.L. Klemperer. (2008). Discontinuous and diachronous evolution of the Main Ethiopian Rift: Implications for the development of continental rifts. *Earth and Planetary Science Letters*, **265**: 96-111, DOI:10.1016/j.epsl.2007.09.038.

Kirschvink, J. (1980). The least-squares line and plane and the analysis of palaeomagnetic data. *Geophysical Journal International,* **62(3):** 699-718.

Koç, A., van Hinsbergen, D. J. J., & Langereis, C. G. (2018). Rotations of normal fault blocks quantify extension in the Central Tauride intermontane basins, SW Turkey. *Tectonics*, **37**. https:// DOI.org/10.1029/2018TC005112.

Kurz, t. et al. (2007). Deformation distribution and type in the MER: a remote sensing study. 100-114.

Le Pichon, X., and J. M. Gaulier. (1988). The rotation of Arabia and the Levant fault system, *Tectonophysics*, **153**: 271–294.

Levitte, D., Columba, J., and Mohr, P. (1974). Reconnaissance geology of the Amaro Horst, Southern Ethiopia. *Geological Society of American Bulletin*, **85**: 417-422.

Maguire, P., et al. (2006). Crustal structure of the northern main Ethiopian rift from the EAGLE controlled-source survey; a snapshot of an incipient lithospheric break-up. *Special publication-geological Society of London,* **259**: 269.

McFadden, P. and McElhinny, M. (1988). The combined analysis of remagnetization circles and direct observations in palaeomagnetism. *Earth and Planetary Science Letters,* **87(1):** 161-172.

Mehatsente, R., Jentzsch, G., Jahr, T. (1999). Crustal structure of the Main Ethiopian Rift from gravity data: 3-dimensional modeling. *Tectonophysics* **313 (4):** 363–382.

Melanie Siegburg , Jonathan M. Bull , Casey W. Nixon , Derek Keir, Thomas M. Gernon, Giacomo Corti , Bekele Abebe , David J. Sanderson , Atalay Ayele. (2020).

Quantitative constraints on faulting and fault slip--rates in the northern Main Ethiopian Rift. American Geophysical Union, DOI:10.1029/2019TC006046.

Meyer, W., Pilger, A., Rosler, A. and Stets, J. (1975). Tectonic evolution of the northern part of the main Ethiopian rift in southern Ethiopia and Afar Depression of Ethiopia. Schweizerbart Stuttgart, **14**: 352-362.

Mohr, P. (1962). The Ethiopian Rift System. *Bulletin of the Geophysical Observatory of Addis Ababa*. **5**: 33–62.

Mohr, P. (1967). Major volcano-tectonic lineament in the Ethiopian Rift System. *Nature*, **213**: 664-665.

Mohr, P. (1971). The Ethiopian triple-rift junction in terms of plate tectonics. *Bull*. *Geophys*. *Obs*., *Addis Ababa,* **13:** 1-17.

Mohr, P., Mitchell, J.G., Raynolds, R.G.H. (1980). Quaternary volcanism and faulting at O'a caldera, central Ethiopian rift. Bulletin Volcanologique **43**: 173–189.

Peccerillo, A., Barberio, M.R., Gezahegn Yirgu, Dereje Ayalew, Barberi, M. (2003). Relationships between mafic and acid peralkaline magmatism in continental rift settings. A petrological, geochemical and isotopic study of the Gedemsa volcano, central Ethiopian Rift. J. Petrol. **44**:2003–2032.

Samson Tesfaye, Harding, D. J. and Kusky, T. M. (2003). Early continental breakup boundary and migration of the Afar triple junction, Ethiopia. *Geological Society of America Bulletin*, **115(9):** 1053-1067.

Schult, A. (1974). Paleomagnetism of tertiary volcanic-rocks from Ethiopian southern-plateau and Danakil-block. *Journal of geophysics Zeitschrift fur geophysik*, **40(2):** 203-212.

Tadiwos Chernet, Hart, W. K., Aronson, J. L. and Walter, R. C. (1998). New age constraints on the timing of volcanism and tectonism in the northern main Ethiopian rift–southern Afar transition zone, Ethiopia. *Journal of Volcanology and Geothermal Research*, **80(3):** 267-280.

Tarling, D.H., (1983). Palaeomagnetism: principles and applications in Geology, Geophysics and Archeology, Chapman and Hall, London, 379 P.

Tazieff, H. and Varet, J. (1972). Tectonic significance of the Afar (or Danakil) depression. *Nature*, **235:** 144-147.

Tesfaye Kidane, J. Carlut, V. Courtillot, Y. Gallet, X.Quidelleur, PY. Gillot & Tigistu Haile. (1999). Paleomagnetic and geochronological identification of the Réunion subchron in Ethiopian, Afar. *Journal of Geophysical Research: Solid Earth*, **104(B5):** 10405- 10419

Tesfaye Kidane, Courtillot, V., Manighetti, I., Audin, L., Lahitte, P., Quidelleur, X. and Tigistu Haile. (2003). New paleomagnetic and geochronologic results from Ethiopian, Afar: Block rotations linked to rift overlap and propagation and determination of a~ 2 Ma reference pole for stable Africa. *Journal of Geophysical Research: Solid Earth*, **108(B2)**.

Tesfaye Kidane, Platzman, E., Ebinger, C., Bekele Abebe and Rochette, P. (2006). Palaeomagnetic constraints on continental break-up processes: observations from the main Ethiopian rift. *Geological Society, London, Special Publications,* **259(1)**: 165-183.

Tesfaye Kidane, Otofuji, Y.I., Komatsu, Y., Shibasaki, H. and Rowland, J. (2009). Paleomagnetism of the Fentale-magmatic segment, main Ethiopian rift: New evidence for counterclockwise block rotation linked to transtensional deformation. *Physics of the Earth and Planetary Interiors,* **176(1)**, 109-123.

Tesfaye Kidane, Otofuji, Y.I., Komatsu, Y., Shibasaki, H. and Yokoyama, M. (2010). Structural and geochronological implications of the Fentale Volcanics at a nascent passive margin of the main Ethiopian rift: Constraints from magnetostratigraphy study at the Kereyou Lodge, Ethiopia. *Tectonophysics,* **495(3):** 159-170.

Tesfaye Korme , Chorowicz, J., Collet, B., Bonavia, F.F. (1997). Volcanic vents rooted on extension fractures and their geodynamic implications in the Ethiopian Rift. J. *Volcanol*. *Geotherm*. *Res*. **79:** 205–222.

Turner, G.M., D.M. Michalk, and T. A. Little. (2012). Paleomagnetic constraints on Cenozoic deformation along the northwest margin of the Pacific-Australian plate boundary zone through New Zealand. *Tectonics*, DOI:10.1029/2011TC002931.

Wolfenden, E. (2003). Evolution of the southern Red Sea Rift: Birth of a magmatic margin, PhD thesis, Royal Holloway, University of London, UK.

Wolfenden, E., Ebinger, C., Gezahegn Yirgu, Deino, A. and Dereje Ayalew. (2004). Evolution of the northern main Ethiopian rift: birth of a triple junction. *Earth and Planetary Science Letters*, **224(1)**: 213-228.

Zijderveld, J. (1967). AC demagnetization of rocks: analysis of results. Methods in paleomagnetism, **3:** 254.

Appendix: A

Appendix-A Paleomagnetic data from Alternative field Demagnetization

ID	Steps	X	Y	Z	M	ID	Steps	X	Y	Z	M	ID	Steps	X	Y	Z	M
GMS1-1A	NRM	-17.94	4.01	-6.5	0.1942	GMS2-1A	NRM	-4.32	-3.4	-1.35	0.05658	GMS15-1A	NRM	-13.52	4.61	-9.45	1.712
	M5	-16.96	3.53	-6.05	0.1836		M5	-4.14	-3.19	-1.19	0.05354		M5	-13.25	4.33	-9.26	1.674
	M10	-15.56	2.69	-5.05	0.1658		M10	-3.76	-2.99	-1.05	0.04923		M10	-11.83	4.75	-8.34	1.524
	M15	-13.87	3.24	-4.76	0.1502		M15	-3.38	-2.73	-0.95	0.04444		M15	-9.22	3.71	-6.84	1.207
	M20	-12.25	2.95	-4.38	0.1334		M20	-3.16	-2.51	-0.8	0.04116		M20	-6.88	3.33	-5.23	0.9263
	M25	-10.66	2.62	-3.49	0.1152		M25	-2.72	-2.22	-0.71	0.03578		M25	-5.05	2.63	-3.98	0.6952
	M30	-9.24	1.74	-3.01	0.09873		M30	-2.36	-1.96	-0.64	0.0313		M30	-3.55	2.09	-3.04	0.5127
	M40	-7.76	1.52	-2.36	0.08255		M40	-2.07	-1.55	-0.49	0.02629		M40	-19.13	14.3	-17.29	0.2948
	M60	-6.05	1.03	-1.91	0.06428		M60	-13.8	-11.12	-3.84	0.01813		M60	-3.56	6.11	-4.77	0.08533
	M80	-4.82	0.97	-1.49	0.05141		M80	-11.26	-8.48	-3.43	0.01451		M80	-1.26	3.72	-2.82	0.04831
	M100	-3.56	0.84	-1.26	0.03864		M100	-8.24	-6.15	-1.51	0.01039		M100	-1.53	3.44	-1.96	0.04247
	M100	-3.56	0.84	-1.26	0.03864		M100	-8.24	-6.15	-1.51	0.01039		M100	-1.53	3.44	-1.96	0.04247
GMS1-1B	NRM	-2.79	0.74	-0.87	0.3018	GMS2-2A	NRM	-3.79	-2.6	-1.55	0.0485	GMS15-2A	NRM	-14.4	5.57	-10.44	1.864
	M5	-2.64	0.59	-0.8	0.282		M5	-3.42	-2.5	-1.22	0.04407		M5	-14.2	5.16	-10.29	1.828
	M10	-2.39	0.59	-0.7	0.2563		M10	-2.55	-2.03	-0.92	0.03384		M10	-12.52	4.72	-9.42	1.636
	M15	-2.09	0.48	-0.65	0.2236		M15	-2.05	-1.65	-0.75	0.02732		M15	-10.13	4.31	-7.64	1.34
	M20	-17.78	3.93	-5.33	0.1898		M20	-17.84	-15.03	-6.45	0.0242		M20	-7.25	3.78	-6.02	1.015
	M25	-14.81	3.27	-4.5	0.1582		M25	-15.75	-13.4	-5.21	0.02132		M25	-5.68	3.24	-4.58	0.7984
	M30	-12.07	2.86	-3.68	0.1294		M30	-0.11	-0.1	-0.03	0.01558		M30	-4.24	2.47	-3.58	0.6079
	M40	-9.76	2.07	-3.17	0.1047		M40	-11.41	-9.36	-3.65	0.0152		M40	-2.18	1.64	-2.07	0.3425
	M60	-7.54	1.9	-2.22	0.08087		M60	-9.12	-6.42	-2.94	0.01153		M60	-4.09	6.93	-5.51	0.09754
	M80	-5.88	1.37	-1.55	0.06235		M80	-6.42	-5.4	-2.68	0.008813		M80	-0.99	3.44	-3.53	0.05029
	M100	-4.32	0.78	-1.42	0.0461		M100	-5.02	-4.16	-1.45	0.006684		M100	-1.17	2.94	-2.22	0.03864
	M100	-4.32	0.78	-1.42	0.0461		M100	-5.02	-4.16	-1.45	0.006684		M100	-1.17	2.94	-2.22	0.03864
GMS1-1C	NRM	-3.47	1.28	-1.24	0.3901	GMS2-3A	NRM	-3.44	-4.04	-0.62	0.05343	GMS15-3A	NRM	-12.96	4.65	-9.53	1.674
	M5	-3.83	1.17	-1.5	0.4277		M5	-3.24	-3.88	-0.57	0.05081		M5	-13.25	4.59	-9.3	1.683
	M10	-3.53	1.04	-1.4	0.3938		M10	-2.85	-3.63	-0.48	0.04639		M10	-11.16	4.36	-8.54	1.471
	M15	-3.11	0.97	-1.26	0.3492		M15	-2.62	-3.46	-0.39	0.04359		M15	-8.7	3.84	-6.75	1.166
	M20	-2.68	0.85	-1.1	0.3016		M20	-2.44	-3.2	-0.29	0.04038		M20	-6.3	3.02	-5.27	0.8748
	M25	-2.28	0.76	-0.91	0.2573		M25	-2.16	-2.88	-0.21	0.03605		M25	-4.85	2.55	-3.95	0.6753
	M30	-2.01	0.71	-0.78	0.2274		M30	-1.99	-2.62	-0.19	0.03299		M30	-3.41	2.06	-2.88	0.4916
	M40	-15.75	5.55	-6.53	0.1793		M40	-1.62	-2.2	-0.15	0.02738		M40	-17.24	14.4	-16.26	0.2773
	M60	-11.2	4.39	-5.13	0.01308		M60	-11.78	-16.11	-0.91	0.01998		M60	-4.75	6.94	-4.15	0.09379
	M80	-8.36	3.09	-3.47	0.09562		M80	-7.59	-12	0.19	0.0142		M80	-1.68	4.26	-2.23	0.05095
	M100	-6.05	2.06	-2.48	0.06854		M100	-6.39	-9.23	-0.68	0.01124		M100	-0.33	3.53	-1.43	0.03828
	M100	-6.05	2.06	-2.48	0.06854		M100	-6.39	-9.23	-0.68	0.01124		M100	-0.33	3.53	-1.43	0.03828
GMS1-2A	NRM	-16.26	0.46	-7.08	0.1774	GMS2-4A	NRM	-5.71	-4.17	-2.45	0.07482	GMS15-4A	NRM	-10.61	6.7	-8.22	1.501
	M5	-15.7	0.84	-6.89	0.1717		M5	-5.12	-3.99	-2.12	0.06826		M5	-9.54	6.21	-8.18	1.401
	M10	-14.2	0.94	-6.14	0.155		M10	-4.35	-3.57	-1.65	0.05869		M10	-8.65	5.35	-7.4	1.258
	M15	-12.65	0.5	-5.63	0.1386		M15	-3.78	-3.18	-1.57	0.05184		M15	-6.77	4.7	-5.98	1.018
	M20	-11.06	0.61	-4.73	0.1205		M20	-3.18	-2.61	-1.17	0.04272		M20	-5.03	3.98	-4.69	0.7944
	M25	-9.41	0.15	-4.19	0.103		M25	-2.71	-2.34	-0.98	0.03712		M25	-3.51	2.88	-3.49	0.5729
	M30	-8.51	0.03	-3.62	0.09251		M30	-2.48	-2.19	-0.85	0.0342		M30	-2.76	2.45	-2.79	0.4623
	M40	-7.13	0.11	-3.03	0.07751		M40	-2.06	-1.82	-0.73	0.02845		M40	-13.83	16.15	-15.21	0.2614
	M60	-5.83	0.01	-2.48	0.06337		M60	-15.06	-13.29	-5.18	0.02075		M60	-2.95	6.6	-5.18	0.08894
	M80	-4.59	0.26	-1.61	0.04873		M80	-11.81	-10.78	-3.27	0.01632		M80	-0.92	4.07	-2.52	0.04871
	M100	-3.46	-0.1	-1.45	0.03754		M100	-9.74	-8.45	-3.35	0.01332		M100	0.11	2.98	-2.56	0.03931
	M100	-3.46	-0.1	-1.45	0.03754		M100	-9.74	-8.45	-3.35	0.01332		M100	0.11	2.98	-2.56	0.03931
GMS1-3A	NRM	-17.58	-5.6	8.55	0.2034	GMS2-5A	NRM	-3.29	-3.42	-1.22	0.04902	GMS15-5A	NRM	-12.16	2.34	-7.06	1.425
	M5	-16.58	-6.35	6.56	0.1893		M5	-2.69	-2.94	-0.73	0.04053		M5	-11.96	2.06	-6.92	1.397
	M10	-15.36	-6.75	5.39	0.1762		M10	-2.5	-2.96	-0.77	0.03949		M10	-10.2	1.65	-6.27	1.209
	M15	-13.72	-5.74	4.83	0.1564		M15	-2.14	-2.51	-0.65	0.03361		M15	-7.7	1.35	-4.75	0.9147
	M20	-1.07	-0.52	0.4	0.1253		M20	-1.93	-2.21	-0.52	0.02981		M20	-5.89	1.33	-3.69	0.7079
	M25	-0.79	-0.37	0.34	0.09335		M25	-16.95	-18.55	-4.83	0.02559		M25	-4.09	1.43	-2.84	0.5182
	M30	-0.67	-0.31	0.32	0.08093		M30	-14.11	-17.15	-4.53	0.02267		M30	-2.93	0.98	-2.14	0.3752
	M40	-0.54	-0.26	0.26	0.06566		M40	-11.02	-13.8	-2.75	0.01787		M40	-15.55	8.06	-12.59	0.2157
	M60	-6.23	-3.15	2.14	0.07304		M60	-7.64	-9.94	-2.07	0.01271		M60	-2.76	3.83	-4.21	0.0632
	M80	-4.58	-2.83	1.47	0.05582		M80	-5.77	-7.46	-0.67	0.009455		M80	-1.39	2.81	-2.53	0.04028
	M100	-3.54	-2.25	1.6	0.04491		M100	-4.19	-5.87	-1.19	0.007311		M100	-0.8	2.96	-1.71	0.03512
	M100	-3.54	-2.25	1.6	0.04491		M100	-4.19	-5.87	-1.19	0.007311		M100	-0.8	2.96	-1.71	0.03512
GMS1-4A	NRM	-5.64	3.35	-0.96	0.06634	GMS2-6A	NRM	-4.34	-4.14	-1.34	0.06147	GMS15-6A	NRM	-12.02	6.22	-7.41	1.543
	M5	-6.48	4.68	-1.66	0.08163		M5	-4.06	-4.16	-1.16	0.05928		M5	-11.49	6.24	-7.25	1.496
	M10	-7.43	6.84	-3.32	0.1063		M10	-3.42	-3.68	-0.92	0.05111		M10	-10.18	6.53	-6.38	1.368
	M15	-7.39	7.9	-3.98	0.1153		M15	-2.88	-3.19	-0.77	0.04365		M15	-7.84	4.71	-5.33	1.059
	M20	-6.88	8.12	-4.26	0.1146		M20	-2.46	-2.81	-0.55	0.03775		M20	-5.83	3.99	-3.91	0.8072
	M25	-6.59	7.79	-4.1	0.11		M25	-2.21	-2.38	-0.47	0.03278		M25	-3.86	3.13	-3.12	0.5865
	M30	-6.1	7.24	-3.97	0.1026		M30	-1.91	-2.03	-0.32	0.02803		M30	-2.93	2.49	-2.32	0.4493
	M40	-5.17	6.56	-3.44	0.09037		M40	-15.1	-16.97	-3.22	0.02295		M40	-13.71	16.04	-12.25	0.244
	M60	-4.01	5.28	-2.92	0.0725		M60	-9.34	-11.33	-2.1	0.01483		M60	-2.4	6.56	-3.51	0.07817
	M80	-3.34	4.7	-2.43	0.06257		M80	-7.14	-8.2	-2.05	0.01106		M80	0.81	3.76	-2.53	0.04609
	M100	-2.53	4.05	-2.28	0.0529		M100	-5.12	-6.22	-1.7	0.008236		M100	-0.94	3.34	-1.57	0.03806
	M100	-2.53	4.05	-2.28	0.0529		M100	-5.12	-6.22	-1.7	0.008236		M100	-0.94	3.34	-1.57	0.03806
GMS1-5A	NRM	-14.35	8.94	-3.07	0.1718	GMS2-7A	NRM	-12.28	-13.71	-2.81	0.1862	GMS18-1A	NRM	-7.76	17.54	4.88	1.979
	M5	-13.12	8.23	-3.06	0.1579		M5	-11.19	-13.21	-2.45	0.1749		M5	-7.3	15.29	4.41	1.75
	M10	-12.22	7.57	-2.8	0.1465		M10	-10.83	-12.51	-1.85	0.1665		M10	-6.35	12.58	4.56	1.481
	M15	-11.24	6.86	-2.53	0.1341		M15	-9.84	-11.69	-1.51	0.1536		M15	-4.62	11.04	4.02	1.262
	M20	-10.25	6.18	-2.29	0.1219		M20	-8.31	-10.53	-1.24	0.1348		M20	-3.83	9.56	3.53	1.088
	M25	-8.99	5.72	-2.13	0.1087		M25	-7.13	-9.05	-1.25	0.1159		M25	-4.25	8.18	2.75	0.9618

	M30	-7.62	4.96	-1.99	0.09306		M30	-6.5	-8.42	-1.04	0.1069		M30	-3.13	7.12	2.43	0.8142
	M40	-6.88	4.22	-1.73	0.08254		M40	-5.27	-6.62	-0.72	0.08494		M40	-2.4	5.56	1.67	0.6278
	M60	-5.38	3.35	-1.23	0.06456		M60	-4.53	-5.41	-0.54	0.07074		M60	-1.31	3.57	0.93	0.3914
	M80	-0.34	0.18	-0.08	0.03903		M80	-3.64	-4.54	-0.32	0.05823		M80	-0.93	2.77	0.64	0.2985
	M100	-0.22	0.13	-0.06	0.02647		M100	-2.93	-3.57	-0.5	0.04644		M100	-0.68	2.26	0.38	0.2393
	M100	-0.22	0.13	-0.06	0.02647		M100	-2.93	-3.57	-0.5	0.04644		M100	-0.68	2.26	0.38	0.2393
GMS1-6A	NRM	-0.96	0.36	-0.35	0.1083	GMS2-8A	NRM	-9.78	-13.37	1.02	0.0166	GMS18-2A	NRM	-9.22	10.82	5.93	1.54
	M5	-0.96	0.33	-0.34	0.1072		M5	-9.59	-13.35	1.32	0.01649		M5	-8.75	9.5	5.67	1.411
	M10	-0.9	0.33	-0.31	0.1001		M10	-9.73	-13.05	1.54	0.01635		M10	-7.74	8.5	5.21	1.262
	M15	-0.83	0.33	-0.31	0.09453		M15	-8.08	-11.65	1.62	0.01427		M15	-6.45	7.37	4.68	1.085
	M20	-0.74	0.28	-0.26	0.08354		M20	-7.25	-10.62	1.63	0.01296		M20	-5.73	6.78	4.1	0.9776
	M25	-0.65	0.23	-0.24	0.07314		M25	-6.38	-9.4	1.79	0.0115		M25	-5.43	5.97	3.48	0.8785
	M30	-0.62	0.22	-0.19	0.06808		M30	-5.18	-8.22	1.51	0.009831		M30	-4.18	5.18	3.02	0.7307
	M40	-0.5	0.21	-0.17	0.05704		M40	-3.69	-6.44	1.05	0.007495		M40	-3.22	3.79	2.01	0.5363
	M60	-0.39	0.16	-0.15	0.04463		M60	-2.39	-4.15	0.73	0.004848		M60	-1.74	2.47	1.15	0.3238
	M80	-0.31	0.11	-0.08	0.03406		M80	-2.12	-3.09	0.5	0.003788		M80	-10.96	19.78	7.9	0.2395
	M100	-0.22	0.08	-0.07	0.02471		M100	-1.24	-2.38	0.37	0.002709		M100	-11.09	15.69	7.45	0.2062
	M100	-0.22	0.08	-0.07	0.02471		M100	-1.24	-2.38	0.37	0.002709		M100	-11.09	15.69	7.45	0.2062
GMS1-7A	NRM	-1.41	1	-0.22	0.1739	GMS2-9A	NRM	-6.78	-4.85	0.03	0.08337	GMS18-3A	NRM	-2.6	18.68	5.88	1.976
	M5	-1.36	0.93	-0.22	0.1662		M5	-6.13	-4.78	0.3	0.07775		M5	-2.86	16.3	5.14	1.733
	M10	-1.2	0.84	-0.16	0.1478		M10	-4.99	-4.16	0.41	0.06505		M10	-2.4	13.84	4.61	1.479
	M15	-0.53	0.79	-0.21	0.09753		M15	-4.43	-3.74	0.5	0.05815		M15	-1.84	12.17	4.2	1.3
	M20	-7.51	5.75	-1.5	0.09575		M20	-3.64	-3.35	0.38	0.04962		M20	-2.11	10.49	3.84	1.137
	M25	-5.74	5.04	-1.15	0.07724		M25	-3.28	-2.91	0.34	0.04398		M25	-1	9.21	3.16	0.9792
	M30	-4.84	4.34	-1.42	0.0665		M30	-3.02	-2.6	0.34	0.04001		M30	-1.22	8.14	2.62	0.8635
	M40	-0.38	0.24	-0.09	0.04603		M40	-2.46	-2.07	0.37	0.03236		M40	-0.81	6.26	1.9	0.6596
	M60	-2.95	2.37	-0.68	0.0384		M60	-14.33	-13.99	2.45	0.02018		M60	-0.45	3.97	0.75	0.4065
	M80	-2.24	1.84	-0.51	0.02942		M80	-10.88	-10.8	1.13	0.01537		M80	-0.48	3.13	0.67	0.324
	M100	-18.29	11.29	-2.48	0.02164		M100	-7.37	-8.36	0.88	0.01118		M100	-0.38	2.68	0.72	0.2803
	M100	-18.29	11.29	-2.48	0.02164		M100	-7.37	-8.36	0.88	0.01118		M100	-0.38	2.68	0.72	0.2803
GMS1-8A	NRM	-2.61	-0.2	-0.79	0.2735	GMS2-10A	NRM	-3.77	-4.29	0.47	0.05731	GMS18-4A	NRM	11.61	13.47	15.71	2.373
	M5	-2.48	-0.15	-0.7	0.258		M5	-2.91	-4.15	0.68	0.05114		M5	9.55	11.87	14.09	2.075
	M10	-2.12	-0.19	-0.58	0.2204		M10	-2.79	-3.79	0.67	0.04756		M10	6.75	10.2	11.82	1.701
	M15	-15.34	-1.55	-4.22	0.1598		M15	-2.38	-3.25	0.62	0.04073		M15	6.38	9.17	10.15	1.509
	M20	-11.37	-1.46	-2.77	0.118		M20	-1.94	-2.76	0.55	0.03421		M20	5.09	8	8.66	1.284
	M25						M25	-1.62	-2.3	0.27	0.02822		M25	4.08	6.89	7.46	1.095
	M30	-7.64	-0.96	-1.92	0.07936		M30	-12.95	-19.62	3.75	0.0238		M30	3.49	5.94	6.38	0.9391
	M40	-6.29	-0.76	-1.74	0.06572		M40	-11.47	-16.35	3.43	0.02027		M40	2.31	4.55	4.48	0.6789
	M60	-4.28	-0.38	-1.26	0.04482		M60	-8.32	-11.76	2.25	0.01458		M60	1.59	3.06	2.85	0.4473
	M80	-2.93	-0.08	-0.86	0.03054		M80	-6.2	-9.05	1.87	0.01113		M80	1.01	1.01	1.78	0.3046
	M100	-0.13	-0.02	-0.02	0.01368		M100	-4.78	-7.38	1.78	0.00897		M100	8.96	18.11	10.4	0.2272
	M100	-0.13	-0.02	-0.02	0.01368		M100	-4.78	-7.38	1.78	0.00897		M100	8.96	18.11	10.4	0.2272
GMS1-9A	NRM	-16.79	8.08	-7.29	0.2001	GMS2-11A	NRM	-3.01	-3.21	0.23	0.04412	GMS18-5A	NRM	-3.26	17.29	6.81	1.887
	M5	-16.07	8.02	-6.84	0.1922		M5	-2.56	-2.97	0.35	0.03938		M5	-2.7	15.24	6.57	1.682
	M10	-14.59	7.5	-6.22	0.1755		M10	-2.04	-2.67	0.4	0.03381		M10	-2.33	13.21	5.8	1.461
	M15	-12.19	6.1	-5.32	0.1464		M15	-1.84	-2.25	0.42	0.02934		M15	-2.23	11.63	5.37	1.3
	M20	-9.45	5.78	-4.54	0.1197		M20	-14.78	-19.28	3.46	0.02454		M20	-2.01	10.25	4.55	1.139
	M25	-6.98	4.6	-3.62	0.09111		M25	-10.66	-14.94	2.85	0.01857		M25	-1.91	9.15	4.15	1.023
	M30	-6.01	3.95	-3	0.07795		M30	-10.66	-14.94	2.85	0.01857		M30	-1.71	7.86	3.17	0.8645
	M40	-4.67	2.99	-2.1	0.05933		M40	-9.83	-12.14	2.25	0.01579		M40	-1.28	6.08	2.29	0.662
	M60	-3.84	2.06	-1.85	0.04736		M60	-6.69	-8.94	1.76	0.0113		M60	-0.94	4.07	1.29	0.4373
	M80	-3.03	1.22	-1.09	0.03447		M80	-5.11	-7.09	1.19	0.00882		M80	-0.4	3.03	0.94	0.3199
	M100	-2.35	1.16	-1.08	0.02839		M100	-3.88	-6.3	1.13	0.007483		M100	-0.68	2.47	0.55	0.262
	M100	-2.35	1.16	-1.08	0.02839		M100	-3.88	-6.3	1.13	0.007483		M100	-0.68	2.47	0.55	0.262
GMS3-1A	NRM	-3.78	-2.15	-3.26	5.437	GMS4-1A	NRM	8.01	4.17	8.54	12.43	GMS18-6A	NRM	9.28	13.19	16.28	2.291
	M5	-3.08	-2.14	-2.45	4.481		M5	8.06	4.21	8.51	12.46		M5	7.78	11.86	14.78	2.049
	M10	-2.35	-1.63	-1.75	3.355		M10	7.64	3.93	8.1	11.81		M10	6.69	10.38	12.02	1.723
	M15	-18.62	-11.5	-11.94	2.493		M15	6.76	3.38	7.35	10.54		M15	5.64	9.22	10.08	1.478
	M20	-15.55	-10.16	-10.74	2.145		M20	6.11	2.99	6.38	9.322		M20	4.7	7.95	8.74	1.272
	M25	-12.62	-9.12	-9.84	1.842		M25	5.12	2.64	5.57	8.016		M25	4.21	7.18	7.43	1.116
	M30	-11.45	-8.33	-8.53	1.653		M30	4.38	2.1	4.89	6.893		M30	3.27	6.17	6.16	0.9306
	M40	-9.43	-6.32	-6.2	1.294		M40	3.19	1.69	2.83	4.589		M40	2.44	4.86	4.45	0.7023
	M60	-5.98	-4.28	-3.42	0.8114		M60	2.25	1.26	1.96	3.24		M60	1.25	3.25	2.84	0.4487
	M80	-3.18	-4.42	-3.65	0.6553		M80	18.62	10.69	16.31	2.696		M80	0.82	2.25	1.58	0.287
	M100	-2.93	-3.41	-1.62	0.478		M100	16.89	11.13	14.51	2.489		M100	1	2.01	1.4	0.2646
	M100	-2.93	-3.41	-1.62	0.478		M100	16.89	11.13	14.51	2.489		M100	1	2.01	1.4	0.2646
GMS3-2A	NRM	-3.66	-2.95	-3.53	5.88	GMS4-2A	NRM	7.2	5.16	8.97	12.61	GMS20-1A	NRM	9.76	16.32	11.67	0.002231
	M5	-2.85	-2.5	-2.42	4.503		M5	7.25	4.9	9.04	12.58		M5	8.76	13.2	9.96	0.001871
	M10	-2.14	-1.93	-1.65	3.322		M10	6.8	4.32	8.67	11.84		M10	6.38	7.39	4.21	0.001063
	M15	-17.08	-14.67	-12.65	2.582		M15	6.15	4.08	7.82	10.75		M15	5.8	3.85	1.27	0.0007075
	M20	-13.37	-12.33	-10.6	2.105		M20	5.14	3.48	6.01	8.639		M20	4.89	2.4	0.44	0.0005463
	M25	-12.19	-10.12	-9.12	1.828		M25	4.56	3.13	5.18	7.577		M25	4.43	1.82	0.13	0.0004788
	M30	-10.46	-8.5	-5.89	1.471		M30	4	2.65	4.15	6.346		M30	3.53	1.39	-0.19	0.0003801
	M40	-7.64	-6.99	-6.06	1.2		M40	2.94	2.02	2.91	4.6		M40	3.03	0.9	-0.15	0.0003168
	M60	-5.23	-5.39	-3.81	0.8419		M60	2.01	1.45	2.02	3.196		M60	2	0.7	0.21	0.0002131
	M80	-2.6	-3.74	-1.54	0.4813		M80	16.5	12.59	16.51	2.652		M80	13	5.86	4.72	0.0001503
	M100	-2.4	-1.2	0.81	0.2801		M100	15	11.81	14.74	2.412		M100	8.65	5.33	5.35	0.0001149
	M100	-2.4	-1.2	0.81	0.2801		M100	15	11.81	14.74	2.412		M100	8.65	5.33	5.35	0.0001149
GMS3-3A	NRM	-2.84	-3.36	-2.54	5.083	GMS4-3A	NRM	5.72	3.71	6.1	9.151	GMS20-2A	NRM	4.08	6.5	5.13	0.0009236
	M5	-2.07	-2.84	-1.81	3.952		M5	5.86	3.38	6.13	9.134		M5	2.83	4.79	3.08	0.000636
	M10	-1.54	-2.03	-1.18	2.812		M10	5.52	3.5	5.78	8.725		M10	1.6	2.25	0.89	0.0002899
	M15	-11.85	-15.95	-8.65	2.167		M15	5.11	3.11	5.29	7.988		M15	12.98	11.23	2.14	0.000173

	M20	-9.64	-12.72	-6.93	1.74		M20	4.45	2.8	4.67	7.028		M20	9.2	8.18	1.75	0.0001244
	M25	-8.39	-11.27	-6.38	1.543		M25	3.88	2.29	4.07	6.07		M25	6.05	4.9	0.03	0.00007781
	M30	-7.14	-9.79	-5.02	1.312		M30	3.47	1.98	3.55	5.341		M30	9.43	4.11	0.91	0.0001033
	M40	-5.49	-8.14	-4.17	1.067		M40	2.69	1.58	2.77	4.166		M40	7.32	-1.74	1.03	0.00007593
	M60	-3.67	-5.59	-2.43	0.7116		M60	1.9	1.19	1.94	2.967		M60	3.67	1.7	1.07	0.0000418
	M80	-2.11	-3.94	-4.26	0.6178		M80	16.25	10.36	16.27	2.522		M80	0.62	0.33	3.54	0.00003612
	M100	-1.78	-3.53	-1.18	0.4128		M100	14.3	9.75	14.82	2.279		M100	2.88	-1.35	2.28	0.00003914
	M100	-1.78	-3.53	-1.18	0.4128		M100	14.3	9.75	14.82	2.279		M100	2.88	-1.35	2.28	0.00003914
GMS3-4A	NRM	-2.73	-3.65	-3.15	5.536	GMS4-4A	NRM	6.7	-1.05	6.25	9.221	GMS20-3A	NRM	7.88	16.49	10.32	0.002099
	M5	-2.01	-3.04	-2.25	4.284		M5	6.66	-1.15	6.23	9.19		M5	5.06	11.99	5.87	0.001427
	M10	-1.77	-2.33	-1.52	3.293		M10	6.24	-1.18	6.02	8.753		M10	2.34	5.81	1.73	0.0006496
	M15	-12.64	-18.55	-11.59	2.526		M15	5.74	-1.26	5.51	8.059		M15	1.47	3.28	0.32	0.000361
	M20	-10.79	-15.74	-9.15	2.116		M20	4.96	-1.41	5.01	7.193		M20	1.6	2.5	-0.22	0.0002976
	M25	-9.58	-12.91	-7.91	1.792		M25	4.41	-1.27	4.4	6.356		M25	1.17	1.86	-0.23	0.000221
	M30	-8.07	-11.32	-7.01	1.558		M30	3.79	-1.32	3.92	5.609		M30	8.85	14.92	-1.11	0.0001738
	M40	-6.1	-9.6	-5.27	1.253		M40	3	-1.06	3.07	4.425		M40	9.3	5.92	-5.48	0.0001231
	M60	-4.17	-6.82	-3.02	0.8548		M60	2.13	-0.71	2.15	3.108		M60	1.76	3.41	-4.55	0.00005949
	M80	-2.09	-5.29	-1.57	0.5905		M80	17.74	-4.82	17.63	2.547		M80	3.03	2.58	-2.26	0.00004575
	M100	-2.18	-4.47	-0.6	0.5011		M100	15.87	-3.92	15.46	2.25		M100	2.78	-0.31	-5.41	0.00006094
	M100	-2.18	-4.47	-0.6	0.5011		M100	15.87	-3.92	15.46	2.25		M100	2.78	-0.31	-5.41	0.00006094
GMS3-5A	NRM	-3.94	-2.95	-2.65	5.592	GMS4-5A	NRM	6.39	2.64	7.55	10.24	GMS20-4A	NRM	6.9	14.49	15.46	0.002229
	M5	-2.89	-2.41	-1.81	4.175		M5	6.1	2.81	5.77	8.857		M5	4.81	9.98	9.44	0.001455
	M10	-19.46	-15.89	-12.09	2.788		M10	5.94	2.85	5.42	8.537		M10	2.53	3	2.48	0.0004639
	M15	-15.39	-12.7	-9.05	2.191		M15	5.4	2.35	4.88	7.655		M15	2.04	0.53	0.42	0.0002148
	M20	-11.65	-10.63	-7.04	1.727		M20	4.6	1.98	4.4	6.667		M20	17.76	3.04	3.53	0.0001836
	M25	-10.03	-8.52	-6.06	1.449		M25	4.02	1.78	3.84	5.836		M25	7.4	-2.66	-6.52	0.0001022
	M30	-8.67	-7.45	-4.92	1.244		M30	3.58	1.49	3.31	5.093		M30	7.85	-3.23	-2.23	0.00008773
	M40	-7.46	-6.81	-4.06	1.088		M40	2.7	1.11	2.63	3.931		M40	11.3	-6.17	-2.77	0.0001317
	M60	-3.82	-4.79	-2.74	0.671		M60	19.62	8.99	18.68	2.854		M60	4.98	-3.96	-6.62	0.00009178
	M80	-2.91	-4.09	-1.39	0.5206		M80	16.81	8	15.37	2.415		M80	2.96	-3.54	-3.24	0.00005644
	M100	-1.86	-3.47	-1.33	0.4159		M100	15.06	7.95	13.96	2.202		M100	3.35	-2.18	-9.95	0.0001072
	M100	-1.86	-3.47	-1.33	0.4159		M100	15.06	7.95	13.96	2.202		M100	3.35	-2.18	-9.95	0.0001072
GMS3-6A	NRM	-2.93	-3.87	-2.22	5.336	GMS4-6A	NRM	6.5	5.46	7.19	11.12	GMS21-1A	NRM	-0.29	4.07	1.21	0.4257
	M5	-2.56	-3.34	-1.63	4.514		M5	5.91	5.14	5.33	9.474		M5	-0.42	3.92	1.1	0.4092
	M10	-1.96	-2.47	-1.06	3.324		M10	5.76	4.7	5.13	9.031		M10	-0.41	3.76	0.99	0.3906
	M15	-13.91	-19.24	-7.96	2.504		M15	5.08	4.46	4.58	8.168		M15	-0.34	3.54	0.9	0.3664
	M20	-11.62	-16.23	-6.47	2.098		M20	4.54	3.86	3.98	7.17		M20	-0.37	3.25	0.76	0.3362
	M25	-10.15	-14.07	-5.48	1.819		M25	3.91	3.28	3.37	6.113		M25	-0.14	2.8	0.5	0.2845
	M30	-8.75	-12.5	-5.21	1.612		M30	3.34	2.99	2.88	5.329		M30	-0.19	2.29	0.26	0.2314
	M40	-6.86	-9.51	-3.5	1.224		M40	2.56	2.07	2.27	3.999		M40	-1.44	14.28	1.14	0.1439
	M60	-5.2	-7.08	-1.86	0.898		M60	16.6	14.9	15.92	2.74		M60	-0.46	7.28	2.1	0.07593
	M80	-3.16	-5.94	-1.05	0.6809		M80	13.97	12.84	12.72	2.284		M80	-0.1	5.35	2.44	0.05883
	M100	-2.5	-4.42	-0.18	0.5077		M100	12.47	12.02	11.31	2.068		M100	-0.57	4.2	2.57	0.04959
	M100	-2.5	-4.42	-0.18	0.5077		M100	12.47	12.02	11.31	2.068		M100	-0.57	4.2	2.57	0.04959
GMS3-7A	NRM	-3.43	-4.26	-2.55	6.033	GMS4-7A	NRM	6.04	4.63	5.92	9.64	GMS21-2A	NRM	1.14	4.32	0.6	0.4511
	M5	-2.44	-3.7	-1.91	4.827		M5	6.49	4.82	7.63	11.11		M5	1.09	4.23	0.53	0.4403
	M10	-1.91	-2.82	-1.37	3.67		M10	5.84	4.5	5.4	9.143		M10	1.06	4.07	0.51	0.4233
	M15	-1.59	-2.22	-1.01	2.913		M15	5.41	3.93	4.9	8.288		M15	0.89	3.91	0.42	0.4036
	M20	-12.51	-18.79	-8.66	2.418		M20	4.76	3.37	4.3	7.244		M20	0.92	3.65	0.32	0.3775
	M25	-11.15	-16.4	-7.4	2.116		M25	4.07	2.87	3.67	6.184		M25	0.78	3.18	0.15	0.3282
	M30	-9.89	-14.3	-5.33	1.819		M30	3.44	2.5	3.18	5.313		M30	0.62	2.56	-0.06	0.2631
	M40	-8.14	-11.82	-4.52	1.504		M40	2.65	1.96	2.41	4.083		M40	2.55	16.35	-0.74	0.1656
	M60	-4.66	-8.65	-3.2	1.034		M60	18.43	14.33	17.09	2.893		M60	2.42	8.79	0.63	0.09134
	M80	-3.22	-6.68	-1.97	0.7676		M80	15.72	11.94	14.33	2.439		M80	2.37	6.31	1.48	0.069
	M100	-2.66	-5.59	-0.82	0.6246		M100	14.21	10.63	12.92	2.195		M100	1.86	5.21	1.78	0.5813
	M100	-2.66	-5.59	-0.82	0.6246		M100	14.21	10.63	12.92	2.195		M100	1.86	5.21	1.78	0.5813
GMS3-8A	NRM	-3.47	-5.03	-2.55	6.621	GMS4-8A	NRM	7.55	1.47	9.3	12.06	GMS21-3A	NRM	4.14	0.94	1.55	0.4518
	M5	-3.06	-4.47	-2.01	5.776		M5	7.13	1.47	7.19	10.23		M5	4.03	0.8	1.46	0.4358
	M10	-2.49	-3.69	-1.46	4.685		M10	6.76	1.73	6.67	9.651		M10	3.85	0.89	1.4	0.4192
	M15	-2.06	-3.12	-1.2	3.927		M15	6.11	1.34	5.95	8.634		M15	3.59	0.91	1.33	0.3938
	M20	-1.78	-2.75	-0.98	3.422		M20	5.11	1.05	5.11	7.303		M20	3.35	0.84	1.21	0.3657
	M25	-1.6	-2.37	-0.88	2.989		M25	4.19	0.74	4.18	5.961		M25	2.79	0.61	1.03	0.3039
	M30	-1.28	-2.11	-0.76	2.581		M30	3.46	0.57	3.47	4.934		M30	2.11	0.44	0.79	0.2298
	M40	-10.09	-15.97	-5.31	1.963		M40	2.38	0.23	2.43	3.409		M40	11.72	1	5.63	0.1304
	M60	-6.4	-11.29	-4.03	1.359		M60	12.96	1.6	13.18	1.855		M60	8.29	-0.36	4.49	0.09434
	M80	-4.27	-8.75	-2.76	1.012		M80	8.21	2.07	8.37	1.191		M80	7.07	-0.6	4.29	0.08292
	M100	-3.22	-7.28	-1.9	0.8179		M100	6.33	2.41	5.65	0.8827		M100	6.87	-0.72	3.92	0.07946
	M100	-3.22	-7.28	-1.9	0.8179		M100	6.33	2.41	5.65	0.8827		M100	6.87	-0.72	3.92	0.07946
GMS3-9A	NRM	-0.36	-4.83	3.13	5.769	GMS6-1A	NRM	3.64	-6.71	0.54	7.651	GMS21-5A	NRM	16.54	-2.69	12.41	0.2085
	M5	-0.59	-4.65	2.57	5.341		M5	3.7	-6.93	0.87	7.906		M5	16.22	-2.37	11.92	0.2026
	M10	-0.73	-3.79	2.06	4.376		M10	4.12	-6.72	1.03	7.949		M10	15.16	-2.03	11.49	0.1913
	M15	-0.47	-3.16	1.75	3.644		M15	3.99	-6.45	1.08	7.66		M15	13.07	-2.98	9.89	0.1666
	M20	-0.55	-2.75	1.54	3.203		M20	3.72	-6.1	1.06	7.221		M20	10.19	-3.11	8.2	0.1345
	M25	-0.47	-2.49	1.36	2.873		M25	2.97	-5.41	0.97	6.246		M25	6.81	-3.28	6.19	0.09769
	M30	-0.42	-2.23	1.22	2.574		M30	2.87	-4.88	0.91	5.731		M30	4.4	-3.33	4.74	0.07278
	M40	-3.8	-18.72	10.37	2.174		M40	2.05	-4	0.84	4.574		M40	2.25	-2.92	3.15	0.04847
	M60	-2.37	-14.14	7.45	1.616		M60	1.35	-2.77	0.55	3.131		M60	1.06	-2.07	2.01	0.03073
	M80	-0.71	-10.91	6.19	1.257		M80	1.09	-2.02	0.45	2.339		M80	10.38	-18.19	14.76	0.02562
	M100	-0.56	-9.01	4.91	1.027		M100	7.55	-16.17	3.31	1.815		M100	10.21	-15.85	11.67	0.02217
	M100	-0.56	-9.01	4.91	1.027		M100	7.55	-16.17	3.31	1.815		M100	10.21	-15.85	11.67	0.02217
GMS5-1A	NRM	3.85	6.36	9.59	12.14	GMS6-2A	NRM	2.58	-7.44	1.38	7.995	GMS21-6A	NRM	1.34	2.25	1.04	0.2814
	M5	4.07	6.16	7.17	10.29		M5	2.3	-7.77	1.62	8.26		M5	1.25	2.2	0.97	0.2705
	M10	3.35	5.64	6.77	9.427		M10	2.42	-7.51	1.78	8.091		M10	1.27	2.1	0.95	0.2629
	M15	3.09	5.13	6.15	8.583		M15	2.29	-7.14	1.79	7.712		M15	1.09	2	0.86	0.2436

	M20	2.72	4.5	5.43	7.559		M20	2.19	-6.58	1.72	7.147		M20	9.81	18.64	7.44	0.2233
	M25	2.66	3.91	4.69	6.664		M25	1.88	-5.82	1.68	6.346		M25	8.5	15.44	5.61	0.185
	M30	2.08	3.45	4.1	5.75		M30	1.36	-5.29	1.58	5.688		M30	5.22	11.61	11.61	0.1323
	M40	1.63	2.72	3.2	4.506		M40	1.25	-4.31	1.27	4.66		M40	3.33	6.44	1.72	0.07453
	M60	1.09	1.84	2.08	2.983		M60	0.71	-2.9	0.91	3.124		M60	1.78	2.1	1.75	0.03268
	M80	7.49	13.82	14.55	2.142		M80	0.47	-2.12	0.71	2.285		M80	16.08	4.91	15.22	0.02268
	M100	6.01	11.68	11.04	1.716		M100	4.06	-16.88	4.97	1.806		M100	1.35	0	2.03	0.02435
	M100	6.01	11.68	11.04	1.716		M100	4.06	-16.88	4.97	1.806		M100	1.35	0	2.03	0.02435
GMS5-2A	NRM	4.7	2.05	9.13	10.47	GMS6-3A	NRM	2.47	-6.83	1.44	7.408	GMS23-5A	NRM	-12.84	16.68	-1.9	2.113
	M5	4.63	2.42	6.96	8.696		M5	2.81	-7.1	1.84	7.85		M5	-12.62	15.81	-1.75	2.03
	M10	4.38	2.16	6.45	8.087		M10	2.71	-7.03	1.99	7.791		M10	-11.97	14.54	-2.23	1.897
	M15	3.9	1.93	5.76	7.214		M15	2.94	-6.68	1.88	7.532		M15	-10.28	13.13	-1.93	1.678
	M20	3.21	1.33	5.02	6.106		M20	2.45	-6.08	1.87	6.819		M20	-9.36	12.04	-1.97	1.537
	M25	2.8	1.11	4.14	5.12		M25	1.94	-5.58	1.64	6.13		M25	-8.36	10.81	-1.83	1.379
	M30	2.24	0.95	3.59	4.335		M30	1.99	-4.98	1.57	5.586		M30	-7.53	10.13	-1.64	1.273
	M40	1.67	0.66	2.62	3.174		M40	1.33	-3.99	1.31	4.402		M40	-5.62	8.13	-1.43	0.9984
	M60	10.25	4.38	16.43	1.985		M60	0.86	-2.72	0.92	2.998		M60	-3.78	5.62	-1.02	0.6848
	M80	7.35	3.36	12.06	1.452		M80	0.6	-2.02	0.69	2.22		M80	-2.53	3.87	-0.98	0.4724
	M100	6.35	3.73	9.55	1.206		M100	4.61	-15.69	5.47	1.724		M100	-1.81	2.94	-0.74	0.3532
	M100	6.35	3.73	9.55	1.206		M100	4.61	-15.69	5.47	1.724		M100	-1.81	2.94	-0.74	0.3532
GMS5-3A	NRM	3.61	5.24	9.26	11.24	GMS6-4A	NRM	2.88	-7.23	1.93	8.024	GMS16-4A	NRM	-1.45	-13.52	-2.42	0.1381
	M5	3.75	5.09	6.89	9.35		M5	2.77	-7.36	2.37	8.212		M5	-1.18	-13.04	-2.01	0.1324
	M10	3.59	4.63	6.38	8.66		M10	2.65	-7.24	2.5	8.104		M10	-0.89	-12.39	-1.73	0.1254
	M15	3.22	4.03	5.65	7.653		M15	2.75	-6.85	2.47	7.785		M15	-0.76	-11.7	-1.46	0.1181
	M20	2.58	3.55	4.8	6.497		M20	2.43	-6.31	2.34	7.155		M20	-1.02	-10.88	-1.14	0.1098
	M25	2.13	2.95	3.93	5.362		M25	2.35	-5.75	2.1	6.552		M25	-0.93	-10.02	-1.16	0.1013
	M30	1.8	2.37	3.25	4.406		M30	2.25	-5.15	1.97	5.957		M30	-1.19	-9.35	-0.95	0.09478
	M40	1.31	1.65	2.22	3.064		M40	1.73	-4.21	1.62	4.834		M40	-1.04	-8.04	-0.77	0.0814
	M60	7.58	10.45	12.77	1.816		M60	0.99	-2.95	1.05	3.285		M60	-0.86	-6.13	-0.59	0.06215
	M80	5.61	8.52	9.56	1.398		M80	0.74	-2.19	0.78	2.442		M80	-0.65	-4.62	-0.39	0.04677
	M100	4.35	6.64	7.4	1.085		M100	5.28	-16.63	6.98	1.879		M100	-0.2	-3.44	-0.12	0.03449
	M100	4.35	6.64	7.4	1.085		M100	5.28	-16.63	6.98	1.879		M100	-0.2	-3.44	-0.12	0.03449
GMS5-4A	NRM	5.03	5.63	9.34	12.01	GMS6-5A	NRM	2.25	-6.53	2.33	7.292	GMS17-1A	NRM	6.49	-6.33	7.75	0.1193
	M5	5.07	5.2	8.91	11.49		M5	2.5	-6.83	2.66	7.75		M5	5.51	-7.75	7.16	0.119
	M10	4.63	4.86	8.16	10.57		M10	2.89	-6.67	2.82	7.793		M10	4.92	-8.48	6.45	0.1174
	M15	4.05	4.32	7.19	9.317		M15	2.71	-6.23	2.74	7.318		M15	3.58	-7.29	5.66	0.09907
	M20	3.29	3.75	6.05	7.838		M20	2.35	-5.86	2.47	6.784		M20	2.89	-6.57	4.72	0.08588
	M25	2.88	3.13	5.07	6.614		M25	1.96	-5.28	2.36	6.104		M25	2.69	-5.61	3.82	0.07302
	M30	2.39	2.57	4.27	5.522		M30	1.89	-4.81	2.1	5.577		M30	1.89	-4.64	3.05	0.05866
	M40	1.73	1.88	2.93	3.886		M40	1.34	-3.85	1.74	4.429		M40	1.25	-3.31	2.26	0.04198
	M60	1.15	1.29	2.03	2.664		M60	0.82	-2.63	1.17	2.988		M60	0.84	-2.03	1.37	0.02587
	M80	7.16	9.67	14.24	1.864		M80	7.08	-19.25	8.74	2.229		M80	6.27	-14.27	10.9	0.01902
	M100	5.03	8.44	11.88	1.541		M100	4.37	-15.52	7.12	1.762		M100	6.02	-11.82	8.65	0.01584
	M100	5.03	8.44	11.88	1.541		M100	4.37	-15.52	7.12	1.762		M100	6.02	-11.82	8.65	0.01584
GMS5-5A	NRM	5.87	6	8.63	12.04	GMS6-6A	NRM	2.74	-6.92	2.2	7.756	GMS17-2A	NRM	7.11	-16.92	0.79	0.1837
	M5	5.73	5.44	8.25	11.42		M5	2.98	-7.18	2.55	8.179		M5	5.22	-18.42	-0.7	0.1916
	M10	5.26	5.24	7.57	10.6		M10	3.26	-7.08	2.68	8.244		M10	5.77	-16.52	-0.58	0.1751
	M15	4.73	4.55	6.73	9.4		M15	3.09	-6.65	2.72	7.816		M15	4.33	-14.5	-0.14	0.1514
	M20	3.93	3.98	5.77	8.034		M20	2.99	-6.16	2.53	7.301		M20	4.05	-12.3	0.18	0.1295
	M25	3.44	3.34	4.86	6.826		M25	2.52	-5.59	2.32	6.556		M25	3.3	-10.19	0.46	0.1072
	M30	2.9	3.01	4.09	5.843		M30	2.18	-5.05	2.1	5.892		M30	2.44	-8.43	0.6	0.08798
	M40	2.02	2.2	3.13	4.326		M40	1.78	-4.09	1.75	4.794		M40	1.57	-5.81	0.73	0.06064
	M60	1.46	1.5	2.02	2.911		M60	1.09	-2.83	1.21	3.263		M60	0.99	-3.53	0.55	0.03713
	M80	9.87	11.14	14.56	2.082		M80	0.77	-2.08	0.91	2.394		M80	0.77	-2.69	0.32	0.02814
	M100	7.67	9.43	10.94	1.635		M100	5.46	-16.38	6.68	1.851		M100	0.58	-2.15	0.25	0.02241
	M100	7.67	9.43	10.94	1.635		M100	5.46	-16.38	6.68	1.851		M100	0.58	-2.15	0.25	0.02241
GMS5-6A	NRM	2.45	6.97	8.82	11.51	GMS6-7A	NRM	3.42	-6.27	2.47	7.557	GMS17-3A	NRM	1.22	-5.08	0.05	0.05229
	M5	2.2	6.83	8.5	11.12		M5	3.54	-6.42	3.02	7.929		M5	0.7	-5.41	-0.6	0.05492
	M10	1.98	6.43	7.91	10.38		M10	3.55	-6.43	3.09	7.967		M10	0.64	-4.79	-0.45	0.04855
	M15	1.67	5.73	7.06	9.247		M15	3.27	-6.12	2.96	7.541		M15	48.55	-4.02	-0.24	0.04044
	M20	1.72	5	6.05	8.03		M20	2.87	-5.54	2.85	6.862		M20	0.42	-3.23	-0.13	0.03258
	M25	1.17	4.22	4.97	6.624		M25	2.29	-5.15	2.51	6.169		M25	0.3	-2.61	-0.04	0.02628
	M30	1.12	3.57	4.14	5.584		M30	2.18	-4.63	2.39	5.648		M30	0.29	-2.02	0.08	0.02041
	M40	0.75	2.61	2.83	3.918		M40	1.76	-3.74	1.94	4.57		M40	2.18	-14.33	0.67	0.01451
	M60	3.41	15.79	16.39	2.301		M60	1.02	-2.51	1.3	3.002		M60	0.98	-9.09	0.19	0.009147
	M80	2.91	12.14	11.1	1.671		M80	7.59	-19.31	9.44	2.279		M80	0.5	-7.12	0.01	0.007134
	M100	1.73	10.91	9.14	1.434		M100	7.82	-15.87	9.44	2.005		M100	0.62	-5.32	0.54	0.005382
	M100	1.73	10.91	9.14	1.434		M100	7.82	-15.87	9.44	2.005		M100	0.62	-5.32	0.54	0.005382
GMS5-7A	NRM	3.31	6.51	9.47	11.96	GMS6-8A	NRM	-2.92	-7.43	2.19	8.279	GMS17-4A	NRM	2.44	-4.25	-0.12	0.4902
	M5	3.33	6.2	9.17	11.56		M5	-3.13	-7.71	2.54	8.696		M5	2.46	-4.09	-0.17	0.4778
	M10	2.99	5.78	8.58	10.77		M10	-2.87	-7.62	2.56	8.53		M10	2.37	-3.72	-0.18	0.4413
	M15	2.51	5.25	7.82	9.745		M15	-2.75	-7.25	2.58	8.17		M15	2.1	-3.46	-0.11	0.4052
	M20	2.6	4.63	6.83	8.652		M20	-2.4	-6.77	2.4	7.573		M20	1.69	-2.91	-0.01	0.3367
	M25	2.13	4.07	5.96	7.523		M25	-1.89	-6.04	2.19	6.701		M25	1.49	-2.66	0.04	0.3048
	M30	1.73	3.64	5.19	6.575		M30	-1.62	-5.5	1.99	6.073		M30	1.13	-2.24	0.12	0.2514
	M40	1.42	2.94	4.16	5.291		M40	-1.29	-4.47	1.69	4.953		M40	8.92	-16.07	1.17	0.1841
	M60	0.98	2.02	2.75	3.551		M60	-0.72	-3.1	1.17	3.395		M60	5.73	-10.94	0.98	0.1239
	M80	5.14	15.88	18.84	2.517		M80	-0.62	-2.27	0.93	2.536		M80	4.51	-8.79	0.91	0.09918
	M100	4.09	12.4	13.69	1.892		M100	-4.67	-18.02	7.27	1.999		M100	4.37	-7.41	0.46	0.08611
	M100	4.09	12.4	13.69	1.892		M100	-4.67	-18.02	7.27	1.999		M100	4.37	-7.41	0.46	0.08611
GMS5-8A	NRM	6.01	4.81	8.95	11.81	GMS6-9A	NRM	3.21	-6.13	2.53	7.366	GMS17-5A	NRM	2.26	-1.86	1.45	0.3265
	M5	5.75	4.67	7.63	10.64		M5	3.06	-6.32	2.89	7.597		M5	2.16	-1.72	1.25	0.3031
	M10	5.9	4.25	8.06	10.86		M10	2.97	-6.15	2.97	7.446		M10	2.01	-1.64	1.13	0.2835
	M15	4.93	3.55	7.39	9.56		M15	2.77	-5.88	2.8	7.078		M15	16.45	-14.71	9.97	0.2422
	M20	4.6	3.26	6.54	8.635		M20	2.51	-5.44	2.67	6.558		M20	12.74	-12.51	8.37	0.1972

	M25	4.07	2.86	5.68	7.544		M25	2.24	-4.96	2.4	5.955		M25	9.54	-10.71	6.86	0.159
	M30	3.42	2.46	5.04	6.564		M30	2.02	-4.55	2.2	5.439		M30	7.42	-8.63	5.57	0.1268
	M40	2.74	1.99	3.94	5.195		M40	1.41	-3.66	1.86	4.341		M40	4.26	-6.26	3.81	0.08477
	M60	1.83	1.35	2.59	3.447		M60	0.94	-2.5	1.31	2.976		M60	2.7	-3.76	2.15	0.05108
	M80	12.84	11.27	18.14	2.492		M80	8.14	-18.45	9.73	2.239		M80	2.18	-2.76	1.56	0.03846
	M100	9.43	8.88	13.42	1.865		M100	6.44	-14.93	7.88	1.807		M100	1.84	-2.07	1.49	0.03148
	M100	9.43	8.88	13.42	1.865		M100	6.44	-14.93	7.88	1.807		M100	1.84	-2.07	1.49	0.03148
GMS7-1A	NRM	0.15	4.01	-4.74	0.0621	GMS6-10A	NRM	2.79	-6.59	2.53	7.587	GMS17-6A	NRM	0.84	-2.65	0.87	0.2917
	M5	0.31	4.1	-3.51	0.05401		M5	3.13	-6.96	2.86	8.147		M5	0.86	-2.61	0.8	0.2859
	M10	0.58	3.88	-0.42	0.03946		M10	3	-6.87	3.07	8.104		M10	0.86	-2.38	0.75	0.2638
	M15	0.66	3.29	0.93	0.03482		M15	-0.25	-6.67	1.53	6.843		M15	0.77	-2.11	0.67	0.2347
	M20	0.55	2.65	1.33	0.03014		M20	2.55	-6.14	2.69	7.168		M20	5.05	-17.57	6.48	0.194
	M25	0.47	2.14	1.36	0.02579		M25	2.22	-5.63	2.49	6.544		M25	5.68	-15.15	5.25	0.1701
	M30	3.74	18.12	12.27	0.0222		M30	2.18	-5.15	2.3	6.043		M30	3.01	-12.5	4.32	0.1356
	M40	2.13	13.26	9.91	0.01669		M40	1.51	-4.14	1.88	4.794		M40	2.47	-8.34	3.13	0.09246
	M60	1.95	9.35	6.85	0.01175		M60	1.01	-2.86	1.22	3.267		M60	1.66	-4.43	1.44	0.0495
	M80	1.41	6.73	4.61	0.008279		M80	0.68	-2.1	0.92	2.393		M80	1.13	-3.44	1.22	0.03822
	M100	0.95	4.86	3.12	0.00585		M100	5.93	-16.52	7.68	1.916		M100	0.89	-2.75	0.96	0.03048
	M100	0.95	4.86	3.12	0.00585		M100	5.93	-16.52	7.68	1.916		M100	0.89	-2.75	0.96	0.03048
GMS7-2A	NRM	0.65	-5.03	-9.57	0.1084	GMS8-1A	NRM	0.14	3.4	1.2	3.61	GMS19-1A	NRM	-0.84	2.6	0.55	0.2786
	M5	0.48	-4.31	-7.75	0.08879		M5	0.08	2.83	0.93	2.978		M5	-0.8	2.48	0.5	0.2652
	M10	0.61	-2.86	-2.29	0.0372		M10	0.06	2.46	0.73	2.565		M10	-5.39	19.8	3.74	0.2086
	M15	0.45	-2.48	0.68	0.02607		M15	0.04	2.14	0.57	2.213		M15	-5.04	15.29	2.52	0.163
	M20	0.44	-2.25	1.55	0.02764		M20	0.22	17.98	3.9	1.84		M20	-4.06	12.11	1.54	0.1287
	M25	4.16	-19.67	16.88	0.02625		M25	0.47	15.49	3.6	1.591		M25	-2.69	9.58	0.87	0.09986
	M30	4.01	-17.66	16.14	0.02425		M30	-0.03	13.36	2.53	1.36		M30	-2.36	7.86	0.74	0.08245
	M40	2.45	-14.1	13.33	0.01955		M40	0.8	10.42	1.18	1.051		M40	-1.58	6.07	0.66	0.06303
	M60	1.93	-9.37	9.43	0.01343		M60	-0.32	6.45	0.11	0.6455		M60	-1.21	4.87	0.64	0.0506
	M80	1.32	-6.99	6.94	0.009944		M80	0.3	4.49	-0.01	0.45		M80	-1.25	4.15	0.29	0.04339
	M100	1.07	-5.4	5.39	0.007704		M100	-0.02	3.63	0.02	0.363		M100	-1.25	3.95	0.34	0.04155
	M100	1.07	-5.4	5.39	0.007704		M100	-0.02	3.63	0.02	0.363		M100	-1.25	3.95	0.34	0.04155
GMS7-3A	NRM	1.9	2.74	-8.47	0.09103	GMS8-2A	NRM	-0.34	3.33	1.37	3.618	GMS19-2A	NRM	0.35	2.33	0.71	0.2459
	M5	1.91	3.13	-7.41	0.08268		M5	-0.41	2.61	1.04	2.844		M5	0.31	2.12	0.64	0.2238
	M10	1.51	3.54	-3.54	0.05229		M10	-0.37	2.23	0.84	2.413		M10	3.18	16.8	4.73	0.1774
	M15	1.18	3.23	-0.58	0.03492		M15	-3.08	18.93	6.43	2.023		M15	1.44	12.64	3.19	0.1312
	M20	0.98	2.91	0.38	0.03089		M20	-2.57	15.89	4.65	1.676		M20	1.31	9.92	2.19	0.1025
	M25	0.71	2.43	0.88	0.02677		M25	-2.06	13.66	3.61	1.428		M25	1.11	7.8	1.76	0.08071
	M30	0.51	2.02	0.95	0.02292		M30	-2.21	11.59	2.48	1.206		M30	1.16	6.6	1.41	0.06851
	M40	2.88	15.09	8.41	0.01751		M40	-1.49	8.82	1.66	0.91		M40	0.93	5.11	1.22	0.05333
	M60	2.06	9.85	6.49	0.01197		M60	-0.77	5.56	0.79	0.5664		M60	0.75	3.98	0.79	0.04128
	M80	2.59	7.4	4.3	0.008944		M80	-0.75	4.19	0.83	0.4333		M80	0.63	3.55	0.81	0.03699
	M100	1.42	5.55	3.38	0.006654		M100	-0.67	3.27	0.33	0.3357		M100	0.6	3.3	0.71	0.03424
	M100	1.42	5.55	3.38	0.006654		M100	-0.67	3.27	0.33	0.3357		M100	0.6	3.3	0.71	0.03424
GMS7-4A	NRM	7.33	-0.31	-17.71	0.1917	GMS8-3A	NRM	-0.34	4.51	1.11	4.661	GMS19-3A	NRM	-1.62	2.11	0.59	0.2731
	M5	5.98	-0.51	-15.52	0.1664		M5	-0.36	3.26	0.88	3.397		M5	-15.2	19.4	5.47	0.2524
	M10	3.6	1.34	-8.31	0.09157		M10	-0.36	2.65	0.7	2.766		M10	-11.58	15.08	4.06	0.1944
	M15	2.05	2.09	-2.97	0.04172		M15	-0.37	2.21	0.49	2.295		M15	-8.56	11.47	2.65	0.1455
	M20	12.77	19.56	-7.22	0.02445		M20	-2.75	19.06	3.46	1.957		M20	-6.44	9.12	1.87	0.1132
	M25	8.93	18.13	1.53	0.02027		M25	-2.72	15.69	2.27	1.609		M25	-4.95	7.11	1.39	0.0877
	M30	6.53	15.16	5.08	0.01727		M30	-1.54	13.83	1.97	1.406		M30	-3.92	6.07	1.28	0.07337
	M40	4.61	12.18	6.8	0.0147		M40	-1.75	10.55	0.76	1.072		M40	-3.24	4.74	1.06	0.05842
	M60	2.96	8.31	5.68	0.01049		M60	-0.81	6.77	0.12	0.6818		M60	-2.63	3.71	0.77	0.04607
	M80	1.79	6.49	4.14	0.007906		M80	-0.57	4.76	0.13	0.4797		M80	-2.03	3.28	0.61	0.03901
	M100	1.6	4.7	2.57	0.005592		M100	-0.06	3.61	-0.15	0.3615		M100	-1.83	3	0.45	0.03545
	M100	1.6	4.7	2.57	0.005592		M100	-0.06	3.61	-0.15	0.3615		M100	-1.83	3	0.45	0.03545
GMS7-5A	NRM	0.61	-0.25	-1.55	0.1687	GMS8-4A	NRM	-1.89	-3.83	-4.21	5.997	GMS19-4A	NRM	-0.87	2.71	0.54	0.2897
	M5	0.52	-0.2	-1.44	0.1548		M5	-11.67	8.37	-8.58	1.673		M5	-0.92	2.52	0.47	0.2727
	M10	0.37	-0.05	-0.91	0.09832		M10	-8.98	17.98	-1.37	2.015		M10	-6.58	19.39	2.98	0.2069
	M15	0.2	0.15	-0.41	0.04772		M15	-6.49	17.62	-0.89	1.879		M15	-5.68	14.51	2.05	0.1572
	M20	0.16	0.16	-0.16	0.02765		M20	-5.55	15.82	-1.41	1.682		M20	-3.16	11.23	1.24	0.1173
	M25	14.58	18.88	-4.38	0.02425		M25	-4.68	9.71	-1.61	1.09		M25	-2.74	8.81	0.76	0.09259
	M30	10.54	16.6	1.4	0.01972		M30	-3.73	10.51	-1.36	1.124		M30	-2.61	7.22	0.66	0.077
	M40	7.45	12.98	4.52	0.01563		M40	-2.82	8.96	-2.3	0.9672		M40	-1.87	5.59	0.61	0.05927
	M60	4.53	9.06	4.78	0.0112		M60	-1.7	5.79	-2.51	0.6537		M60	-0.97	4.4	0.49	0.04534
	M80	3.02	6.81	3.79	0.008359		M80	0.01	2.37	-1.04	0.2591		M80	-1.16	3.77	0.32	0.03959
	M100	1.96	5.51	2.52	0.006368		M100	-1.09	2.2	-1.82	0.3052		M100	-1.11	3.44	0.25	0.03629
	M100	1.96	5.51	2.52	0.006368		M100	-1.09	2.2	-1.82	0.3052		M100	-1.11	3.44	0.25	0.03629
GMS7-6A	NRM	3.73	1.78	-14.63	0.152	GMS8-5A	NRM	-0.28	-7.44	9.75	12.27	GMS19-5A	NRM	-0.56	2.67	0.66	0.2805
	M5	2.97	2.02	-13.21	0.1369		M5	0.1	-3.82	6.36	7.422		M5	-0.56	2.5	0.55	0.2617
	M10	1.96	3.04	-7.31	0.08153		M10	-0.38	-0.26	3.35	3.379		M10	-5.01	19.45	3.5	0.2038
	M15	1.14	3.03	-2.55	0.04122		M15	-0.37	0.75	2.15	2.307		M15	-3.04	14.56	2.43	0.1507
	M20	0.85	2.52	-0.6	0.0273		M20	-3.9	9.62	16.36	1.938		M20	-2.2	11.41	1.57	0.1173
	M25	0.68	2.15	0.18	0.02257		M25	-2.77	9.71	13.15	1.658		M25	-1.98	9.03	1.08	0.09309
	M30	5.18	18.27	4.48	0.01951		M30	-2.69	9.13	10.75	1.436		M30	-1.57	7.43	1.09	0.07668
	M40	3.25	13.37	5.45	0.0148		M40	-1.78	7.63	7.41	1.078		M40	-0.49	5.63	0.73	0.05694
	M60	1.93	9.47	4.83	0.0108		M60	-1.46	4.92	3.75	0.6356		M60	-0.73	4.47	0.55	0.04563
	M80	1.67	6.98	3.74	0.008093		M80	-1	3.15	2.6	0.4206		M80	-0.68	3.98	0.47	0.04068
	M100	1.05	5.71	2.63	0.006376		M100	0.31	2.74	2.01	0.3416		M100	-0.59	3.55	0.28	0.03613
	M100	1.05	5.71	2.63	0.006376		M100	0.31	2.74	2.01	0.3416		M100	-0.59	3.55	0.28	0.03613
GMS9-1A	NRM	-0.2	-2.29	-0.8	243.3	GMS10-1A	NRM	-0.6	-5.12	-4.81	7.048	GMS19-6A	NRM	-0.77	2.73	0.62	0.2899
	M5	-0.2	-2.2	-0.74	232.6		M5	0.01	-4.85	-3.54	6.005		M5	-0.51	2.54	0.5	0.2638
	M10	-1.4	-17.25	-4.98	180.1		M10	0.31	-4.66	-2.17	5.153		M10	-4.95	19.48	3.36	0.2038
	M15	-0.82	-12.62	-2.68	129.2		M15	0.19	-4.39	-1.72	4.715		M15	-3.64	14.83	2.13	0.1542
	M20	-0.53	-9.05	-1.55	91.99		M20	0.38	-3.93	-1.38	4.18		M20	-2.5	11.39	1.44	0.1175
	M25	-0.68	-6.46	-0.57	65.18		M25	0.16	-3.47	-1.09	3.642		M25	-2.19	8.97	0.97	0.0928

	M30	-0.31	-4.64	-0.22	46.55		M30	0.3	-3.04	-0.92	3.19		M30	-2.02	7.29	0.61	0.0759
	M40	-0.25	-2.48	0.03	24.93		M40	0.12	-2.42	-0.66	2.513		M40	-1.13	5.68	0.68	0.05827
	M60	-1.45	-9.43	0.13	9.545		M60	1.58	-16.61	-4.24	1.722		M60	-0.96	4.38	0.59	0.04524
	M80	-0.72	-4.69	-0.11	4.749		M80	1.42	-12.89	-3.33	1.339		M80	-0.69	3.91	0.43	0.03998
	M100	-0.7	-2.79	-0.17	2.88		M100	0.64	-10.66	-2.78	1.103		M100	-0.89	3.53	0.29	0.03651
	M100	-0.7	-2.79	-0.17	2.88		M100	0.64	-10.66	-2.78	1.103		M100	-0.89	3.53	0.29	0.03651
GMS9-2A	NRM	9.8	-18.71	-11.09	238.5	GMS10-2A	NRM	-0.05	-6.37	-5.16	8.197	GMS22-1A	NRM	-0.92	-3.94	-3.71	0.5491
	M5	8.73	-17.69	-10.63	224.1		M5	0.46	-5.78	-3.4	6.723		M5	-0.79	-3.86	-3.43	0.5224
	M10	6.27	-13.59	-7.56	167.6		M10	0.65	-5.11	-1.72	5.428		M10	-0.69	-3.47	-2.98	0.462
	M15	4.12	-9.86	-4.61	116.4		M15	0.58	-4.75	-1.33	4.967		M15	-0.58	-2.96	-2.54	0.3939
	M20	2.79	-6.75	-2.74	77.97		M20	0.64	-4.26	-0.96	4.409		M20	-0.61	-2.5	-2.13	0.334
	M25	1.32	-4.73	-1.56	51.55		M25	0.86	-3.73	-0.74	3.897		M25	-0.41	-2.19	-1.8	0.2862
	M30	0.82	-3.11	-0.93	33.46		M30	0.47	-3.24	-0.56	3.323		M30	-4.28	-18.84	-15.8	0.2495
	M40	2.84	-15.51	-3.4	16.13		M40	0.27	-2.61	-0.43	2.662		M40	-2.91	-13.84	-12.17	0.1866
	M60	1.4	-6.62	-1.24	6.883		M60	3.69	-18.78	-3.14	1.94		M60	-2.51	-9.83	-8.92	0.1351
	M80	0.32	-3.65	-0.81	3.755		M80	2.78	-14.63	-2.27	1.506		M80	-1.56	-8.09	-7.06	0.1085
	M100	0.06	-2.34	-0.65	2.426		M100	2.02	-12.36	-1.81	1.265		M100	-1.72	-6.73	-5.72	0.09004
	M100	0.06	-2.34	-0.65	2.426		M100	2.02	-12.36	-1.81	1.265		M100	-1.72	-6.73	-5.72	0.09004
GMS9-3A	NRM	8.57	-4.52	-5.49	111.4	GMS10-3A	NRM	0.9	-7.16	-5.69	9.187	GMS22-2A	NRM	-0.99	-4.35	-4.73	0.65
	M5	8.45	-4.39	-5.61	110.6		M5	1.48	-6.46	-3.63	7.553		M5	-0.97	-4.04	-4.47	0.6098
	M10	7.46	-4.23	-4.83	98.42		M10	1.5	-5.56	-1.76	6.02		M10	-0.68	-3.73	-3.99	0.5505
	M15	5.5	-3.27	-3.43	72.59		M15	1.4	-4.95	-1.28	5.303		M15	-0.57	-3.34	-3.46	0.4841
	M20	3.84	-2.47	-2.22	50.73		M20	1.19	-4.46	-0.94	4.714		M20	-0.64	-2.9	-3.11	0.43
	M25	2.41	-1.76	-1.38	32.82		M25	0.51	-4.01	-0.71	4.1		M25	-0.52	-2.67	-2.69	0.3829
	M30	15.86	-13.85	-8.07	22.55		M30	0.97	-3.45	-0.55	3.623		M30	-0.5	-2.34	-2.44	0.3415
	M40	7.97	-8.48	-3.3	12.09		M40	0.79	-2.58	-0.36	2.723		M40	-0.45	-1.93	-2.04	0.2841
	M60	2.99	-4.21	-0.73	5.212		M60	3.24	-17.72	-1.97	1.813		M60	-3.49	-15.02	-15.81	0.2209
	M80	1.62	-2.74	-0.23	3.19		M80	3.32	-12.24	-1.55	1.277		M80	-1.78	-12.06	-12.75	0.1764
	M100	11.04	-18.9	-1.16	2.192		M100	2.23	-10.42	-1.32	1.074		M100	-1.97	-9.82	-10.7	0.146
	M100	11.04	-18.9	-1.16	2.192		M100	2.23	-10.42	-1.32	1.074		M100	-1.97	-9.82	-10.7	0.146
GMS9-4A	NRM	2.02	-3.97	3.44	56.33	GMS10-4A	NRM	0.68	-5.98	-4.97	7.799	GMS22-3A	NRM	-0.96	-2.75	-3.74	0.4745
	M5	1.23	-3.82	3.01	50.17		M5	0.86	-5.4	-3.25	6.361		M5	-0.82	-2.75	-3.51	0.4536
	M10	0.6	-3.16	1.76	36.72		M10	1.11	-4.65	-1.88	5.143		M10	-0.96	-2.42	-3.19	0.4118
	M15	0.31	-2.23	1.08	24.94		M15	1.18	-4.31	-1.28	4.646		M15	-0.7	-2.17	-2.72	0.3554
	M20	1.99	-16.42	7.57	18.19		M20	0.89	-3.86	-0.98	4.079		M20	-0.61	-1.85	-2.32	0.3032
	M25	1.16	-12.46	5.94	13.85		M25	0.9	-3.29	-0.77	3.499		M25	-0.51	-1.59	-1.97	0.2582
	M30	0.51	-10.22	4.49	11.18		M30	0.73	-2.95	-0.65	3.105		M30	-4.02	-13.53	-17.31	0.2234
	M40	-0.25	-7.14	2.72	7.649		M40	0.57	-2.38	-0.48	2.496		M40	-2.66	-10.21	-13.48	0.1712
	M60	-0.09	-4.22	1.46	4.464		M60	4.36	-16.59	-3.28	1.747		M60	-2.98	-7.61	-10.11	0.13
	M80	-0.04	-2.88	0.93	3.026		M80	4.17	-13.49	-2.63	1.436		M80	-1.62	-6.17	-8.47	0.106
	M100	0.05	-2.12	0.74	2.248		M100	2.73	-11.38	-1.94	1.186		M100	-1.59	-5.37	-7.44	0.09312
	M100	0.05	-2.12	0.74	2.248		M100	2.73	-11.38	-1.94	1.186		M100	-1.59	-5.37	-7.44	0.09312
GMS9-5A	NRM	1.69	-2.94	3.2	46.63	GMS10-5A	NRM	-4.84	-10.55	-7.5	13.82	GMS22-4A	NRM	-0.44	-4.58	-3.86	0.6004
	M5	1.42	-2.84	2.8	42.33		M5	-2.93	-9.1	-5.68	11.12		M5	-0.32	-4.48	-3.53	0.5717
	M10	0.77	-2.44	1.7	30.7		M10	-0.68	-6.16	-2.33	6.616		M10	-0.2	-4.03	-3.08	0.5077
	M15	2.91	-17.74	10.56	20.85		M15	-0.16	-5.16	-1.47	5.364		M15	-0.29	-3.53	-2.67	0.4434
	M20	1.76	-13.1	7.49	15.19		M20	-0.17	-4.64	-1.05	4.761		M20	-0.18	-3.07	-2.28	0.3832
	M25	1.17	-10.19	5.44	11.61		M25	0.11	-3.79	-0.67	3.846		M25	-0.12	-2.68	-1.97	0.3326
	M30	0.71	-8.23	3.95	9.159		M30	0	-4.16	-0.88	4.251		M30	-0.12	-2.35	-1.69	0.2897
	M40	-0.09	-5.65	2.8	6.306		M40	0.2	-3.79	-0.71	3.86		M40	0.41	-19.03	-13.74	0.2347
	M60	0.05	-3.33	1.61	3.702		M60	0.15	-2.23	-0.28	2.248		M60	-0.24	-13.79	-10.21	0.1716
	M80	-0.06	-2.25	1.12	2.516		M80	0.96	-16.83	-1.8	1.695		M80	-0.29	-11.41	-8.35	0.1414
	M100	0.63	-17.08	7.16	1.853		M100	1.16	-13.81	-1.6	1.395		M100	-0.39	-9.77	-6.91	0.1198
	M100	0.63	-17.08	7.16	1.853		M100	1.16	-13.81	-1.6	1.395		M100	-0.39	-9.77	-6.91	0.1198
GMS9-6A	NRM	2.55	-1.96	3.08	44.56	GMS10-6A	NRM	-1.83	-2.49	-4.29	52.89	GMS23-1A	NRM	-11.71	12.24	-3.75	1.735
	M5	2.07	-1.94	2.8	39.83		M5	-1.39	-1.73	-3.12	38.31		M5	-10.77	11.77	-3.73	1.638
	M10	1.05	-1.98	1.69	28.09		M10	-4.2	-4.43	-9.61	11.39		M10	-9.8	10.95	-3.46	1.51
	M15	7.52	-15.37	10.16	19.9		M15	-1.5	-1.88	-4.14	4.79		M15	-9.2	9.99	-3.33	1.399
	M20	3.78	-11.25	7.32	13.95		M20	-0.7	-1.56	-2.42	2.965		M20	-7.91	9.24	-3	1.253
	M25	2.52	-9.07	5.11	10.71		M25	-3.76	-14.11	-16.32	2.19		M25	-6.7	7.71	-2.56	1.053
	M30	2.45	-7.35	3.95	8.697		M30	-2.78	-12.88	-12.77	1.835		M30	-5.95	7.26	-2.45	0.9703
	M40	1.22	-5.47	2.57	6.162		M40	-1.06	-10.58	-8.32	1.35		M40	-4.62	5.83	-2.03	0.771
	M60	0.7	-3.3	1.48	3.682		M60	-0.72	-8.36	-5.81	1.021		M60	-2.68	3.86	-1.62	0.4969
	M80	0.68	-2.29	0.96	2.576		M80	-0.38	-7.01	-4.72	0.846		M80	-2.25	2.95	-0.94	0.3826
	M100	3.36	-17.38	7.9	1.939		M100	-0.8	-5.73	-2.92	0.6479		M100	-1.84	2.21	-0.72	0.2971
	M100	3.36	-17.38	7.9	1.939		M100	-0.8	-5.73	-2.92	0.6479		M100	-1.84	2.21	-0.72	0.2971
GMS11-1A	NRM	5.09	1.14	-0.32	0.5229	GMS12-2A	NRM	1.01	-18.83	5.74	1.972	GMS23-2A	NRM	-16.85	-3.24	-2.41	1.733
	M5	5	1.12	-0.35	0.5135		M5	1.72	-18.68	5.68	1.96		M5	-16.45	-3.06	-1.46	1.68
	M10	4.83	1.01	-0.35	0.4942		M10	1.22	-17.88	5.28	1.869		M10	-15.35	-3.05	-1.77	1.575
	M15	4.5	0.98	-0.33	0.4616		M15	1.33	-15.87	5.15	1.673		M15	-13.84	-2.56	-1.55	1.416
	M20	4.12	0.98	-0.27	0.4247		M20	1.37	-13.47	4.36	1.423		M20	-12.17	-2.39	-1.19	1.246
	M25	3.71	0.7	-0.3	0.3783		M25	1.05	-10.9	3.78	1.158		M25	-10.74	-1.99	-1.2	1.098
	M30	3.28	0.81	-0.26	0.3384		M30	0.79	-8.74	3.2	0.9335		M30	-9.5	-1.83	-0.96	0.9725
	M40	2.61	0.64	-0.24	0.2693		M40	0.51	-6.12	2.23	0.6534		M40	-7.47	-1.31	-0.75	0.7621
	M60	17.08	4.05	-2.01	0.1767		M60	0.34	-3.71	1.24	0.3925		M60	-5.03	-0.74	-0.59	0.5116
	M80	11.4	3.12	-1.15	0.1188		M80	0.26	-2.42	0.81	0.2562		M80	-3.72	-0.7	-0.6	0.3832
	M100	8.26	2.27	-0.73	0.08603		M100	2.29	-16.4	5.45	0.1743		M100	-2.86	-0.49	-0.23	0.2907
	M100	8.26	2.27	-0.73	0.08603		M100	2.29	-16.4	5.45	0.1743		M100	-2.86	-0.49	-0.23	0.2907
GMS11-2A	NRM	-0.67	-2.76	-0.43	0.2874	GMS12-3A	NRM	1.14	-16.74	4.72	1.743	GMS23-3A	NRM	14.22	15.69	-5.56	2.189
	M5	-0.77	-2.74	-0.42	0.2878		M5	0.23	-16.55	4.76	1.722		M5	13.8	15.55	-5.16	2.142
	M10	-0.64	-2.63	-0.39	0.2738		M10	0.9	-15.61	4.78	1.635		M10	12.41	14.25	-4.7	1.948
	M15	-0.53	-2.5	-0.35	0.2581		M15	0.73	-14.2	4.39	1.488		M15	11.08	12.52	-4.43	1.729
	M20	-0.67	-2.35	-0.3	0.2464		M20	0.83	-12.13	3.88	1.276		M20	9.8	11.59	-3.91	1.567
	M25	-0.49	-2.19	-0.25	0.2255		M25	0.42	-10.09	3.1	1.057		M25	8.41	10.3	-3.69	1.38
	M30	-0.41	-2.01	-0.19	0.2057		M30	0.2	-8.28	2.63	0.8685		M30	7.36	8.91	-3.31	1.202

	M40	-2.82	-16.78	-1.47	0.1708		M40	0.49	-5.82	2.01	0.6179		M40	5.86	7.36	-2.65	0.9775
	M60	-2.14	-11.78	-0.68	0.1199		M60	0.35	-3.43	1.14	0.3629		M60	3.95	4.83	-2.1	0.658
	M80	-1.75	-8.45	-0.28	0.08632		M80	0.16	-2.31	0.77	0.2437		M80	2.52	3.45	-1.45	0.4508
	M100	-1.14	-6.1	-0.21	0.06207		M100	1.27	-15.85	4.49	0.1652		M100	2.08	2.65	-1.3	0.3609
	M100	-1.14	-6.1	-0.21	0.06207		M100	1.27	-15.85	4.49	0.1652		M100	2.08	2.65	-1.3	0.3609
GMS11-3A	NRM	0.2	-5.55	-1.18	0.5676	GMS12-5A	NRM	-2.15	-17.3	1.5	1.75	GMS23-4A	NRM	-0.76	2.02	-0.41	2.196
	M5	0.17	-5.48	-1.19	0.5606		M5	-1.09	-17.12	1.83	1.725		M5	-6.63	19.09	-3.87	2.058
	M10	0.08	-5.34	-1.04	0.5437		M10	-1.29	-16.38	1.59	1.651		M10	-7.79	17.74	-3.58	1.97
	M15	0.14	-5.1	-0.99	0.5201		M15	-0.64	-14.7	1.84	1.483		M15	-6.36	16.29	-3.72	1.787
	M20	0.16	-4.82	-0.88	0.4898		M20	-0.45	-12.55	1.74	1.268		M20	-5.53	14.96	-3.34	1.629
	M25	0.19	-4.47	-0.74	0.4535		M25	-0.03	-10.4	1.57	1.052		M25	-4.4	13.5	-3.13	1.454
	M30	0.05	-4.06	-0.64	0.4107		M30	-0.3	-8.58	1.42	0.8706		M30	-4.35	11.99	-2.84	1.306
	M40	0.01	-3.3	-0.46	0.3335		M40	-0.07	-6.04	1.07	0.6135		M40	-3.68	9.93	-2.26	1.083
	M60	0.17	-2.2	-0.2	0.2217		M60	-0.03	-3.57	0.67	0.3633		M60	-1.8	6.72	-1.75	0.7177
	M80	0.7	-15.35	-1.45	0.1544		M80	-0.06	-2.31	0.43	0.2356		M80	-1.6	4.75	-1.25	0.5162
	M100	0.6	-11.15	-0.72	0.1119		M100	-0.01	-16.65	2.53	0.1684		M100	-0.83	3.51	-0.87	0.3706
	M100	0.6	-11.15	-0.72	0.1119		M100	-0.01	-16.65	2.53	0.1684		M100	-0.83	3.51	-0.87	0.3706
GMS11-4A	NRM	-0.45	-2.91	-0.19	0.2952	GMS14-1A	NRM	7.81	8.52	-10.39	15.54	GMS13-4A	NRM	-11.77	6.15	-6.91	14.97
	M5	-0.51	-2.88	-0.19	0.2936		M5	7.07	8.4	-11.24	15.71		M5	-10.77	5.31	-6.7	13.76
	M10	-0.51	-2.81	-0.15	0.2863		M10	7.56	8.38	-10.38	15.34		M10	-8.96	3.7	-6.13	11.47
	M15	-0.36	-2.69	-0.13	0.2722		M15	6.32	7.67	-8.71	13.21		M15	-7.73	2.49	-5.5	9.81
	M20	-0.42	-2.53	-0.1	0.2568		M20	5.95	6.65	-6.63	11.12		M20	-6.75	1.94	-4.86	8.546
	M25	-0.34	-2.34	-0.04	0.2362		M25	5.44	5.69	-5.09	9.378		M25	-5.66	1.82	-4.17	7.262
	M30	-0.33	-2.14	-0.04	0.2169		M30	4.5	4.86	-4.16	7.819		M30	-4.77	1.56	-3.61	6.186
	M40	-3.16	-17.84	-0.26	0.1812		M40	3.68	3.41	-2.69	5.688		M40	-3.43	1.39	-2.68	4.569
	M60	-1.16	-12.23	0.3	0.1229		M60	1.91	1.98	-1.61	3.189		M60	-18.9	9.3	-15.16	2.595
	M80	-0.66	-8.7	0.42	0.08732		M80	12.04	12.47	-9.48	1.975		M80	-10.76	5.86	-9.99	1.581
	M100	-0.53	-6.38	0.24	0.06407		M100	7.7	8.73	-6.59	1.337		M100	-8.59	4.24	-7.07	1.191
	M100	-0.53	-6.38	0.24	0.06407		M100	7.7	8.73	-6.59	1.337		M100	-8.59	4.24	-7.07	1.191
GMS11-5A	NRM	-0.91	-2.73	-0.49	0.292	GMS14-2A	NRM	-2.5	-7.62	6.56	10.36	GMS13-6A	NRM	-12.1	-5.32	-5.65	14.38
	M5	-0.87	-2.7	-0.45	0.2871		M5	-1.9	-7.59	5.91	9.799		M5	-10.76	-5.66	-5.51	13.35
	M10	-0.88	-2.61	-0.45	0.2789		M10	-0.77	-7.2	3.6	8.085		M10	-8.66	-6.16	-4.82	11.67
	M15	-0.79	-2.45	-0.38	0.2602		M15	-0.41	-6.58	2.51	7.058		M15	-7.75	-6.36	-4.25	10.89
	M20	-0.69	-2.28	-0.36	0.2407		M20	-0.4	-6.09	1.89	6.39		M20	-6.5	-5.82	-3.62	9.444
	M25	-0.64	-2.09	-0.27	0.2204		M25	-0.17	-5.62	1.48	5.815		M25	-5.2	-5.29	-2.87	7.955
	M30	-5.66	-19.02	-2.24	0.1998		M30	0.03	-5.12	1.34	5.293		M30	-4.4	-4.53	-2.31	6.728
	M40	-3.78	-15.29	-1.52	0.1582		M40	-0.17	-4.3	1.02	4.427		M40	-2.88	-3.17	-1.47	4.529
	M60	-2.98	-10.41	-0.91	0.1086		M60	0.03	-2.97	0.76	3.062		M60	-14.53	-19.35	-6.57	2.507
	M80	-1.7	-7.13	-0.41	0.07337		M80	0.15	-2.15	0.61	2.234		M80	-8.7	-11.5	-3.64	1.487
	M100	-1.3	-5.25	-0.24	0.05416		M100	1.57	-16.1	5.77	1.717		M100	-6.12	-7.79	-2.63	1.025
	M100	-1.3	-5.25	-0.24	0.05416		M100	1.57	-16.1	5.77	1.717		M100	-6.12	-7.79	-2.63	1.025
GMS11-6A	NRM	-1.39	-3.16	-0.4	0.3476	GMS14-3A	NRM	0.55	-6.7	9.63	11.75	GMS13-7A	NRM	-13.37	-4.06	-5.85	15.15
	M5	-1.37	-3.09	-0.38	0.3403		M5	0.37	-6.73	7.87	10.36		M5	-12.2	-4.87	-5.61	14.29
	M10	-1.37	-2.98	-0.38	0.3305		M10	1.03	-6.57	3.98	7.749		M10	-9.72	-5.76	-4.99	12.35
	M15	-1.11	-2.86	-0.3	0.3088		M15	1.3	-5.86	2.42	6.478		M15	-8.52	-5.73	-4.41	11.17
	M20	-1.2	-2.68	-0.25	0.2944		M20	1.13	-5.28	1.72	5.669		M20	-7.2	-5.5	-3.72	9.795
	M25	-1.02	-2.47	-0.19	0.2683		M25	1.09	-4.79	1.31	5.085		M25	-5.98	-4.88	-2.82	8.217
	M30	-0.97	-2.27	-0.17	0.2472		M30	1.01	-4.38	1.04	4.612		M30	-5.14	-3.99	-2.38	6.926
	M40	-6.68	-18.65	-1.08	0.1984		M40	0.72	-3.69	0.78	3.839		M40	-3.1	-3.02	-1.55	4.597
	M60	-4.78	-12.94	-0.41	0.138		M60	0.69	-2.56	0.63	2.726		M60	-17.44	-17.36	-7.26	2.566
	M80	-2.87	-9.13	-0.17	0.09576		M80	4.15	-19.55	4.67	2.053		M80	-10.96	-11.52	-4.46	1.651
	M100	-2.33	-6.59	0.07	0.06984		M100	3.08	-13.85	4.96	1.503		M100	-7.51	-7.76	-3.26	1.127
	M100	-2.33	-6.59	0.07	0.06984		M100	3.08	-13.85	4.96	1.503		M100	-7.51	-7.76	-3.26	1.127
GMS13-1A	NRM	0.64	3.75	-0.72	38.74	GMS14-4A	NRM	-14.69	-18.21	18.87	30.06	GMS16-1A	NRM	-4.39	-11.37	-2.97	0.1255
	M5	0.49	3.55	-0.74	36.6		M5	-13.76	-18.69	17.4	29.01		M5	-4.6	-11.22	-2.75	0.1244
	M10	-0.05	2.54	-0.83	26.75		M10	-10.25	-17.06	13.45	24.02		M10	-4.14	-10.69	-2.56	0.1175
	M15	-3.1	16.42	-7.06	18.14		M15	-7.12	-14.54	8.84	18.44		M15	-4.1	-9.99	-2.26	0.1103
	M20	-3.54	11.92	-5.55	13.61		M20	-4.46	-11.47	5.99	13.69		M20	-3.55	-9.25	-1.96	0.101
	M25	-2.94	8.85	-4.6	10.4		M25	-3.21	-10.18	4.74	11.68		M25	-3.2	-8.43	-1.69	0.09176
	M30	-2.67	7.2	-3.94	8.637		M30	-2.04	-8.28	3.34	9.16		M30	-2.57	-7.59	-1.41	0.08132
	M40	-2.49	4.95	-2.94	6.276		M40	-1.34	-6.21	1.92	6.641		M40	-2.07	-6.26	-1.21	0.06707
	M60	-1.73	2.95	-1.86	3.89		M60	-0.47	-3.76	1.13	3.954		M60	-1.49	-4.42	-0.85	0.04744
	M80	-1.02	2.02	-1.15	2.536		M80	-0.27	-2.58	0.72	2.692		M80	-0.81	-3.24	-0.54	0.03385
	M100	-6.5	14.44	-8.49	1.797		M100	-1.43	-18.96	5.81	1.988		M100	-0.7	-2.38	-0.42	0.02519
	M100	-6.5	14.44	-8.49	1.797		M100	-1.43	-18.96	5.81	1.988		M100	-0.7	-2.38	-0.42	0.02519
GMS13-2A	NRM	-15.68	7.15	-7.99	19	GMS14-5A	NRM	-4.98	5.94	8.6	11.58	GMS16-2A	NRM	-2.28	-11.05	0.17	0.1129
	M5	-14.32	6.34	-7.81	17.5		M5	-5.28	4.38	5.92	9.064		M5	-1.43	-10.74	0.31	0.1084
	M10	-10.56	3.97	-6.75	13.15		M10	-6.04	1.15	1.51	6.337		M10	-1.97	-10.2	0.24	0.1039
	M15	-8.54	1.71	-5.71	10.42		M15	-5.77	-0.24	0.22	5.779		M15	-1.43	-9.53	0.31	0.09642
	M20	-7.31	0.9	-4.77	8.778		M20	-5.33	-0.63	-0.27	5.373		M20	-1.15	-8.79	0.29	0.08872
	M25	-6.13	0.52	-4.06	7.373		M25	-4.82	-0.87	-0.52	4.924		M25	-1.54	-8.02	0.44	0.08178
	M30	-5.04	0.49	-3.44	6.12		M30	-4.36	-0.93	-0.55	4.496		M30	-1.21	-7.23	0.53	0.07345
	M40	-3.63	0.39	-2.5	4.425		M40	-3.37	-1.01	-0.53	3.562		M40	-0.84	-5.97	0.41	0.06039
	M60	-19.07	1.97	-14.26	2.389		M60	-2.1	-0.65	-0.29	2.22		M60	-0.62	-4.18	0.34	0.04236
	M80	-11.41	1.43	-8.26	1.416		M80	-13.52	-4.04	-1.35	1.418		M80	-0.46	-2.94	0.3	0.02988
	M100	-7.41	1.41	-5.83	0.9537		M100	-9.39	-2.9	-1.12	0.9895		M100	-0.31	-2.25	0.26	0.02286
	M100	-7.41	1.41	-5.83	0.9537		M100	-9.39	-2.9	-1.12	0.9895		M100	-0.31	-2.25	0.26	0.02286
GMS13-3A	NRM	-12.01	8.95	-5.74	16.04	GMS14-6A	NRM	-11.1	-5.56	7.87	14.69	GMS16-3A	NRM	-0.76	-13.77	0.65	0.1381
	M5	-11.27	7.61	-5.73	14.76		M5	-10.07	-5.79	6.97	13.55		M5	-0.65	-13.31	0.71	0.1335
	M10	-9.03	5.04	-5.49	11.71		M10	-6.93	-6.34	3.35	9.972		M10	-0.63	-12.74	0.85	0.1278
	M15	-7.51	3.84	-4.65	9.635		M15	-4.9	-6.06	1.21	7.886		M15	-0.33	-11.92	0.93	0.1196
	M20	-6.46	2.64	-4.1	8.095		M20	-3.39	-5.74	0.38	6.679		M20	-0.75	-11.06	0.87	0.1112
	M25	-5.44	2.51	-3.55	6.966		M25	-2.57	-5.22	-0.01	5.818		M25	-0.09	-10.09	1.09	0.1015
	M30	-4.89	2	-3.07	6.104		M30	-2.2	-4.74	-0.26	5.235		M30	-0.36	-9.18	0.95	0.09237
	M40	-3.41	1.37	-2.36	4.371		M40	-1.47	-3.83	-0.23	4.11		M40	-0.46	-7.43	0.76	0.07486

	M60	-19.44	10.05	-13.16	2.554		M60	-0.8	-2.59	-0.16	2.716		M60	-0.35	-5.5	0.52	0.05534
	M80	-12.89	6.48	-9.22	1.712		M80	-6.04	-17.99	0.01	1.897		M80	0.01	-4.07	0.27	0.04077
	M100	-8.18	5.22	-5.75	1.128		M100	-3.48	-13.09	0.29	1.354		M100	0.1	-2.97	0.45	0.03001
	M100	-8.18	5.22	-5.75	1.128		M100	-3.48	-13.09	0.29	1.354		M100	0.1	-2.97	0.45	0.03001

Appendix-B: Paleomagnetic data from Thermal Demagnetization

ID	Steps	X	Y	Z	M	ID	Steps	X	Y	Z	M	ID	Steps	X	Y	Z	M
GMS1-2B	NRM	-19.83	-0.11	9	0.2178	GMS1-3B	NRM	-17.51	8.27	-5.79	0.2021	GMS13-5B	NRM	-2.06	-14.61	-3.5	15.16
	T150	-19.38	0.08	8.69	0.2124		T150	-17.59	7.85	-5.28	0.1997		T150	-1.32	-13.08	-3.44	13.59
	T200	-2.05	-0.05	0.84	0.2211		T200	-17.58	8.75	-5.55	0.204		T200	-0.19	-10.91	-3.41	11.43
	T250	-17.84	1.36	8.65	0.1987		T250	-18.6	7.77	-6.63	0.2122		T250	0.44	-9.57	-3.27	10.12
	T300	-17.23	0.09	7.88	0.1895		T300	-12.66	5.22	-4.84	0.1452		T300	0.64	-8.3	-2.78	8.777
	T330	-14.96	0.49	6.83	0.1646		T330	-10.15	6.23	-2.85	0.1224		T330	1.72	-7.37	-2.69	8.03
	T360	-14.6	-0.03	6.35	0.1592		T360	-13.78	3.85	-6.19	0.1559		T360	1.54	-7.35	-2.76	7.997
	T390	-13.24	1.36	5.74	0.1449		T390	-10.53	9.25	-2.45	0.1423		T390	1.44	-6.65	-2.45	7.228
	T420	-10.98	0.57	4.83	0.1201		T420	-17.05	5.28	-1.96	0.1795		T420	1.69	-6.41	-2.39	7.048
	T450	-9.71	0.4	4.31	0.1063		T450	-3.35	5.05	-4.4	0.07488		T450	1.67	-5.79	-2.19	6.413
	T490	-7.82	0.57	3.65	0.08649		T490	-13.64	7.98	-0.32	0.1581		T490	1.44	-4.56	-1.82	5.116
	T520	-5.58	-0.16	2.9	0.06293		T520	-4.61	-4.18	-2.07	0.06558		T520	1.15	-3.6	-1.46	4.048
	T540	-4.46	0.15	2.33	0.0503		T540	-4.09	-0.01	-1.43	0.04336		T540	0.96	-2.47	-1	2.835
	T560	-2.56	0.19	1.34	0.02896		T560	-2.1	0.47	-0.75	0.02282		T560	6.78	-19.29	-7.94	2.193
	T580	-8.94	0.68	6.02	0.01079		T580	-7.28	0	-1.04	0.007356		T580	3.59	-8.51	-3.38	0.9832
	T600	-5.51	-0.23	5.15	0.007545		T600	-3.8	0.59	0.78	0.00392		T600	8.22	-19.65	-3	0.2151
	T640	-1.19	0.59	2.88	0.003169		T640	-3.3	16.7	14.35	0.002227		T640	1.62	-4.46	0.42	0.04759
	T680	0.56	0.45	1.98	0.002106		T680	0.53	0.45	1.41	0.001574		T680	0.26	-0.07	2.49	0.02506
	T680	0.56	0.45	1.98	0.002106		T680	0.53	0.45	1.41	0.001574		T680	0.26	-0.07	2.49	0.02506
GMS1-6B	NRM	-16.69	5.74	-6.31	0.1875	GMS1-7B	NRM	-2.22	1.51	-0.32	0.2699	GMS14-1B	NRM	3.88	10.41	-8.48	13.98
	T150	-16.19	5.06	-5.81	0.1793		T150	-2.18	1.42	-0.33	0.2623		T150	4.19	9.6	-8.51	13.5
	T200	-16.55	4.58	-5.62	0.1807		T200	-2.19	1.3	-0.3	0.2563		T200	4.62	8.7	-7.75	12.54
	T250	-14.84	3.04	-4.35	0.1576		T250	-2.07	1.18	-0.25	0.2393		T250	4.14	7.61	-6.86	11.05
	T300	-16.55	3.43	-5.72	0.1785		T300	-1.95	1.85	-0.27	0.2702		T300	4.44	6.76	-6.17	10.18
	T330	-13.09	2.29	-5.04	0.1422		T330	-2.09	1.13	0.07	0.238		T330	4.68	5.45	-5.19	8.862
	T360	-12.95	5.2	-0.37	0.1397		T360	-16.31	14.38	-2.77	0.2192		T360	5.07	5.33	-5.06	8.928
	T390	-6.17	0.17	-1.23	0.06296		T390	-6.8	13.29	0.35	0.1493		T390	4.83	4.95	-4.53	8.27
	T420	-5.12	2.5	-3.68	0.06784		T420	-18.29	15.63	1.77	0.2412		T420	4.62	4.32	-4.14	7.559
	T450	-11.33	5.77	-3.73	0.1325		T450	-2.36	1.73	-0.33	0.2941		T450	4.04	3.72	-3.37	6.442
	T490	-9.13	4.97	0.6	0.1042		T490	-16.5	1.43	-4.02	0.1704		T490	3.77	2.96	-2.53	5.423
	T520	-3.74	3.85	-0.97	0.05462		T520	-13.14	5.75	-3.69	0.1481		T520	3.01	1.98	-1.7	3.982
	T540	-2.14	-4.28	-4.48	0.06559		T540	-8.67	-0.83	5.8	0.1047		T540	2.18	1.35	-1.17	2.816
	T560	-5.61	1.91	-3.13	0.06697		T560	-5.5	-0.74	3.31	0.06462		T560	16.26	9.76	-7.83	2.052
	T580	-10.41	4.32	-3.69	0.01186		T580	-2.23	0.83	0.58	0.0245		T580	6.88	3.62	-2.03	0.8032
	T600	-5.4	2.67	-0.61	0.006056		T600	-12.31	4.05	1.72	0.01307		T600	2.71	1.12	0.02	0.2937
	T640	-0.79	0.99	1.92	0.0023		T640	-0.49	1.2	1.85	0.002259		T640	8.31	2.93	0.24	0.08815
	T680	0.53	0.69	1.5	0.001735		T680	0.78	0.91	2.65	0.002905		T680	0.93	1.1	3.25	0.03558
	T680	0.53	0.69	1.5	0.001735		T680	0.78	0.91	2.65	0.002905		T680	0.93	1.1	3.25	0.03558
GMS2-3B	NRM	-4.67	-5.74	-0.88	0.07453	GMS2-5B	NRM	-2.42	-2.51	-0.59	0.03539	GMS15-4B	NRM	-7.58	5.53	-6.55	1.145
	T150	-4.53	-5.74	-0.6	0.07338		T150	-2.29	-2.55	-0.56	0.03474		T150	-7.43	4.83	-6.04	1.072
	T200	-4.69	-5.64	-0.93	0.07394		T200	-2.16	-2.28	-0.42	0.03168		T200	-7.39	4.79	-5.96	1.063
	T250	-4.28	-5.06	-0.7	0.06662		T250	-1.94	-2.08	-0.46	0.02878		T250	-6.55	5.63	-5.86	1.044
	T300	-4.1	-5.37	-0.62	0.06785		T300	-2.01	-2.11	-0.41	0.02945		T300	-7.08	4.48	-5.72	1.015
	T330	-3.43	-4.81	-0.48	0.05928		T330	-2.08	-1.7	-0.4	0.02713		T330	-6.55	4.31	-5.37	0.9502
	T360	-3.16	-4.1	-0.49	0.05197		T360	-18.7	-16.96	-2.52	0.02537		T360	-6.32	4.41	-5.25	0.9324
	T390	-2.51	-4.7	-0.75	0.05384		T390	-17.69	-18.8	-2.17	0.02591		T390	-6.06	4.02	-4.95	0.8799
	T420	-2.48	-3.43	-0.54	0.04268		T420	-17.05	-14.14	-4.58	0.02261		T420	-6.23	4.02	-4.81	0.8843
	T450	-3.18	-4.13	-0.02	0.05214		T450	-14.12	-14.86	-2.41	0.02064		T450	-5.88	3.93	-4.62	0.8444
	T490	-3	-3.14	-0.32	0.04359		T490	-12.82	-12.64	-3.4	0.01832		T490	-5.47	3.53	-4.16	0.7724
	T520	-2.35	-3.63	0.13	0.04331		T520	-8.56	-10.84	0.22	0.01381		T520	-5	3.33	-4.06	0.7252
	T540	-2.44	-3.17	-0.25	0.04011		T540	-9.39	-9.36	-1.6	0.01335		T540	-4.53	3.03	-3.53	0.6492
	T560	-1.84	-2.64	-0.03	0.03215		T560	-6.97	-7.23	-1.28	0.01013		T560	-4.04	2.63	-3.1	0.5731
	T580	-11.99	-15.63	-0.73	0.01971		T580	-5.07	-5.17	-0.72	0.007281		T580	-3.67	2.32	-2.77	0.5145
	T600	-7.89	-9.81	-0.05	0.01259		T600	-3.1	-3.29	-0.26	0.004521		T600	-2.96	1.98	-2.13	0.4151
	T640	1.17	-1.84	7.87	0.000817		T640	-0.09	0.1	7.1	0.0007097		T640	-2.12	1.99	0.7	0.02986
	T680	3.38	2.08	10.62	0.001133		T680	-0.02	3.36	10.76	0.001127		T680	-0.19	1.22	2.13	0.02463
	T680	3.38	2.08	10.62	0.001133		T680	-0.02	3.36	10.76	0.001127		T680	-0.19	1.22	2.13	0.02463
GMS2-8B	NRM	-8.42	-12.53	0.61	0.01511	GMS2-9B	NRM	-17.01	-14.71	-0.16	0.02248	GMS16-5A	NRM	5.99	-2.68	-2.19	0.06917
	T150	-9.05	-12.68	1.02	0.01561		T150	-16.45	-13.73	1	0.02145		T150	5.72	-2.45	-2.21	0.06604
	T200	-8.98	-11.91	0.92	0.01494		T200	-15.31	-13.63	0.92	0.02052		T200	5.57	-2.41	-2.16	0.06441
	T250	-8.57	-12.22	0.75	0.01494		T250	-13.1	-12.8	0.65	0.01833		T250	5.47	-2.19	-2.06	0.06243
	T300	-9.04	-11.47	0.29	0.01461		T300	-13.42	-13.22	3.19	0.0191		T300	5.23	-2	-1.98	0.05943
	T330	-7.57	-10.93	0.58	0.01331		T330	-10.37	-11.72	1.5	0.01572		T330	4.94	-2.13	-1.83	0.05681
	T360	-7.67	-10.72	0.71	0.0132		T360	-13.03	-11.38	0.32	0.01731		T360	4.87	-2.08	-1.81	0.05598
	T390	-6.5	-9.8	0.54	0.01178		T390	-10.24	-7.81	0.81	0.01291		T390	4.62	-1.93	-1.78	0.05309
	T420	-6.8	-10.16	0.8	0.01225		T420	-11.02	-8.26	0.21	0.01377		T420	4.48	-1.99	-1.67	0.05175
	T450	-5.75	-8.97	0.57	0.01067		T450	-10.78	-7.58	-0.4	0.01319		T450	3.99	-1.83	-1.57	0.0466
	T490	-5.28	-7.59	0.7	0.009274		T490	-9.69	-6.78	0.22	0.01182		T490	3.46	-1.71	-1.24	0.04052
	T520	-4.48	-6.53	0.71	0.00795		T520	-7.47	-5.39	0.04	0.009208		T520	2.49	-1.28	-0.94	0.02952
	T540	-3.39	-5.24	0.46	0.006259		T540	-6.42	-5.99	-0.36	0.008782		T540	2.03	-0.92	-0.67	0.02324
	T560	-2.32	-3.71	0.64	0.004418		T560	-5.49	-4.6	0.61	0.007191		T560	16.84	-7.86	-5.58	0.0194
	T580	-1.49	-2.36	0.58	0.002847		T580	-4.08	-3.41	0.58	0.005343		T580	8.63	-4.84	-2.48	0.0102
	T600	-10.05	-15.93	4.71	0.001942		T600	-2.05	-1.97	0.51	0.002888		T600	4.4	-2.02	-0.05	0.04841
	T640	0.87	0.41	6.98	0.000705		T640	-0.45	1.08	6.12	0.0006228		T640	5.07	2.35	5.38	0.00078
	T680	3.85	4	13.23	0.001435		T680	2.54	2.6	9.92	0.001057		T680	0.42	-0.05	2.6	0.00264
	T680	3.85	4	13.23	0.001435		T680	2.54	2.6	9.92	0.001057		T680	0.42	-0.05	2.6	0.00264

GMS2-10B						GMS3-1B						GMS18-1B				
	NRM	-2.06	-2.79	0.3	0.03478		NRM	-3.27	-2.02	-3.03	4.89		NRM	-4.72	12.25	3.82	1.367
	T150	-1.8	-2.69	0.46	0.03272		T150	-1.62	-3.4	-1.12	3.931		T150	-4.84	10.52	4.2	1.232
	T200	-1.88	-2.6	0.42	0.03238		T200	-3.95	-2.26	-0.81	4.623		T200	-4.5	9.59	3.85	1.127
	T250	-1.77	-2.49	0.43	0.0309		T250	-1.5	-3.97	-1.2	4.409		T250	-3.97	8.36	3.29	0.9823
	T300	-1.45	-2.23	0.22	0.0267		T300	6.91	-1.43	13.51	1.524		T300	-3.38	7.45	3.39	0.8855
	T330	-1.4	-2.08	0.48	0.02558		T330	-2.19	-1.02	0.08	2.419		T330	-2.77	6.6	2.91	0.7722
	T360	-1.33	-2.04	0.33	0.02462		T360	-2.32	-1.4	0.17	2.719		T360	-2.46	5.89	2.58	0.6886
	T390	-0.95	-2.01	0.19	0.02234		T390	-2.09	-0.31	0.14	2.118		T390	-2.85	5.07	1.59	0.6032
	T420	-11.31	-18.77	3.94	0.02226		T420	-17.43	7.97	1.15	1.92		T420	-2	4.14	1.84	0.4953
	T450	-13.22	-16	2.72	0.02093		T450	-3.08	2.94	0.03	0.4263		T450	-1.51	3.67	1.75	0.4335
	T490	-14.52	-17.56	3.97	0.002313		T490	-9.41	10.45	6.43	1.547		T490	-1.3	2.96	1.58	0.3601
	T520	-12.39	-18.26	2.69	0.02223		T520	-6.34	5.19	6.37	1.037		T520	-0.77	2.44	1.17	0.2817
	T540	-13.38	-17.17	2.95	0.02196		T540	-4.52	0.11	2.51	0.5171		T540	-4.88	14.25	8.47	0.1728
	T560	-11.81	-16.56	3.51	0.02064		T560	2.27	18.45	13.56	0.2301		T560	-3.1	7.4	6.11	0.1009
	T580	-9.18	-14.09	2.93	0.01707		T580	1.05	0.61	2.15	0.2463		T580	-2.01	4.52	4.56	0.06733
	T600	-5.76	-8.61	1.73	0.0105		T600	-0.09	0.69	1.96	0.2076		T600	-0.66	2.96	3.79	0.04856
	T640	0.83	-0.32	7.78	0.000783		T640	0.49	-0.08	2.17	0.2228		T640	-4.5	12.57	15.84	0.02072
	T680	-0.11	3.57	10.95	0.001152		T680	-0.17	0.55	2.22	0.2297		T680	3.36	3.58	13.8	0.01465
	T680	-0.11	3.57	10.95	0.001152		T680	-0.17	0.55	2.22	0.2297		T680	3.36	3.58	13.8	0.01465
GMS3-9B	NRM	-0.49	-5.15	2.78	5.872	GMS3-10B	NRM	-0.6	-5.51	2.64	6.137	GMS18-4B	NRM	6.29	9.96	9.87	1.537
	T150	-1.08	-4.16	1.84	4.675		T150	-0.54	-3.85	2.28	4.506		T150	5.53	8.86	9.03	1.381
	T200	-0.63	-3.16	2.42	4.023		T200	-0.49	-3.29	2.27	4.028		T200	5.26	8	7.95	1.244
	T250	-0.37	-2.9	1.53	3.301		T250	-0.63	-2.95	1.53	3.382		T250	3.7	6.67	7.49	1.069
	T300	-0.69	-2.74	2.17	3.56		T300	-0.52	-2.77	2.5	3.773		T300	3.7	5.46	6.32	0.9137
	T330	-0.8	-2.13	2.27	3.215		T330	-0.88	-1.88	2.08	2.94		T330	3	4.8	5.27	0.7733
	T360	-0.79	-2.08	1.95	2.957		T360	-0.9	-2.43	1.71	3.106		T360	3.01	4.27	4.54	0.6926
	T390	-0.24	-2	2.38	3.117		T390	-0.49	-2.47	2.06	3.252		T390	2.26	3.47	3.98	0.5743
	T420	-0.48	-1.79	2.12	2.82		T420	-0.62	-1.9	2.04	2.857		T420	2.24	2.76	3.54	0.5015
	T450	0.03	-1.42	2.28	2.685		T450	-3.97	-14.36	19.1	2.423		T450	1.77	2.65	3.19	0.4508
	T490	-0.28	-0.94	1.98	2.21		T490	-2.61	-9.87	17.68	2.042		T490	1.4	1.86	2.35	0.3302
	T520	-0.55	-5.06	18.36	1.905		T520	-2.58	-4.25	17.23	1.793		T520	10.11	12.46	13.98	0.2129
	T540	-0.61	-0.29	14.49	1.451		T540	-0.29	-3.62	13.47	1.395		T540	2.01	4.11	6.55	0.07988
	T560	0.11	-0.02	13.58	1.358		T560	0.74	-0.24	10.44	1.047		T560	2.86	3.97	4.93	0.06943
	T580	1.06	1.06	12.14	1.223		T580	-0.4	1.04	9.76	0.9823		T580	2.23	2.7	3.66	0.05064
	T600	1.35	0.27	8.17	0.8288		T600	0.63	0.48	6.54	0.6589		T600	1.74	1.4	2.35	0.03245
	T640	-5.59	10.29	7.29	0.138		T640	4.4	1.73	12.82	0.1366		T640	2.33	0.7	8.51	0.00885
	T680	0.38	-0.2	3.18	0.3207		T680	0.29	0.22	2.9	0.2924		T680	-1.2	-1.36	4.72	0.00506
	T680	0.38	-0.2	3.18	0.3207		T680	0.29	0.22	2.9	0.2924		T680	-1.2	-1.36	4.72	0.00506
GMS4-1B	NRM	5.16	3.32	6.4	8.871	GMS4-2B	NRM	6.28	4.01	8.3	11.15	GMS19-2B	NRM	0.23	2.27	0.79	0.2415
	T150	4.78	3.35	6.42	8.675		T150	6.3	3.82	8.27	11.07		T150	3.08	19.78	7.11	0.2124
	T200	5.04	3.32	6.36	8.766		T200	6.19	3.7	8.19	10.91		T200	2.38	18.1	6.27	0.193
	T250	4.86	3.09	6.31	8.54		T250	6.1	3.61	8.19	10.83		T250	1.89	15.04	6.11	0.1634
	T300	4.95	3.29	6.31	8.674		T300	6.3	3.73	8.14	10.94		T300	0.92	12.44	5.16	0.135
	T330	4.92	3.3	6.27	8.625		T330	6.36	3.24	8.11	10.81		T330	1.03	9.65	4.06	0.1052
	T360	4.95	3.18	6.23	8.571		T360	6.34	3.59	8.04	10.86		T360	1.22	9.18	4.05	0.1011
	T390	4.96	3.41	6.06	8.542		T390	6.31	3.51	7.94	10.73		T390	0.74	8.55	3.83	0.09394
	T420	4.84	3.33	5.89	8.314		T420	6.31	3.37	7.87	10.63		T420	1.13	7.76	3.41	0.08554
	T450	4.68	3.07	5.74	8.012		T450	6.22	3.15	7.61	10.32		T450	0.44	6.8	3.1	0.07482
	T490	4.29	2.86	5.49	7.529		T490	5.78	3.04	7.3	9.791		T490	0.93	6.07	2.9	0.06791
	T520	4.3	2.95	5.16	7.337		T520	5.47	2.95	6.8	9.208		T520	0.61	5.23	2.44	0.05802
	T540	3.68	2.56	4.51	6.36		T540	4.61	2.46	5.74	7.768		T540	0.81	4.38	2.3	0.05013
	T560	3.09	2.07	3.65	5.214		T560	3.88	1.96	4.74	6.431		T560	0.12	4.06	2.01	0.04533
	T580	12.03	6.75	16.21	2.128		T580	11.36	5.76	14.76	1.95		T580	0.46	2.98	1.78	0.03501
	T600	3.8	2.58	5.51	0.7168		T600	4.11	2.17	5.88	0.7495		T600	3.05	19.48	15.01	0.02478
	T640	1.83	1.28	2.69	0.3492		T640	2.2	1.06	3.15	0.3984		T640	1.51	2.6	5.16	0.00598
	T680	8.28	6.15	15	0.1821		T680	4.52	2.72	12.82	0.1387		T680	1.02	1.32	4.77	0.00505
	T680	8.28	6.15	15	0.1821		T680	4.52	2.72	12.82	0.1387		T680	1.02	1.32	4.77	0.00505
GMS4-4B	NRM	4.91	-1.89	5.88	7.894	GMS4-5B	NRM	4.62	1.62	5.49	7.353	GMS19-5B	NRM	-0.49	2.58	0.66	0.2703
	T150	4.78	-2.05	5.89	7.861		T150	4.37	1.18	5.5	7.13		T150	-0.44	2.37	0.55	0.2478
	T200	4.73	-2.16	5.82	7.804		T200	4.55	1.46	5.37	7.191		T200	-0.42	2.17	0.5	0.2265
	T250	4.58	-2.18	5.73	7.651		T250	4.38	1.2	5.39	7.049		T250	-4.29	19.19	5.72	0.2048
	T300	4.84	-1.95	5.69	7.721		T300	4.51	1.57	5.21	7.068		T300	-2.69	13.25	3.93	0.1408
	T330	4.58	-2.06	5.67	7.58		T330	4.3	1.53	5.17	6.897		T330	-1.79	11.84	3.48	0.1247
	T360	4.61	-1.99	5.67	7.57		T360	4.37	1.69	5	6.855		T360	-1.59	10.17	3.44	0.1086
	T390	4.61	-1.8	5.48	7.385		T390	4.29	1.31	4.93	6.663		T390	-1.76	9.2	2.75	0.09761
	T420	4.48	-1.94	5.33	7.224		T420	4.12	1.47	4.61	6.35		T420	-2.07	8.8	3.01	0.09528
	T450	4.4	-1.85	5.11	6.995		T450	3.89	1.32	4.58	6.152		T450	-2.12	8.02	2.55	0.08676
	T490	4.09	-1.86	4.92	6.661		T490	3.42	1.17	4.1	5.463		T490	-0.74	6.52	2.29	0.06945
	T520	4.08	-1.78	4.69	6.466		T520	2.62	0.99	3.15	4.22		T520	-1.15	5.29	2.2	0.0584
	T540	3.45	-1.34	3.95	5.413		T540	12.27	3.97	15.19	1.992		T540	-0.79	4.02	1.78	0.04471
	T560	2.85	-1.05	3.29	4.472		T560	4.44	1.48	5.34	0.7099		T560	-0.55	3.14	1.6	0.03562
	T580	15.34	-6.06	17.86	2.431		T580	2.78	0.99	3.37	0.4479		T580	-1.05	14.8	12.41	0.01934
	T600	4.77	-2.16	6.14	0.8069		T600	1.93	0.66	2.69	0.3374		T600	0.59	6.87	10.18	0.01229
	T640	2.27	-0.87	2.9	0.3784		T640	9.04	2.43	13.52	0.1645		T640	1.09	2.09	6.59	0.007
	T680	10.3	-4.84	15.67	0.1937		T680	-0.33	0.8	3.37	0.03478		T680	1.5	0.99	7.42	0.00763
	T680	10.3	-4.84	15.67	0.1937		T680	-0.33	0.8	3.37	0.03478		T680	1.5	0.99	7.42	0.00763
GMS4-6B	NRM	6.04	4.07	6.75	9.935	GMS2-3-4B	NRM	-5.73	18.47	-3.74	1.97	GMS2-1-2B	NRM	1.12	3.1	0.54	0.3335
	T150	5.01	4.38	6.1	9.028		T150	-4.27	17.75	-3.49	1.858		T150	1.14	3.15	0.48	0.3386
	T200	4.94	4.52	5.93	8.945		T200	-4.71	16.93	-3.33	1.788		T200	1.11	3.08	0.48	0.3308
	T250	4.65	4.46	5.86	8.712		T250	-4.8	16.16	-2.92	1.711		T250	1.2	3.05	0.48	0.3317

	T300	4.93	4.43	5.8	8.804		T300	-4.09	15.08	-2.76	1.586		T300	1.05	3.01	0.43	0.3214
	T330	4.59	4.53	5.87	8.72		T330	-4.98	14.07	-2.54	1.514		T330	1	2.87	0.42	0.3065
	T360	4.86	4.33	5.75	8.688		T360	-4.16	13.7	-2.31	1.45		T360	1.19	2.87	0.44	0.3144
	T390	4.45	4.55	5.66	8.516		T390	-4.52	13.05	-2.18	1.399		T390	0.93	2.78	0.47	0.2972
	T420	4.39	4.47	5.52	8.346		T420	-3.84	12.57	-2.38	1.336		T420	0.94	2.73	0.45	0.292
	T450	4.43	4.26	5.26	8.094		T450	-3.75	11.68	-2.1	1.245		T450	0.88	2.62	0.39	0.2787
	T490	4.33	4.02	5.05	7.77		T490	-2.9	10.28	-1.98	1.087		T490	0.79	2.18	0.33	0.2341
	T520	3.83	3.93	4.7	7.225		T520	-3.38	9.07	-1.58	0.9806		T520	6.02	15.74	2.98	0.1711
	T540	3.22	3.28	3.88	6.009		T540	-2.52	7.65	-1.3	0.8157		T540	4.28	10.13	2	0.1118
	T560	2.47	2.47	3.06	4.638		T560	-1.83	5.8	-0.96	0.6154		T560	2.6	6.96	1.27	0.07534
	T580	10.26	10.62	13.72	2.015		T580	-0.79	2.32	-0.14	0.2455		T580	0.9	3.36	0.8	0.03567
	T600	3.95	4.24	5.66	0.8101		T600	-4.29	14.48	0.39	0.1511		T600	5.54	12.1	5.9	0.01456
	T640	2.18	2.04	2.82	0.4107		T640	-0.26	2.37	1.57	0.02855		T640	1.77	3.64	2.79	0.00492
	T680	5.13	5.59	11.27	0.1359		T680	0.13	0.62	2.1	0.02193		T680	-0.45	0.25	2.49	0.00254
	T680	5.13	5.59	11.27	0.1359		T680	0.13	0.62	2.1	0.02193		T680	-0.45	0.25	2.49	0.00254
GMS4-7B	NRM	6.04	4.07	6.75	9.935	GMS5-1B	NRM	3.31	8.34	11.18	14.33	GMS20-5B	NRM	9.73	15.66	14.98	0.00238
	T150	5.88	4.04	6.7	9.784		T150	2.78	7.8	10.89	13.68		T150	8.59	13.62	12.85	0.00206
	T200	5.53	3.88	6.71	9.517		T200	3.4	7.21	10.92	13.52		T200	7.83	11.9	11.67	0.00184
	T250	5.68	3.98	6.59	9.562		T250	3.14	7.77	10.65	13.56		T250	7.11	10.03	9.24	0.00154
	T300	5.7	4.03	6.46	9.513		T300	3.82	8.24	10.33	13.75		T300	5.87	8.32	9.01	0.00136
	T330	5.84	3.58	6.42	9.389		T330	0.19	5.29	4.99	7.276		T330	4.51	7.26	6.68	0.00109
	T360	5.83	3.53	6.45	9.38		T360	3.87	7.56	10.26	13.32		T360	3.87	7.01	6.54	0.00103
	T390	5.59	3.92	6.09	9.148		T390	4.01	7.32	10.24	13.21		T390	4	5.43	5.52	0.00087
	T420	5.49	3.85	5.87	8.908		T420	3.6	6.64	9.62	12.23		T420	3.41	6.38	5.05	0.00088
	T450	5.17	3.36	5.69	8.389		T450	3.51	7.01	9.26	12.13		T450	3.24	4	5.2	0.00073
	T490	4.85	3.15	5.33	7.862		T490	2.98	6.1	8.65	11		T490	2.51	1.54	4.87	0.00057
	T520	4.09	2.61	4.38	6.536		T520	2.11	5.11	6.51	8.54		T520	1.63	0.57	3.6	0.0004
	T540	2.07	1.51	2.37	3.496		T540	0.28	2.06	3.52	4.086		T540	1.46	-0.4	2.8	0.00032
	T560	12.07	8.23	13.81	2.011		T560	-2.19	13.28	11.92	1.798		T560	0.75	-0.98	7.29	0.00074
	T580	5.26	3.5	6.54	0.9096		T580	2.04	3.88	5.42	0.6969		T580	0.23	0.3	12.8	0.00128
	T600	3.48	2.37	4.67	0.6285		T600	1.22	1.83	3.93	0.45		T600	0.57	-0.03	2.53	0.0026
	T640	1.95	1.24	2.55	0.344		T640	0.48	1.03	2.42	0.267		T640	0.79	-0.54	2.16	0.00236
	T680	0.39	0.6	5.71	0.05757		T680	4.03	3.82	11.19	0.125		T680	0.37	-0.66	3.91	0.00398
	T680	0.39	0.6	5.71	0.05757		T680	4.03	3.82	11.19	0.125		T680	0.37	-0.66	3.91	0.00398
GMS5-2B	NRM	6.3	2.44	12.77	14.45	GMS5-8B	NRM	4.71	2.57	7.09	8.892	GMS23-1B	NRM	-9.22	7.46	-2.81	1.219
	T150	6.52	2.1	12.36	14.13		T150	4.65	2.91	6.95	8.852		T150	-9.11	6.65	-2.48	1.155
	T200	5.84	1.73	12.25	13.68		T200	4.52	2.8	6.81	8.644		T200	-8.91	6.64	-2.55	1.14
	T250	5.92	2.4	11.87	13.48		T250	4.62	2.75	6.66	8.558		T250	-8.21	6.06	-2.34	1.047
	T300	6.11	2.54	11.86	13.58		T300	4.58	2.73	6.61	8.494		T300	-7.52	5.66	-2.14	0.9649
	T330	6	2.15	11.51	13.16		T330	4.56	2.5	6.4	8.246		T330	-6.73	5.43	-1.92	0.8854
	T360	5.89	2.05	11.48	13.06		T360	4.38	2.48	6.42	8.162		T360	-6.69	5.21	-1.69	0.8649
	T390	5.9	2.42	11.29	12.96		T390	4.52	2.56	6.24	8.121		T390	-6.59	4.91	-1.71	0.8393
	T420	5.76	2.24	11.12	12.72		T420	4.35	2.34	6.17	7.904		T420	-5.87	4.58	-1.55	0.7605
	T450	5.55	1.95	10.57	12.09		T450	3.94	2.14	5.91	7.412		T450	-5.65	4.33	-1.45	0.7263
	T490	4.95	1.81	9.91	11.23		T490	3.82	1.81	5.4	6.858		T490	-5.05	3.72	-1.4	0.6428
	T520	4.24	1.55	7.95	9.137		T520	3.2	1.67	4.52	5.786		T520	-4.22	3.18	-1.09	0.5398
	T540	2.23	0.73	4.9	5.437		T540	2.05	1.01	2.92	3.705		T540	-3.49	2.64	-0.87	0.4457
	T560	1.45	0.59	3.1	3.471		T560	13.68	5.93	19.79	2.478		T560	-2.98	2.33	-0.72	0.3848
	T580	4.35	0.92	10.01	1.096		T580	4.54	2.29	7.17	0.8789		T580	-16.44	12	-2.99	0.2057
	T600	1.98	0.49	6.35	0.6669		T600	2.3	1.08	4.22	0.4931		T600	-8.18	6.06	-0.43	0.1019
	T640	0.8	0.24	2.7	0.283		T640	9.59	5.91	18.95	0.2205		T640	-17.22	14.36	5.5	0.02308
	T680	1.41	1.69	14.23	0.144		T680	1.92	2.04	9.31	0.09722		T680	-0.48	0.27	11.71	0.01172
	T680	1.41	1.69	14.23	0.144		T680	1.92	2.04	9.31	0.09722		T680	-0.48	0.27	11.71	0.01172
GMS6-2B	NRM	1.56	-7.56	1.04	7.793	GMS6-4B	NRM	2.72	-7.03	1.9	7.777	GMS9-1B	NRM	0.29	-18.11	-5.02	188
	T150	1.79	-7.59	1.25	7.893		T150	2.64	-7.18	2.08	7.924		T150	0.1	-16.54	-4.94	172.6
	T200	1.46	-7.51	1.26	7.752		T200	2.52	-7.03	2.15	7.773		T200	0.14	-14.68	-4.51	153.6
	T250	1.71	-7.37	1.4	7.696		T250	2.9	-6.9	2.04	7.762		T250	0.49	-13.01	-4.02	136.2
	T300	1.36	-6.63	1.62	6.956		T300	2.68	-6.87	2.31	7.733		T300	0.41	-11.25	-3.81	118.8
	T330	1.4	-6.53	1.67	6.885		T330	2.62	-6.88	2.39	7.741		T330	0.52	-10.12	-3.26	106.4
	T360	1.05	-7.33	1.54	7.565		T360	2.59	-6.84	2.26	7.653		T360	0.75	-9.56	-3.12	100.8
	T390	1.24	-7.17	1.73	7.483		T390	2.87	-6.66	2.43	7.647		T390	0.31	-8.63	-2.84	90.92
	T420	1.22	-6.96	1.7	7.268		T420	2.45	-6.53	2.45	7.393		T420	0.19	-7.67	-2.49	80.63
	T450	1.15	-6.33	1.78	6.671		T450	2.71	-5.85	2.37	6.868		T450	0.45	-6.44	-2.03	67.69
	T490	0.58	-4.45	1.45	4.715		T490	1.96	-4.18	1.86	4.972		T490	0.29	-4.52	-1.53	47.8
	T520	0.42	-2.5	0.99	2.722		T520	1.19	-2.62	1.42	3.212		T520	0.02	-3.46	-1.14	36.41
	T540	3.19	-14.29	7.82	1.66		T540	6.79	-17.22	9.94	2.101		T540	0.11	-2.24	-0.74	23.65
	T560	1.55	-7.35	5.58	0.9359		T560	6.07	-11.72	8.52	1.571		T560	1.15	-15.47	-5.03	16.31
	T580	0.87	-2.17	3.99	0.4623		T580	2.26	-3.65	4.92	0.6532		T580	-0.24	-5.62	-1.79	5.901
	T600	0.27	-1.1	3.25	0.3441		T600	1.24	-1.56	3.66	0.4165		T600	-0.05	-6.11	-1.66	0.633
	T640	1.72	-4.51	13.31	0.1416		T640	3.92	-7.13	11.31	0.1393		T640	-0.5	-9.66	-2.47	0.09983
	T680	1.2	1.57	18.2	0.1831		T680	2.03	-0.84	15.5	0.1566		T680	0.57	-1.93	2.46	0.03178
	T680	1.2	1.57	18.2	0.1831		T680	2.03	-0.84	15.5	0.1566		T680	0.57	-1.93	2.46	0.03178
GMS6-5B	NRM	0.89	-5.99	1.97	6.368	GMS6-7B	NRM	3.08	-6.94	2.53	8.006	GMS10-2B	NRM	0.24	-5.85	-5.03	7.721
	T150	1.28	-6.07	2.07	6.535		T150	3.16	-6.8	2.83	8.017		T150	0.47	-5.52	-4.93	7.421
	T200	1.2	-5.97	2.05	6.421		T200	3.37	-6.86	2.77	8.131		T200	0.02	-5.46	-4.66	7.174
	T250	1.05	-5.89	2.03	6.321		T250	3.67	-6.91	2.83	8.321		T250	0.48	-5.4	-4.31	6.925
	T300	1.12	-5.79	2.19	6.293		T300	3.05	-6.83	2.89	8.018		T300	0.42	-5.28	-4.11	6.699
	T330	0.94	-5.7	2.22	6.192		T330	2.96	-6.91	3.09	8.125		T330	0.63	-5.24	-3.54	6.356
	T360	1.11	-5.72	2.17	6.219		T360	2.9	-6.85	3.02	8.025		T360	0.64	-5.11	-3.53	6.244
	T390	0.93	-5.35	2.17	5.845		T390	3	-6.23	2.83	7.47		T390	0.3	-4.92	-3.28	5.922
	T420	0.81	-4.69	2.02	5.166		T420	2.32	-5.85	3	6.973		T420	0.11	-4.72	-2.95	5.565
	T450	0.67	-3.67	1.67	4.085		T450	2.14	-5.9	2.77	6.86		T450	0.28	-4.39	-2.6	5.113
	T490	0.47	-2.07	1.07	2.382		T490	1.19	-3.36	1.57	3.896		T490	0.29	-3.66	-1.77	4.082
	T520	2.44	-10.35	6.59	1.251		T520	0.61	-2.22	1.31	2.647		T520	0.31	-3.04	-1.47	3.387
	T540	0.67	-3.34	3.55	0.4921		T540	0.91	-2.49	1.05	2.855		T540	0.43	-2.42	-1.09	2.688
	T560	0.39	-1.8	2.76	0.3318		T560	6.54	-12.93	7.64	1.638		T560	1.49	-8.36	-3.73	0.9271
	T580	0.41	-0.61	2.04	0.2165		T580	1.72	-3.46	4.08	0.5617		T580	0.48	-3.86	-1.55	0.4191
	T600	1.03	-5.19	18.42	0.1917		T600	0.55	-2.12	2.58	0.3381		T600	0.44	-2.29	-0.37	0.2363

	T640	0.54	-0.41	5.97	0.06011		T640	2.77	-8.25	19.36	0.2122		T640	1.52	-7.3	2.51	0.07869
	T680	0.86	2.38	11.84	0.121		T680	-0.91	1.1	15.12	0.1519		T680	0.86	-0.2	4	0.04093
	T680	0.86	2.38	11.84	0.121		T680	-0.91	1.1	15.12	0.1519		T680	0.86	-0.2	4	0.04093
GMS6-8B	NRM	-2.37	-6.88	1.79	7.491	GMS6-9B	NRM	3.54	-6.29	2.76	7.726	GMS6-9C	NRM	2.04	-6.04	2.22	6.755
	T150	-2.78	-7	1.89	7.762		T150	2.9	-6.46	2.86	7.636		T150	2.48	-6.09	2.31	6.968
	T200	-2.65	-6.88	1.77	7.582		T200	2.92	-6.3	3.02	7.567		T200	2.41	-5.99	2.45	6.902
	T250	-2.48	-6.86	1.84	7.528		T250	3.08	-6.15	2.98	7.502		T250	2.32	-5.87	2.47	6.776
	T300	-2.38	-6.7	2.03	7.39		T300	3.09	-6.28	3.04	7.629		T300	2.21	-5.67	2.59	6.618
	T330	-2.63	-6.64	2.07	7.44		T330	2.49	-6.2	3.09	7.364		T330	2.07	-5.68	2.6	6.583
	T360	-2.38	-6.63	1.95	7.306		T360	2.69	-6.31	2.99	7.489		T360	2.26	-5.73	2.47	6.637
	T390	-2.74	-6.54	2.14	7.413		T390	2.52	-6.07	3.11	7.27		T390	2.11	-5.56	2.6	6.492
	T420	-2.55	-6.24	2.19	7.088		T420	2.38	-5.85	3.09	7.035		T420	1.89	-5.31	2.56	6.189
	T450	-1.71	-5.5	1.96	6.084		T450	2.06	-5.11	2.85	6.209		T450	1.67	-4.38	2.26	5.199
	T490	-1.42	-4.07	1.58	4.589		T490	1.83	-3.91	2.33	4.91		T490	1.31	-3.19	1.77	3.877
	T520	-0.81	-2.64	1.15	2.989		T520	1.15	-2.35	1.69	3.112		T520	6.83	-17.82	11.9	2.249
	T540	-4.83	-19.47	8.95	2.196		T540	7.52	-17.27	13.04	2.291		T540	4.23	-12.89	9.27	1.643
	T560	-3.79	-14.61	7.85	1.702		T560	6.05	-13.13	10.44	1.783		T560	3.78	-9.23	7.79	1.266
	T580	-0.96	-4.55	4.56	0.6511		T580	2.7	-4.6	5.68	0.7794		T580	0.85	-2.72	4.47	0.5299
	T600	-0.68	-1.74	3.26	0.3758		T600	1.02	-1.99	3.87	0.4469		T600	0.52	-1.4	3.44	0.3753
	T640	-1.26	-7.77	9.01	0.1196		T640	3.61	-7.83	13.15	0.1572		T640	1.75	-5.12	12.38	0.1351
	T680	0.94	-1.49	12.76	0.1289		T680	0.84	-0.87	14.33	0.1438		T680	0.74	-0.76	14.6	0.1464
	T680	0.94	-1.49	12.76	0.1289		T680	0.84	-0.87	14.33	0.1438		T680	0.74	-0.76	14.6	0.1464
GMS7-3B	NRM	2.53	2.22	-9.43	0.1001	GMS7-4B	NRM	3.45	0.27	-8.63	0.09302	GMS1-1B	NRM	5.5	0.06	0.15	0.5498
	T150	2.42	2.18	-9.39	0.09942		T150	3.41	0.09	-8.71	0.09355		T150	5.34	0.22	0.22	0.5348
	T200	2.39	1.73	-9.32	0.09771		T200	3.65	0.19	-8.62	0.0936		T200	5.19	-0.02	0.13	0.5196
	T250	2.31	2	-8.97	0.09477		T250	3.26	0.11	-8.55	0.09151		T250	5.07	0.09	0.27	0.5073
	T300	2.28	1.21	-8.77	0.0914		T300	3.36	-0.03	-8.39	0.09034		T300	4.96	-0.03	0.18	0.4959
	T330	2.1	1.55	-7.53	0.0797		T330	2.97	-0.04	-7.6	0.08159		T330	4.58	-0.24	0.19	0.4586
	T360	1.87	1.62	-6.85	0.07279		T360	2.93	0.02	-7.3	0.07868		T360	4.51	-0.34	0.24	0.4532
	T390	1.58	1.59	-5.11	0.05583		T390	2.8	0.19	-6.53	0.07111		T390	4.35	-0.13	0.16	0.4357
	T420	1.26	1.72	-3.89	0.04439		T420	2.35	0.29	-5.48	0.05967		T420	4.22	-0.07	0.19	0.4221
	T450	1.33	1.74	-2.84	0.03589		T450	1.86	0.48	-4.25	0.04659		T450	4	-0.25	0.13	0.4013
	T490	10.11	16.79	-14.33	0.02427		T490	1.51	0.73	-2.9	0.03348		T490	3.67	-0.23	0.18	0.3679
	T520	7.33	15	-7	0.01811		T520	12.45	7.78	-17.92	0.02317		T520	3.02	-0.25	0.17	0.3035
	T540	6.53	13.51	-1.52	0.01509		T540	8.44	7.68	-9.48	0.01484		T540	2.28	-0.19	0.15	0.2291
	T560	4.7	9.73	0.82	0.01084		T560	6.91	6.96	-8.28	0.01283		T560	17.96	-1.98	1.12	0.181
	T580	2.56	6.05	1.27	0.00669		T580	6.53	6.45	-5.52	0.01071		T580	9.47	-0.47	0.88	0.0952
	T600	1.46	3.88	2	0.004607		T600	4.06	4.53	-3.29	0.006917		T600	4.34	-0.3	1	0.04466
	T640	-0.47	1.78	14.51	0.001463		T640	16.99	15.53	-9.05	0.002473		T640	2.12	-0.79	4.88	0.00538
	T680	-0.27	0.39	2.23	0.002278		T680	4.75	2.58	8.7	0.001025		T680	0.83	-0.26	7.16	0.00721
	T680	-0.27	0.39	2.23	0.002278		T680	4.75	2.58	8.7	0.001025		T680	0.83	-0.26	7.16	0.00721
GMS7-5B	NRM	6.58	0.86	-19.76	0.2085	GMS8-1B	NRM	-0.16	3.52	1.53	3.841	GMS1-7B	NRM	-1.25	-2.25	-0.55	0.2633
	T150	6.8	0.39	-19.75	0.2089		T150	-0.3	3.07	1.4	3.382		T150	-0.99	-2.26	-0.45	0.2508
	T200	6.2	0.35	-19.65	0.2061		T200	-0.31	2.78	1.27	3.071		T200	-1.17	-2.16	-0.47	0.2498
	T250	5.9	0.04	-19.47	0.2034		T250	-0.2	2.57	1.01	2.772		T250	-1.15	-2.1	-0.59	0.2462
	T300	6.05	0.31	-18.73	0.1969		T300	-0.26	2.4	1.23	2.706		T300	-10.67	-19.55	-4.3	0.2269
	T330	5.55	0.27	-17.49	0.1835		T330	-0.44	2.23	1.22	2.583		T330	-8.58	-18.4	-5.29	0.2099
	T360	5.35	0.05	-15.83	0.1671		T360	-0.43	2.16	1.01	2.419		T360	-9.34	-17.26	-4.46	0.2012
	T390	4.1	0.41	-13.05	0.1369		T390	-2.9	19.47	11.19	2.264		T390	-7.83	-18.48	-3.73	0.2042
	T420	3.73	0.47	-10.7	0.1134		T420	-3.25	18.68	11	2.192		T420	-7.87	-16.3	-4.52	0.1865
	T450	2.9	0.81	-8.4	0.08923		T450	-2.84	14.85	10.02	1.814		T450	-7.48	-13.66	-2.73	0.1582
	T490	1.93	1.07	-4.3	0.04839		T490	-1.87	10.88	9.11	1.431		T490	-7.21	-11.03	-4.62	0.1396
	T520	13.91	7.68	-19.65	0.02527		T520	-0.56	4.4	6.59	0.7947		T520	-4.14	-8.14	-3.27	0.09701
	T540	8.9	6.05	-9.66	0.01446		T540	-0.34	2.28	4.69	0.5229		T540	-2.68	-4.76	-1.9	0.05785
	T560	6.48	4.94	-4.51	0.009314		T560	0.69	1.61	4.1	0.4454		T560	-10.83	-17.7	-4.23	0.02118
	T580	2.1	1.52	0.36	0.00262		T580	0.06	1.32	3.49	0.3728		T580	-2.73	-5.42	-1.43	0.00623
	T600	5.62	2.6	13.06	0.001445		T600	-0.14	0.7	3.1	0.3181		T600	5.27	6.42	12.28	0.00148
	T640	3.25	0.58	13.33	0.001373		T640	-0.73	3.17	14.13	0.145		T640	14.33	12.82	8.01	0.00208
	T680	0.45	0.73	2.77	0.002904		T680	1.47	2.18	17.78	0.1797		T680	16.4	6.92	12.66	0.00219
	T680	0.45	0.73	2.77	0.002904		T680	1.47	2.18	17.78	0.1797		T680	16.4	6.92	12.66	0.00219
GMS8-2B	NRM	-0.1	3.78	1.43	4.041	GMS18-6B	NRM	7.39	10.5	10.15	1.637	GMS12-2B	NRM	1.24	-15.83	5.02	1.665
	T150	-0.24	3.21	1.15	3.414		T150	6.2	8.64	10.23	1.475		T150	0.44	-15.29	5.05	1.611
	T200	-0.39	2.8	1.16	3.06		T200	5.62	8.15	9.58	1.377		T200	1.37	-14.64	4.4	1.535
	T250	-0.45	2.52	1	2.75		T250	5.46	7.5	8.2	1.238		T250	1.15	-14.12	4.65	1.491
	T300	-0.25	2.28	1.17	2.576		T300	4.98	7.07	8.63	1.222		T300	1.16	-13.01	4.55	1.383
	T330	-0.32	2.1	1.17	2.43		T330	3.72	4.96	7	0.9351		T330	0.34	-11.36	3.98	1.204
	T360	-3.28	19.83	9.7	2.231		T360	3.25	4.91	6.23	0.8572		T360	-0.99	-11.09	3.89	1.18
	T390	-2.26	18.21	10.15	2.098		T390	3.68	4.11	6.24	0.8331		T390	-0.17	-10.77	3.76	1.141
	T420	-1.84	15.18	10.05	1.83		T420	2.88	4.17	5.49	0.7471		T420	-0.13	-10.33	3.71	1.098
	T450	-2.04	11.77	8.75	1.481		T450	2.4	3.56	5.47	0.695		T450	-0.71	-9.71	3.55	1.036
	T490	-1.01	7.81	7.69	1.101		T490	1.95	3.14	4.98	0.6205		T490	-0.24	-9.09	3.47	0.9731
	T520	-0.17	2.19	5.28	0.5722		T520	1.7	2.49	4.15	0.5127		T520	0.34	-8.26	3.26	0.8885
	T540	0.5	1.01	3.97	0.4125		T540	1.08	1.51	2.8	0.3359		T540	0.24	-7.4	3.03	0.8
	T560	0.22	0.96	3.31	0.3451		T560	1.1	1.26	2.55	0.3053		T560	-0.08	-6.61	2.92	0.7225
	T580	0.18	0.92	3.17	0.3306		T580	3.88	5.5	15.14	0.1657		T580	-0.12	-5.05	2.43	0.5608
	T600	0.32	1.26	2.6	0.2903		T600	2.18	4.58	11.62	0.1268		T600	-0.02	-3.44	1.94	0.3953
	T640	1.15	2.31	13.5	0.1375		T640	0.75	1.74	5.16	0.05495		T640	1.04	-0.45	6.9	0.06992
	T680	2.46	0.32	16.78	0.1696		T680	0.65	0.92	3.59	0.03765		T680	0.84	1.12	7.47	0.07604
	T680	2.46	0.32	16.78	0.1696		T680	0.65	0.92	3.59	0.03765		T680	0.84	1.12	7.47	0.07604
GMS9-3B	NRM	9.21	-4.44	-5.42	115.7	GMS19-4B	NRM	-0.93	2.7	0.59	0.2913	GMS12-5B	NRM	-0.96	-17.15	1.68	1.726
	T150	8.91	-4.4	-5.26	112.4		T150	-0.84	2.47	0.62	0.2684		T150	-0.76	-16.24	1.97	1.638
	T200	8.38	-4.18	-4.92	105.8		T200	-0.64	2.1	0.48	0.2245		T200	-0.4	-15.43	1.94	1.555
	T250	7.62	-3.84	-4.43	96.17		T250	-6.65	19.15	5.01	0.2088		T250	-0.58	-14.71	1.85	1.483
	T300	6.61	-3.57	-3.99	85.08		T300	-3.64	15.83	4.37	0.1682		T300	-0.73	-13.58	1.82	1.372
	T330	5.67	-3.07	-3.35	72.66		T330	-3.4	12.86	4.19	0.1395		T330	-0.11	-12.38	1.71	1.25
	T360	5.48	-2.89	-3.24	69.9		T360	-1.25	12.64	3.55	0.1319		T360	-0.74	-11.83	1.62	1.196
	T390	5.08	-2.7	-3	64.94		T390	-1.42	10.82	3.47	0.1145		T390	0.22	-11.17	1.51	1.127
	T420	4.57	-2.35	-2.74	58.23		T420	-4.05	7.08	3.1	0.08733		T420	-0.9	-10.72	2	1.094

	T450	3.96	-2.32	-2.38	51.72		T450	-2.92	8.94	2.4	0.09703		T450	-0.03	-10.25	1.7	1.04
	T490	3.17	-1.83	-1.83	40.9		T490	-1.48	8.51	2.43	0.08977		T490	-0.3	-8.83	1.7	0.8996
	T520	2.4	-1.35	-1.44	31.06		T520	-1.38	5.79	1.97	0.06267		T520	-0.56	-8.17	1.49	0.8323
	T540	17.52	-8.94	-10.17	22.14		T540	-0.55	5.57	2.25	0.06038		T540	-0.08	-6.97	1.52	0.7131
	T560	14.7	-8.99	-8.89	19.39		T560	-0.86	4.54	1.93	0.05007		T560	-0.44	-5.29	1.47	0.551
	T580	9.84	-6.09	-5.5	12.82		T580	-0.77	3.32	1.67	0.03791		T580	-0.06	-3.13	1.26	0.3375
	T600	3.85	-2.45	-2.17	5.055		T600	-0.53	2.32	1.33	0.02722		T600	1.03	-13.17	11.35	0.1741
	T640	2.45	-1.6	-1.07	0.3118		T640	1.58	3.44	6.75	0.007736		T640	2.32	1.24	7.21	0.07677
	T680	2.84	-1.24	1.41	0.03408		T680	1.92	0.96	7.73	0.008025		T680	0.96	1.45	8.41	0.08583
	T680	2.84	-1.24	1.41	0.03408		T680	1.92	0.96	7.73	0.008025		T680	0.96	1.45	8.41	0.08583
GMS10-5B	NRM	-4.16	-9.89	-7.45	13.06	GMS21-1B	NRM	0.33	3.64	1.06	0.3803	GMS13-2B	NRM	-18.11	13.24	-9.9	24.52
	T150	-4.49	-9.76	-7.32	13		T150	0.2	3.58	1.03	0.3735		T150	-16	11.36	-8.45	21.37
	T200	-3.38	-9.51	-7	12.28		T200	0.19	3.54	1.03	0.369		T200	-13.57	8.98	-7.27	17.82
	T250	-3.37	-9.14	-6.5	11.71		T250	0.11	3.7	1	0.3831		T250	-9.93	5.39	-5.37	12.51
	T300	-2.87	-8.62	-5.98	10.88		T300	0.19	3.46	1.01	0.3608		T300	-8.62	4.58	-4.68	10.82
	T330	-2.41	-7.9	-5.42	9.879		T330	0.28	3.25	0.93	0.3397		T330	-7.3	3.97	-3.84	9.154
	T360	-2.06	-8	-5.23	9.777		T360	0.47	3.19	0.89	0.3341		T360	-6.98	3.64	-3.86	8.765
	T390	-2.45	-7.53	-4.88	9.305		T390	0.2	3.04	0.92	0.318		T390	-6.31	3.28	-3.34	7.856
	T420	-1.99	-7.25	-4.36	8.694		T420	0.08	2.95	0.87	0.3079		T420	-5.98	2.54	-3.06	7.177
	T450	-1.49	-6.58	-3.73	7.713		T450	0.22	2.95	0.96	0.3114		T450	-5.18	2.03	-2.62	6.156
	T490	-1.2	-5.58	-3	6.45		T490	0.11	2.18	0.68	0.2286		T490	-4.16	1.46	-2.05	4.859
	T520	-0.74	-4.46	-2.16	5.01		T520	3.04	15.06	2.9	0.1564		T520	-3.35	0.97	-1.67	3.863
	T540	-0.48	-3.33	-1.49	3.684		T540	0.79	10.22	4.5	0.112		T540	-2.35	0.54	-1.17	2.684
	T560	-0.14	-2.29	-0.88	2.455		T560	-0.42	2.34	1.6	0.02861		T560	-18.03	3.2	-9.46	2.061
	T580	0.59	-8.29	-1.99	0.8549		T580	2.35	13.81	12.39	0.0187		T580	-9.04	1.79	-4.28	1.016
	T600	0.6	-3.95	-0.51	0.4028		T600	3.82	3.98	9.22	0.01075		T600	-17.67	2.27	-1.31	0.1786
	T640	2.34	-15.4	-1.29	0.1563		T640	0.63	2.85	5.46	0.006189		T640	-2.56	1.33	1.67	0.03333
	T680	0.63	-2.16	3.33	0.04019		T680	0.69	0.77	3.35	0.003509		T680	-1.18	-0.05	2.18	0.0248
	T680	0.63	-2.16	3.33	0.04019		T680	0.69	0.77	3.35	0.003509		T680	-1.18	-0.05	2.18	0.0248
GMS5-4B	NRM	2.95	3.72	6.13	7.753	GMS21-5B	NRM	-11.12	-2.51	8.45	0.1419	GMS13-4B	NRM	-12.21	9.74	-7.13	17.17
	T150	2.92	3.32	6.15	7.572		T150	-11.19	-2.99	8.31	0.1426		T150	-10.48	6.75	-6.08	13.87
	T200	2.58	3.53	5.98	7.407		T200	-10.97	-2.39	8.22	0.1392		T200	-9.4	5.08	-5.68	12.1
	T250	2.6	3.44	5.89	7.301		T250	-10.91	-2.39	7.88	0.1367		T250	-6.99	3.96	-4.57	9.244
	T300	2.73	3.19	5.77	7.139		T300	-10.53	-2.47	7.87	0.1338		T300	-6.71	3.88	-4.16	8.801
	T330	2.56	3.25	5.63	6.989		T330	-10.23	-2.18	7.57	0.1292		T330	-8.73	4.11	-1.72	9.798
	T360	2.6	3.11	5.49	6.828		T360	-10.08	-2.25	7.53	0.1278		T360	-7.32	3.89	-4.1	9.245
	T390	2.57	2.93	5.37	6.64		T390	-9.53	-2.33	7.16	0.1214		T390	-5.83	0.23	-4.59	7.427
	T420	2.48	2.86	5.05	6.307		T420	-8.28	-2.71	6.36	0.1079		T420	-5.41	2.91	-3.54	7.091
	T450	2.4	2.81	4.71	5.988		T450	-6.46	-1.54	5.01	0.08315		T450	-4.74	4.37	-3.28	7.238
	T490	1.86	2.23	4.04	4.971		T490	-4.1	-1.07	3.31	0.05371		T490	-4.78	2.57	-3.17	6.288
	T520	1.37	1.43	2.5	3.19		T520	-11.28	-3.61	13.14	0.01769		T520	-3.64	0.91	-2.35	4.427
	T540	2.51	2.84	5.26	0.6486		T540	-3.9	-1.84	4.46	0.006199		T540	-13.93	16.73	-8.79	2.348
	T560	1.45	1.62	3.02	0.3718		T560	-4.29	-1.3	5.13	0.006817		T560	-8.92	0	-7.86	1.189
	T580	9.63	9.05	17.49	0.2192		T580	-3.17	-0.1	4.04	0.005134		T580	-2.74	2.14	-1.11	0.365
	T600	6.57	7.47	14.14	0.1729		T600	-1.04	-0.98	3.93	0.004183		T600	-15.81	6.35	-4.45	0.1761
	T640	2.88	2.21	5.8	0.06847		T640	-0.9	-0.43	2.59	0.002776		T640	-3.52	1.16	1.77	0.04105
	T680	4.58	-0.77	10.71	0.01167		T680	-0.58	0.35	2.6	0.002684		T680	-0.1	1.57	2.94	0.03337
	T680	4.58	-0.77	10.71	0.01167		T680	-0.58	0.35	2.6	0.002684		T680	-0.1	1.57	2.94	0.03337
GMS11-4B	NRM	-0.51	-2.81	-0.27	0.2868	GMS22-5A	NRM	-0.85	-4.5	-3.2	0.5586	GMS13-6B	NRM	-6.8	-0.78	-5.93	9.057
	T150	-0.43	-2.75	-0.27	0.2794		T150	-0.83	-4.39	-3.11	0.5442		T150	-11.65	-2.56	-5.37	13.08
	T200	-0.48	-2.66	-0.27	0.2722		T200	-0.8	-4.17	-3.06	0.5231		T200	-9.94	-2.47	-5.01	11.4
	T250	-0.43	-2.6	-0.26	0.2646		T250	-0.8	-3.92	-2.83	0.4897		T250	-8.24	-2.97	-4.31	9.763
	T300	-0.48	-2.53	-0.24	0.2584		T300	-0.63	-3.7	-2.64	0.4587		T300	-7.64	-3.2	-3.99	9.193
	T330	-0.4	-2.39	-0.2	0.2428		T330	-0.93	-3.3	-2.36	0.4169		T330	-7	-3.29	-3.7	8.571
	T360	-0.29	-2.34	-0.22	0.2368		T360	-0.57	-3.36	-2.13	0.4017		T360	-6.42	-3.75	-3.51	8.215
	T390	-0.46	-2.29	-0.19	0.2341		T390	-0.19	-2.89	-1.95	0.349		T390	-5.8	-3.84	-3.31	7.705
	T420	-0.35	-2.22	-0.19	0.2251		T420	-0.35	-2.63	-1.93	0.3279		T420	-5.59	-3.85	-3.19	7.505
	T450	-0.32	-2.1	-0.16	0.2132		T450	-0.47	-2.11	-1.37	0.256		T450	-5.15	-3.24	-2.91	6.739
	T490	-3.07	-19.28	-1.77	0.196		T490	-0.25	-13.95	-11.5	0.1808		T490	-3.96	-2.62	-2.32	5.288
	T520	-2.68	-15.92	-1.16	0.1618		T520	-2.89	-11.04	-8.64	0.1431		T520	-2.92	-2.09	-1.9	4.06
	T540	-1.92	-12.52	-0.68	0.1268		T540	-0.47	-8.73	-5.27	0.1021		T540	-2.11	-1.68	-1.25	2.979
	T560	-1.64	-10.1	-0.52	0.1024		T560	0.53	-6.83	-4.23	0.08055		T560	-16.06	-12.59	-9.16	2.237
	T580	-0.97	-5.04	-0.05	0.05136		T580	-0.48	-4.34	-2.21	0.04894		T580	-6.81	-5.3	-3.82	0.9435
	T600	-2.11	-17.63	1.87	0.01785		T600	-0.14	-2.29	-0.57	0.02368		T600	-13.66	-13.27	-5.93	0.1994
	T640	8.51	-0.64	10.68	0.001367		T640	2.64	-0.12	7.17	0.007643		T640	-3.95	-3.72	-1.2	0.05551
	T680	0.2	-0.24	3.61	0.003627		T680	2.39	0.43	9.31	0.009624		T680	-0.74	-7.06	8.99	0.01146
	T680	0.2	-0.24	3.61	0.003627		T680	2.39	0.43	9.31	0.009624		T680	-0.74	-7.06	8.99	0.01146
GMS9-2B	NRM	7.39	-12.23	-7.4	160.9	GMS23-2B	NRM	-15.38	-4.73	-2.75	1.632	GMS15-1B	NRM	-14.17	5.12	-9.95	1.806
	T150	6.71	-10.94	-6.94	145.9		T150	-14.86	-4.95	-2.57	1.587		T150	-14.46	4.94	-9.7	1.809
	T200	6.31	-10.09	-6.31	134.7		T200	-14.16	-4.89	-2.98	1.527		T200	-14.38	4.81	-9.66	1.798
	T250	5.2	-8.87	-5.72	117.7		T250	-13.1	-4.83	-2.28	1.415		T250	-13.91	4.18	-9.2	1.72
	T300	4.85	-7.68	-4.91	103.3		T300	-12.63	-3.9	-2.09	1.338		T300	-13.29	3.93	-8.79	1.641
	T330	4.45	-7.23	-4.46	95.89		T330	-11.57	-4.19	-1.98	1.247		T330	-12.27	4.6	-8.2	1.546
	T360	3.43	-6.49	-4.16	84.36		T360	-11.6	-3.81	-1.86	1.235		T360	-12.17	4.71	-8.11	1.536
	T390	3.53	-6.13	-3.67	79.71		T390	-11.01	-3.9	-1.61	1.179		T390	-12.13	3.99	-7.85	1.499
	T420	2.91	-5.36	-3.33	69.5		T420	-10.35	-3.28	-1.5	1.096		T420	-11.6	3.31	-7.6	1.426
	T450	2.47	-4.47	-2.8	58.21		T450	-9.72	-3.63	-1.37	1.047		T450	-11.3	3.87	-7.12	1.391
	T490	1.61	-3.14	-2.06	40.89		T490	-8.63	-2.73	-1.27	0.9144		T490	-10.01	3.15	-6.64	1.242
	T520	1.23	-2.53	-1.52	32		T520	-7.64	-2.39	-1.07	0.808		T520	-9.21	2.96	-6.01	1.139
	T540	8.98	-15.5	-9.89	20.47		T540	-6.47	-1.99	-0.76	0.6806		T540	-8.17	2.93	-5.1	1.006
	T560	5.45	-9.95	-6.25	12.96		T560	-5.1	-1.94	-0.59	0.549		T560	-7.27	2.03	-4.6	0.8843
	T580	1.2	-2.43	-1.54	3.117		T580	-2.18	-0.76	-0.03	0.2312		T580	-6.86	1.98	-4.24	0.8306
	T600	1.82	-3.03	-1.66	0.3908		T600	-11.84	-3.18	0.92	0.1229		T600	-5.33	1.86	-3.31	0.6549
	T640	2.95	-5.59	-3.08	0.07027		T640	-16.84	-4.5	14.48	0.02266		T640				
	T680	0.36	0.01	1.68	0.01721		T680	0	0.19	1.95	0.0196		T680				
	T680	0.36	0.01	1.68	0.01721		T680	0	0.19	1.95	0.0196		T680				

GMS12-3B						GMS13-3B						GMS15-4C					
	NRM	0.35	-15.69	5.15	1.652		NRM	-14.55	14.41	-5.82	21.29		NRM	-7.17	5.79	-6.17	1.109
	T150	0.24	-12.58	4.83	1.347		T150	-12.31	10.87	-5.35	17.27		T150	-7.4	5.29	-6	1.089
	T200	-0.23	-14.24	5.42	1.524		T200	-10.74	8.6	-4.87	14.59		T200	-7.59	5.48	-5.68	1.095
	T250	0.07	-12.91	4.51	1.367		T250	-8.87	6.32	-4.39	11.75		T250	-6.56	5.26	-5.61	1.011
	T300	0.93	-12.23	4.69	1.313		T300	-7.55	5.05	-3.43	9.71		T300	-6.86	4.92	-5.23	0.9929
	T330	0.61	-10.86	4.64	1.182		T330	-6.69	3.63	-2.94	8.164		T330	-6.47	4.1	-4.97	0.9129
	T360	0.72	-11.15	4.66	1.21		T360	-6.43	3.42	-2.87	7.824		T360	-5.94	4.66	-4.93	0.9018
	T390	0.26	-10.46	4	1.12		T390	-6.05	3.18	-2.53	7.285		T390	-6.06	4.5	-4.73	0.8909
	T420	0.11	-9.92	4.2	1.077		T420	-5.54	2.74	-2.39	6.627		T420	-5.95	3.86	-4.67	0.8497
	T450	0.54	-9.33	4.01	1.017		T450	-4.99	2.21	-2.16	5.867		T450	-5.58	4.07	-4.42	0.8207
	T490	0.53	-8.27	3.62	0.904		T490	-4.13	1.74	-1.74	4.804		T490	-5.38	4.15	-4	0.7881
	T520	0.53	-7.73	3.57	0.8528		T520	-2.97	1.19	-1.24	3.434		T520	-4.8	3.73	-3.65	0.7095
	T540	0.37	-7.06	3.27	0.7791		T540	-2.12	0.77	-1.03	2.481		T540	-4.22	3.11	-3.16	0.6122
	T560	0.47	-5.54	2.81	0.623		T560	-16.39	6.01	-8.29	1.932		T560	-4.02	2.86	-3.1	0.5828
	T580	0.55	-3.89	2.31	0.4557		T580	-8.04	3.11	-4.22	0.9599		T580	-3.82	2.78	-2.74	0.5464
	T600	-0.33	-18.89	16.62	0.2516		T600	-16.29	7.54	-1.11	0.1798		T600	-3.41	2.51	-2.43	0.4889
	T640	1.96	2.3	10.81	0.1122		T640	-2.71	0.38	0.16	0.02745		T640	-14.45	12.42	-11.1	0.2203
	T680	0.18	1.51	10.28	0.1039		T680	0.24	0.24	2.33	0.02355		T680	-7.31	-1.68	12.77	0.01481
	T680	0.18	1.51	10.28	0.1039		T680	0.24	0.24	2.33	0.02355		T680	-7.31	-1.68	12.77	0.01481
GMS13-1B	NRM	1.22	4.35	-0.65	45.63	GMS18-3B	NRM	-2.1	17.17	6.61	1.852	GMS17-1A	NRM	4.46	-3.32	4.66	0.07258
	T150	0.99	3.86	-0.55	40.25		T150	-2.17	15.08	6.47	1.655		T150	4.39	-3.45	4.39	0.07099
	T200	0.79	3.06	-0.46	31.98		T200	-2.12	13.63	6.11	1.508		T200	4.16	-3.34	4.16	0.06761
	T250	0.42	2.32	-0.43	23.94		T250	-1.35	12.74	5.02	1.376		T250	3.9	-3.7	3.98	0.06691
	T300	3.17	17.15	-3.09	17.71		T300	-1.03	11.6	6.37	1.328		T300	3.79	-3.86	3.82	0.06625
	T330	2.54	13.96	-2.65	14.44		T330	-0.31	9.74	6.12	1.151		T330	2.96	-3.81	3.3	0.05847
	T360	3.34	13.41	-2.85	14.11		T360	-1.37	9.12	4.68	1.035		T360	2.75	-3.67	3.19	0.05583
	T390	1.71	12.14	-2.45	12.5		T390	-0.71	6.95	5.3	0.8768		T390	2.51	-3.28	2.83	0.05008
	T420	0.57	10.72	-2.35	10.99		T420	-0.47	6.48	4.93	0.8154		T420	1.98	-2.31	2.32	0.03823
	T450	1.82	9.08	-2.02	9.48		T450	-0.64	5.81	4.33	0.7274		T450	14.91	-15.09	16.6	0.02693
	T490	0.36	6.82	-1.62	7.023		T490	-0.65	4.69	4.05	0.6232		T490	7.8	-8.6	10.07	0.01537
	T520	0.06	4.96	-1.24	5.112		T520	-0.27	3.37	3.43	0.4815		T520	5.19	-3.97	6.96	0.00955
	T540	-0.2	3.26	-1	3.418		T540	-0.4	2.17	2.48	0.3319		T540	4.17	-2.58	5.6	0.00744
	T560	-0.22	2.33	-0.76	2.458		T560	-1.73	14.6	18.26	0.2345		T560	3.58	-1.88	5.3	0.00667
	T580	-2.67	9.65	-3.21	1.051		T580	0.2	7.39	11.26	0.1346		T580	2.43	-0.63	3.74	0.0045
	T600	-6.57	18.62	-0.48	0.1975		T600	-0.11	4.58	9.3	0.1037		T600	1.42	-0.04	2.7	0.00305
	T640	-1.64	2.25	1.58	0.03205		T640	-0.88	2.6	4.2	0.05016		T640	0.53	-0.14	1.95	0.00203
	T680	-0.57	0.43	2.21	0.02324		T680	-0.3	0.5	3.83	0.03877		T680	0.47	0.37	2.6	0.00267
	T680	-0.57	0.43	2.21	0.02324		T680	-0.3	0.5	3.83	0.03877		T680	0.47	0.37	2.6	0.00267

Appendix C: Paleomagnetic data from IRM Experiment

ID	Steps (mT)	X	Y	Z	M
GMS1-9B	NRM	-2.13	1.31	-0.84	0.2636
	10	-1.97	14.41	-8.19	0.1669
	20	7.28	-0.35	0.08	0.7285
	30	12.58	-0.31	-0.05	1.259
	40	18.15	0.86	-0.58	1.818
	60	2.55	-0.26	0.15	2.562
	80	2.91	-0.16	-0.1	2.917
	100	3.14	0.09	-0.17	3.15
	150	3.54	-0.34	0.14	3.558
	300	3.74	-0.14	-0.08	3.747
	400	3.75	-0.48	0.46	3.811
	500	3.69	0.87	0.9	3.894
	750	3.78	0.67	0.53	3.87
	900	3.84	-0.54	-0.16	3.88
	1000	3.82	-0.35	0.09	3.84
	1000	3.82	-0.35	0.09	3.84
GMS1-8B	NRM	-6.93	-1.48	-1.5	0.7244
	10	19.91	-1.23	-3.35	2.023
	20	16.53	0.46	-1.74	16.63
	30	3.6	0.02	-0.41	36.21
	40	3.69	0.27	-0.35	37.17
	60	4.48	0.67	-0.33	45.41
	80	4.86	0.84	-0.47	49.57
	100	5.13	-0.58	0.18	51.66
	150	5.4	0.73	-0.3	54.61
	300	5.45	-1.03	-0.33	55.57
	400	5.45	0.32	-0.99	55.5
	500	5.35	-0.85	0.68	54.64
	750	5.48	0.84	-0.53	55.73
	900	5.54	-0.11	-0.52	55.66
	1000	5.56	0.45	-0.38	55.89
	1000	5.56	0.45	-0.38	55.89
GMS2-2B	NRM	-10.17	-11.34	-4.06	0.1577
	10	3.01	-1.32	-0.33	0.3304
	20	17.35	-0.44	-0.15	1.736
	30	4.32	-0.14	0.01	4.325
	40	7.1	0.31	0.19	7.113
	60	9.68	0.96	0.23	9.735
	80	11.46	-0.01	0.39	11.46
	100	12.81	0.08	0.3	12.81
	150	14.47	1.09	0.42	14.52
	300	15.83	0.07	0.36	15.83
	400	16.09	-0.63	0.36	16.11
	500	16.13	-0.04	0.36	16.14
	750	16.21	0.85	0.32	16.23
	900	16.12	1.63	0.35	16.21
	1000	16.22	-0.24	0.39	16.23
	1000	16.22	-0.24	0.39	16.23
GMS3-2B	NRM	-2.52	-2.02	-2.33	3.983
	10	11.24	-4.35	0.3	120.6
	20	2.14	-0.19	0.14	215.2
	30	3.04	0.09	0.26	305.4
	40	3.37	0.07	0.33	338.6
	60	3.87	0.18	0.07	387.1
	80	4.05	-0.14	0.34	406.3
	100	4.1	-0.08	0.36	411.5
	150	4.21	0.06	0.36	422.8
	300	4.05	-1.14	0.24	421.8
	400	4.22	-0.11	0.37	423.7
	500	4.23	0.21	0.44	425.7
	750	4.23	0.05	0.43	425.4
	900	4.22	0.39	0.42	426
	1000	4.23	-0.1	0.43	424.8
	1000	4.23	-0.1	0.43	424.8
GMS4-8B	NRM	6.28	0.4	8.33	10.44
	10	4.74	-0.3	0.65	47.96
	20	2.41	-0.02	-0.03	240.9
	30	4.35	0.27	-0.15	436.1
	40	5.32	0.55	-0.18	535.6
	60	9.56	0.98	-0.49	962.4
	80	10.32	1.7	-0.59	1048
	100	11.92	0.91	-0.51	1197
	150	10.94	0.77	-1.16	1103
	300	11.65	1	-1.25	1176
	400	11.66	0.95	-1.33	1178
	500	11.61	0.77	-1.4	1172

ID	Steps (mT)	X	Y	Z	M
GMS9-4B	NRM	1.71	-3.3	3.15	48.77
	10	7.18	-3.25	2.33	82.19
	20	19.19	-2.05	0.49	193
	30	2.43	-0.07	-0.02	243
	40	2.73	-0.08	-0.33	275.3
	60	2.95	-0.14	-0.14	295.3
	80	3.42	0.16	-0.12	342.2
	100	3.57	-0.09	-0.14	357.5
	150	3.7	0.02	-0.2	370.2
	300	3.8	-0.07	-0.14	380.4
	400	3.75	0.46	-0.2	378.7
	500	3.8	-0.57	-0.14	384.3
	750	3.82	0.17	-0.04	382.6
	900	3.83	0.1	-0.08	383.1
	1000	3.82	0.15	-0.08	382
	1000	3.82	0.15	-0.08	382
GMS10-4B	NRM	1.09	-6.27	-5.78	8.599
	10	17.57	-5.41	-5.32	19.14
	20	10.23	-1.49	-0.47	103.5
	30	12.95	-0.76	-0.67	129.9
	40	2.48	-0.23	-0.09	249.7
	60	3.85	-0.44	-0.09	387.5
	80	4.78	-0.17	-0.13	478.4
	100	5.25	-0.36	-0.12	526.3
	150	5.7	0.13	-0.16	570.2
	300	6.08	-0.04	-0.14	608.6
	400	6.13	0.23	-0.16	614.1
	500	6.16	-0.2	-0.11	616.2
	750	6.2	0.24	-0.16	620.8
	900	6.22	0.21	-0.18	622.5
	1000	6.21	0.08	-0.13	621.5
	1000	6.21	0.08	-0.13	621.5
GMS11-2B	NRM	-1.68	2.94	0.82	0.3479
	10	1.64	2.54	-1.22	0.326
	20	2.27	0	-1.58	2.77
	30	4.62	0.44	-2.88	5.463
	40	9.45	0.74	-6.55	11.52
	60	15.17	0.93	-8.82	17.58
	80	18.75	1.29	-13.27	23.01
	100	2.25	0.02	-1.45	26.78
	150	2.48	0.05	-1.69	30.03
	300	2.82	0.17	-1.89	34.02
	400	2.98	0.63	-1.58	34.36
	500	2.92	0.58	-1.64	33.95
	750	2.86	-0.12	-2.01	35
	900	2.98	-0.06	-1.86	35.13
	1000	2.97	-0.1	-1.9	35.32
	1000	2.97	-0.1	-1.9	35.32
GMS12-6B	NRM	1.85	-17.82	2.9	1.815
	10	2.27	-1.71	0.25	2.856
	20	2.18	0.05	-0.02	21.8
	30	4.02	-0.13	-0.05	40.18
	40	6.33	0.27	-0.04	63.32
	60	9.69	-0.08	0.09	96.91
	80	11.5	0.41	-0.12	115
	100	13.23	0.02	-0.12	132.3
	150	14.62	1.01	-0.19	146.5
	300	15.64	2.33	-0.05	158.1
	400	15.96	0.23	-0.06	159.6
	500	15.9	0.87	-0.06	159.2
	750	16.07	0.11	-0.21	160.7
	900	16.1	-0.28	-0.07	161.1
	1000	16.05	-2.22	-0.16	162
	1000	16.05	-2.22	-0.16	162
GMS13-7B	NRM	-13.64	-0.96	-5.29	14.66
	10	3.31	0.16	-0.49	33.52
	20	14.67	1.19	-0.42	147.3
	30	2.68	-0.12	-0.05	268.2
	40	3.92	-0.01	-0.08	391.8
	60	6.6	-0.22	-0.05	660.1
	80	7.86	0.63	-0.06	788.5
	100	8.73	0.91	-0.1	878.2
	150	9.99	0.8	-0.15	1002
	300	10.61	0.67	-0.11	1063
	400	10.67	0.58	-0.08	1069
	500	10.72	0.97	0.12	1076

ID	Steps (mT)	X	Y	Z	M
GMS7-6B	NRM	2.74	1.46	-9.15	0.09658
	10	2.58	0.35	-0.85	0.2739
	20	4.66	0.44	-0.77	0.4743
	30	9.68	1.89	-0.74	0.9894
	40	11.62	1.31	-0.43	1.17
	60	15.69	1.08	-0.67	1.574
	80	18.44	1.15	-0.78	1.849
	100	19.52	2.76	-0.89	1.973
	150	2.28	-0.07	-0.09	2.281
	300	2.56	0.2	-0.16	2.576
	400	2.62	0.04	-0.16	2.629
	500	2.6	0.06	-0.17	2.609
	750	2.65	0.24	-0.16	2.668
	900	2.66	0.04	-0.16	2.667
	1000	2.66	-0.03	-0.15	2.669
	1000	2.66	-0.03	-0.15	2.669
GMS8-3B	NRM	-0.66	4.04	0.92	4.194
	10	3.22	0.47	0.01	32.57
	20	13.66	-1.07	-0.29	137.1
	30	2.84	0.28	-0.06	285.1
	40	3.27	0.08	-0.04	327.1
	60	6.37	0.25	-0.09	637.5
	80	7.54	0.6	-0.17	756.9
	100	9.28	0.88	-0.29	933
	150	9.35	-0.42	-0.2	936
	300	9.48	0.34	-0.22	949.2
	400	9.39	-1.5	-0.21	951.5
	500	9.5	0.18	-0.15	950.7
	750	9.44	0.23	-0.17	944.1
	900	9.52	0.39	-0.19	952.9
	1000	9.52	-0.02	-0.16	952.2
	1000	9.52	-0.02	-0.16	952.2
GMS19-6B	NRM	-0.48	2.53	0.63	0.2647
	10	14.7	3.03	0.46	1.502
	20	2.54	0.39	0.06	2.573
	30	4.67	1.07	0.01	4.79
	40	6.29	0.52	-0.01	6.316
	60	8.41	0.98	-0.02	8.47
	80	9.32	0.6	0.03	9.336
	100	9.66	0.15	-0.05	9.664
	150	10.29	0.66	-0.12	10.31
	300	11.28	0.6	0.06	11.3
	400	11.44	0.99	-0.16	11.49
	500	11.53	-0.35	0.06	11.53
	750	11.6	-0.29	-0.12	11.6
	900	11.58	0.88	0.01	11.61
	1000	11.7	-0.17	-0.06	11.71
	1000	11.7	-0.17	-0.06	11.71
GMS20-4B	NRM	8.59	16.56	15.74	0.000244
	10	3.18	1.32	1.19	0.000365
	20	8.41	1.35	0.79	0.000855
	30	11.89	0.36	0.57	0.001191
	40	16.86	0.08	0.78	0.001688
	60	3.04	0.36	0.25	0.003075
	80	3.67	0.55	0.35	0.003731
	100	4.56	0.34	0.49	0.004602
	150	5.21	-0.03	0.65	0.005251
	300	6.18	0.76	0.85	0.006284
	400	6.51	1.32	0.9	0.006704
	500	6.75	1.13	0.93	0.006905
	750	6.96	1.37	0.96	0.007159
	900	7.06	1.21	0.92	0.007225
	1000	7.09	1.04	0.95	0.007228
	1000	7.09	1.04	0.95	0.007228
GMS23-6B	NRM	-6.44	8.81	-1.01	1.096
	10	11.14	11.41	-0.98	1.597
	20	5.22	1.38	0.02	5.398
	30	14.79	2.07	-0.19	14.94
	40	2.29	-0.07	0.02	22.88
	60	3.15	-0.14	0.01	31.5
	80	3.76	0.06	-0.04	37.65
	100	4.22	0.18	-0.06	42.27
	150	4.57	-0.1	0.07	45.75
	300	4.86	0.09	0.06	48.61
	400	4.91	0.15	0	49.12
	500	4.98	0.3	-0.04	49.92

GMS5-9B	750	11.7	1.26	-1.28	1183
	900	11.63	0.86	-1.34	1174
	1000	11.79	-0.5	-1.13	1186
	1000	11.79	-0.5	-1.13	1186
	NRM	4.68	4.93	7.56	10.17
	10	6.11	0.38	0.56	61.43
	20	10.85	0.78	0.41	108.8
	30	2.36	0.06	0.02	236
	40	4.13	-0.23	-0.04	414.1
	60	6.52	0.46	-0.13	654.1
	80	8.19	0	-0.24	819.3
	100	9.5	0.55	-0.32	951.9
	150	10.56	0	-0.23	1057
	300	11.45	-0.63	-0.26	1147
	400	11.6	-0.86	-0.34	1164
	500	11.64	0.12	-0.26	1164
	750	11.71	-0.92	-0.4	1176
	900	11.59	-2.26	-0.38	1181
	1000	11.77	-0.56	-0.32	1179
	1000	11.77	-0.56	-0.32	1179
GMS6-10B	NRM	2.57	-7.36	2.21	8.099
	10	3.63	-0.11	0.14	36.35
	20	18.37	-1.07	-0.17	184
	30	2.62	-0.2	-0.01	263.2
	40	4.35	0.26	-0.1	436
	60	6.26	0.36	-0.17	627.4
	80	6.96	1.26	-0.18	707.9
	100	7.93	0.81	-0.18	797.8
	150	8.9	0.41	-0.22	891.7
	300	9.41	-0.19	-0.04	941.6
	400	9.52	0.39	-0.21	953.4
	500	9.56	-0.58	-0.17	958.3
	750	9.61	0.47	-0.27	962
	900	9.53	1.23	-0.18	960.6
	1000	9.6	0.25	-0.15	960
	1000	9.6	0.25	-0.15	960
GMS22-6B	NRM	-19.33	7.69	-7.52	0.2212
	10	16.6	8.62	-8.78	0.2066
	20	9.45	0.53	-1.15	0.953
	30	2.24	-0.01	-0.12	2.246
	40	3.51	0.09	-0.2	3.521
	60	5.33	0.15	-0.15	5.338
	80	6.22	0.26	-0.25	6.23
	100	7.78	0.6	-0.25	7.809
	150	8.74	0.53	-0.25	8.762
	300	10.32	0.55	-0.08	10.34
	400	10.54	-0.46	-0.12	10.55
	500	10.75	0.54	-0.1	10.76
	750	11.02	-0.4	-0.14	11.03
	900	11.14	1.04	-0.2	11.19
	1000	11.25	0.92	-0.24	11.29
	1000	11.25	0.92	-0.24	11.29

GMS14-4B	750	10.71	0.85	-0.05	1074
	900	10.69	-1.33	-0.13	1077
	1000	10.72	-0.21	-0.07	1072
	1000	10.72	-0.21	-0.07	1072
	NRM	-8.6	-6.71	12.4	16.51
	10	3.45	-1.1	0.99	37.56
	20	19.12	1.74	0.11	192
	30	2.04	0.32	-0.02	206.9
	40	3.05	0.1	-0.06	305.1
	60	4.28	-0.15	-0.13	428.2
	80	5.13	-0.42	-0.17	515.1
	100	6.02	0.53	-0.15	604.7
	150	6.87	-0.08	-0.83	692.5
	300	7.37	-0.59	-0.21	739.3
	400	7.42	-0.86	-0.22	747.6
	500	7.49	0.51	-0.25	751.5
	750	7.53	-0.29	-0.24	753.8
	900	7.53	-0.01	-0.25	753.9
	1000	7.53	-0.26	-0.23	754.1
	1000	7.53	-0.26	-0.23	754.1
GMS15-5B	NRM	-8.56	2.3	-5.36	1.036
	10	13.55	1.35	-5.18	1.456
	20	11.28	0.29	-0.49	11.29
	30	2.55	0.04	-0.05	25.5
	40	3.93	-0.57	0.01	39.74
	60	5.76	0.19	0.09	57.59
	80	6.12	-1.16	0.01	62.31
	100	6.36	-0.34	0.05	63.73
	150	6.52	-0.03	0.08	65.21
	300	6.62	-0.12	0.03	66.18
	400	6.68	-0.06	0.07	66.84
	500	6.75	-0.26	0.07	67.53
	750	6.76	-0.14	0.11	67.67
	900	6.74	-0.64	0.14	67.75
	1000	6.74	-0.72	0.1	67.78
	1000	6.74	-0.72	0.1	67.78
GMS17-4B	NRM	0.76	-3.67	-0.34	0.3759
	10	3.55	-3.13	-0.32	0.4744
	20	8.66	-1.94	-0.04	0.8872
	30	14.22	-2.78	0.18	1.449
	40	2.07	-0.05	0.01	2.074
	60	2.16	-0.16	0.03	2.168
	80	2.85	0.48	0.06	2.895
	100	3.07	0.06	0.03	3.071
	150	3.38	0.2	0.06	3.384
	300	3.58	-0.04	0.21	3.584
	400	3.61	-0.49	0.03	3.638
	500	3.69	0.25	0.12	3.705
	750	3.81	0.21	0.08	3.812
	900	3.88	-0.06	0.07	3.88
	1000	3.95	-0.03	0.12	3.948
	1000	3.95	-0.03	0.12	3.948

GMS18-7B	750	5.09	0.48	0.02	51.08
	900	5.15	-0.18	0	51.58
	1000	5.25	0.02	0.08	52.52
	1000	5.25	0.02	0.08	52.52
	NRM	11.46	6.95	12.98	1.866
	10	3.6	0.35	0.12	36.23
	20	12.57	1.26	0.1	126.4
	30	2.1	0.07	-0.03	210.1
	40	3.61	-0.03	-0.03	361.1
	60	4.2	-0.2	-0.07	420.7
	80	4.87	0.09	-0.05	487.1
	100	5.21	-0.33	0	522.2
	150	5.81	-0.04	-0.07	580.6
	300	5.93	0.19	-0.01	593.5
	400	5.97	-0.19	-0.12	596.9
	500	5.99	0.08	-0.06	599.1
	750	6.01	0.07	-0.08	601.1
	900	5.98	0.54	-0.02	600.8
	1000	6	0.19	0	600.7
	1000	6	0.19	0	600.7
GMS21-6B	NRM	8.73	10.17	5.77	0.1459
	10	4.47	0.96	0.41	0.4589
	20	7.35	0.8	0.17	0.7399
	30	10.98	0.81	0.01	1.101
	40	12.74	-0.19	-0.23	1.274
	60	14.7	-0.46	-0.54	1.472
	80	15.75	1.71	-0.45	1.584
	100	16.3	0.81	-0.53	1.632
	150	16.58	-0.41	-0.37	1.659
	300	17.06	1.09	-0.45	1.71
	400	17.12	0.49	-0.5	1.714
	500	17.25	-0.4	-0.61	1.727
	750	17.09	2.82	-0.3	1.733
	900	17.33	1.2	-0.42	1.737
	1000	17.4	0.71	-0.54	1.742
	1000	17.4	0.71	-0.54	1.742

Appendix D: Paleomagnetic Data during field work									
Site Name	Elev (m)	Coordinates		Sample no	Field orientation			Local time (GMT+3)	Field remarks
		Lat	Long		αmag	β	αsol		
GMS1	1567±5	522920	936682	GMS1-1	233	54	270	10:45	Sample broken, hole oriented
				GMS1-2	200	50	235	10:52	Sample broken, hole oriented
				GMS1-3	239	51	265	10:59	
				GMS1-4	223	57	251	11:11	Sample broken, hole oriented
				GMS1-5	238	50	264	11:15	Cap broken
				GMS1-6	224	50	249	11:19	
				GMS1-7	250	48	268	11:23	
				GMS1-8	190	42	214	11:28	
				GMS1-9	230	54	249	11:31	
				GMS1-10	227	51	246	11:34	
				GMS1-11	246	59	265	11:36	
				GMS1-12	241	54	261	11:49	
GMS2	1527±5	522932	936717	GMS2-1	150	59	145	12:53	Sample broken, hole oriented
				GMS2-2	143	56	150	12:57	
				GMS2-3	141	56	134	13:00	
				GMS2-4	157	58	149	13:02	cap broken
				GMS2-5	150	58	140	13:04	
				GMS2-6	146	55	136	13:06	
				GMS2-7	182	41	169	13:09	sample broken, hole oriented
				GMS2-8	138	42	124	13:14	
				GMS2-9	150	39	134	13:17	
				GMS2-10	138	38	120	13:20	
				GMS2-11	132	45	114	13:22	
				GMS2-12	157	45	140	13:25	
				GMS2-13	129	36	109	13:27	core broken, hole oriented
				GMS2-14	132	47	112	13:29	
GMS3	1727±5	518693	913105	GMS3-1	149	58	96	15:23	
				GMS3-2	140	61	89	15:23	
				GMS3-3	127	67	75	15:24	
				GMS3-4	133	67	81	15:24	
				GMS3-5	131	62	79	15:25	
				GMS3-6	127	60	74	15:25	
				GMS3-7	127	62	74	15:26	
				GMS3-8	123	59	70	15:26	
				GMS3-9	58	77	63	12:25	
				GMS3-10	63	75	69	12:27	
				GMS3-11	67	59	78	12:18	
				GMS3-12	69	69	78	12:20	
				GMS3-13	79	50	84	12:22	
GMS4	1697±4	517978	914366	GMS4-1	330	58	Shadow	-	
				GMS4-2	335	60	Shadow	-	
				GMS4-3	337	61	Shadow	-	
				GMS4-4	341	59	Shadow	-	
				GMS4-5	342	59	Shadow	-	
				GMS4-6	330	57	Shadow	-	
				GMS4-7	335	56	Shadow	-	
				GMS4-8	357	61	Shadow	-	
				GMS4-9	346	63	Shadow	-	
				GMS4-10	359	65	Shadow	-	

				GMS4-11	350	66	Shadow	-	
				GMS4-12	305	80	Shadow	-	
GMS5	1697±4	517978	914366	GMS5-1	325	79	Shadow	-	
				GMS5-2	340	74	Shadow	-	
				GMS5-3	330	76	Shadow	-	
				GMS5-4	333	70	Shadow	-	
				GMS5-5	332	64	Shadow	-	
				GMS5-6	324	81	Shadow	-	
				GMS5-7	325	75	Shadow	-	
				GMS5-8	333	63	Shadow	-	
				GMS5-9	327	67	Shadow	-	
				GMS5-10	332	67	Shadow	-	
				GMS5-11	339	64	Shadow	-	Core broken, hole oriented
				GMS5-12	342	62	Shadow	-	
GMS6	1735±5	520581	912560	GMS6-1	270	57	10	16:48	
				GMS6-2	65	62	6	16:52	
				GMS6-3	63	62	6	16:54	
				GMS6-4	58	60	0	16:55	
				GMS6-5	56	64	56	16:57	
				GMS6-6	55	55	5	16:59	
				GMS6-7	67	61	359	17:01	
				GMS6-8	60	65	0	17:03	
				GMS6-9	53	66	357	17:05	
				GMS6-10	55	56	354	17:07	
				GMS6-11	52	59	350	17:09	
				GMS6-12	54	65	355	17:11	
				GMS6-13	50	72	347	17:14	
				GMS6-14	40	70	339	17:16	
GMS7	1708±5	519179	913329	GMS7-1	320	56	9	10:15	
				GMS7-2	324	55	12	10:18	core broken, hole oriented
				GMS7-3	320	56	9	10:22	
				GMS7-4	323	54	10	10:23	
				GMS7-5	323	52	11	10:25	
				GMS7-6	319	55	5	10:26	
				GMS7-7	324	55	9	10:27	
				GMS7-8	321	55	7	10:30	
				GMS7-9	321	59	8	10:31	Core not recovered
GMS8	1732±5	520809	913763	GMS8-1	269	38	315	11:35	
				GMS8-2	289	39	316	11:38	
				GMS8-3	287	41	307	11:40	
				GMS8-4	280	73	302	11:43	
				GMS8-5	307	58	327	11:46	
				GMS8-6	299	54	318	11:47	core broken, hole oriented
				GMS8-7	299	62	315	11:51	
				GMS8-8	315	75	330	11:54	
GMS9	1761±5	522684	912915	GMS9-1	215	30	139	13:03	
				GMS9-2	212	30	140	13:04	
				GMS9-3	105	45	149	13:07	
				GMS9-4	145	39	130	13:11	
				GMS9-5	140	36	126	13:15	
				GMS9-6	130	33	112	13:21	
				GMS9-7	162	26	142	13:25	
				GMS9-8	160	26	138	13:29	
				GMS9-9	170	32	147	13:33	
GMS10	1757±5	523556	914437	GMS10-1	107	89	64	14:42	
				GMS10-2	105	85	54	15:04	
				GMS10-3	104	88	52	15:05	
				GMS10-4	108	83	55	15:08	
				GMS10-5	113	69	49	15:12	
				GMS10-6	120	77	56	15:14	

				GMS10-7	100	58	36	15:16	
				GMS10-8	105	73	56	15:19	
				GMS10-9	107	65	61	15:22	
GMS11	1760±5	524118	916290	GMS11-1	98	75	41	16:33	
				GMS11-2	115	51	62	16:37	
				GMS11-3	141	31	85	16:40	
				GMS11-4	114	45	55	16:45	
				GMS11-5	127	37	68	16:47	
				GMS11-6	132	31	72	16:54	
				GMS11-7	130	43	69	16:56	
				GMS11-8	105	56	45	16:58	
				GMS11-9	150	13	90	17:01	
				GMS11-10	150	67	Shadow	-	core broken, hole oriented
GMS12	1699±3	524371	916560	GMS12-1	73	65	126	9:57	Core broken, hole oriented
				GMS12-2	79	61	133	9:59	
				GMS12-3	78	63	133	10:01	
				GMS12-4	90	67	142	10:02	
				GMS12-5	90	70	Shadow	-	
				GMS12-6	89	70	Shadow	-	
				GMS12-7	92	76	Shadow	-	
				GMS12-8	86	65	Shadow	-	
				GMS12-9	87	68	Shadow	-	
GMS13	1716±3	524718	916579	GMS13-1	190	25	238	10:21	
				GMS13-2	176	30	223	10:25	
				GMS13-3	189	29	235	10:27	
				GMS13-4	186	34	231	10:29	
				GMS13-5	195	28	240	10:32	Core broken, hole oriented
				GMS13-6	151	22	198	10:34	
				GMS13-7	152	20	198	10:37	
				GMS13-8	166	28	210	10:39	
				GMS13-9	119	19	167	10:41	
GMS14	1732±4	525522	916501	GMS14-1	96	46	137	11:21	
				GMS14-2	87	48	123	11:30	Core broken, hole oriented
				GMS14-3	87	35	123	11:34	
				GMS14-4	102	43	137	11:39	
				GMS14-5	97	44	132	11:58	Core broken, hole oriented
				GMS14-6	110	49	shadow	-	
				GMS14-7	110	42	133	11:56	
				GMS14-8	105	52	128	11:56	
				GMS14-9	106	59	130	11:54	
GMS15	1751±3	527808	916837	GMS15-1	207	53	195	13:01	
				GMS15-2	206	53	193	13:03	
				GMS15-3	206	54	192	13:05	
				GMS15-4	211	57	197	13:06	
				GMS15-5	215	54	200	13:07	
				GMS15-6	216	52	200	13:09	
				GMS15-7	212	55	196	13:11	
				GMS15-8	213	50	196	13:13	
				GMS15-9	210	58	190	13:18	Core broken, hole oriented
GMS16	1656±4	533254	919355	GMS16-1	116	70	70	15:13	
				GMS16-2	100	51	53	15:16	
				GMS16-3	90	81	42	15:18	
				GMS16-4	99	84	52	15:20	
				GMS16-5	336	10	286	15:22	
				GMS16-6	338	9	285	15:26	
				GMS16-7	9	6	316	15:30	
				GMS16-8	97	87	47	15:32	Core not recovered
GMS 17	1707 ±5	517452	921844	GMS17-1	33	53	85	10:16	Core broken, hole oriented
				GMS17-2	84	54	132	10:19	
				GMS17-3	90	47	131	10:22	Core broken, hole oriented

				GMS17-4	95	49	143	10:26	Core broken, hole oriented
				GMS17-5	33	23	82	10:30	
				GMS17-6	75	50	122	10:33	
				GMS17-7	68	30	115	10:36	
				GMS17-8	80	34	126	10:38	Core broken, hole oriented
				GMS17-9	90	30	134	10:43	
GMS18	1546±4	524822	935333	GMS18-1	247	10	186	17:30	
				GMS18-2	257	7	195	17:32	
				GMS18-3	262	15	200	17:34	Core broken, hole oriented
				GMS18-4	318	24	Shadow	_	
				GMS18-5	266	6	210	17:41	
				GMS18-6	317	21	255	17:46	
				GMS18-7	339	22	sunset	-	
				GMS18-8	329	19	sunset	-	
				GMS18-9	291	8	sunset	-	
GMS19	1714±4	520530	922336	GMS19-1	280	37	340	9:22	
				GMS19-2	294	28	353	9:24	Core broken, hole oriented
				GMS19-3	281	37	340	9:26	Core broken, hole oriented
				GMS19-4	279	43	336	9:29	
				GMS19-5	281	44	338	9:30	
				GMS19-6	282	42	339	9:32	
				GMS19-7	270	40	326	9:33	Core broken, hole oriented
				GMS19-8	281	45	337	9:36	
				GMS19-9	279	39	335	9:40	
GMS20	1654±3	522724	924711	GMS20-1	79	46	123	10:53	
				GMS20-2	82	42	125	10:55	
				GMS20-3	76	40	118	10:57	
				GMS20-4	78	42	121	10:59	
				GMS20-5	75	42	117	11:02	
				GMS20-6	76	46	117	11:04	
				GMS20-7	79	26	120	11:06	
				GMS20-8	78	40	118	11:09	
				GMS20-9	79	50	118	11:12	Core not recovered
GMS21	1666±4	521969	927210	GMS21-1	308	32	319	12:13	
				GMS21-2	310	19	318	12:15	
				GMS21-3	316	52	325	12:17	
				GMS21-4	310	71	317	12:20	
				GMS21-5	312	73	317	12:25	
				GMS21-6	314	35	316	12:31	
				GMS21-7	306	22	316	12:36	
				GMS21-8	316	28	314	12:39	
				GMS21-9	250	32	246	12:40	
GMS22	1650±4	522490	927946	GMS22-1	135	68	100	14:18	
				GMS22-2	137	74	101	14:19	
				GMS22-3	151	77	105	14:21	
				GMS22-4	128	72	92	14:22	
				GMS22-5	125	70	89	14:23	
				GMS22-6	207	30	170	14:25	
				GMS22-7	161	25	123	14:27	
				GMS22-8	152	37	114	14:28	
				GMS22-9	196	47	156	14:30	core broken, hole oriented
GMS23	1578±4	522148	932645	GMS23-1	231	29	172	16:31	
				GMS23-2	240	31	180	16:32	Core broken, hole oriented
				GMS23-3	234	32	175	16:35	
				GMS23-4	223	30	176	16:37	
				GMS23-5	237	29	176	16:39	
				GMS23-6	245	27	184	16:46	
				GMS23-7	230	21	169	16:51	

Appendix E: Field structural data/Joint

Structure		Orientation				Structure		Orientation			
Name	No	Strike	Dip	Dip direction	Host rock	Name	No	Strike	Dip	Dip direction	Host rock
Joint	J1	55	70	SE	Ignimbrite	Joint	J29	45	85	E	Volcanic tuff
	J2	70	85	SE	Ignimbrite		J30	5	85	E	Volcanic tuff
	J3	215	90	SE	Ignimbrite		J31	335	70	SW	Volcanic tuff
	J4	220	80	SE	Ignimbrite		J32	320	60	NW	Volcanic tuff
	J5	265	88	S	Ignimbrite		J33	10	75	SE	Volcanic tuff
	J6	310	75	NE	Basaltic lava flow		J34	340	90	SW	Ignimbrite
	J7	120	60	NE	Basaltic lava flow		J35	75	75	SE	Ignimbrite
	J8	50	90	SE	Basaltic lava flow		J36	10	80	NW	Ignimbrite
	J9	345	90	NE	Basaltic lava flow		J37	330	80	SW	Ignimbrite
	J10	60	86	SE	Basaltic lava flow		J38	230	90	SW	Rhyolitic lava flow
	J11	345	84	NE	Basaltic lava flow		J39	245	85	SW	Rhyolitic lava flow
	J12	30	85	NW	Basaltic lava flow		J40	350	90	SW	Rhyolitic lava flow
	J13	60	90	SE	Basaltic lava flow		J41	110	90	SW	Ignimbrite
	J14	335	90	NE	Basaltic lava flow		J42	30	85	SE	Ignimbrite
	J15	55	85	SE	Basaltic lava flow		J43	95	80	S	Ignimbrite
	J16	345	90	NE	Basaltic lava flow		J44	60	90	SE	Ignimbrite
	J17	357	88	SW	Basaltic lava flow		J45	85	90	S	Ignimbrite
	J18	5	85	SW	Basaltic lava flow		J46	355	90	SW	Ignimbrite
	J19	10	85	SW	Basaltic lava flow		J47	330	80	SW	Ignimbrite
	J20	350	90	SW	Basaltic lava flow		J48	55	70	SE	Ignimbrite
	J21	240	85	SE	Basaltic lava flow		J49	245	85	SE	Ignimbrite
	J22	330	85	SW	Ignimbrite		J50	350	90	SW	Ignimbrite
	J23	310	90	SW	Ignimbrite		J51	80	75	SE	Ignimbrite
	J24	340	65	NE	Ignimbrite		J52	25	85	SE	Ignimbrite
	J25	305	88	SW	Ignimbrite		J53	75	80	S	Ignimbrite
	J26	60	90	NE	Ignimbrite		J54	80	90	SE	Ignimbrite
	J27	240	90	SE	Ignimbrite		J55	85	90	S	Ignimbrite
	J28	325	85	NE	Volcanic tuff						

Appendix F: Field structural data/Fault

Structure		Orientations			
Name	No	Strike	Dip	Dip direction	Host rock
Fault	F1	35	85	SE	Ignimbrite
	F2	12	83	SE	Ignimbrite
	F3	18	80	SE	Ignimbrite
	F4	20	88	E	Ignimbrite
	F5	22	84	E	Pumice
	F6	10	79	E	Pumice
	F7	33	84	SE	Pumice
	F8	28	82	SE	Pumice
	F9	30	87	SE	Ignimbrite
	F10	17	86	SE	Ignimbrite
	F11	30	84	SE	Ignimbrite
	F12	12	85	SE	Ignimbrite
	F13	25	90	SE	Rhyolitic lava flow
	F14	21	88	SE	Rhyolitic lava flow
	F15	17	86	SE	Basaltic lava flow
	F16	345	90	SW	Basaltic lava flow
	F17	357	88	SW	Basaltic lava flow
	F18	5	85	SW	Basaltic lava flow
	F19	10	85	SW	Basaltic lava flow
	F20	350	90	SW	Basaltic lava flow